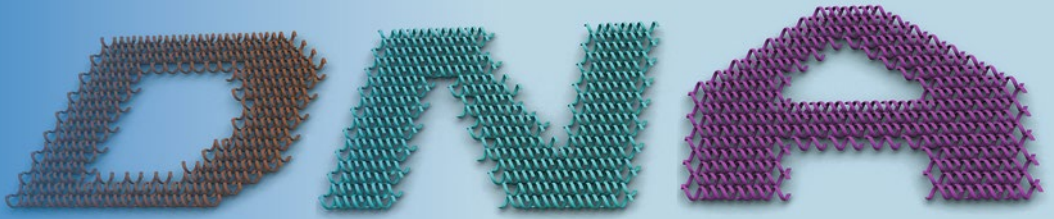


Methods in
Molecular Biology 1500

Springer Protocols



Yonggang Ke
Pengfei Wang *Editors*

3D DNA Nanostructure

Methods and Protocols

 Humana Press

METHODS IN MOLECULAR BIOLOGY

Series Editor
John M. Walker
School of Life and Medical Sciences
University of Hertfordshire
Hatfield, Hertfordshire, AL10 9AB, UK

For further volumes:
<http://www.springer.com/series/7651>

3D DNA Nanostructure

Methods and Protocols

Edited by

Yonggang Ke

Biomolecular Nanoengineering Laboratory, Emory University, Atlanta, GA, USA

Pengfei Wang

Biomolecular Nanoengineering Laboratory, Emory University, Atlanta, GA, USA

Editors

Yonggang Ke
Biomolecular Nanoengineering Laboratory
Emory University
Atlanta, GA, USA

Pengfei Wang
Biomolecular Nanoengineering Laboratory
Emory University
Atlanta, GA, USA

ISSN 1064-3745 ISSN 1940-6029 (electronic)
Methods in Molecular Biology
ISBN 978-1-4939-6452-9 ISBN 978-1-4939-6454-3 (eBook)
DOI 10.1007/978-1-4939-6454-3

Library of Congress Control Number: 2016954329

© Springer Science+Business Media New York 2017

This work is subject to copyright. All rights are reserved by the Publisher, whether the whole or part of the material is concerned, specifically the rights of translation, reprinting, reuse of illustrations, recitation, broadcasting, reproduction on microfilms or in any other physical way, and transmission or information storage and retrieval, electronic adaptation, computer software, or by similar or dissimilar methodology now known or hereafter developed.

The use of general descriptive names, registered names, trademarks, service marks, etc. in this publication does not imply, even in the absence of a specific statement, that such names are exempt from the relevant protective laws and regulations and therefore free for general use.

The publisher, the authors and the editors are safe to assume that the advice and information in this book are believed to be true and accurate at the date of publication. Neither the publisher nor the authors or the editors give a warranty, express or implied, with respect to the material contained herein or for any errors or omissions that may have been made.

Printed on acid-free paper

This Humana Press imprint is published by Springer Nature
The registered company is Springer Science+Business Media LLC
The registered company address is: 233 Spring Street, New York, NY 10013, U.S.A.

Preface

DNA is known for its biological role as the genetic information carrier for most living organisms. However, DNA is far beyond just the secret of life. Thanks to Nadrian Seeman's seminal contributions in the early 1980s, the field of DNA nanotechnology was founded based on the groundbreaking idea of utilizing DNA as building materials towards the organization of guest molecules such as proteins. In the past three decades, started from solely demonstrating the beauty of DNA self-assembly to actively exploring a large diversity of applications, we have witnessed the rapid growth and expansion of the field of DNA nanotechnology.

This book, *3D DNA Nanostructure: Methods and Protocols*, aims to present a comprehensive technical overview of DNA nanotechnology with an emphasis on 3D DNA nanostructure design and applications. Towards this end, we have invited leading scientists across the world in the field of DNA nanotechnology to contribute to this book, aiming to provide the most up-to-date tutorial style overview or technical style protocols to benefit the whole scientific society. Coverage of this book spans from basic design principles for DNA and RNA nanostructures to their cutting-edge applications in a variety of fields.

This book is composed of two parts. Part I covers basic DNA and RNA nanostructure design strategies ranging from conventional tile-based assembly, single-stranded DNA bricks, to the origami approach. Part II has a comprehensive inclusion of applications utilizing DNA nanostructures that have been continually explored, including but not limited to nanomedicine, bioimaging, biosensing, nanoplasmonics, nanoelectronics, nanofabrication, crystallography, biophysics, and analytical chemistry.

Taking this opportunity, we would like to show our sincere appreciation to all the authors of the book, who have spent tremendous effort and done fabulous work on putting all the materials together to make this book. In addition, we would like to thank the organizational and editorial help from the editorial team of Springer.

Atlanta, GA, USA

*Yonggang Ke
Pengfei Wang*

Contents

<i>Preface</i>	<i>v</i>
<i>Contributors</i>	<i>ix</i>

PART I DNA/RNA STRUCTURE DESIGN

1	Designed 3D DNA Crystals	3
	<i>Nadrian C. Seeman, Ruojie Sha, Jens Birktoft, Jianping Zheng, Wenyan Liu, Tong Wang, and Chengde Mao</i>	
2	Three-Dimensional DNA Nanostructures Assembled from DNA Star Motifs	11
	<i>Cheng Tian and Chuan Zhang</i>	
3	Design of Wireframe DNA Nanostructures—DNA Gridiron	27
	<i>Dongran Han</i>	
4	Complex DNA Brick Assembly	41
	<i>Luvena Ong and Yonggang Ke</i>	
5	Computer-Aided Design of RNA Origami Structures	51
	<i>Steffen L. Sparvath, Cody W. Geary, and Ebbe S. Andersen</i>	
6	Assembling RNA Nanoparticles	81
	<i>Shou-Jun Xiao</i>	

PART II APPLICATIONS OF DNA STRUCTURES

7	DNA Functionalization of Nanoparticles	99
	<i>Fang Lu and Oleg Gang</i>	
8	Purification Techniques for Three-Dimensional DNA Nanostructures	109
	<i>Travis A. Meyer</i>	
9	DNA Nanostructure as Smart Carriers for Drug Delivery	121
	<i>Xiangyuan Ouyang, Jie Chao, Shao Su, and Chunhai Fan</i>	
10	DNA G-Quadruplex-Based Assay of Enzyme Activity	133
	<i>Zhuoliang Liu, Kaiyu He, Wang Li, Xin Liu, Xiahong Xu, Zhou Nie, and Shouzhuo Yao</i>	
11	Spatial Organization of Enzyme Cascade on a DNA Origami Nanostructure	153
	<i>Jinglin Fu and Tianran Li</i>	
12	Lipid Membrane Encapsulation of a 3D DNA Nano Octahedron	165
	<i>Steven D. Perrault and William M. Shih</i>	
13	DNA-PAINT Super-Resolution Imaging for Nucleic Acid Nanostructures	185
	<i>Mingjie Dai</i>	
14	Designing DNA Nanotube Liquid Crystals as a Weak-Alignment Medium for NMR Structure Determination of Membrane Proteins	203
	<i>John Min, William M. Shih, and Gaëtan Bellot</i>	

15	Direct Nanofabrication Using DNA Nanostructure	217
	<i>Feng Zhou and Haitao Liu</i>	
16	Confined Growth of Metal Nanoparticles Within 3D DNA Origami Molds	237
	<i>Wei Sun and Jie Shen</i>	
17	DNA-Directed Self-Assembly of Highly Ordered and Dense Single-Walled Carbon Nanotube Arrays	245
	<i>Hareem Maune and Si-ping Han</i>	
18	A Proximity-Based Programmable DNA Nanoscale Assembly Line	257
	<i>Xiaoyan Zhang, Xiaoqiang Ding, Jianzhou Zou, and Hongzhou Gu</i>	
19	DNA Walkers as Transport Vehicles of Nanoparticles Along a Carbon Nanotube Track	269
	<i>Jing Pan, Tae-Gon Cha, Haorong Chen, Feiran Li, and Jong Hyun Choi</i>	
	<i>Index</i>	281

Contributors

- EBBE S. ANDERSEN • *iNANO, Aarhus University, Aarhus, Denmark*
- GAËTAN BELLOT • *Institut de Génomique Fonctionnelle, Centre National de la Recherche Scientifique, CNRS Unité Mixte de Recherche UMR 5203, Institut National de la Santé et de la Recherche Médicale, INSERM U1191, Montpellier, France; Université de Montpellier, Montpellier, France*
- JENS BIRKTOFT • *Department of Chemistry, New York University, New York, NY, USA*
- TAE-GON CHA • *School of Mechanical Engineering, Purdue University, West Lafayette, IN, USA*
- JIE CHAO • *Laboratory of Physical Biology, Chinese Academy of Sciences, Shanghai Institute of Applied Physics, Shanghai, China; Key Laboratory for Organic Electronics and Information Displays and Institute of Advanced Materials (IAM), Jiangsu National Synergetic Innovation Center for Advanced Materials (SICAM), Nanjing University of Posts and Telecommunications, Nanjing, Jiangsu, China*
- HAORONG CHEN • *School of Mechanical Engineering, Purdue University, West Lafayette, IN, USA*
- JONG HYUN CHOI • *School of Mechanical Engineering, Purdue University, West Lafayette, IN, USA*
- MINGJIE DAI • *Program in Biophysics, Harvard University, Boston, MA, USA; Wyss Institute for Biologically Inspired Engineering, Boston, MA, USA*
- XIAOQIANG DING • *Kidney and Dialysis Institute of Shanghai, Shanghai, China; Kidney and Blood Purification Laboratory of Shanghai, Shanghai, China; Department of Nephrology, Zhongshan Hospital, Shanghai Medical College, Fudan University, Shanghai, China*
- CHUNHAI FAN • *Laboratory of Physical Biology, Chinese Academy of Sciences, Shanghai Institute of Applied Physics, Shanghai, China*
- JINGLIN FU • *Center for Computational and Integrative Biology, Rutgers University, Camden, NJ, USA; Department of Chemistry, Rutgers University, Camden, NJ, USA*
- OLEG GANG • *Brookhaven National Laboratory, Center for Functional Nanomaterials, Upton, NY, USA*
- CODY W. GEARY • *iNANO, Aarhus University, Aarhus, Denmark*
- HONGZHOU GU • *Kidney and Dialysis Institute of Shanghai, Shanghai, China; Kidney and Blood Purification Laboratory of Shanghai, Shanghai, China; Department of Nephrology, Zhongshan Hospital, Shanghai Medical College, Fudan University, Shanghai, China*
- DONGRAN HAN • *Department of Systems Biology, Harvard Medical School, Boston, MA, USA; Wyss Institute for Biologically Inspired Engineering, Harvard University, Boston, MA, USA*
- SI-PING HAN • *Materials and Process Simulation Center, California Institute of Technology, Pasadena, CA, USA*

- KAIYU HE • *State Key Laboratory Breeding Base for Zhejiang Sustainable Pest and Disease Control, Key Laboratory for Pesticide Residue Detection of Ministry of Agriculture, Zhejiang Academy of Agricultural Sciences, Institute of Quality and Standard for Agro-Products, Hangzhou, People's Republic of China*
- YONGGANG KE • *The Wallace H. Coulter Department of Biomedical Engineering, Georgia Institute of Technology and Emory University, Atlanta, GA, USA*
- FEIRAN LI • *School of Mechanical Engineering, Purdue University, West Lafayette, IN, USA*
- TIANRAN LI • *Center for Computational and Integrative Biology, Rutgers University, Camden, NJ, USA*
- WANG LI • *State Key Laboratory of Chemo/Biosensing and Chemometrics, College of Chemistry and Chemical Engineering, Hunan University, Changsha, People's Republic of China*
- HAITAO LIU • *Department of Chemistry, University of Pittsburgh, Pittsburgh, PA, USA*
- WENYAN LIU • *Department of Chemistry, New York University, New York, NY, USA*
- XIN LIU • *State Key Laboratory of Chemo/Biosensing and Chemometrics, College of Chemistry and Chemical Engineering, Hunan University, Changsha, People's Republic of China*
- ZHUOLIANG LIU • *State Key Laboratory of Chemo/Biosensing and Chemometrics, College of Chemistry and Chemical Engineering, Hunan University, Changsha, People's Republic of China*
- FANG LU • *Brookhaven National Laboratory, Center for Functional Nanomaterials, Upton, NY, USA*
- CHENGDE MAO • *Department of Chemistry, Purdue University, West Lafayette, IN, USA*
- HAREEM MAUNE • *IBM Almaden Research Center, San Jose, CA, USA*
- TRAVIS A. MEYER • *The Wallace H. Coulter Department of Biomedical Engineering, Georgia Institute of Technology and Emory University, Atlanta, GA, USA; Biomolecular Nanoengineering Lab, Emory School of Medicine, Atlanta, GA, USA*
- JOHN MIN • *Department of Genetics, Harvard Medical School, Boston, MA, USA; Wyss Institute for Biologically Inspired Engineering, Boston, MA, USA; Sculpting Evolution Group, Media Lab, Massachusetts Institute of Technology, Cambridge, MA, USA*
- ZHOU NIE • *State Key Laboratory of Chemo/Biosensing and Chemometrics, College of Chemistry and Chemical Engineering, Hunan University, Changsha, People's Republic of China*
- LUVENA ONG • *Wyss Institute for Biologically Inspired Engineering, Harvard University, Boston, MA, USA; The Harvard-MIT Health Sciences and Technology Program, Massachusetts Institute of Technology, Cambridge, MA, USA*
- XIANGYUAN OUYANG • *Laboratory of Physical Biology, Chinese Academy of Sciences, Shanghai Institute of Applied Physics, Shanghai, China; Key Laboratory of Synthetic and Natural Function Molecule Chemistry of Ministry of Education, College of Chemistry and Material Science, Northwest University, Xi'an, China*
- JING PAN • *School of Mechanical Engineering, Purdue University, West Lafayette, IN, USA*
- STEVEN D. PERRAULT • *Department of Biological Chemistry and Molecular Pharmacology, Harvard Medical School, Boston, MA, USA; Wyss Institute for Biologically Inspired Engineering, Boston, MA, USA; Department of Cancer Biology, Dana Farber Cancer Institute, Boston, MA, USA*
- NADRIAN C. SEEMAN • *Department of Chemistry, New York University, New York, NY, USA*
- RUOJIE SHA • *Department of Chemistry, New York University, New York, NY, USA*

- JIE SHEN • *Wyss Institute for Biologically Inspired Engineering, Harvard University, Boston, MA, USA; Department of Systems Biology, Harvard Medical School, Boston, MA, USA*
- WILLIAM M. SHIH • *Department of Biological Chemistry and Molecular Pharmacology, Harvard Medical School, Boston, MA, USA; Wyss Institute for Biologically Inspired Engineering, Boston, MA, USA; Department of Cancer Biology, Dana Farber Cancer Institute, Boston, MA, USA*
- STEFFEN L. SPARVATH • *iNANO, Aarhus University, Aarhus, Denmark*
- SHAO SU • *Key Laboratory for Organic Electronics and Information Displays and Institute of Advanced Materials (IAM), Jiangsu National Synergetic Innovation Center for Advanced Materials (SICAM), Nanjing University of Posts and Telecommunications, Nanjing, Jiangsu, People's Republic of China*
- WEI SUN • *Wyss Institute for Biologically Inspired Engineering, Harvard University, Boston, MA, USA; Department of Systems Biology, Harvard Medical School, Boston, MA, USA*
- CHENG TIAN • *Department of Chemistry, Purdue University, West Lafayette, IN, USA*
- TONG WANG • *Department of Chemistry, New York University, New York, NY, USA*
- SHOU-JUN XIAO • *School of Chemistry and Chemical Engineering, Nanjing University, Nanjing, People's Republic of China*
- XIAHONG XU • *State Key Laboratory Breeding Base for Zhejiang Sustainable Pest and Disease Control, Key Laboratory for Pesticide Residue Detection of Ministry of Agriculture, Zhejiang Academy of Agricultural Sciences, Institute of Quality and Standard for Agro-Products, Hangzhou, People's Republic of China*
- SHOUZHUO YAO • *State Key Laboratory of Chemo/Biosensing and Chemometrics, College of Chemistry and Chemical Engineering, Hunan University, Changsha, People's Republic of China*
- CHUAN ZHANG • *School of Chemistry and Chemical Engineering, Shanghai Jiao Tong University, Shanghai, People's Republic of China*
- XIAOYAN ZHANG • *Fudan University Shanghai Cancer Center, Institutes of Biomedical Sciences, Shanghai Medical College of Fudan University, Shanghai, China; Kidney and Dialysis Institute of Shanghai, Shanghai, China; Kidney and Blood Purification Laboratory of Shanghai, Shanghai, China; Department of Nephrology, Zhongshan Hospital, Shanghai Medical College, Fudan University, Shanghai, China*
- JIANPING ZHENG • *Department of Chemistry, New York University, New York, NY, USA*
- FENG ZHOU • *Department of Chemistry, University of Pittsburgh, Pittsburgh, PA, USA*
- JIANZHOU ZOU • *Kidney and Dialysis Institute of Shanghai, Shanghai, China; Kidney and Blood Purification Laboratory of Shanghai, Shanghai, China; Department of Nephrology, Zhongshan Hospital, Shanghai Medical College, Fudan University, Shanghai, China*

Part I

DNA/RNA Structure Design

Chapter 1

Designed 3D DNA Crystals

Nadrian C. Seeman, Ruojie Sha, Jens Birktoft, Jianping Zheng,
Wenyan Liu, Tong Wang, and Chengde Mao

Abstract

The simplest practical route to producing precisely designed 3D macroscopic objects is to form a crystalline arrangement by self-assembly, because such a periodic array has only conceptually simple requirements: a motif that has a robust 3D structure, dominant affinity interactions between parts of the motif when it self-associates, and predictable structures for these affinity interactions. Fulfilling these three criteria to produce a 3D periodic system is not easy, but should readily be achieved with well-structured branched DNA motifs tailed by sticky ends (Zheng et al., *Nature* 461:74–77, 2009). Herein, a brief introduction to designed 3D DNA crystals from tensegrity triangle is presented.

Key words DNA crystal, Self-assembly

1 Introduction

A key goal of structural DNA nanotechnology is the control of the structure of matter in three dimensions. Crystals are the most prominent form of 3D matter, and they are also the easiest form to characterize, because they are amenable to diffraction analysis by X-ray crystallography. As we are all aware, a crystal is a periodic array of matter. In principle, one-dimensional, two-dimensional, and three-dimensional arrays are all possible, but the most intriguing arrays are those in 3D. Such arrangements bring us into touch with the 3D world that we all inhabit, and they enable us to establish structures that are “statues,” not merely 2D representations or projections.

Molecular crystals typically self-assemble themselves when conditions are arranged to make them insoluble; it is usually the job of the crystallographer to establish the organization of matter within them. However, DNA has provided us with the means to design the internal structures of crystals, including their intermolecular contacts. This is done by designing well-structured

components that will self-assemble into a crystal from branched DNA molecules [1]. To our knowledge, this is a unique situation available for the design of crystalline matter.

2 3D DNA Crystal Design

Crystal design components require three features: Predictable intermolecular interactions based on affinity, predictable local product structures, and “structural integrity.” The first two of these properties are readily provided by sticky-ended cohesion. Sticky ends consist of single-stranded overhangs that occur when one strand of the double helix is longer than its Watson–Crick complement (Fig. 1, top). If they are complementary, two sticky ends will cohere to produce a single molecular complex in conventional conditions for nucleic acid solutions. The bottom of Fig. 1 shows the two sticky ends from the top image (colored magenta) cohering with each other by Watson–Crick base pairing. It is important to indicate that when working with synthetic DNA, it is possible to program sticky ends for numerous orthogonal affinities all within the same pot.

The predictability of the local product structure is another feature for which sticky ends are responsible. When two sticky ends cohere, they form B-DNA, as shown in Fig. 2 [2]. Thus, we know, *a priori*, not only affinity, but also structure. This is in contrast

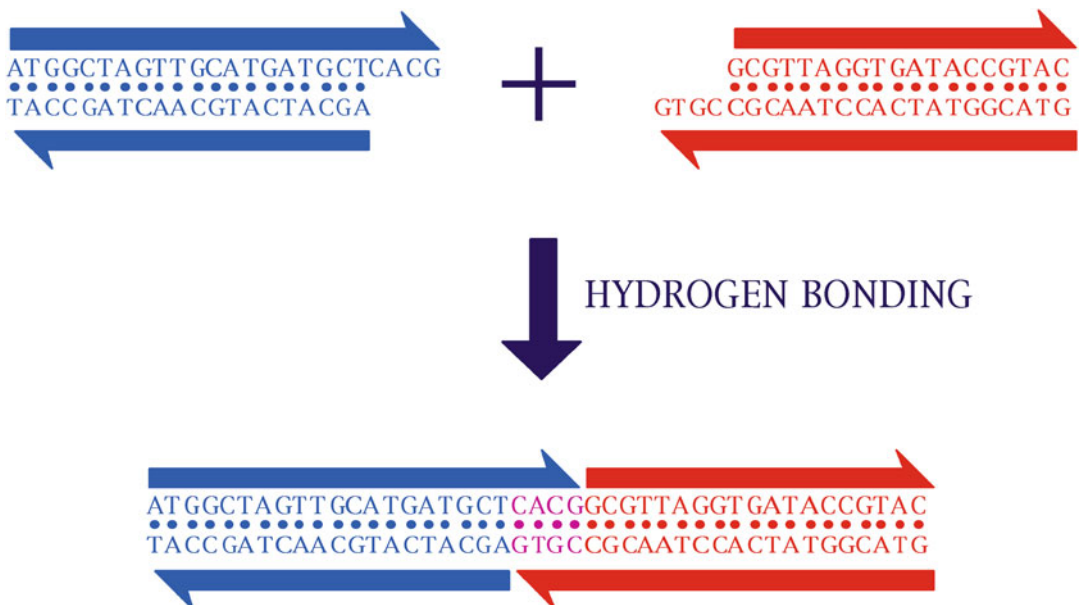


Fig. 1 Sticky-ended cohesion. Two unwound double helices are shown at the *top*. Their strands are slightly different lengths, creating overhangs that are called sticky ends. If the sticky ends are complementary and conditions are proper, the two molecules can cohere, as shown at the *bottom*

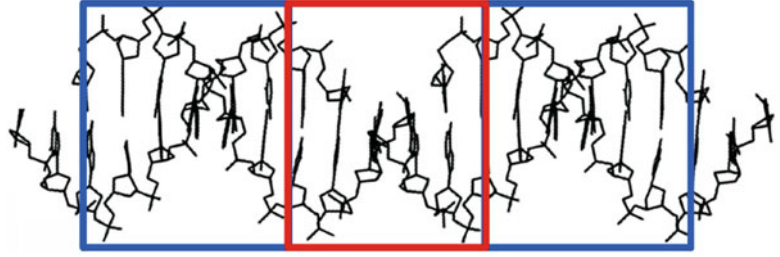


Fig. 2 A crystal structure showing sticky ended cohesion. This is the crystal structure of a self-complementary DNA decamer. Sticky ended cohesion is shown in the *red box* in the middle, where the two gaps lacking phosphate groups are prominent. The DNA in the *red box* has the same B-DNA structure as the DNA in the *blue boxes*, even though it is upside down, because it is a half-turn away. Thus, if one knows the coordinates of the DNA in the *blue box* on the right, one knows the coordinates of the DNA in the *blue box* on the left, even in solution

other well-known affinity interactions. For example, one can know the 3D structure of an antigen and an antibody to it, but the exact geometry of their interaction requires at least a sophisticated docking experiment, if not a crystal structure. By contrast, we know that whatever the programming and lengths of the sticky ends, the product will be B-DNA.

“Structural integrity” is a fancy way of saying that the motif must be stiff. This is the hardest of the criteria to satisfy. Although it is possible to define relatively stiff DNA motifs that are branched [3], they largely suffer from another flaw, namely that their helix axes are all parallel. Both in 2D and in 3D, the structures that seem to lead best to propagation of the lattice in multiple dimensions are those that entail DNA motifs whose helix axes span all of the dimensions of the target array. Nobody understands the reason for this, but to date, it has proved unwise to ignore this lesson. For example, in the case of 2D DNA origami, a cross-shaped motif was far more successful than a conventional origami with parallel helix axes (Fig. 3a, b) [4]. The same is true in 3D: The main motif that has led to 3D crystals that diffract to significant resolution is the “tensegrity triangle,” first devised by Mao and his colleagues [5]. This motif consists of a series of stressed double helices that span 3-space. The triangle consists of three four-arm junctions that are connected in a stressed arrangement. The triangle with two helical turns is highly stressed, and has never been made successfully with its junctions flanked by anything but the particularly robust J1 junction sequence [6, 7].

The experimental details of self-assembling two-turn tensegrity triangles into 3D crystals are given in ref. [8]. This concatenation of tensegrity triangles into a 3D crystal results in a 6-connected lattice, shown in Fig. 4a, which illustrates a tensegrity triangle and all of its nearest neighbors [8]. It is clear from this stereographic

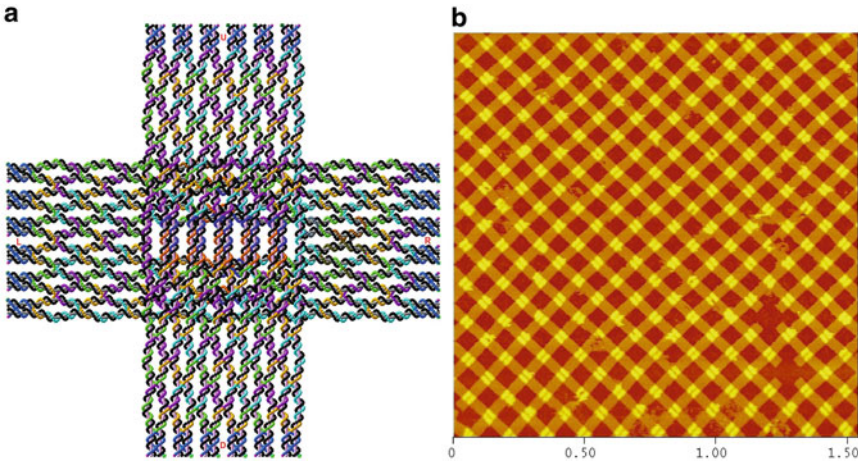


Fig. 3 A 2D origami array. **(a)** A DNA origami motif with helix axes pointing at right angles to each other. **(b)** A 2D origami array self-assembled from the motif in **(a)**

image that the tensegrity motif spans 3-space: The red direction proceeds from the rear to the front, as does the green direction, and the yellow direction. Figure 4b indicates another way to look at the lattice: An arrangement of eight tensegrity triangles flank a rhombohedral cavity. The red triangle flanks a vertex at the rear, and it is connected to three yellow triangles that flank vertices somewhat nearer to us. The yellow triangles are, in turn, connected to three green triangles that flank vertices nearer to us yet. The front vertex of the rhombohedron has been left without a flanking triangle for clarity, but another red triangle clearly belongs in that position.

Although the successful tensegrity triangles made so far have certain limitations, their size is not one of them. Crystals have been made with edges two, three, and four turns long [8]. These structures are shown in Fig. 5. There appear to be no limitations on the sequences of the junctions that flank the larger triangles. The sticky ends used in crystals are typically two nucleotides long, but they can be both symmetric (all three sets the same) or asymmetric. We do not understand why, but symmetric triangles diffract better than asymmetric triangles. It is possible that variations are averaged out, but it is also possible that the purification of the three strands of a symmetric triangle is more effective than the purification of the seven strands of an asymmetric triangle.

Because sticky ends constitute a programmable intermolecular contact, they can be used to control the number of molecules in an asymmetric unit of the unit cell. Figure 6a shows the nearest neighbors of a triangle in a crystal containing two different molecules in the asymmetric unit [9]. The rhombohedral arrangement corresponding to this crystal is shown in Fig. 6b. It is clear that each

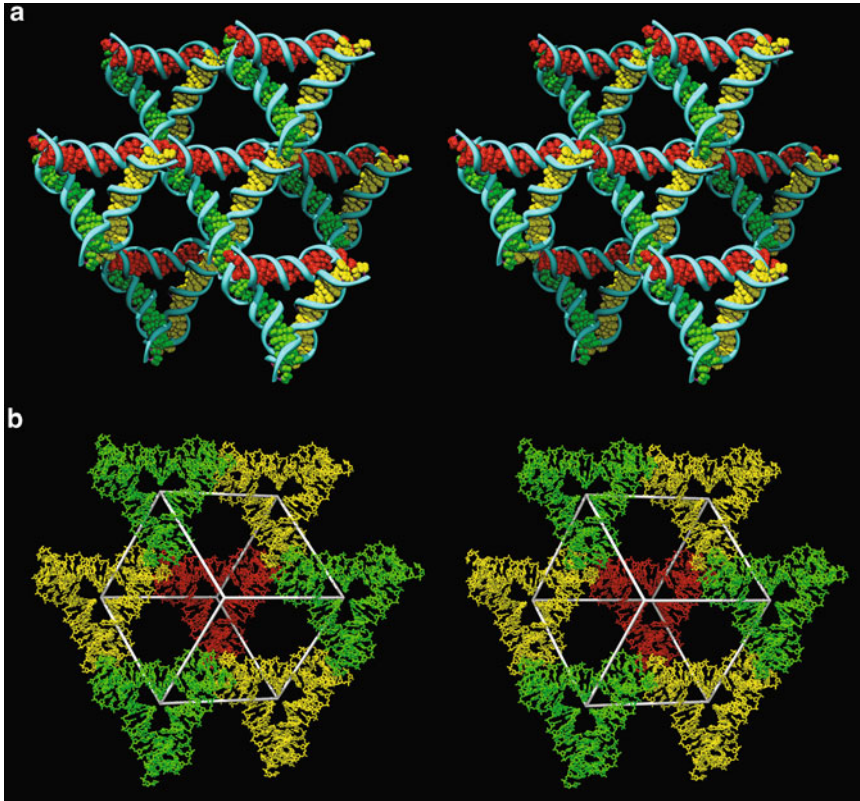


Fig. 4 Stereographic images of a tensegrity triangle crystal structure. **(a)** The surroundings of a triangle. Each triangle is joined to six other triangles by sticky-ended cohesion. The schematic shows that the three directions defined by the helix axes span 3-space. The *red* direction goes from rear to front, as does the *green* direction and the *yellow* direction. **(b)** Eight triangles surround the vertices of a rhombohedron. The *red* triangle sits on the rear vertex of a rhombohedron. It is connected to the three *yellow* triangles that flank vertices nearer to the viewer. The *yellow* triangles are connected to the *green* triangles that flank vertices nearer yet to the viewer. The front vertex has been left vacant for clarity, but would contain another *red* triangle

edge of the rhombohedron is flanked by triangles of a different color, indicating different molecules. The presence of multiple independent molecules in the unit cell can be used further to control a macroscopic property of the crystal, such as its color [9]. Figure 7 shows the labeling of various molecules within the unit cell. In the top row, the pink dye CY3 is attached to the A molecule, the B molecule or both, yielding a pink crystal. In the bottom row, the blue dye CY5 is similarly attached to the A molecule, the B molecule or both, yielding a blue crystal. On the ends of the middle row, the CY3 is attached to the A molecule and CY5 is attached to the B molecule or *vice versa*, yielding a purple crystal.

One of the troublesome features of designed 3D DNA crystals is that their resolutions are mediocre (typically 4–5 Å), and as their edge lengths increase, and the volumes of their cavities do too,

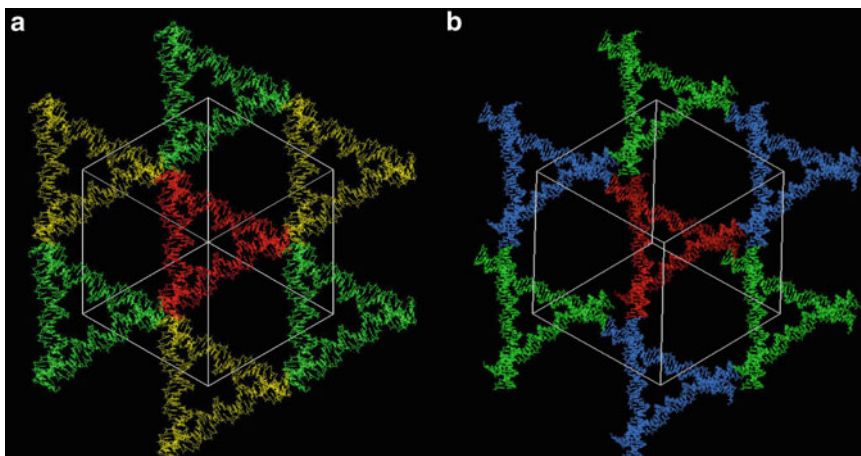


Fig. 5 Larger crystals. **(a)** A crystal structure constructed from triangles containing three turns per edge. **(b)** A crystal structure constructed from triangles containing 4 turns per edge. These crystals are not significantly different from the 2-turn-per-edge crystal, except for the quality of their diffraction

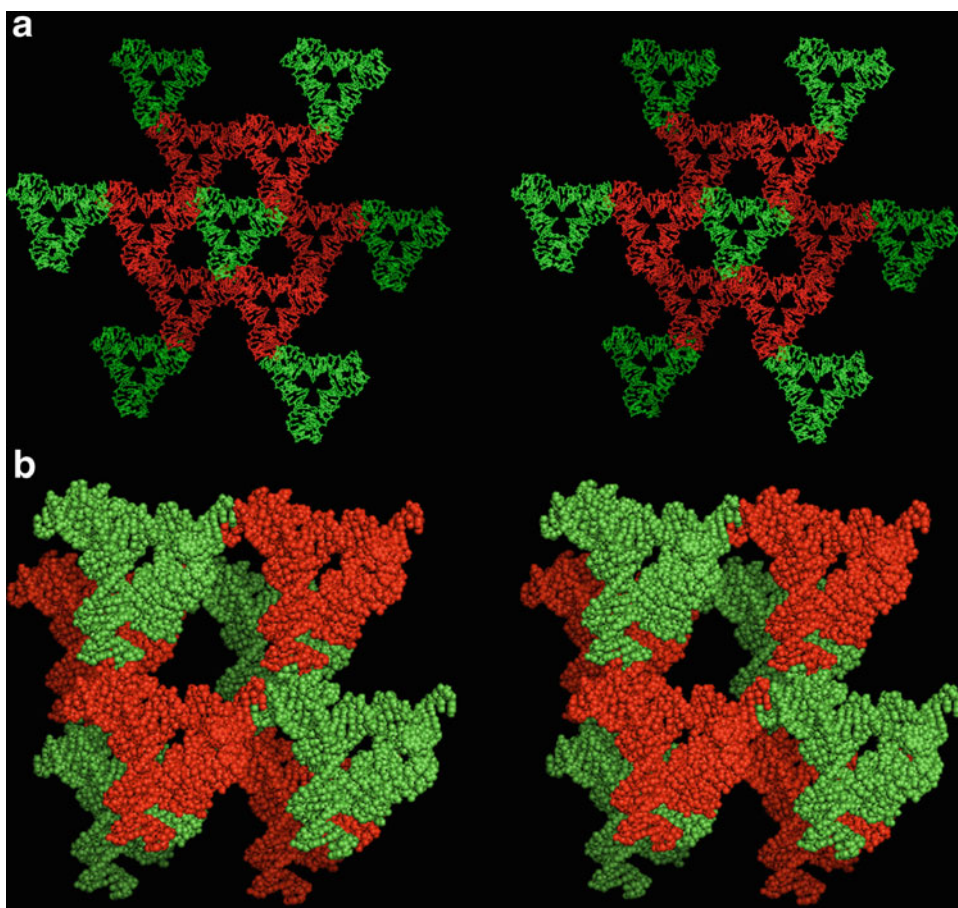


Fig. 6 A crystal programmed to contain two molecules per asymmetric unit. Both panels are stereographic images of the crystal structure. One molecule is drawn in *red* and the other in *green*. **(a)** The surroundings of an individual triangle. The *green* triangle in the center is connected to six *red* triangles, just as in Fig. 4. The next-nearest neighbors in the same direction (only) are shown in *green*. **(b)** The rhombohedron formed by four molecules of each kind. Eight molecules are shown. The opposite vertices along each edge contain triangles of different species

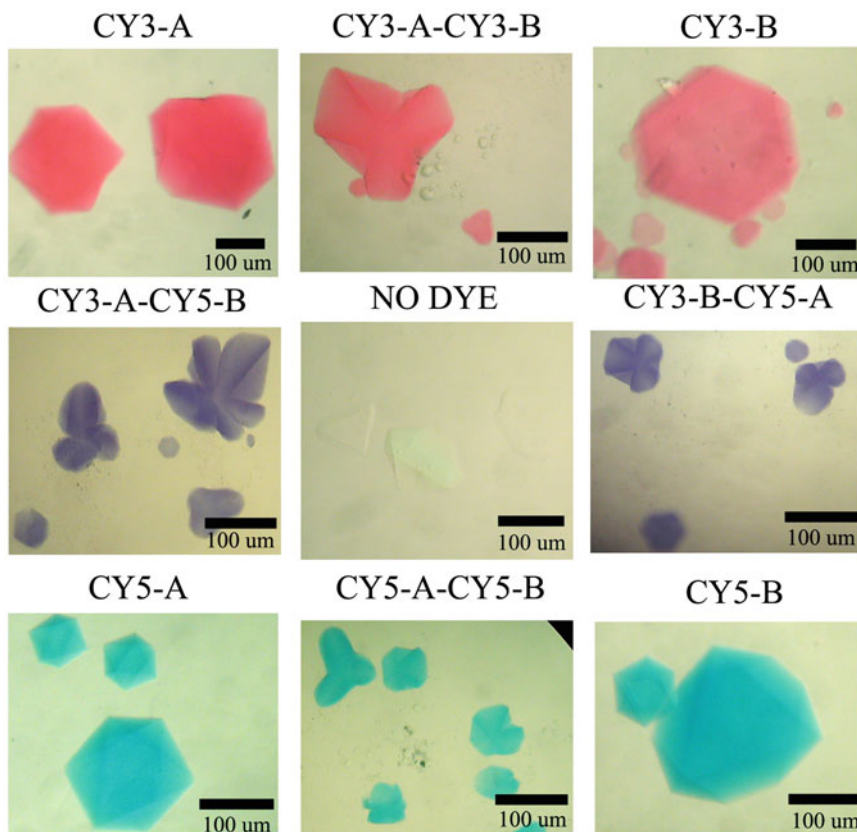


Fig. 7 Controlling the color: a macroscopic property of a crystal containing two independent molecules. Two dyes have been employed, CY-3, a *pink* dye, and CY-5, a *blue* dye. In the top row, the A-molecule (*left*), the B-molecule (*right*) or both (*center*) have had CY-3 attached to it. The crystals are consequently colored *pink*. In the bottom row, the A-molecule (*left*), the B-molecule (*right*), or both (*center*) have had CY-5 attached to them. The crystals are now colored *blue*. The *left* image in the middle row has CY-3 attached to the A molecule, and CY-5 attached to the B molecule, whereas the order has been reversed on the *right*. The crystals are colored *purple*, as expected. The central image contains control crystals to which no dye has been attached. Thus, a macroscopic property, the color, has been programmed using a microscopic chemical attachment

their resolution decreases. We do not understand this completely. Obviously something involving the heterogeneity of the individual molecules is involved, either as a fixed phenomenon or in the freezing process. In unpublished work, we have shown at LCLS that it is probably not the freezing process, because nanocrystals (about 1 μm in size) diffract no better at room temperature. Addition of phosphates to the sticky ends seems to improve the quality of diffraction by about 1 \AA in tensegrity triangles with two turns per edge [10]. Control of the sticky ends has revealed that resolution can be changed by varying the lengths of the sticky ends, but that the process appears not to be thermodynamic: At least in the case of the 2-turn triangle, shorter sticky ends are better than longer ones (in preparation). 3D DNA crystals have been proposed as

scaffolding for nanoelectronics [11], an application that probably does not require very high resolution. However, the original goal of 3D DNA crystals, acting as scaffolds for macromolecular guests [1], will require more experimentation to bring to fruition.

The control of structure in three dimensions by DNA on the macroscopic scale is likely to impinge on our abilities to organize bottom-up nanoelectronics [11], as noted above. In addition, it will ultimately enable our examination of well-oriented optical phenomena on the molecular scale. For these purposes, the X-ray diffraction experiment is likely to prove a valuable concomitant. However, for the time being, diffraction experiments will need to be relatively insensitive to resolution to be able to aid the analysis of other systems oriented by DNA in 3D crystals.

Acknowledgement

This research has been supported by the following grants to NCS: EFRI-1332411, and CCF-1526650 from the NSF, MURI W911NF-11-1-0024 from ARO, MURI N000140911118 from ONR, DE-SC0007991 from DOE for partial salary support, and grant GBMF3849 from the Gordon and Betty Moore Foundation.

References

1. Seeman NC (1982) Nucleic acid junctions and lattices. *J Theor Biol* 99:237–247.
2. Qiu H, Dewan JC, Seeman NC (1997) A DNA decamer with a sticky end: the crystal structure of d-CGACGATCGT. *J Mol Biol* 267:881–898.
3. Li X, Yang X, Qi J, Seeman NC (1996) Antiparallel DNA double crossover molecules as components for nanoconstruction. *J Am Chem Soc* 118:6131–6140.
4. Liu W, Zhong H, Wang R, Seeman NC (2011) Crystalline two-dimensional DNA origami arrays. *Angew Chem* 50:264–267.
5. Liu D, Wang W, Deng Z, Walulu R, Mao C (2004) Tensegrity: construction of rigid DNA triangles with flexible four-arm junctions. *J Am Chem Soc* 126:2324–2325.
6. Nguyen N, Birktoft JJ, Sha R, Wang T, Zheng J, Constantinou PE, Ginell SL, Chen Y, Mao C, Seeman NC (2012) The absence of tertiary interactions in a self-assembled DNA crystal structure. *J Mol Recogn* 25:234–237.
7. Kallenbach NR, Ma R-I, Seeman NC (1983) An immobile nucleic acid junction constructed from oligonucleotides. *Nature* 305:829–831.
8. Zheng J, Birktoft JJ, Chen Y, Wang T, Sha R, Constantinou PE, Ginell SL, Mao C, Seeman NC (2009) From molecular to macroscopic *via* the rational design of a self-assembled 3D DNA crystal. *Nature* 461:74–77.
9. Wang T, Sha R, Birktoft JJ, Zheng J, Mao C, Seeman NC (2010) A DNA crystal designed to contain two molecules per asymmetric unit. *J Am Chem Soc* 132:15471–15473.
10. Sha R, Birktoft JJ, Nguyen N, Chandrasekaran AR, Zheng J, Zhao X, Mao C, Seeman NC (2013) Self-assembled DNA crystals: the impact on resolution of 5'-phosphates and the DNA source. *Nano Lett* 13:793–797.
11. Robinson BH, Seeman NC (1987) The design of a biochip: a self-assembling molecular-scale memory device. *Protein Eng* 1:295–300.

Three-Dimensional DNA Nanostructures Assembled from DNA Star Motifs

Cheng Tian and Chuan Zhang

Abstract

Tile-based DNA self-assembly is a promising method in DNA nanotechnology and has produced a wide range of nanostructures by using a small set of unique DNA strands. DNA star motif, as one of DNA tiles, has been employed to assemble varieties of symmetric one-, two-, three-dimensional (1, 2, 3D) DNA nanostructures. Herein, we describe the design principles, assembly methods, and characterization methods of 3D DNA nanostructures assembled from the DNA star motifs.

Key words DNA nanostructure, Star motif, Three-dimensional (3D), Self-assembly, Gel electrophoresis, Atomic force microscopy, Cryogenic electron microscopy, Single particle reconstruction, Dynamic light scattering

1 Introduction

1.1 DNA Three-Dimensional (3D) Self-Assembly

In the past three decades, rather than its genetic functions in biology, DNA has been invoked as a generic superb macromolecule in bottom-up self-assembly in materials science, rising a new discipline that is called “DNA nanotechnology” [1–3]. To date, hundreds of different one-, two-, three-dimensional (1, 2, 3D) DNA nanostructures with controllable size, geometry, topology, and functions have been synthesized in a rational design fashion. Among them, DNA 3D nanostructures are particularly of interests to scientists since they can be programmably tuned to mimic many molecular machines and functional subcellular organelles in cell. Thus, artificial DNA nanostructures with specific functions are highly expected to play an important role in biomedical applications.

However, the synthesis of DNA 3D nanostructures is challenging. In early childhood of DNA nanotechnology, DNA 3D nanostructures were synthesized by stepwise and tedious enzymatic ligation, as evident by the construction of connective cube [4] and truncated octahedron [5]. One drawback of this strategy is that the overall yield is extremely low. To develop more facile

procedure for 3D nanostructure synthesis, later on, one pot self-assembly strategy was invented, in which multiple DNA strands with predesigned sequences recognized with each other and hybridized together to form predesigned 3D nanostructures during the annealing process. The first example was demonstrated in 2004 where four oligonucleotides were used to construct a DNA tetrahedron [6]. Since then, one-pot synthesis strategy has dominated the DNA 3D assembly and two different approaches were invented independently. One is called tile-based self-assembly and the other is called DNA origami. The former method redesigns the DNA motifs previously used for 1D and 2D assembly and enables them suitable to form 3D nanostructures. For instance, Mao et al. introduced long and flexible hinges into rigid DNA star motifs, by which DNA polyhedra with different geometries were constructed [7–10]. In the case of DNA origami, researchers employ hundreds of staple strands to fold a long genetic viral DNA strand back and forth into predesigned 3D nanostructures [11]. For example, Shih and his coworkers folded a long viral DNA into a highly symmetric octahedron [12]. Later on, DNA box [13], sphere, nanoflask, and structures with other specific morphologies [14] were successfully synthesized. Thus far, origami method is capable of constructing 3D nanostructures with almost any arbitrary shapes and topologies. Moreover, the combination of aforementioned two strategies can further extend the diversity of DNA 3D nanostructures. As an example, giant DNA tiles assembled via the origami method served as building blocks to construct very large 3D objects, allowing us to synthesize more sophisticated nanostructures that may mimic functional cellular components [15].

1.2 DNA 3D Nanostructures Assembled by Star Motifs

Although DNA origami has been demonstrated as a facile and powerful method in constructing DNA 3D nanostructures, the synthesis of each object requires a huge number of staple strands. As the 3D objects become large and complicated, the number of helper strands with unique sequence dramatically increases. Alternatively, biosystem evolves a smarter way to construct nanomachines with different biological functions. In nature, the living organism usually employs multiple copies of component biomolecules, to construct a desired structure, by which the workload of gene coding can be significantly reduced. For instance, the capsids of spherical viruses are highly symmetric, icosahedral structures, which are composed by many copies of identical subunit proteins through non-covalent binding. Inspired by this process, we successfully designed and synthesized a series of DNA star motifs and assembled them into highly symmetric DNA polyhedra and nanocages, resembling the viral capsid formation [7–10, 16–20].

As shown in schematic drawing (Fig. 1), a DNA star motif with n -fold rotational symmetry consists of three types of DNA strands: one long repetitive central strand (L_n , n is an integer

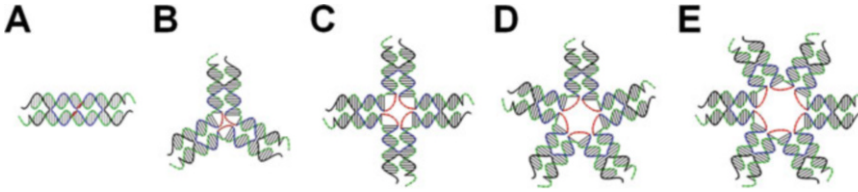


Fig. 1 DNA star motifs with n fold rotational symmetry. n equals (a) 2, (b) 3, (c) 4, (d) 5, and (e) 6. Each DNA star motif consists of one long repetitive central strand (colored *black* and *red*), n copies of identical medium strands (colored *green*), and n copies of identical short peripheral strands (colored *black*). n pieces of single-stranded loops (colored *red*) at the center of the motif hinge branched arms together

number larger than 1, which determines the symmetry), n copies of identical medium strands (**M**) and n copies of identical short peripheral strands (**S**). After the self-assembly, each branch consists of two antiparallel pseudo-continuous DNA duplexes that are linked together by strand crossovers. Meanwhile, there are n pieces of single-stranded loops (colored red) that hinge branched arms together at the center of star motif, the length of which determines the flexibility of the motif. In general, longer loops provide the DNA motifs with higher flexibility, which plays as a key factor in some cases (vide infra). At the termini of each branch of the motif, there are two self-complementary, single-stranded sticky ends. Association between the sticky-ends allows finite numbers of DNA tiles to assemble into 3D nanostructures.

1.3 Design Principles

To form well-defined DNA 3D nanostructures, a key step is to design the basic building blocks for aforementioned bionic self-assembly. In the past few years, a series of DNA star motifs have been employed to construct a large number of DNA nanocages with varied size, geometry, and chirality. Following these studies, design rules of star motif based 3D self-assembly have been gradually illustrated, such as the number of arms, flexibility of motifs, concentration of motifs, the length of each arm, and the sticky end sequence of each arm. Herein, we list each parameter separately and discuss their effects on DNA 3D assembly accordingly.

1.3.1 Number of Arms

Based on the symmetric design of sequence in a DNA star motif, the number of branches directly determines its rotational symmetry. As we know, the polyhedron's morphology is highly related to the symmetry of its component building blocks. The branch number of DNA star motif can be varied by introducing repetitive sequence in the central strands, resulting in 2-, 3-, 4-, 5-, and 6-point star motifs, etc. According to the geometry theory, a normal polyhedron exhibits a higher symmetry compared to the component building blocks (here are the DNA star motifs). Therefore, the symmetry of a star motif should be a subgroup of its assembled DNA polyhedral symmetry. Theoretically, in those building blocks, the star motif with

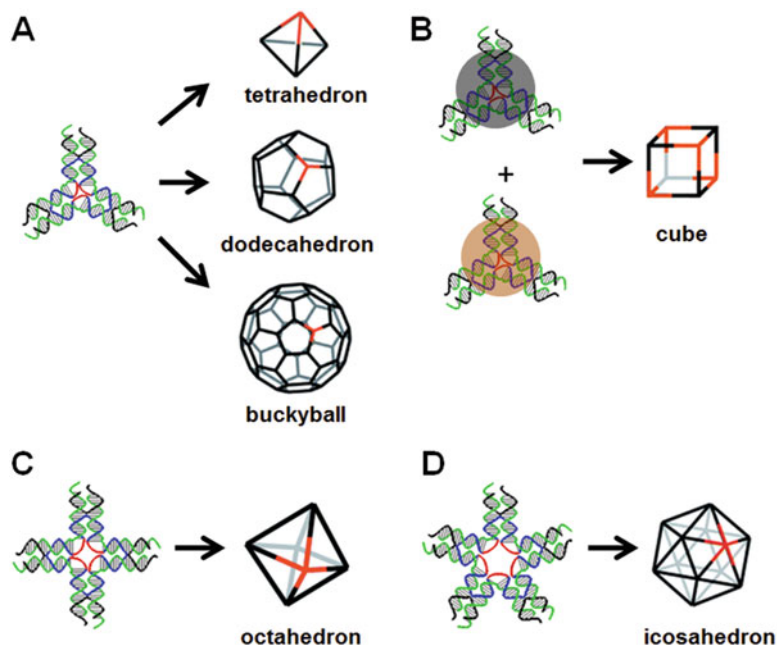


Fig. 2 Assembly of DNA polyhedra from DNA star motifs. (a) DNA tetrahedron, dodecahedron and buckyball assembled by 3-point star motifs. (b) DNA cube assembled by two different component 3-point star motifs. (c) DNA octahedron assembled by 4-point star motifs. (Reproduced in part with permission from Ref. [10]. Copyright 2010 John Wiley & Sons) (d) DNA icosahedron assembled by 5-point star-motifs. (Reproduced in part from Ref. [21] with permission from The Royal Society of Chemistry)

threefold rotational symmetry can assemble into the largest number of DNA polyhedra. In our experiments, 3-point star motifs have been revealed to form tetrahedron [7], dodecahedron [7], buckyball [7], cube [9], etc., as summarized in the Fig. 2. Comparatively, we further employed the 4-point star motifs to construct a well-defined octahedron [10]. When the branch number increases to 5, only icosahedron that contains fivefold rotational symmetry can be synthesized by a single type of DNA star motif [8]. If branch number further increases, simple normal polyhedron cannot be assembled with only one type of motif. Instead, large spherical DNA nanocages with the size of 200–300 nm in diameter can be obtained by the self-assembly [21]. Moreover, it is worthy to note that although 2-arm motif cannot directly assemble into any 3D objects by itself, it can be used to tune the size of the DNA polyhedron due to its linear feature. When incorporating 2-arm motifs in the 3D assembly, the strut length of a polyhedron can be extended, resulting in larger objects with the same geometry [19].

1.3.2 Flexibility of DNA Motifs

As we mentioned above, flexibility of the DNA motif is another key parameter to determine the morphology of 3D nanostructure. When a discrete 3D polyhedron forms, it requires each arm of the

star motif bends off from its original plane. Thus, balancing the flexibility and rigidity of the motif is crucial for the formation of desired nanocages. Compared to the motifs previously used for 2D array self-assembly, the motifs for the self-assembly of DNA nanocages usually contain longer single-stranded loops at the central long strand. The star motif could be imagined as multiple rigid sticks hinged by soft ropes. Flexibility of the motif can be easily tuned by changing the loop length. The longer the free loop is, the more flexible the motif would be. For DNA polyhedron with small size, such as tetrahedron, cube, prism, octahedron, and icosahedron, it requires each motif bending in large extent from their planar configuration. Therefore, the loop length is usually designed to be 5 bases long. When a larger polyhedron or nanocage is synthesized, such as dodecahedron, buckyball, and irregular cages, the bending of each motif will be in less extent. Therefore, three or four bases long free loops are often designed in the component motifs [21].

Moreover, the central free loop not only tunes the flexibility of the entire building block, but also the length of each segment can be varied in an individual motif, resulting in asymmetric DNA star motifs. This can be applied to control the chirality of the assembled DNA 3D nanocages. For instance, we once designed a series of asymmetric 3-point star motifs by changing their free loop length and arrangement [16]. As shown in Fig. 3, different lengths of the single-stranded loops (color red) at the center of the motif provide varied flexibility to each arm, resulting in the synthesis of pairs of twisted and chiral DNA triangular prisms. Notably, the twisted orientation and angle can also be tuned by changing the design of asymmetric motif.

In a certain condition, very long free loops can be introduced in the motif, which provides the motif with extremely high flexibility. As such, the arms of each motif can fully bend from its original plane, enabling two motifs to associate together through their sticky ends and form a closed structure. Instead of a 3D polyhedron, discrete rods like DNA nanotube were observed [22].

1.3.3 Concentration of DNA Motifs

It is worthy to note that the DNA self-assembly is an inter-unit process. When component star motifs associate with each other under native condition, the flexibility of the assemblies quickly builds up, resulting in closed DNA 3D nanostructures. Therefore, the size and geometry of the closed structures is concentration-dependent and it would be possible to control the size of polyhedra by controlling the motif concentration. Generally, at sufficiently low DNA concentration, the formation of smaller DNA polyhedra could be expected. On the contrary, high concentration of motif usually leads to larger structures. For instance, to form small DNA polyhedra, such as tetrahedron, octahedron and icosahedron, concentration of the component motif is usually less than 100 nM. Even with more rigid DNA motif, the concentration effect is obvious. For instance,

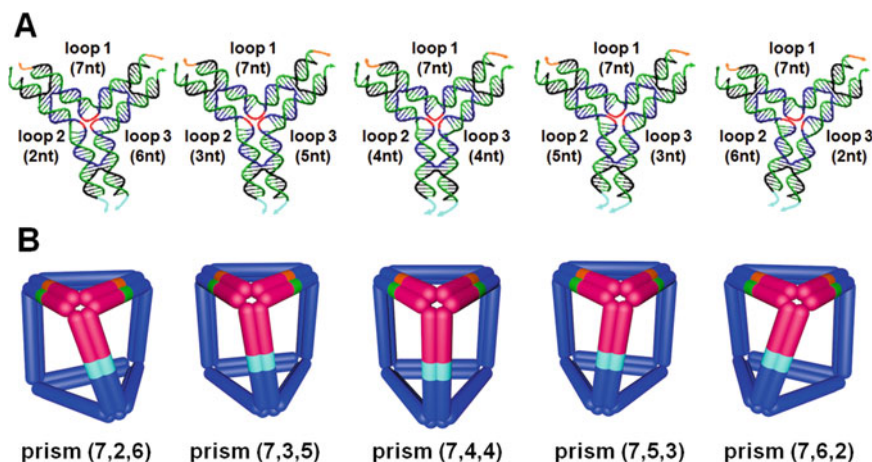


Fig. 3 Self-assembly of chiral DNA triangular prisms. (*Top panel*) Structures of asymmetric 3-point star motifs. The single-stranded loops at the center are colored *red* and can have different lengths. The complementarities of the sticky ends are coded by colors. (*Bottom panel*) Schemes of the resulting chiral triangular prisms. In the prism, one component motif is highlighted. The motifs and their resulting prisms are designated by the loop lengths. (Reproduced in part with permission from Ref. [16]. Copyright 2014 John Wiley & Sons)

the 3-point star motifs with three base long loops readily assemble into dodecahedron at a concentration of 50 nM. However, at a high DNA concentration (500 nM), the same star motifs assemble into a buckyball. Further, for any type of DNA star motif, large irregular nanocages are usually obtained when the motif concentration reaches micromolar scale [21].

1.3.4 Length of Each Arm

In general, the branch length of the motif directly determines the size of DNA 3D polyhedra. For the star motifs, the arms are usually designed to be two turn helices in length. After sticky end association, two arms in the neighbor motifs connect with each other and form a polyhedron's strut with a total length of four turn helices. As such, two neighbored motifs face to the same side and allow the curvature accumulation to form closed 3D structures. To synthesize 3D nanostructures with different size, larger structures can be assembled by either elongating the branch length of component motif or incorporating 2-point star motif during the assembly as we mentioned above [19]. It is well-known that DNA duplex is a double helix structure, which means the structural features repeat after each turn. Instead of integer number of helical turns in the strut, when two motifs are separated by odd number of half helical turns, their configurations are opposite due to the helical nature of DNA duplex. Based on this consideration, a 3-point star motif with a length of 2.25 turns could be designed. After the self-assembly, the odd half turn (4.5 turn) duplex led two adjacent tiles to face oppositely along their original planes. When folded into a closed 3D structure, half of tiles faced inward and the other half

faced outward, resulting in a DNA cube [9]. Therefore, it is believed that exploiting the helical nature of the DNA double helix structure allows us to synthesize more complicated DNA 3D nanostructures.

1.3.5 Sticky End Sequence of Each Arm

In most DNA star motifs mentioned above, the sticky ends on each branch are identical. To further increase the diversity and complexity of assembled DNA nanocages, various sticky ends combinations can be designed in an individual star motif. Also, DNA motifs with different symmetries and sticky ends can cooperate to direct the self-assembly. Figure 4 shows an example of this design principle, in which two different types of DNA motifs are employed: directing motifs (D-motifs) and assembly motifs (A-motifs) [18]. D-motifs are designed to direct the assembly behavior of A-motifs and cannot associate with themselves. Each A-motif contains two sets of sticky ends: one (a and a') is self-complementary to assemble A-motifs into larger structures; the other (b and b') is complementary to the sticky ends of D-motifs to allow A-motifs to be directed by D-motifs. The loops with five bases are introduced in the central strand of both motifs to offer sufficient flexibility. Without D-motifs, A-motifs self-associate into a mixture of homooligomeric complexes with different sizes. With the direction of D-motif, the interaction of A-motifs and D-motifs leads to a certain complex. A wide range of nanocages including bipyramids and the Kleetopes of polyhedra can be assembled by this strategy.

2 Materials

2.1 Purification of DNA Single Strand

1. Denaturing gel electrophoresis buffer (1× TBE buffer): 89 mM Tris base, 2 mM EDTA (disodium salt, dihydrate), and 89 mM boric acid; pH 8.0.
2. 20% Denaturing gel: Add 100 mL 10× TBE buffer and 500 mL 40% acrylamide and bis-acrylamide solution (19:1) to a 1-L glass beaker. Weigh and transfer 500,000 g urea to the glass beaker. Add water to a volume of 1 L to dissolve the chemical reagents.
3. 0% Denaturing gel: Add 100 mL 10× TBE buffer to a 1-L glass beaker. Weigh and transfer 500,000 g urea to the glass beaker. Add water to a volume of 1 L to dissolve the chemical reagents.
4. Denaturing gel with a concentration between 0 and 20%: Mix the 0% denaturing gel and 20% denaturing gel with a certain ratio.
5. Denaturing loading buffer: 0.3% bromophenol blue and 0.3% xylene cyanol in formamide. Weigh 0.300 g bromophenol blue

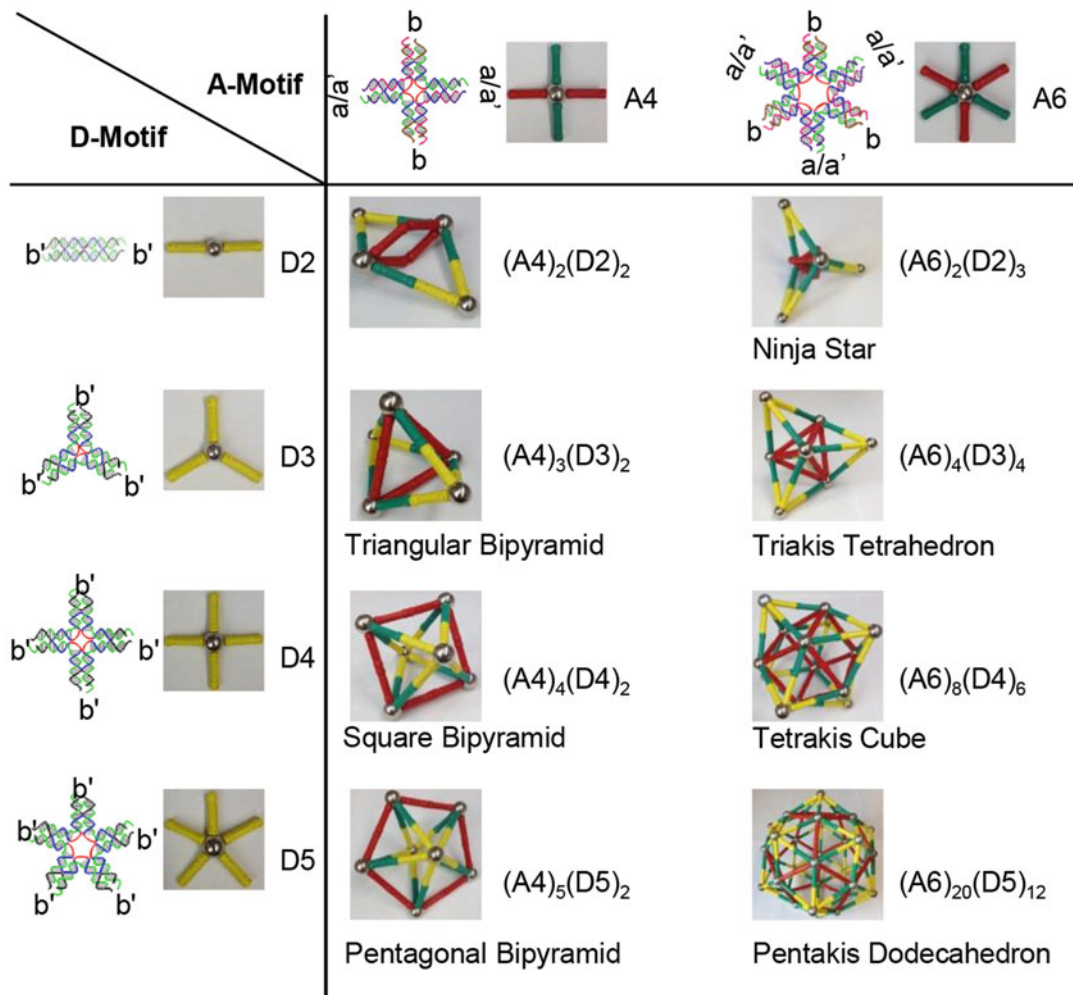


Fig. 4 Self-assembly of DNA nanocages through different combinations of sticky ends. A chart of the component motifs and the resulting DNA cages. (Reproduced in part with permission from Ref. [18]. Copyright 2014 John Wiley & Sons)

and 0.300 g xylene cyanol, and transfer both dyes to a 100-mL glass beaker. Add 100 mL formamide to the beaker to dissolve the dyes.

6. Elution buffer: 500 mM ammonium acetate, 10 mM magnesium acetate tetrahydrate, and 2 mM EDTA (disodium salt, dihydrate).

2.2 Assembly of DNA Nanocages and Native Gel Electrophoresis

1. Assembly buffer and native gel electrophoresis buffer (1× TAE/Mg²⁺ buffer): 40 mM Tris base, 2 mM EDTA (disodium salt, dihydrate), 20 mM acetic acid, and 12.5 mM magnesium acetate tetrahydrate; pH 8.0. Dilute 10× TAE/Mg²⁺ buffer with deionized water by ten times to make assembly buffer and native gel electrophoresis buffer.

2. Native polyacrylamide gel: Add 2 mL 10× TAE/Mg²⁺ buffer and certain volume of 40% acrylamide and bis-acrylamide solution (19:1) to a 50-mL glass beaker. Add the deionized water to a volume of 20 mL. Add 75 μL 10% ammonium persulfate and 7.5 μL *N,N,N',N'*-tetramethylethane-1,2-diamine to the beaker immediately before solidifying the gel.
3. Native agarose gel: Dissolve certain amount of agarose in 100 mL 1× TAE/Mg²⁺ buffer in a 250-mL volumetric flask. Heat the agarose solution till the solution boils and the agarose dissolves.
4. Native loading dye: 0.3% bromophenol blue and 0.3% xylene cyanol in 50% glycerol solution. Weigh 0.030 g bromophenol blue and 0.030 g xylene cyanol to a 10-mL tube. Add 5 mL deionized water and 5 mL glycerol to the tube to mix and dissolve the dyes.
5. Stains-all solution: Weigh and transfer 0.1 g stains-all to a 1-L glass bottle covered by the aluminum foil. Add 450 mL formamide and 550 mL deionized water into the beaker to dissolve the stains-all (*see Note 1*).

2.3 Characterization by Atomic Force Microscopy (AFM)

1. AFM probe NSC15-AIBS (MikroMasch) is used to image the sample in the air in the Multimode AFM with Nanoscope IIIa controller (Veeco).
2. AFM probe SNL-10 (Bruker) is used to image the sample in the fluid in the Multimode AFM with Nanoscope IIIa controller (Veeco).
3. SCANASYST-AIR (Bruker) is used to image the sample in the air in the Multimode 8 AFM (Bruker).

3 Methods

3.1 Purification of DNA Single Strand

DNA single strands are synthesized by Integrated DNA Technologies. Crude DNA single strands are subjected to the polyacrylamide gel electrophoresis (PAGE) purification process. The purification process includes denaturing PAGE purification, elution, butanol extraction, ethanol precipitation, and filtration.

3.1.1 Denaturing PAGE Purification

1. Prepare denaturing polyacrylamide gel. Add 75 μL 10% ammonium persulfate and 7.5 μL *N,N,N',N'*-tetramethylethane-1,2-diamine to a 20 mL denaturing gel solution immediately before solidifying the gel.
2. Mix DNA single strand solution and denaturing loading buffer with a volume ratio of 1 to 2. Heat the DNA solution at 95 °C for 5 min to denature the DNA strands. Load the DNA solution into the wells using a syringe.

3. The gel runs on a cooled vertical electrophoresis unit (Hoefer, SE600) (600 V, constant voltage) in $1\times$ TBE buffer at 55 °C.
4. After the gel electrophoresis, stain the gel in 0.5 $\mu\text{g}/\text{mL}$ ethidium bromide solution at 4 °C for 30 min (*see Note 2*).
5. Cut the target bands using a razor blade under the UV illumination.

3.1.2 Elution of DNA Strands

1. Chop the target bands into small pieces and transfer them to the elution buffer in a 1.5-mL microcentrifuge tube.
2. Shake the gel pieces at room temperature for 12 h to elute the DNA strands.
3. Transfer the supernatant of four 1.5-mL microcentrifuge tubes to a 15-mL centrifuge tube. Rinse the gel pieces with elution buffer to recover the residual DNA and combine with the supernatant.

3.1.3 Butanol Extraction

1. Add equal volume of 2-butanol to the eluate, mix the solution, and centrifuge the solution for 1 min to separate two phases.
2. Remove the upper layer of solution, and repeat the butanol extraction till the final volume is $1/3$ of the original volume.

3.1.4 Ethanol Precipitation

1. Transfer 500 μL of concentrated eluate to a 1.5-mL microcentrifuge tube. Add 1 mL of ethanol into the tube and mix them.
2. Incubate the tube in the dry ice for 90 min.
3. Centrifuge the tube with a speed of $16,000\times g$ in a microcentrifuge at 4 °C for 30 min to precipitate the DNA.
4. Remove the supernatant, add 1 mL cold 70% ethanol solution to the tube, and spin the tube with a speed of $16,000\times g$ in a microcentrifuge at 4 °C for 10 min to rinse the DNA pellet. Repeat this rinsing step one more time (*see Note 3*).
5. Dry the DNA solution and dissolve the DNA in the deionized water.

3.1.5 Filtration and Quantification of DNA Single Strands

1. Filter the DNA solution by centrifuge tube filter with 0.22 μm pore membrane to remove small pieces of gel.
2. Quantify the DNA using UV-Visible spectrophotometer at 260 nm.

3.2 Preparation of Circular, Long DNA Central Strands by DNA Kinase and Ligation

DNA kination and ligation are used to prepare central DNA strands for 4-, 5-, and 6-point star motifs (*see Note 4*). Phenol extraction, ethanol precipitation, and PAGE purification are used to purify the ligated central DNA strands. The protocol of ethanol precipitation and PAGE purification are same as that in the Subheading 3.1.

3.2.1 DNA Kination

1. Add 6 nmol purified DNA component strands and 100 μL 10 \times T4 DNA ligase buffer to a 1.5-mL microcentrifuge tube (*see Note 5*). Add the deionized water to a volume of 1000 μL and mix the solution (*see Note 6*).
2. Add 10 μL T4 polyacrylamide kinase into the tube. Use the pipette to gently mix the solution.
3. Incubate the solution at 37 $^{\circ}\text{C}$ for 2 h.
4. Incubate the solution at 95 $^{\circ}\text{C}$ for 5 min to deactivate the kinase.

3.2.2 DNA Ligation

1. Add DNA linker strands and 10 \times T4 DNA ligase buffer to make the final solution to be 1 \times T4 DNA ligase buffer.
2. Anneal the solution according to the following protocol: 95 $^{\circ}\text{C}$ (5 min), 65 $^{\circ}\text{C}$ (30 min), 50 $^{\circ}\text{C}$ (30 min), 37 $^{\circ}\text{C}$ (30 min), and 23 $^{\circ}\text{C}$ (30 min).
3. Add 10 μL T4 DNA ligase and incubate the solution at room temperature (~ 23 $^{\circ}\text{C}$) for 24 h.

3.2.3 Phenol Extraction

1. Add an equal volume of saturated phenol to the DNA solution, vortex the solution for 20 s, and centrifuge the solution at room temperature with a speed of 2000 $\times g$ for 1 min.
2. Transfer the top aqueous phase to a new tube. Add a half volume of saturate phenol and half volume of chloroform to the DNA solution. Vortex the solution for 20 s, and centrifuge the solution at room temperature with a speed of 2000 $\times g$ for 1 min.
3. Transfer the top aqueous phase to a new tube again. Add equal volume of chloroform to the DNA solution. Vortex the solution for 20 s, and centrifuge the solution at room temperature with a speed of 2000 $\times g$ for 1 min.
4. Transfer the top aqueous phase to a new tube. Proceed to the ethanol precipitation and PAGE purification.

3.3 Assembly of DNA Nanocages

1. DNA component strands are combined according to the designated molecular ratio and concentration in 1 \times TAE/ Mg^{2+} buffer in a 0.65-mL microcentrifuge tube.
2. Add 1.9 L water to a 2-L glass beaker and heat up the water till boiling.
3. Insert and immobilize the tubes in a microcentrifuge tube mini floating rack. Float the rack on the top of the boiling water.
4. Cover the beaker with aluminum foil, and transfer the beaker to a Styrofoam box. Put the box at room temperature (~ 23 $^{\circ}\text{C}$). The temperature of the DNA solution along with the water in the beaker cools from 95 $^{\circ}\text{C}$ to room temperature in 2 days.

3.4 Characterization by Native Gel Electrophoresis

1. Polyacrylamide and agarose gels are prepared in $1\times$ TAE/ Mg^{2+} buffer. Cool the gel and the buffer at $4\text{ }^{\circ}\text{C}$ before use.
2. Add 10% (v/v) native loading dye to the samples. Load $1\text{ }\mu\text{g}$ of sample in each lane using a syringe.
3. The polyacrylamide gel runs on a cooled vertical electrophoresis unit (Hoefer, SE600) (250 V, constant voltage) in $1\times$ TAE/ Mg^{2+} buffer at $4\text{ }^{\circ}\text{C}$. The agarose gel runs on a mini-horizontal unit of electrophoresis systems (FisherBiotech, FB-2B-710) (65 V, constant voltage) in $1\times$ TAE/ Mg^{2+} buffer at $4\text{ }^{\circ}\text{C}$ (*see Note 7*).
4. After native polyacrylamide gel electrophoresis, stain the native polyacrylamide gel in a tray with stains-all solution for 30 min (*see Note 8*). Then the gel is transferred to a new tray with water and destained under the light illumination till the red color on the background of the gel disappears (*see Note 9*). Scan the gel with a common office HP scanner.
5. After native agarose gel electrophoresis, stain the gel in $0.5\text{ }\mu\text{g}/\text{mL}$ ethidium bromide solution at $4\text{ }^{\circ}\text{C}$ for 1 h. Destain the gel in $1\times$ TAE/ Mg^{2+} buffer at $4\text{ }^{\circ}\text{C}$ if necessary. Photograph the gel under UV illumination with a Nikon camera (Coolpix L22).

3.5 Characterization by AFM

1. To prepare the DNA sample to be imaged in the air, $1.5\text{ }\mu\text{L}$ of annealed DNA solution is deposited on a freshly cleaved mica surface, and incubated for 1 min in a humid chamber to allow DNA to absorb on the substrate (*see Note 10*). Add $50\text{ }\mu\text{L}$ of 2 mM magnesium acetate solution on the top of the DNA sample, and immediately blow away the solution and dry the substrate by the condensed air (*see Note 11*). Proceed to the AFM imaging.
2. To prepare the DNA sample to be imaged in the fluid, $1.5\text{ }\mu\text{L}$ of annealed DNA solution is deposited on a freshly cleaved mica surface, and incubated for 1 min in a humid chamber to allow DNA to absorb on the substrate. Add $50\text{ }\mu\text{L}$ of $1\times$ TAE/ Mg^{2+} buffer on the top of the DNA sample (*see Note 12*). Proceed to the AFM imaging.
3. Perform the AFM imaging in a Multimode AFM with Nanoscope IIIa controller (Veeco) or a Multimode 8 AFM (Bruker). The tip-surface interaction is minimized by optimizing the scan set-point to the highest possible value.

3.6 Characterization by Cryogenic Electron Microscopy (cryoEM) and Single Particle Reconstruction

1. Concentrate assembled DNA nanostructures by 0.5-mL centrifugal filter with a molecular cutting off membrane of 50 kDa or 100 kDa for cryoEM sample preparation. Rinse the centrifugal filter by the deionized water for three times. Add assembled DNA solution into the centrifugal filter and concentrate with a speed of at most 400 g at room temperature

(~23 °C) (*see Note 13*). The final concentration of DNA nanocages is around 1 μM .

2. Glow discharge the TEM grid with 400 mesh holey carbon film (Quantifoil). Put the TEM grid on a glass slide and place the glass slide in the chamber of Emitech K950. Turn on the turbo pump and wait until the turbo pump speed reaches 100% and the vacuum reads 0.2 mbar. Glow discharge the TEM grid for 15 s. Vent the chamber and TEM grid is ready to be used for freezing the sample.
3. Freeze the sample by Vitrobot. Open the nitrogen tank which is used to provide the pressure for the Vitrobot. Fill the reservoir with the water to maintain the humidity. Install two pieces of central punched filter paper as blotting pads in the chamber. Set the temperature as 22 °C, humidity as 100%, blot number as 1, and blot time as 1.5 s (*see Note 14*). Fill the outer chamber of the coolant container with liquid nitrogen until the temperature is stable. Then fill the inside chamber with liquid ethane till reaching a stable temperature. Load a TEM grid onto a tweezer and place the tweezer onto the notched end of the rod. Wait until the tweezer and the coolant container move up to the right position. Add 3 μL of concentrated sample on the TEM grid, start the blotting process and plunge the grid into the liquid ethane. Transfer the grid from the liquid ethane to a grid box in the liquid nitrogen quickly. Store the grid in a liquid nitrogen dewar.
4. Collect the cryoEM images using a Gatan 4K \times 4K CCD camera or by films on a FEI CM200 TEM with accelerating voltage of 200 kV under low-dose condition to minimize radiation damages to the samples. To enhance the image contrast, under-focus in the range of 2–4 μm is used to record the images. The films are developed in a dark room and scanned on a Nikon Super CoolScan 9000.
5. Reconstruct the three-dimensional (3D) DNA nanostructures using “EMAN2” software [23]. For each structure, the experimentally observed, raw particles are first classified into many classes based on reference-free classification method to build class averages. The best 10-15 class averages are selected to build the initial models. Then all the corresponding particles are used for the refinement. The refinement is carried out with a 2° angle interval. A projection matching algorithm is applied for the determination of the center and orientation of raw particles in the iterative refinements. The corresponding symmetry is imposed during the initial model building and reconstruction. The resolution of the density map is determined by using Fourier shell correlation (0.5 threshold criterion) of two 3D maps separately built from even and odd halves of the datasets. The final 3D map is visualized using “UCSF Chimera” software [24].

3.7 Dynamic Light Scattering (DLS) Measurement

1. Before the measurement, samples should be filtered with a 0.22 μm or larger pore size membrane (*see Note 15*).
2. DNA nanocage should have concentration above 100 nM for the DLS measurement (*see Note 16*).
3. Wipe outside of cuvette with lens paper if needed.
4. Pipette 100 μL DNA nanocage-containing sample into the cuvette which is specifically designed for the DLS measurement (10 mm light path facing the incident beam, 2 mm light path facing the detector). Gently tap the cuvette on the bench to remove any bubbles that may appear around the wall of the cuvette. Insert the cuvette in the sample holder on a Malvern Zetasizer Nano-ZS (Malvern Instruments, UK) with a laser wavelength of 633 nm.
5. Setup instrument parameters for DLS analysis. Usually choose room temperature 25 $^{\circ}\text{C}$ during the measurement, use water as solvent, set temperature equilibration time to at least 2 min prior to starting measurements. This allows the temperature control with an accuracy and precision of 0.3 $^{\circ}\text{C}$ or better.
6. Perform 3–10 independent measurements per sample per temperature setting to establish measurement repeatability.

4 Notes

1. The stains-all solution should avoid the light exposure.
2. Lower temperature minimized the migration of DNA single strands.
3. At the end of ethanol precipitation, if there are large amount of white precipitates at the bottom of the tube, repeat the whole process of ethanol precipitation to further remove the salts.
4. DNA central strand without a nick leads to a higher assembly yield of DNA nanocages, especially for 4-, 5-, and 6-point star motifs. DNA single strands with a length of 100 nucleotides or more have to be ligated by short DNA component strands.
5. 1 \times T4 DNA ligase buffer contains 1 mM ATP.
6. The concentration of DNA component strands is important to the yield of DNA ligation. Too high concentration of DNA component strands leads to longer linear structures.
7. Stir the buffer of polyacrylamide gel to make sure that the temperature of the buffer is homogeneous. Change the buffer of agarose gel every 2 h to make sure that the buffer is cool enough and the pH does not change significantly.
8. The tray is covered by the aluminum foil to avoid the light exposure. Shake the gel every 10 min to make sure the whole gel is evenly stained.

9. Shake the gel every 10 min to make sure the whole gel is evenly destained.
10. To set up a humid chamber, put the substrate in a small petri dish covered by wet Kimwipes. The sample should not be dry.
11. Magnesium acetate solution is used to not only remove most salts but also keep the stability of the assembled structures. If there are too many salts left on the surface, magnesium acetate solution with a lower concentration or water can be used to remove the salts.
12. Nickel ions can be used to increase the affinity of small DNA nanostructures to the mica surface. Before depositing the sample on the mica surface, add 50 μL of 1 mM nickel chloride solution on a freshly cleaved mica surface, and immediately dry the surface by the condensed air. After the sample deposition, add 50 μL of $1\times$ TAE/ Mg^{2+} buffer with 1 mM nickel chloride on the top of the DNA sample.
13. Use temperature controlled centrifuge or change the centrifuge every 20 min to keep the samples at room temperature.
14. The humidity, number of blot, and blot time may vary for samples with different components. The combination of these parameters and the volume and chemical components of the sample determine the thickness of the ice.
15. The choice of pore size depends on the maximum dimension of the test particles. Usually the filter with a 0.22 μm is suitable for most nanocage samples.
16. If the starting concentration is lower than 100 nM, use a concentrator with a molecular cutting off membrane of 50 kDa or 100 kDa to concentrate the sample first.

References

1. Seeman NC (2010) Nanomaterials based on DNA. *Annu Rev Biochem* 79:65–87
2. Lin CX, Liu Y, Rinker S, Yan H (2006) DNA tile based self-assembly: building complex nanoarchitectures. *Chemphyschem* 7:1641–1647
3. Aldaye FA, Palmer AL, Sleiman HF (2008) Assembling materials with DNA as the guide. *Science* 321:1795–1799
4. Chen JH, Seeman NC (1991) Synthesis from DNA of a molecule with the connectivity of a cube. *Nature* 350:631–633
5. Zhang YW, Seeman NC (1994) Construction of a DNA-truncated octahedron. *J Am Chem Soc* 116:1661–1669
6. Goodman RP, Berry RM, Turberfield AJ (2004) The single-step synthesis of a DNA tetrahedron. *Chem Commun* 1372–1373
7. He Y, Ye T, Su M, Zhang C, Ribbe AE, Jiang W, Mao CD (2008) Hierarchical self-assembly of DNA into symmetric supramolecular polyhedra. *Nature* 452:198–201
8. Zhang C, Su M, He Y, Zhao X, Fang PA, Ribbe AE, Jiang W, Mao CD (2008) Conformational flexibility facilitates self-assembly of complex DNA nanostructures. *Proc Natl Acad Sci U S A* 105:10665–10669
9. Zhang C, Ko SH, Su M, Leng YJ, Ribbe AE, Jiang W, Mao CD (2009) Symmetry controls the face geometry of DNA polyhedra. *J Am Chem Soc* 131:1413–1415
10. He Y, Su M, P-a F, Zhang C, Ribbe AE, Jiang W, Mao C (2010) On the chirality of self-assembled DNA octahedra. *Angew Chem Int Ed* 49:748–751

11. Rothemund PWK (2006) Folding DNA to create nanoscale shapes and patterns. *Nature* 440:297–302
12. Shih WM, Quispe JD, Joyce GF (2004) A 1.7-kilobase single-stranded DNA that folds into a nanoscale octahedron. *Nature* 427:618–621
13. Andersen ES, Dong M, Nielsen MM, Jahn K, Subramani R, Mamdough W, Golas MM, Sander B, Stark H, Oliveira CLP, Pedersen JS, Birkedal V, Besenbacher F, Gothelf KV, Kjems J (2009) Self-assembly of a nanoscale DNA box with a controllable lid. *Nature* 459:73–76
14. Han DR, Pal S, Nangreave J, Deng ZT, Liu Y, Yan H (2011) DNA origami with complex curvatures in three-dimensional space. *Science* 332:342–346
15. Douglas SM, Dietz H, Liedl T, Hogberg B, Graf F, Shih WM (2009) Self-assembly of DNA into nanoscale three-dimensional shapes. *Nature* 459:414–418
16. Zhang C, Wu W, Li X, Tian C, Qian H, Wang G, Jiang W, Mao C (2012) Controlling the chirality of DNA nanocages. *Angew Chem Int Edit* 51:7999–8002
17. Li X, Zhang C, Hao CH, Tian C, Wang GS, Mao CD (2012) DNA polyhedra with T-linkage. *ACS Nano* 6:5138–5142
18. Tian C, Li X, Liu Z, Jiang W, Wang G, Mao C (2014) Directed self-assembly of DNA tiles into complex nanocages. *Angew Chem Int Edit* 53:8041–8044
19. Liu Z, Tian C, Yu J, Li Y, Jiang W, Mao C (2015) Self-assembly of responsive multilayered DNA nanocages. *J Am Chem Soc* 137:1730–1733
20. Li Y, Tian C, Liu Z, Jiang W, Mao C (2015) Structural transformation: assembly of an otherwise inaccessible DNA nanocage. *Angew Chem Int Edit* 54:5990–5993
21. Zhang C, He Y, Su M, Ko SH, Ye T, Leng Y, Sun X, Ribbe AE, Jiang W, Mao C (2009) DNA self-assembly: from 2D to 3D. *Faraday Discuss* 143:221–233
22. Qian H, Tian C, Yu J, Guo F, Zheng M-S, Jiang W, Dong Q-F, Mao C (2014) Self-assembly of DNA nanotubes with defined diameters and lengths. *Small* 10:855–858
23. Tang G, Peng L, Baldwin PR, Mann DS, Jiang W, Rees I, Ludtke SJ (2007) EMAN2: an extensible image processing suite for electron microscopy. *J Struct Biol* 157:38–46
24. Goddard TD, Huang CC, Ferrin TE (2007) Visualizing density maps with UCSF Chimera. *J Struct Biol* 157:281–287

Chapter 3

Design of Wireframe DNA Nanostructures—DNA Gridiron

Dongran Han

Abstract

Self-assembling nucleic acid molecules have shown merit as versatile materials for organizing and constructing nanoscale structures with both 2D and 3D geometries. This chapter focuses on strategies in designing DNA gridiron nanostructures based on four-arm junction. This design strategies aims at controlling DNA self-assembly with a higher degree of spatial precision by depicting arbitrary 3D geometries with their wireframe outlines using DNA helices (for edges) and four-arm junctions (for vertices).

Key words DNA gridiron, DNA nanotechnology, Self-assembly, Wireframes

1 Introduction

Self-assembling nucleic acid molecules can be used to construct 2D and 3D nanoscale structures from parallelly arranged DNA helices [1–5]. Meanwhile, Geometric shapes can be approximated in the form of wireframes. A few examples of such 3D expression are illustrated in Fig. 1. DNA Gridiron is a DNA nanostructure design strategy to construct complex wireframe architectures, which is one of the important challenges in nanotechnology [6]. In DNA gridiron design, a series of four-arm junctions are used as vertices within a network of double-helical DNA fragments. Linear segments of double stranded DNA are used to connect a series of DNA junction vertices to form designed wireframe structures. Deliberate distortion of the junctions from their most relaxed conformations ensures that a scaffold strand can traverse through individual vertices in multiple directions. DNA gridirons can be used to assemble two-dimensional arrays, multilayer structures, three-dimensional structures, and curved objects.

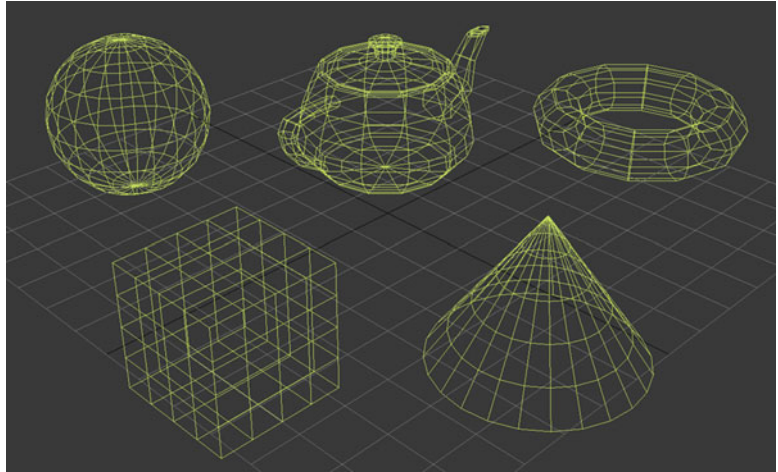


Fig. 1 Wireframe expression of 3D shapes: cube, cone, sphere, teapot, and torus

2 DNA Gridiron Structural Design

In the design of DNA gridiron, an unusual set of immobile Holliday junction analogs (4-arm junctions) is used as the basic structural unit of DNA origami nanostructures as joints to construct a variety of 2D and 3D “gridiron” structures in which the scaffold strand and corresponding double helices are not restricted to a 1D parallel, raster fill pattern. By programming the connection between individual joints with DNA segments of variable lengths, we can construct complex wireframe geometries.

Although intuitively one could imagine threading a single-stranded scaffold through a number of 4-arm junction units in both horizontal and vertical directions to create gridiron like patterns, the structural properties of traditional Holliday junction [7–9] impose certain challenges that require unconventional rearrangement of the junction unit conformation, as revealed by the design principles described below. In Fig. 2a, we compare a gridiron unit to a double crossover motif [10], where the DNA strands are abstracted to display only their polarity with the arrows pointing from 5' to 3'. In the gridiron unit, four 4-arm junctions are linked together to form a two-layer square frame in which the helices on opposite sides lie in the same plane. An anti-parallel arrangement between opposite sides of the square frame permits a single, central strand to traverse each of the helices.

In Fig. 2b, each of the four junctions is depicted in its relaxed conformation such that the helices form a right-handed twist with a 60° torsion angle. Deviation from a relaxed conformation is required of each junction to form the gridiron unit cell. First, the red strands in the horizontally oriented helices (both top and

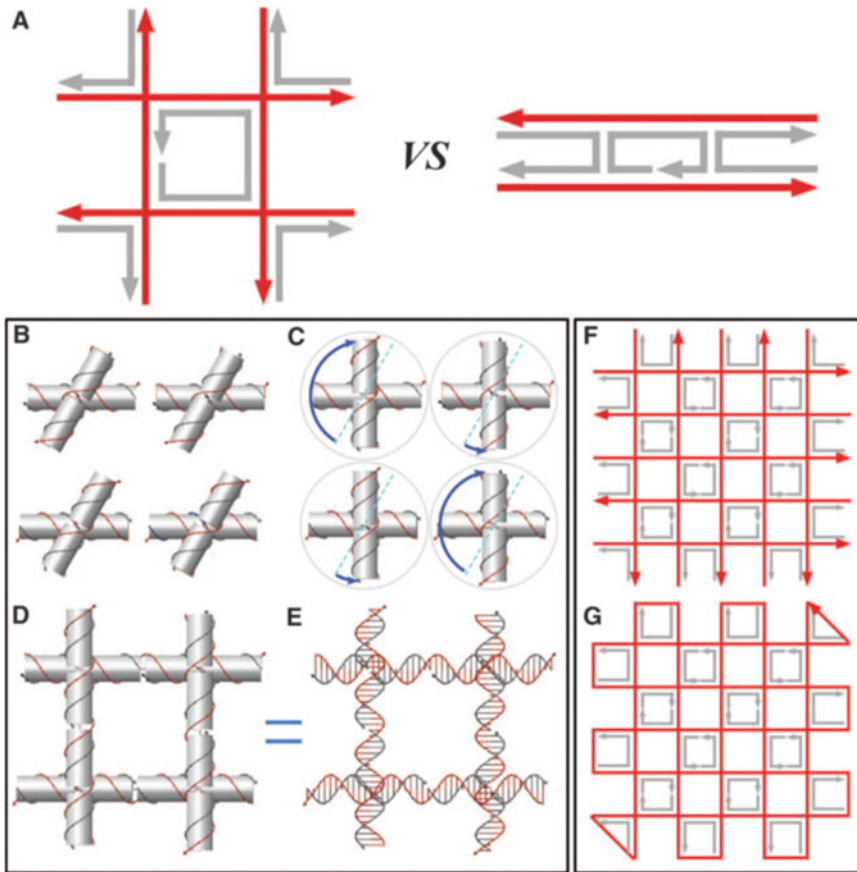


Fig. 2 (a) (Left) Geometry and strand polarity of a single gridiron unit formed from four four-arm junctions. (Right) Geometry and polarity of a double-crossover molecule motif used in conventional DNA origami structures. For both structures, the ssDNAs depicted in red are components of DNA double helices that serve as the scaffold strands. The ssDNA depicted in gray represents staple strands. (b) Models of four four-arm junction molecules in their relaxed conformation. The orientation of the upper two junctions differs from that of the lower two by a 180° in-plane rotation. Thus, the polarities of the continuous red strands in the upper and lower layers of the horizontally oriented helices are antiparallel to one another. (c) Models illustrating the deviation from a relaxed conformation required of the four individual junctions to form a gridiron unit. The blue arrows indicate that the top helix of the junctions in the upper-left and lower-right corners must be rotated $\sim 150^\circ$ clockwise, whereas in the upper-right and lower-left junctions they must be rotated $\sim 30^\circ$ counterclockwise. (d, e) Helical models illustrating a complete gridiron unit. (f, g) Schematics illustrating a typical scaffold-folding path for a 2D DNA gridiron pattern. Figure reproduced from ref. [6] with permission from AAAS

bottom panels) can be linked together to produce continuous strand without reversing the 5' to 3' polarity (Fig. 2b, c). Next, the vertically oriented helices need to be rotated in the plane about the junction points (Fig. 2c) to allow the formation of continuous 5' to 3' connections between the upper and lower junctions (Fig. 2d, e).

Connecting a number of gridiron units leads to the formation of a variety of 2D lattices (Fig. 2f, g). The red lines represent the DNA strands that are expected to retain an unperturbed helical

structure with continuous base stacking. Such continuous base stacking is important for maintaining overall structural rigidity. Meanwhile, the short strands (in gray) form the crossovers between helical domains and function as staples. A long scaffold strand is created by connecting the termini of the red strands with short ssDNA loops. In the most basic design, the scaffold begins at one corner, fills the first layer, changes direction at the opposite corner, and then fills the second layer to produce a structure in which the helices within the two layers are oriented perpendicularly with respect to each other. Finally, the scaffold returns to its initial position to form a closed loop (Fig. 2g).

The cavity size of gridiron structures can be tailored by altering the number of base pairs between the adjacent junction points. Gridiron structures with cavity sizes of 21, 42 and 63 bps are illustrated in Fig. 3a–c, and an example of such design with cavity size of 21 bps (Fig. 3) using software “Tiamat” is shown in Fig. 4. Note that DNA gridiron structures can also be created without the scaffold strand. Figure 3d shows a scaffold-less 2D gridiron design with 21 bps cavity size, and an example of this design using software “Tiamat” is shown in Fig. 5.

The flexibility of the joints makes it possible to control or reconfigure the conformation of the gridiron structure by exerting external forces on selected corners of a gridiron. A modified version of a 15×15 Gridiron structure with 21 bp cavities has approximately one quadrant of the gridiron unfolded and forms a randomly coiled 836 nt single stranded loop between the two “arms” of the tweezers (Fig. 6a), and an example of this design using software “Tiamat” [11] is shown in Fig. 7. Note that the ssDNA loop is long enough to allow the structure to adopt a relaxed conformation.

The ssDNA loop can be contracted and extended by introducing secondary or tertiary structure that generated enough force to control the angle. Sets of staple strands needed to be designed to either contract the ssDNA loop and fix an acute angle via the formation of a 2-helix bundle (Fig. 6b), or to extend the loop to secure a right (Fig. 6c) or obtuse angle (Fig. 6d) via the formation of a 3-helix bundle of specific length.

The gridiron design can be extended into the third dimension by three different strategies. The first involves stacking multiple layers of 2D gridiron lattices at selected connection points (Fig. 8a, b). The second relies on intertwining several gridiron planes in x - y - z direction (Fig. 8c). The third method is based on distorting a single layer of DNA gridiron into 3D structures by controlling their curvatures (Fig. 9). By using the first strategy, a three-layer hexagonal (Fig. 8d) and a four-layer rectangular gridiron (Fig. 8e) structures can be constructed. For all multilayer gridiron structures, the scaffold strand raster fills each layer, with an offset in the angle formed between the helices of adjacent layers. The three-layer

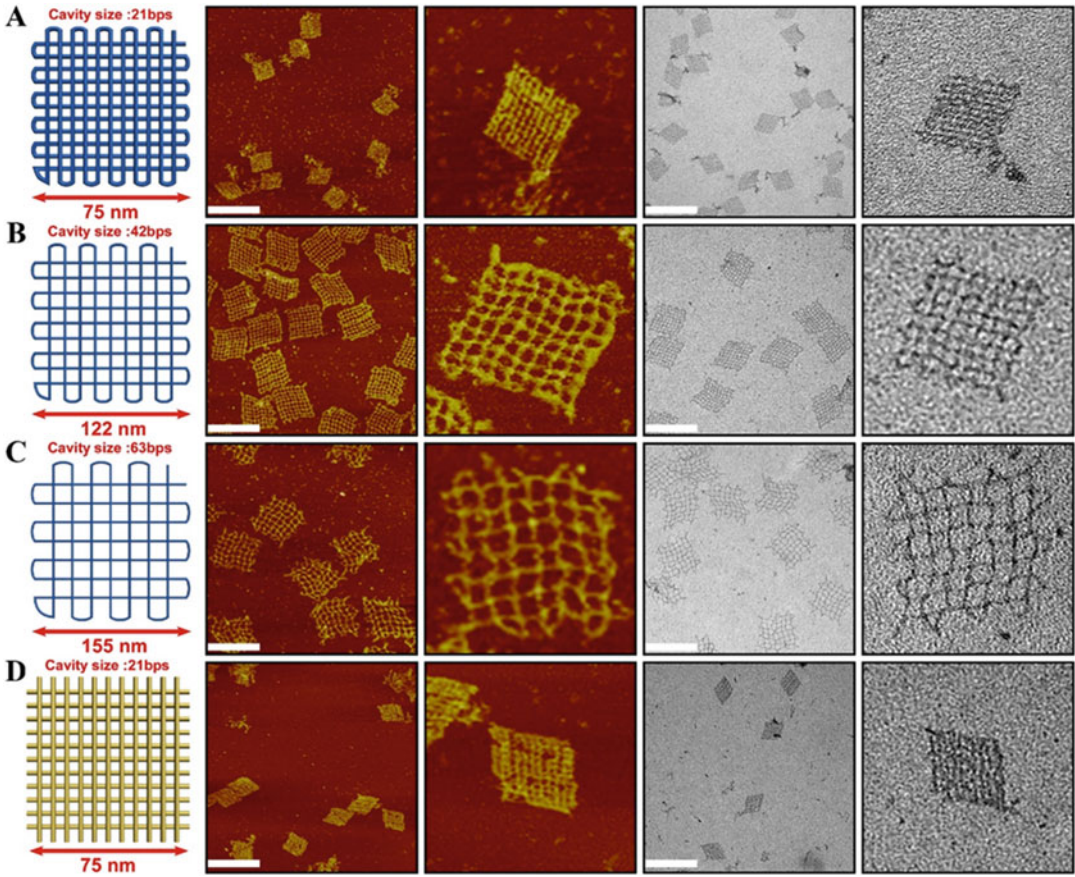


Fig. 3 (a–d) Schematics (first panel from *left*), AFM (second and third panels from *left*) and TEM (fourth and fifth panels from *left*) images of scaffolded 2D gridiron structures with 21 bps (a), 42 bps (b) and 63 bps (c) cavities and scaffold-less 2D gridiron structures with 21 bps cavities (d), respectively. All scale bars are 200 nm in length and all zoom in images are 200 nm \times 200 nm

hexagonal and four-layer rectangular structures maintained a 60° and 90° offset between layers, respectively.

Varying the location and distance between connection points will yield differently patterned multi-layer structures. In contrast to the angle flexibility present in the quasi-2D structures, here, the addition of a third layer fixes the angles at junction points. The only exception to this is for connections through the center of the same unit motif, as shown by the green dashed line (Fig. 8a). In a 3D model of an 8 by 8 by 8 three-layer hexagonal Gridiron structure (Fig. 8d), neighboring junctions in the top and bottom layers are 52 bps apart, and neighboring junctions in the middle layer (alternating connections to the top and bottom layers) are 26 bps apart. Because $X = Y = L$ (Fig. 8b), each junction should adopt a 60° torsion angle. A four-layer rectangular gridiron structure (Fig. 8e) can be broken down into two 6 by 5

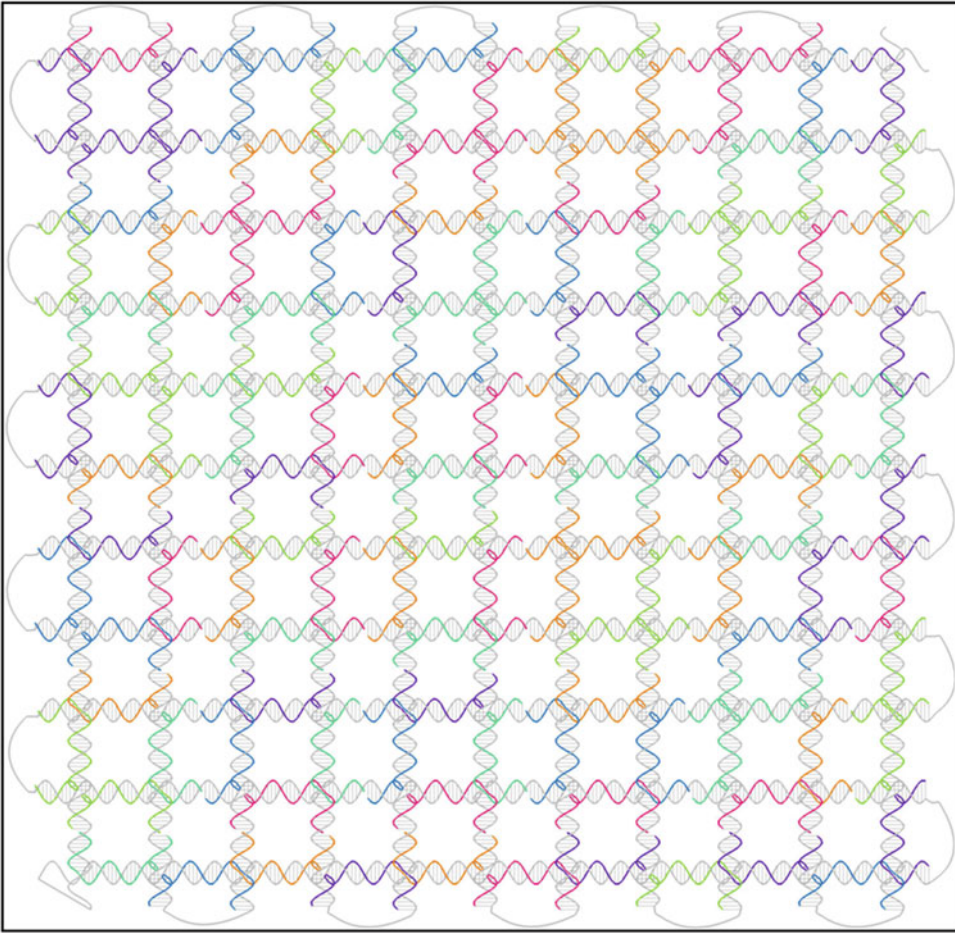


Fig. 4 Design pattern for 21 bps Gridiron structure. Scaffold strand was colored in *gray* and staple strands had different colors

double-layer gridirons (with 52 bp cavities) stacked on top of one another with a 26 bp offset in the connections between the first and third, and second and fourth layers.

The relationships of the lattice planes in gridiron structures are not restricted to stacked multilayer structures. 3D gridiron structures can also be assembled by integrating gridiron lattices with scaffold free elements. Figure 8f presents such a design in which a 9 by 9 gridiron plane (shown in blue) is intertwined with an 8 by 8 scaffold-free gridiron plane (shown in yellow). The complex, interwoven topology of this particular structure required combining scaffolded and scaffold-free components.

Gridiron designs can allow assembly of even more complex structures by inducing a desired curvature in the basic structural unit described in Fig. 2. Maintaining the distance between junctions in one direction while simultaneously shrinking or extending

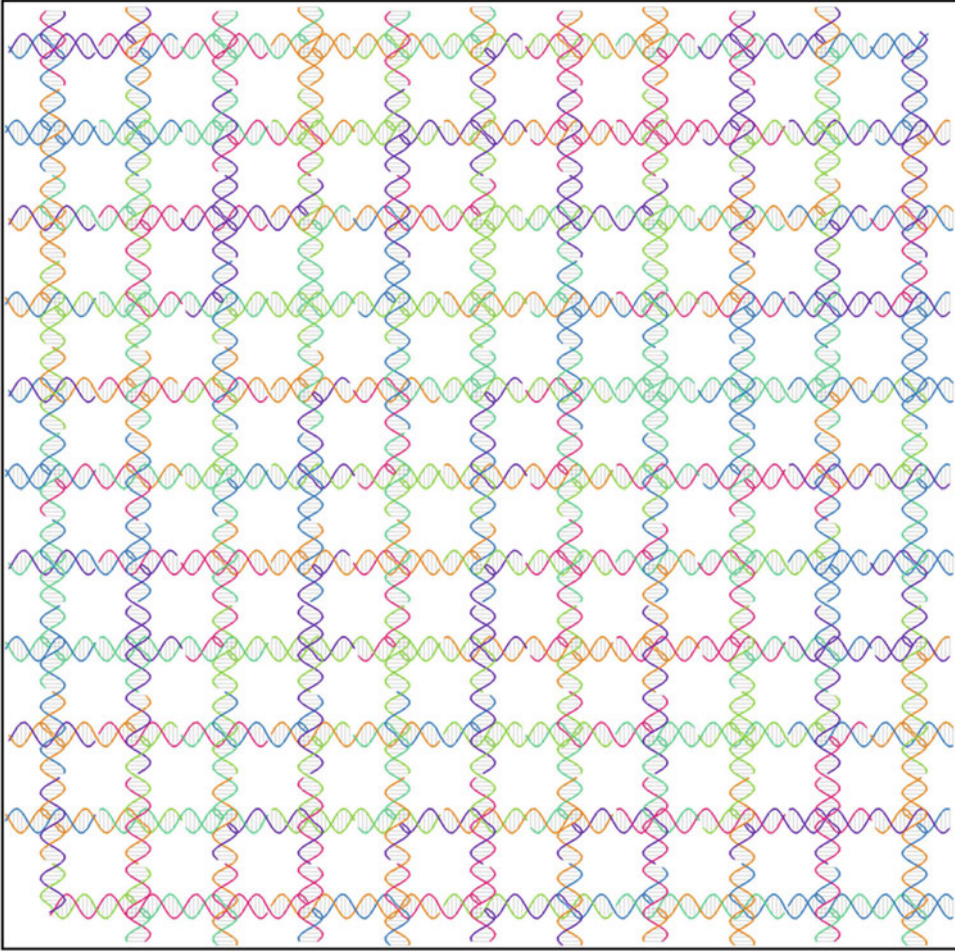


Fig. 5 Design pattern for Scaffold-less 21 bps Gridiron structure. There is no scaffold strand presented in this design

the distance in the other direction (by varying the number of bps) creates an isosceles trapezoid unit. The lengths of the parallel sides of the trapezoidal units can be progressively changed between layers and combined to generate curved gridiron structures such as an S-shaped structure (Fig. 9a), and an example of this design using software “Tiamat” is shown in Fig. 10. One layer is composed of nine concentric, evenly spaced curved helices and the second layer contains 13 linear, non-parallel helices. The relationship between adjacent linear helices (the angles formed by their theoretical intersection) between adjacent linear helices can be varied. 3D gridiron structures that contain curvature, such as the sphere, is shown in Fig. 9b. The helices in concentric ring and radial spoke layers are “stretched” in the center and “shrunk” at the edges forming a latitudinal and longitudinal framework, respectively. This is realized by progressively adjusting the distance between junctions in

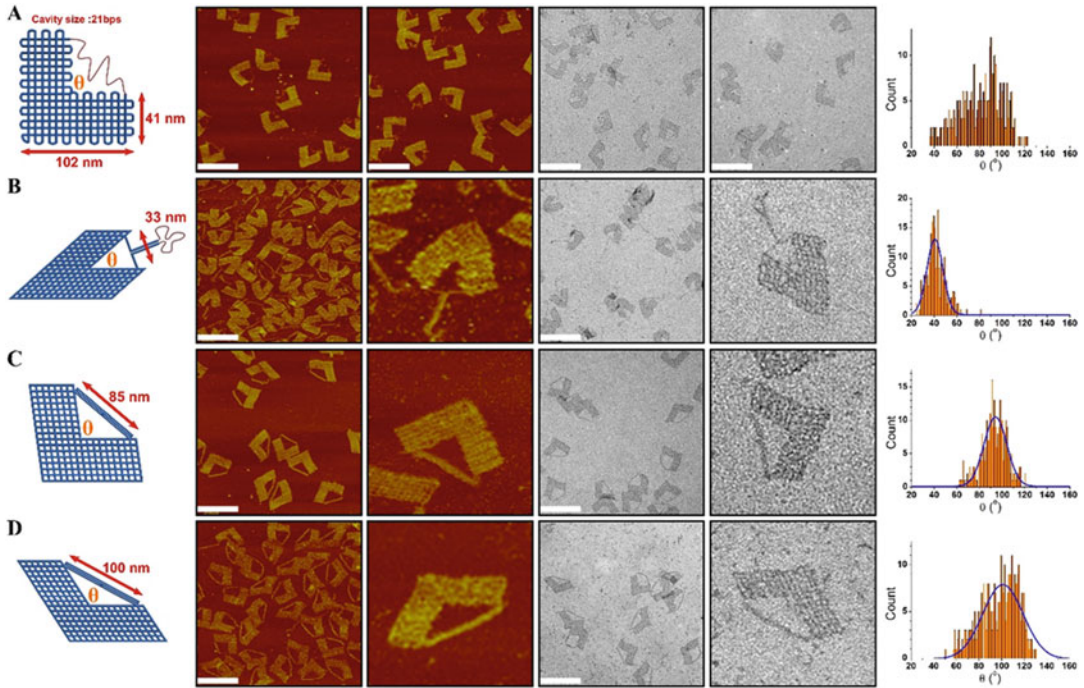


Fig. 6 Angle control of Gridiron tweezers. (a–d) Schematics (first panel from *left*), AFM (second and third panels from *left*) and TEM (fourth and fifth panels from *left*) images, and histogram analysis (sixth panel from *left*) of the angle distributions, respectively. All scale bars are 200 nm in length and all zoom in images are 200 nm \times 200 nm

latitudinal directions. Additional modifications to the basic structural motif can be used to produce other complex structures. In the screw structure (Fig. 9c), the polarity of the DNA strands in the square unit motif differs from what is illustrated in Fig. 2b (where adjacent scaffold helices have an anti-parallel polarity in one direction and the same polarity in the other direction). Here, the scaffold strand is arranged in an anti-parallel configuration to form a wireframe cylinder structure (11 helices are arranged axially), and subsequently wraps around the cylinder (analogous to a left-handed screw) until the two ends meet. The distance between adjacent axial helices is 21 bps and the inter-thread distance is 42 bps.

The design principles of creating gridiron units allow scaffold strands to travel in multiple directions, which represent an important departure from certain aspects of the previous DNA origami methods. Traditional Holliday junctions do not naturally adopt conformations that would allow them to be connected in such a way, and it was surprising to discover that these motifs could (within a larger network of crossovers) endure a 150° rotation of one of the arms while simultaneously maintaining their integrity.

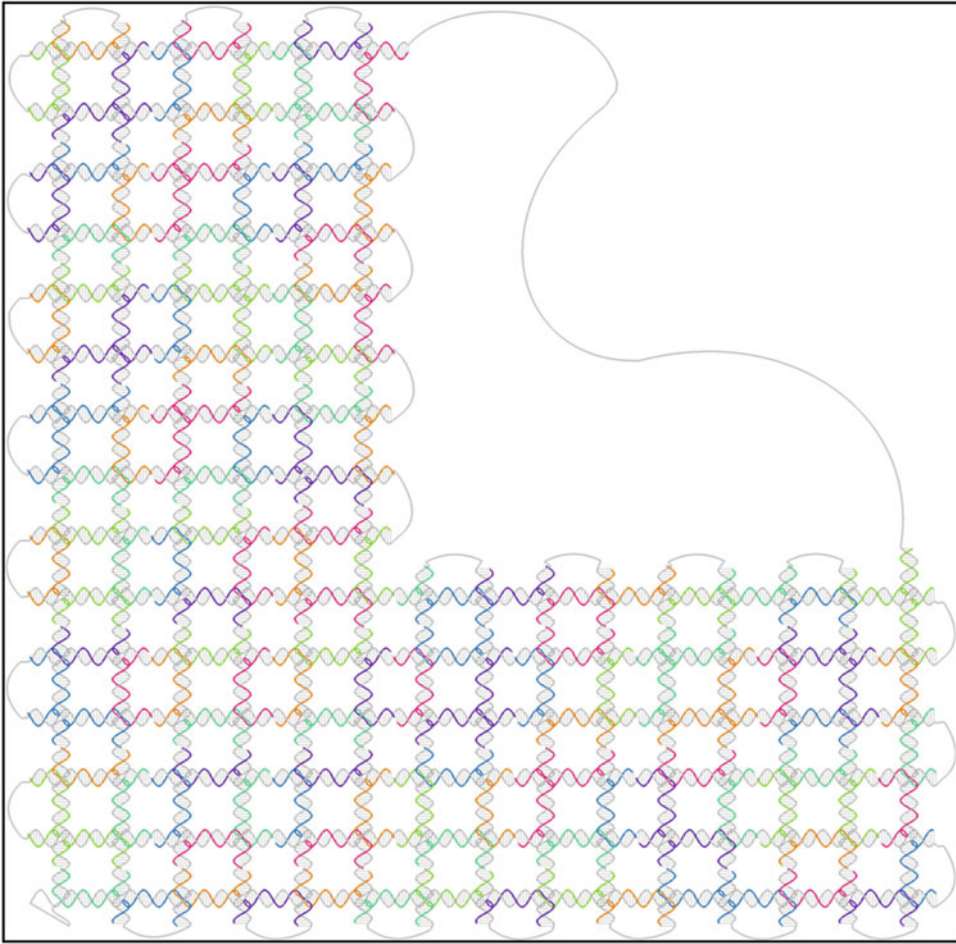


Fig. 7 Design pattern for Gridiron Tweezers structure. Scaffold strand was colored in *gray* and staple strands had different colors. The long single stranded loop left at the upper right corner was used to link the two arms of the tweezers

Indeed, the flexible and dynamic behavior of these motifs may have excluded these types of junction conformations for consideration in scaffolded structures. The ability to engineer DNA gridirons that are analogous to vector-based objects, where a series of points with defined positions in 3D space are connected by lines, is an important milestone in the development of synthetic nucleic acid structures. In particular, this opens up new opportunities to implement the design of complex wireframe structures that are amenable to dynamic controls. A future challenge in DNA origami is to achieve true “folding,” starting from a 2D sheet (miura ori), rather than the 1D M13 scaffolds commonly utilized in traditional DNA origami construction. The loose 2D networks and freely rotating hinges between different planes of DNA Gridirons provide the design features necessary to implement Miura ori type of origami.

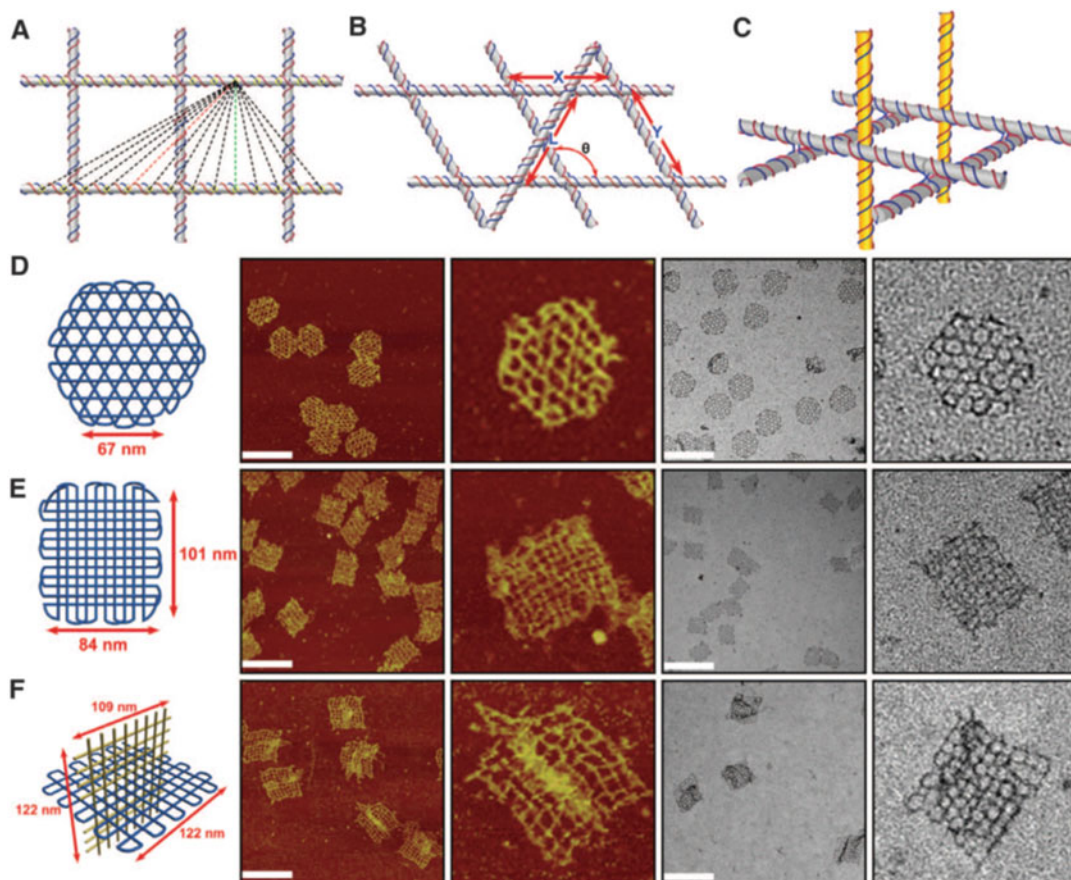


Fig. 8 Multilayer gridiron design strategies. (a, b) Strategy 1 is stacked layers. (a) A portion of a double-layer gridiron lattice with 52-bp cavity size. The *yellow circles* designate the permissible connection points to a third layer. The *dashed lines* correspond to possible connection points to form additional layers. (b) Given the double-layer gridiron lattice (X and Y lengths) and the distance between crossover points in the third layer, the angle q can be calculated as $180^\circ - \cos^{-1} [(X^2 + Y^2 - L^2)/2XY]$. (c) Strategy 2 is intertwining gridiron planes. (d–f) Schematics (*left*), AFM (*middle*), and TEM (*right*) images of (d) a three-layer hexagonal gridiron design, $q = 120^\circ$; (e) a four-layer gridiron design, q is not controlled because the *dashed green line* in (a) represents a connection strategy that cannot fix the angle; and (f) a 3D gridiron assembled by using strategy 2. All scale bars indicate 200 nm, and all zoom-in images (images without scale bars) are 200 by 200 nm. Figure reproduced from ref. [6] with permission from AAAS

3 Materials and Methods

3.1 Materials

1. 50× TAE buffer: 2 M tris base, 1 M acetic acid, 0.1 M EDTA. Filter the solution and store the filtrate at 4 °C.
2. 10× TAE Mg²⁺ buffer: 0.4 M tris base, 0.2 M acetic acid, 20 mM EDTA, and 125 mM Mg²⁺. Filter the solution and store the filtrate at 4 °C.

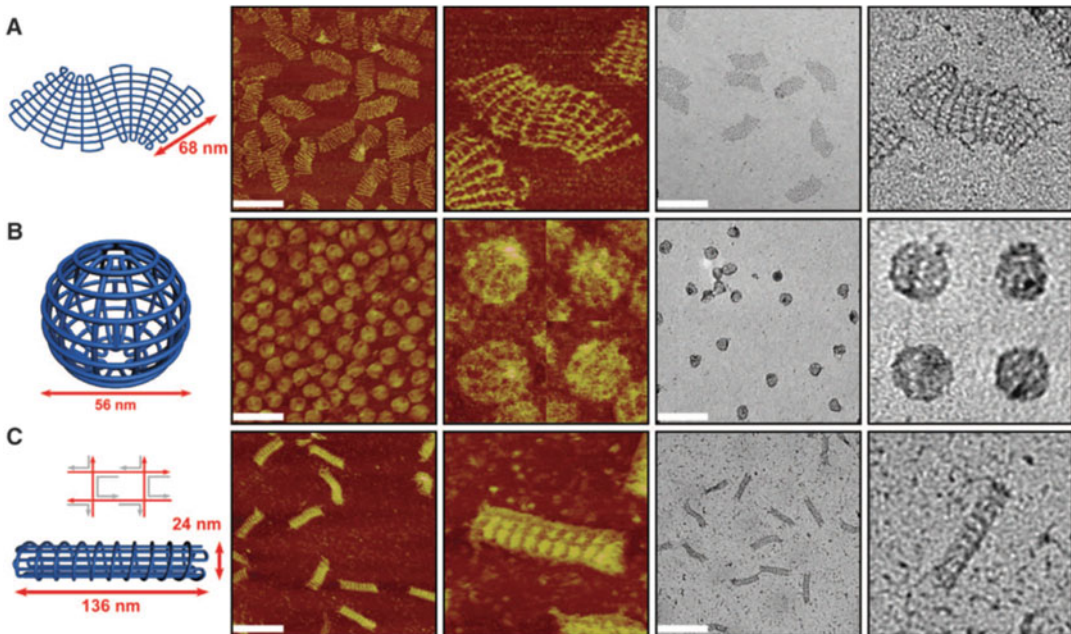


Fig. 9 Schematics (*left*), AFM (*middle*), and TEM (*right*) of (a) an S-shaped structure, (b) a sphere, and (c) a screw. All scale bars are 200 nm in length and all zoom in images are 200 nm \times 200 nm. In **b** and **c**, the diameter and the width, respectively appear to be larger in the AFM images compared to the TEM images. This difference is probably a result of flattening of the 3D objects into two layer structures and AFM tip convolution. Figure reproduced from ref. [6] with permission from AAAS

3. 1 \times TAE Mg²⁺ buffer: Measure 100 mL 10 \times TAE Mg²⁺ buffer and make up to 1 L with water. Store at 4 $^{\circ}$ C.
4. 1 \times TAE buffer: Measure 20 mL 50 \times TAE Mg²⁺ buffer and make up to 1 L with water. Store at 4 $^{\circ}$ C.
5. M13mp18 single stranded DNA (7249 nucleotides).
6. 16–90 nucleotides (nt) rational designed DNA staple strands. Staple strands are mixed at a final concentration of 1 μ M for each strand to make a staple strand mixture.
7. 100 mM NiCl₂. Filter the solution and store the filtrate at 4 $^{\circ}$ C.
8. 0.7% (w/v) uranyl formate solution: Weigh 37 mg of uranyl formate in a glass vial and add 5 mL boiling water to it. Stir this solution on a magnetic stirrer for 5 min in the dark. After 5 min add 50 μ L of 2 M NaOH solution to this solution and again stir it for 5 more minutes in the dark. Then filter the solution using Syringe filter (0.2 μ m) into eppendorf tubes. The filtrate is the 0.7% uranyl Stain solution.
9. EB (ethidium bromide) staining solution (10 mg/mL).

Note: Try to prepare the stain in the dark and always keep it in the dark (cover by Aluminum foil) as uranyl formate is highly sensitive to light.

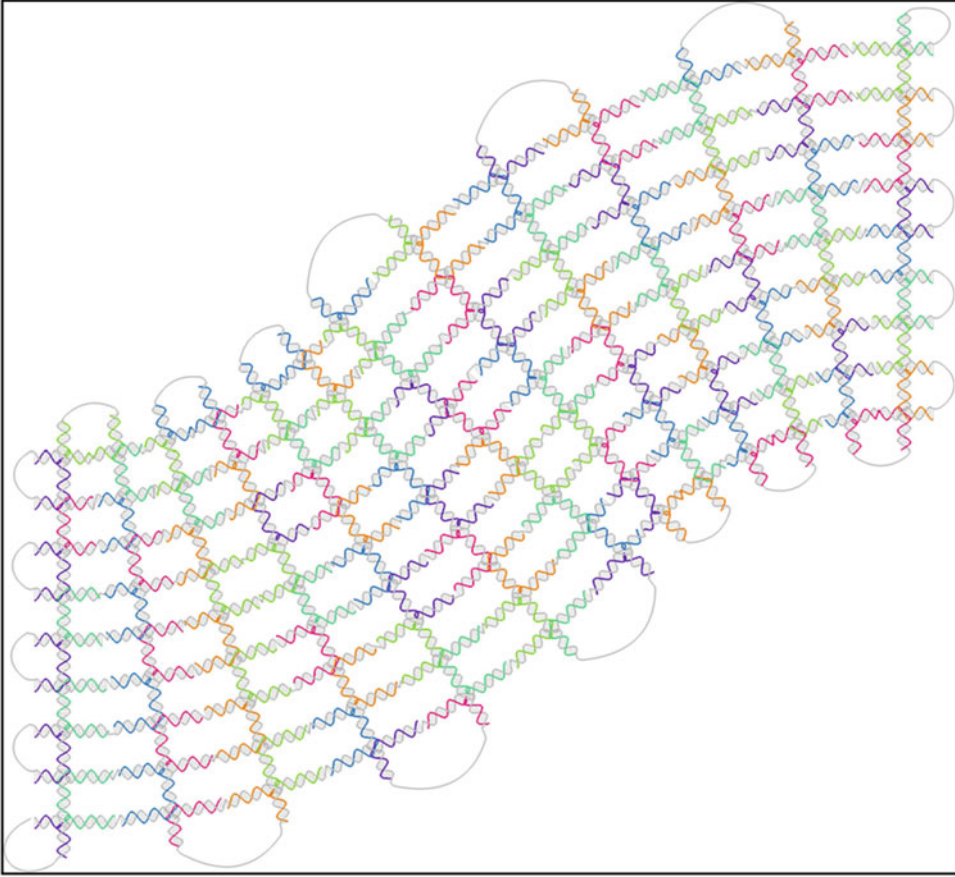


Fig. 10 Design pattern for S-shape Gridiron structure. Scaffold strand was colored in *gray* and staple strands had different colors

3.2 Methods

1. Assembly of 2D and 3D DNA nanostructures.

For each design, 10 nM of single stranded M13mp18 DNA was mixed with a ten times molar excess of staple strands in 1× TAE/Mg²⁺ buffer. For example, 10 μL scaffold strand (M13mp18, 100 nM), 10 μL staple strand mixture (1 μM for each strand) and 10 μL 10× TAE/Mg²⁺ buffer are mixed in a 0.2 mL PCR tube. The resulting solutions were annealed from 95 to 4 °C to form the designed structures. The exact temperature steps for a typical anneal are as follows: 90 to 76 °C at 2 °C per 5 min; 76 to 24 °C at 4 °C per 5 min. For some of the complex 3D structures, longer annealing time can be used to improve the folding yield. The exact temperature steps for a typical long anneal are as follows: 94 to 86 °C at 4 °C per 5 min; 85 to 70 °C at 1 °C per 5 min; 70 to 40 °C at 1 °C per 15 min; 40 to 25 °C at 1 °C per 10 min. All structures form in both anneal protocols and can be subjected to AFM imaging and TEM imaging with or without purification.

2. TEM imaging.

TEM samples were prepared by dropping 2 μL of the sample solution on a carbon-coated grid (400 mesh). Before depositing the sample, the grids were negatively glow discharged (Emitech K100X). After 1 min, the excess sample was wicked away from the grid with a piece of filter paper. To remove the excess salt, the grid was washed with a drop of water and the excess water was wicked away with filter paper. For staining, the grid was treated with a drop of 0.7% uranyl formate solution and the excess solution was removed with filter paper. The grid was treated with a second drop of uranyl formate solution for 20 s, and the excess solution was removed with filter paper. The grid was subsequently held at room temperature in air to evaporate the excess solution. Imaging were conducted with transmission electron microscope, operated at 80 kV in bright field mode.

3. AFM imaging.

For AFM imaging, the sample (2 μL) was deposited onto a freshly cleaved mica surface and left to adsorb for 2 min. 50 μL buffer (1 \times TAE Mg^{2+} buffer, plus 2 μL 100 mM NiCl_2) was added onto the mica, and the sample was scanned in Fluid mode using ScanAsyst in fluid + tips.

4. Agarose gel electrophoresis. The folding products were subject to native gel electrophoresis on 0.75% (g/mL) agarose gel.

Gel casting: For dissolving of agarose, use microwave to heat the solution (60 mL) to facilitate the agarose melt completely in the 1 \times TAE buffer. Stop and shake frequently to prevent bumping. For gel casting, add 2–5 μL EB staining solution to the agarose solution (60 mL) while it cools down to about 45 $^\circ\text{C}$ then cast the gel into horizontal gel box. Insert the combs and wait for 30 min.

Sample loading and electrophoresis: Add 10 \times Non-denaturing dye (1:10) to the annealed DNA structures to prepare the loading samples. Put the horizontal gel box into ice water. Take out the comb. Fill the gel box with 1 \times TAE buffer. The height should be just above the gel surface. Load 10–20 μL samples to each well. Run the gel at constant voltage (80 V) for 2–3 h.

Imaging: Transfer the gel and wipe clean the top of the UV transilluminator and squirt little water to wet the top of the lamp. Place gel onto the UV transilluminator, use 302 nm UV light, turn on the lamp, and observe the DNA bands.

5. DNA sequence design.

Software “Tiamat” is used for designing DNA gridiron structures (Tiamat software and files for all designs are available for downloading from the link: <http://1drv.ms/1OB2SMm>). Tiamat is a basic DNA drawing software and is capable of generating staple strands sequences according to the input scaffold strand sequence.

References

1. Seeman NC (2010) Nanomaterials based on DNA. *Annu Rev Biochem* 79:65
2. Rothemund PW (2006) Folding DNA to create nanoscale shapes and patterns. *Nature* 440(7082):297–302
3. Douglas SM, Dietz H, Liedl T, Högberg B, Graf F, Shih WM (2009) Self-assembly of DNA into nanoscale three-dimensional shapes. *Nature* 459(7245):414–418
4. Dietz H, Douglas SM, Shih WM (2009) Folding DNA into twisted and curved nanoscale shapes. *Science* 325(5941):725–730
5. Han D, Pal S, Nangreave J, Deng Z, Liu Y, Yan H (2011) DNA origami with complex curvatures in three-dimensional space. *Science* 332(6027):342–346
6. Han D, Pal S, Yang Y, Jiang S, Nangreave J, Liu Y, Yan H (2013) DNA gridiron nanostructures based on four-arm junctions. *Science* 339(6126):1412–1415
7. Mao C, Sun W, Seeman NC (1999) Designed two-dimensional DNA Holliday junction arrays visualized by atomic force microscopy. *J Am Chem Soc* 121(23):5437–5443
8. Miick SM, Fee RS, Millar DP, Chazin WJ (1997) Crossover isomer bias is the primary sequence-dependent property of immobilized Holliday junctions. *Proc Natl Acad Sci* 94(17):9080–9084
9. McKinney SA, Déclais AC, Lilley DM, Ha T (2003) Structural dynamics of individual Holliday junctions. *Nat Struct Mol Biol* 10(2):93–97
10. Fu TJ, Seeman NC (1993) DNA double-crossover molecules. *Biochemistry* 32(13):3211–3220
11. Williams S, Lund K, Lin C, Wonka P, Lindsay S, Yan H. Tiamat: a three-dimensional editing tool for complex DNA structures. In: *DNA computing*. Heidelberg, Berlin: Springer; 2008. p. 90–101

Complex DNA Brick Assembly

Luvena Ong and Yonggang Ke

Abstract

DNA nanostructures are a useful technology for precisely organizing and manipulating nanomaterials. The DNA bricks method is a modular and versatile platform for applications requiring discrete or periodic structures with complex three-dimensional features. Here, we describe how structures are designed from the fundamental strand architecture through assembly and characterization of the formed structures.

Key words Structural DNA nanotechnology, DNA bricks, 3D self-assembly, Modular, DNA brick crystals

1 Introduction

In recent years, nucleic acid self-assembly has demonstrated to be a useful technique for nanoscale patterning of different materials. These nucleic acid structures serve as scaffolds, and functional nanomaterials can be simply positioned by conjugating a sequence that is complementary to that of the target position on the scaffold. Three-dimensional assemblies have been of particular interest because of increased structural rigidity and ability to create complex forms in a single pot. The versatility of this approach has been previously demonstrated by current efforts to organize gold nanoparticles for photonic applications [1], arrange proteins to control signaling pathways [2], compartmentalize receptor ligands for targeted delivery [3], and confine growth of inorganic materials [4], among many other endeavors for materials [5] and biophysical applications [6–8].

Since the insight that nucleic acids could serve as a structural code and be programmed to form specific structures [9], progress in structural DNA nanotechnology has occurred quickly—a number of 1D ribbons [10, 11], tubes [12–14], 2D lattices [11, 15], and 3D crystals [16] have been demonstrated. One of the biggest innovations was the DNA origami method where a long single-stranded scaffold often obtained from a biological source with

complementary short oligomer staples [17]. While this approach has allowed for high complex 2D [17] and 3D structures [18] with varying lattice structures [19–21] and curvature [22, 23] to be precisely created, DNA origami is not a modular method. For certain complex shapes, a feasible scaffold routing path may also be difficult to obtain.

Recently, a modular method of assembling 3D discrete [24] and periodic nucleic acid structures [25] was developed. This DNA brick approach uses synthetic short single-stranded oligomers that interact with one another through an eight nucleotide (nt) binding domain. The DNA brick method provides an attractive alternative for designing structures because of its ease of use, scalability, and modularity. The simple architecture and independent components enables assembly of fully addressable features as small as 0.4 MDa to as large as 8 MDa. The modularity allows for facile design of complex 3D shapes by simply choosing to include or removing specific strands in a given canvas structure.

In this chapter, we discuss the design of the discrete and periodic DNA brick structures from strand architecture, shape design, sequence specification, structure annealing, and structure characterization. While hexagonal and honeycomb lattices have been previously developed, we focus on the designs for the square lattice. The architecture for the square lattice structures is periodic and has been thoroughly characterized, and concepts for the design and assembly of these structures can be easily translated to the other lattices. As an example, we design one discrete structure showing an enclosed inner cavity and an ZX-crystal containing pores.

The fundamental structure of a DNA brick within a folded structure contains four 8-nt binding domains in a U-shaped configuration (Fig. 1a). The 8-bp hybridization confers approximately a three-fourths turn for a B-form duplex. As a result, a 90° dihedral

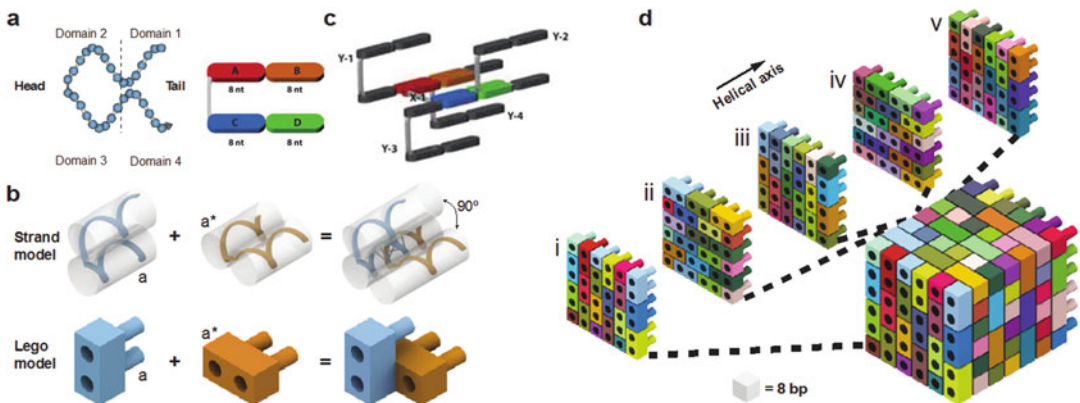


Fig. 1 Design architecture of DNA brick structures. (a) Schematic of a DNA brick, where four 8-nt domains are present. (b) Strand and LEGO model of two interacting DNA bricks, where each domain is represented by a peg or hole. (c) Layers of a cuboid structure. Figure adapted from ref. [24]

angle is present between two interacting bricks (Fig. 1b). Such architecture results in X-bricks interacting only with Y-bricks and vice versa, where X and Y indicate the orientation of the phosphodiester crossover (Fig. 1c). Thus, alternating layers of X- and Y-bricks rotated 270° clockwise in orientation are present within a structure (Fig. 1d). Such periodic design allows for easy assembly of varying shapes and structures since each 8-bp region can serve as a voxel.

Half-strands are present at the face and edges of a structures. Stability of these strands is limited because only 16 bp of hybridization are available. Thus, to increase the binding energy, a half-brick is concatenated to a full brick that precedes it along the Z-axis (Fig. 3f).

A cuboid structure is used to represent a voxel canvas from which desired voxels will be selected for shape design. Each voxel is represented with an 8-bp domain, and the null voxel is represented with a single-stranded polyT region (Figs. 2a and 3a, b). Because each DNA brick will contain four potential voxels, variations of the original DNA brick can be derived depending upon which voxels are present in a structure (Fig. 2b–e). Bricks that

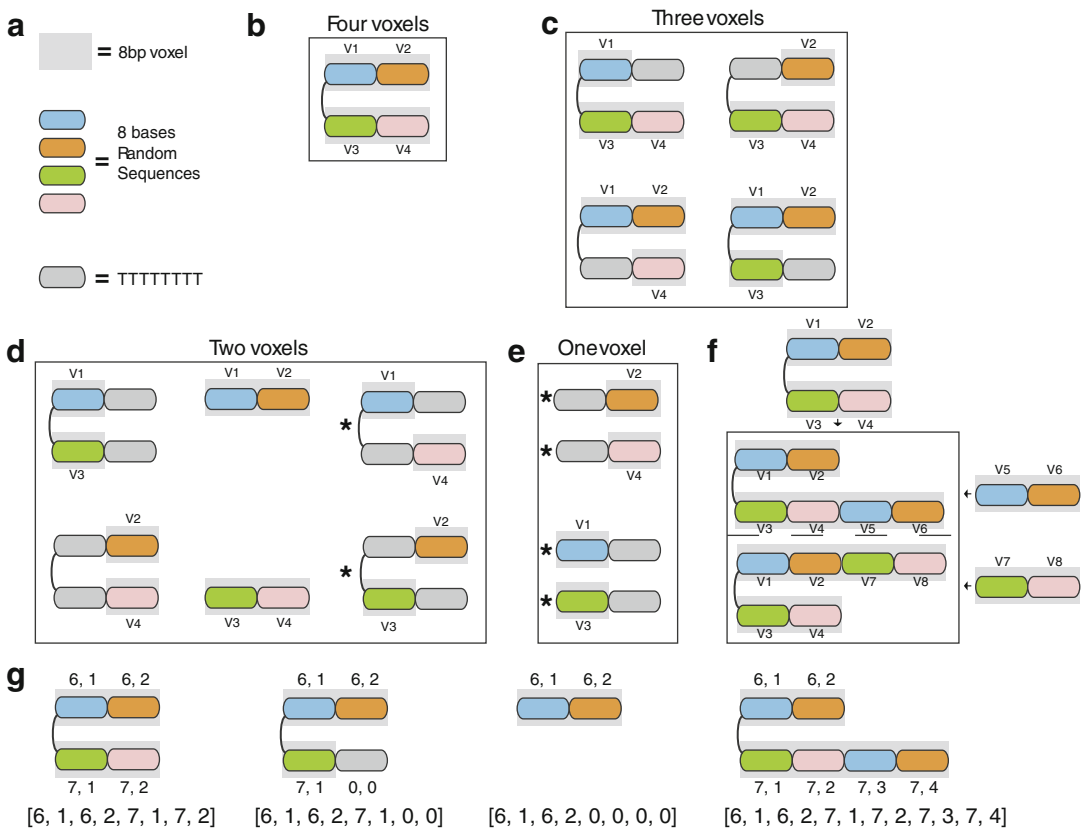


Fig. 2 DNA brick derivatives. (a) Voxels are represented by a *colored rounded rectangle*. The null domain consists of 8 polyT and a *grey rounded rectangle*. Variations of the bricks are shown with all four voxels (b), three voxels (c), two voxels (d), and one voxel (e). Also, boundary strands are shown in (f). Bricks marked with “*” indicate excluded strands that are less frequently used. Figure is adapted from ref. [24]

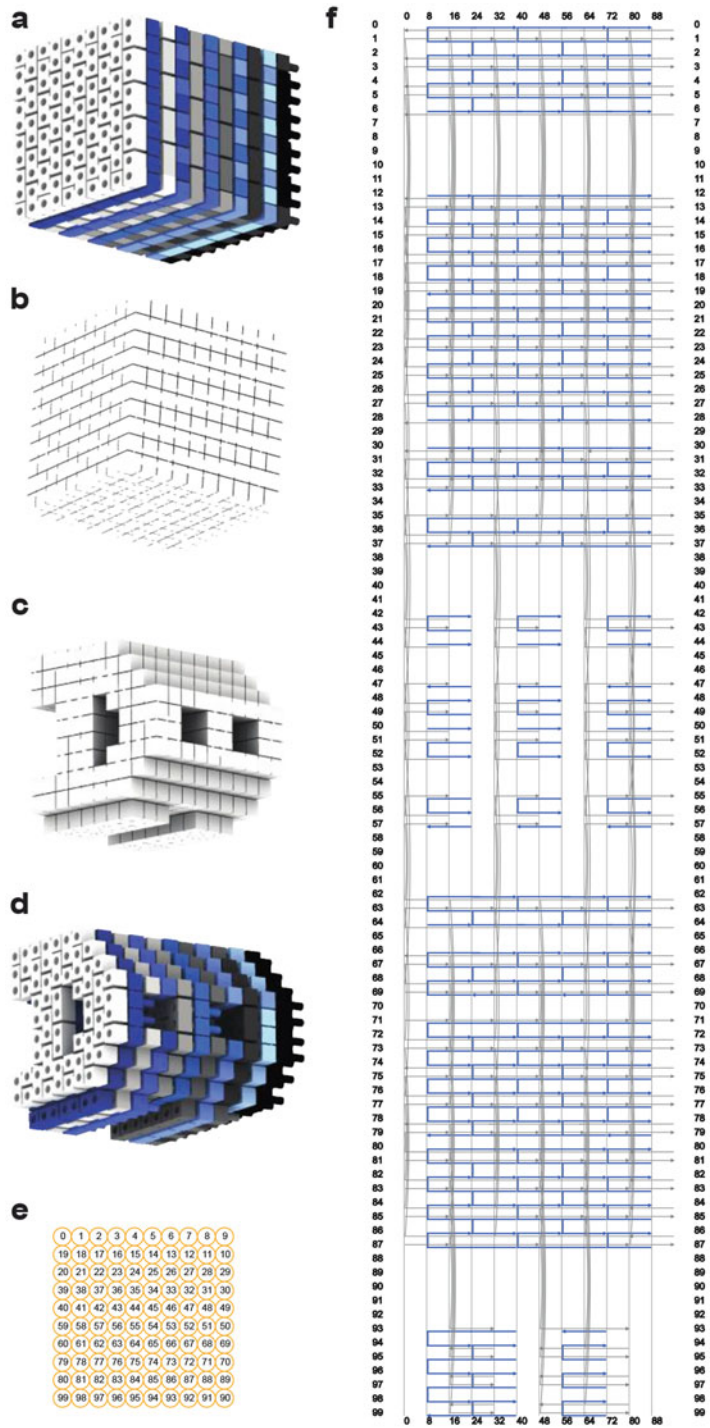


Fig. 3 Assembly of a 3D structure with complex features. (a) In the brick diagram, the X-bricks are depicted in blue and the Y-bricks are in greyscale. Each layer is represented by a different color. Shapes are designed from a $10H \times 10H \times 80B$ cuboid (a) that can be represented by a $10 \times 10 \times 10$ voxel canvas (b). Voxels are selected from this canvas to form a shape (c). This shape can be translated to a brick structure (d). caDNA diagrams are shown in (e) helical projection and (f) strand diagram. Figure adapted from ref. [24]

occur less frequently, such as those where alternating domains contain the null voxel, are excluded from the structure design (Fig. 2, marked by asterisk). Additionally, DNA half-bricks containing only a single domain are excluded due to the weak binding interaction. Such design features also reduces the size of the canvas library necessary to form the different shapes. For single shape designs, these excluded bricks can be used, as the total structure will use fewer strands than the total library.

As an example, we demonstrate the design of a complex cavity structure from a voxel canvas. In Fig. 3a, we see the original 10 helix (H) \times 10 helix (H) \times 80 base pair (B) canvas. This canvas can be represented by a $10 \times 10 \times 10$ voxel canvas (Fig. 3b). Each layer is represented by a different brick color. Similarly colored bricks that penetrate across layers denote the connected boundary strands. From this voxel canvas, a number of shapes can be designed. In this example, we demonstrate a complex cavity shape that shows an “A” projection on one face and a “B” projection on an adjacent face (Fig. 3c). Based on the voxel selection, the bricks from the canvas can be modified to form this designed structure. The underlying brick architecture and caDNAno diagram for this shape is shown in Fig. 3d, e, respectively.

The DNA brick approach can also be used to easily create large micron-sized crystals with defined depths. These crystal structures can be designed by applying complementarity rules to opposing faces on a unit design along the three orthogonal axes (Fig. 4a), where the Z-axis represents the helical axis. In this case, a brick

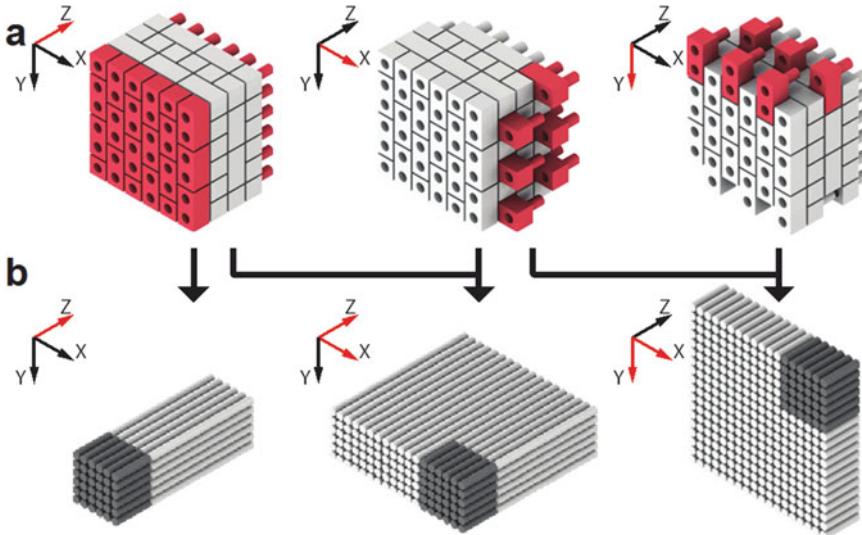


Fig. 4 Assembly of crystals with defined depths. (a) Brick diagrams depicting the “connecting” strands in red across the three different axes. Connecting strands have complementary regions on opposing faces. (b) Combinations of these strands can be used to create crystals with different defined thickness. With connecting strands only in the Z-axis, long rod-like structures can be formed. Figure adapted from ref. [25]

marked by the red color contains domains that are complementary to opposite faces in a structure. The flexibility in selecting which axes have periodic boundary conditions allows us to create crystals with defined thickness either in the helical direction or perpendicular to it (Fig. 4b).

A number of different software can be used to design structures. In our work, we used a custom script that allows for interface between 3D-rendering software for shape design and caDNAno for strand design because of the large number of shapes designed. Generally, this software inputs the voxel coordinates of the shapes, determine the extraneous voxels in the canvas, and removes the unused bricks from the canvas caDNAno file. For design of select shapes, one can directly work in caDNAno from a starting brick canvas file.

Random sequences work well for sequence design. We use a custom script that determines each position in an X-strand, assigns it base, and then assigns the complementary base in the interacting Y-strand. Because this structure is designable in caDNAno, these scripts can work well with the existing “scaffold” and “staple” strand distinction that caDNAno uses.

2 Materials

2.1 Equipment

1. Eppendorf mastergradient thermocycler.
2. JEOL 1200 Transmission Electron Microscope.
3. Vacuum centrifuge.
4. Agarose gel electrophoresis box.
5. Power supply.
6. Blue intensity light.

2.2 Reagents and Supplies

1. Oligonucleotides for structure formation (See above section for sequence design)—can be unpurified and resuspended at 100 μM in DNase and RNase free H_2O . See **Note 1** for extended storage conditions.
2. 10 \times Folding Buffer: 50 mM Tris (pH 7.5), 10 mM EDTA, 400 mM MgCl_2 .
3. PCR tubes.
4. SeaKem LE Agarose.
5. 0.5 \times TBE Buffer: 89 mM Tris-borate, 2 mM EDTA, pH 8.3.
6. Gel running buffer: 0.5 \times TBE Buffer with 10 mM MgCl_2 .
7. 1.2 M MgCl_2 .
8. SYBR Safe.
9. 500 mL beaker.

10. Razor blade.
11. Freeze-“n”-squeeze tubes.
12. Plastic pestles.
13. Formvar carbon grids.
14. 2% (w/w) uranyl formate stain, filtered and pH adjusted: 250 μ L 2% uranyl formate with 2.5 μ L 5 N NaOH.

3 Methods

3.1 Annealing

1. Mix the strands for the structures equimolarly to form a stock solution of strands in water. If the final concentration of the strands is less than 222 nM per strand, solution can be concentrated in a vacuum centrifuge.
2. Dilute the stock strand solutions to at least a 200 nM per strand final concentration in a 20 μ L reaction volume with 1 \times folding buffer.
3. Structures can be annealed in a thermocycler using a 3-day or a 7-day annealing ramp. In both cases, the structures are annealed in a two-step protocol: 80 to 60 $^{\circ}$ C at the rate of 2 min/ $^{\circ}$ C, followed by 60 to 25 $^{\circ}$ C at 2 h/ $^{\circ}$ C or 4.6 h/ $^{\circ}$ C. Discrete structures and ZX-crystals are capable of forming in a 3-day annealing reaction. In contrast, XY-crystals require a 7-day annealing ramp. *See Note 2* for if difficulties arise in forming structures.

3.2 Gel

Electrophoresis: For Discrete Structures Only

1. Measure 1.8 g of dry agarose in a clean 500 mL beaker.
2. Add 0.5 \times TBE buffer until 120 g on the scale is reached.
3. Microwave this solution for 3 min or until the agarose is fully dissolved. Weigh the solution and add the amount of water that had evaporated. Mix by swirling.
4. Cool the agarose solution on ice for 3 min while swirling to avoid uneven gelation.
5. Add in 1 mL of 1.2 M MgCl₂ and mix well.
6. Add in 6 μ L of SYBR Safe for a final concentration of 0.5 \times SYBR Safe and mix well.
7. Carefully pour the agarose solution into the gel box and insert the desired combs. Allow the gel to cool for 1 h before use.
8. Add the gel running buffer to fully cover the agarose gel.
9. Mix 5 μ L of the folded structure with 1 μ L of 6 \times loading dye, and load the full sample into each well.
10. Gel is run for 2 h at 80 V in an ice water bath.
11. Visualize the gel on a gel scanner.

3.3 Structure

Purification: For Discrete Structures Only

1. Gel can be viewed under a high intensity blue light. Often at least two bands can be seen—the target band and a band for the unincorporated strands. Often, there will be several bands above the target band, indicating the formation of dimers and multimers.
2. Target band can be excised using a razor blade and transferred to the column in a Freeze-“n”-Squeeze tube.
3. Gel pieces can be carefully crushed using the flat end of a plastic pestle
4. Tubes are centrifuged at $700 \times g$ for 5 min, and the column containing the gel pieces can be thrown away.

3.4 Imaging

1. Grids can be glow discharged at 25 mA for 45 s in 0.1 mBar with negative HT polarity.
2. Deposit 2.5 μL of sample onto the surface of the grid for 2 min.
3. Sample can be blotted off the edge with filter paper.
4. Deposit 8 μL of 2% uranyl formate stain on the grid for 1 min. See **Notes 3** and **4** for variations on staining times.
5. Remove stain completely using the filter paper.
6. Allow the stain to dry before imaging on the transmission electron microscope.

4 Notes

1. Since the oligomers are stored in water, stock solutions of strands should be stored at $-20\text{ }^\circ\text{C}$ for stability.
2. Difficult structures may benefit from longer annealing times. If yields are low for these structures, a 7-day annealing ramp can be used. Additionally, all these structures are capable of forming using an isothermal folding protocol. The optimal temperature varies depending on size and shape but is generally around $35\text{ }^\circ\text{C}$.
3. Staining times will change depending on the thickness and quality of the structures. Thicker or unpurified samples can be stained for shorter amounts of time.
4. Unpurified discrete structures can also be imaged on the TEM. For preparation and staining of these structures, shorter staining times can be used $\sim 30\text{ s}$.

References

1. Kuzyk A, Schreiber R, Fan Z et al (2012) DNA-based self-assembly of chiral plasmonic nanostructures with tailored optical response. *Nature* 483:311–314
2. Shaw A, Lundin A, Petrova E et al (2014) *Nat Meth* 11:841–846
3. Douglas SM, Bachelet I, Church GM (2012) A logic-gated nanorobot for targeted transport of molecular payloads. *Science* 335:831–834
4. Sun W, Boulais E, Hakobyan Y et al (2014) Casting inorganic structures with DNA molds. *Science* 346:1258361

5. Funke JJ, Dietz H (2015) Placing molecules with Bohr radius resolution using DNA origami. *Nat Nanotech* 11:47–52
6. Douglas SM, Chou JJ, Shih WM (2007) DNA-nanotube-induced alignment of membrane proteins for NMR structure determination. *Proc Natl Acad Sci U S A* 104:6644–6648
7. Udomprasert A, Bongiovanni MN, Sha R et al (2014) *Nat Nanotech* 9:537–541
8. Yan H, Park SH, Finkelstein G et al (2003) DNA-templated self-assembly of protein arrays and highly conductive nanowires. *Science* 301:1882–1884
9. Seeman NC (1982) Nucleic acid junctions and lattices. *J Theor Biol* 99:237–247
10. Schulman R, Winfree E (2007) Synthesis of crystals with a programmable kinetic barrier to nucleation. *Proc Natl Acad Sci U S A* 104:15236–15241
11. Yan H, Labean TH, Feng L et al (2003) Directed nucleation assembly of DNA tile complexes for barcode-patterned lattices. *Proc Natl Acad Sci U S A* 100:8103–8108
12. Yin P, Hariadi RF, Sahu S et al (2008) Programming DNA tube circumferences. *Science* 321:824–826
13. Liu DD, Park SH, Reif JH et al (2004) DNA nanotubes self-assembled from triple-crossover tiles as templates for conductive nanowires. *Proc Natl Acad Sci U S A* 101:717–722
14. Ke Y, Liu Y, Zhang J et al (2006) A study of DNA tube formation mechanisms using 4-, 8-, and 12-helix DNA nanostructures. *J Am Chem Soc* 128:4414–4421
15. Winfree E, Liu F, Wenzler LA et al (1998) Design and self-assembly of two-dimensional DNA crystals. *Nature* 394:539–544
16. Zheng J, Birktoft JJ, Chen Y et al (2009) From molecular to macroscopic via the rational design of a self-assembled 3D DNA crystal. *Nature* 461:74–77
17. Rothmund PWK (2006) Folding DNA to create nanoscale shapes and patterns. *Nature* 440:297–302
18. Douglas SM, Dietz H, Liedl T et al (2009) Self-assembly of DNA into nanoscale three-dimensional shapes. *Nature* 459:414–418
19. Ke Y, Douglas SM, Liu M et al (2009) Multilayer DNA origami packed on a square lattice. *J Am Chem Soc* 131:15903–15908
20. Ke Y, Voigt NV, Gothelf KV et al (2012) Multilayer DNA origami packed on hexagonal and hybrid lattices. *J Am Chem Soc* 134:1770–1774
21. Han D, Pal S, Yang Y et al (2013) DNA grid-iron nanostructures based on four-arm junctions. *Science* 339:1412–1415
22. Han D, Pal S, Nangreave J et al (2011) DNA origami with complex curvatures in three-dimensional space. *Science* 332:342–346
23. Dietz H, Douglas SM, Shih WM (2009) Folding DNA into twisted and curved nanoscale shapes. *Science* 325:725–730
24. Ke Y, Ong LL, Shih WM et al (2012) Three-dimensional structures self-assembled from DNA bricks. *Science* 338:1177–1183
25. Ke Y, Ong LL, Sun W et al (2014) DNA brick crystals with prescribed depths. *Nat Chem* 6:994–1002

Computer-Aided Design of RNA Origami Structures

Steffen L. Sparvath, Cody W. Geary, and Ebbe S. Andersen

Abstract

RNA nanostructures can be used as scaffolds to organize, combine, and control molecular functionalities, with great potential for applications in nanomedicine and synthetic biology. The single-stranded RNA origami method allows RNA nanostructures to be folded as they are transcribed by the RNA polymerase. RNA origami structures provide a stable framework that can be decorated with functional RNA elements such as riboswitches, ribozymes, interaction sites, and aptamers for binding small molecules or protein targets. The rich library of RNA structural and functional elements combined with the possibility to attach proteins through aptamer-based binding creates virtually limitless possibilities for constructing advanced RNA-based nanodevices.

In this chapter we provide a detailed protocol for the single-stranded RNA origami design method using a simple 2-helix tall structure as an example. The first step involves 3D modeling of a double-crossover between two RNA double helices, followed by decoration with tertiary motifs. The second step deals with the construction of a 2D blueprint describing the secondary structure and sequence constraints that serves as the input for computer programs. In the third step, computer programs are used to design RNA sequences that are compatible with the structure, and the resulting outputs are evaluated and converted into DNA sequences to order.

Key words RNA origami, RNA nanotechnology, RNA sequence design, Secondary structure, RNA structure prediction, Computer-aided design

1 Introduction

RNA and DNA nanotechnology have been developing along independent lines during the last decade [1]. In DNA nanotechnology, the design of DNA nanostructures has mainly focused on the use of double-crossover motifs [2], whereas RNA nanotechnology has focused on the use of junctions and motifs that are structurally defined by non-Watson–Crick base pairs [3]. The single-stranded RNA origami method [4] combines double crossovers of the A-form helix with tertiary motifs to form RNA nanostructures designed to fold while they are being transcribed by an RNA polymerase (co-transcriptional folding).

1.1 *The RNA Origami Method*

The single-stranded RNA origami method was developed to allow the creation of large RNA nanostructures that form well-defined scaffolds for combining RNA-based functionalities [4]. A main feature of the method is that it allows you to design an RNA nanostructure that can fold during the transcriptional process, which has the major benefit of allowing the folding to happen autonomously at a constant temperature and possibly inside a cell when expressed from a synthetic RNA gene.

The design of RNA structures that can fold co-transcriptionally requires that the substructures are designed such that they may assemble in a stepwise and coordinated fashion. The RNA origami method uses a combination of hairpins (secondary structure) and kissing-loop complexes (tertiary structure) to stabilize the desired fold during transcription by the T7 RNA polymerase [4]. The kinetics of hairpin formation and kissing-loop formation thus coordinates the folding process as seen in Fig. 1a. First, the hairpins are formed, then junctions are formed, and at last the tertiary contacts lock the final structure into place. In the original study the folded RNA tiles were designed to further assemble into a honeycomb lattice (quaternary structure), to ease the visualization of correctly formed products in the atomic force microscope [4].

The RNA origami method uses double-crossovers (DX) to arrange the RNA helices in parallel to each other. DX molecules are normally constructed using multiple strands (Fig. 1b, left) but for the RNA origami method we devised a way to make DX molecules using only one strand, by adding hairpin motifs to the edges and kissing-loop complexes on internal helices (Fig. 1b, right). When connecting more DX molecules on top of each other an interesting junction is made that we call the dovetail seam. The dovetail contains base pairs that cross between adjacent junctions, and thus makes the structural seam that runs along the junction sequence-specific. An important thing to consider for the design of these structures is the topology of the folding process, i.e., the order in which interactions form can lead to situations where one early interaction blocks a later interaction by forming a physical knot. The kissing-loop interactions and dovetail interactions, due to their length being a half-turn or shorter, do not generate these topological issues, and are thus useful for co-transcriptional folding design.

RNA origami nanostructures are constructed using recurrent structural modules that are found in the structural databases. The RNA origami structures demonstrated in Geary et al. are constructed from only 5 RNA modules (Fig. 1c). The 180° kissing loop is used for coaxial connection of helices internally in the tiles. The tetra loops are used to cap the end of helices and the 120° kissing loop is used to arrange the tiles in a larger hexagonal honeycomb grid. The dovetail seam can be used to adjust the relative positions of helices in relation to each other as described in [5].

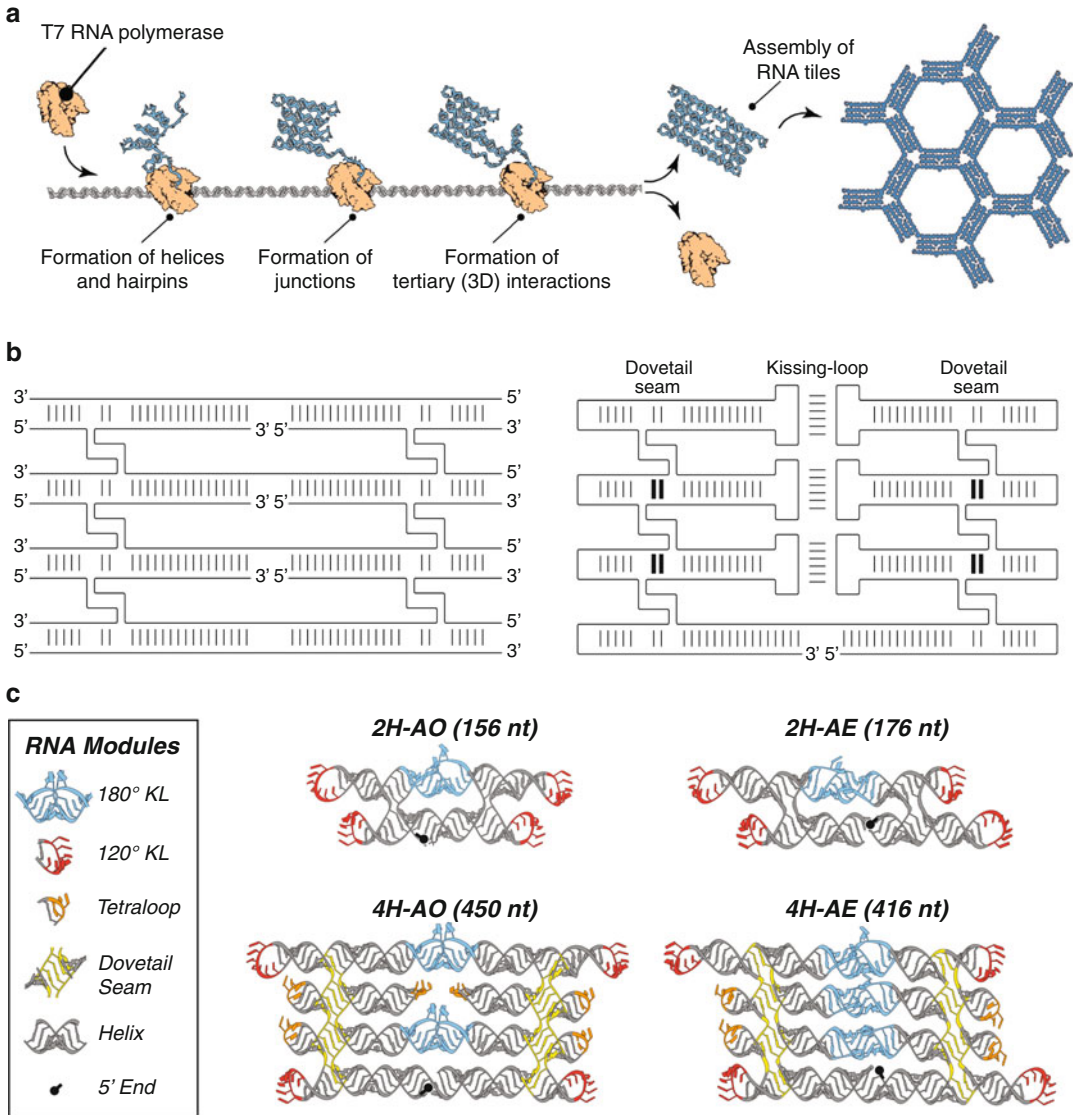


Fig. 1 Design principles for single-stranded RNA origami structures. (a) Co-transcriptional folding by T7 RNA polymerase. RNA hairpins and junctions are formed followed by tertiary interactions. The final RNA tile can be programmed to further assemble into a hexagonal grid. (b) Blueprint schematics showing how a multi-stranded DX structure is converted into a single-stranded RNA origami structure by inserting hairpins and kissing loops. The dovetail seam is shown as thick lines. (c) RNA structural modules are used to compose the final 3D model of the RNA origami structure. 2H and 4H tiles shown here can fold co-transcriptionally

1.2 The Double Crossover (DX) in RNA Origami

The DX has been a fundamental building block of DNA nanotechnology [2] and plays a central role in the single-stranded RNA origami method. To design RNA origami structures it is important to understand the geometry of the A-form RNA helix to be able to construct DX molecules by calculating the optimal position of crossovers.

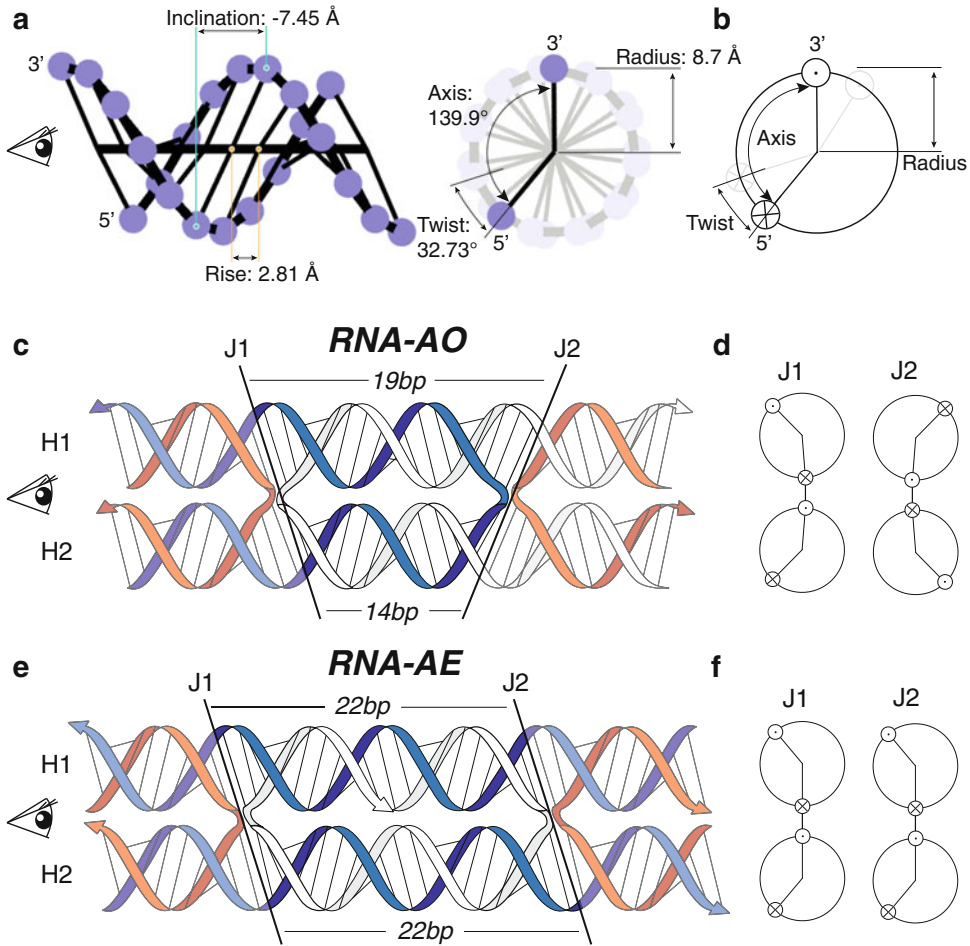


Fig. 2 Calculation of RNA double-crossover molecules. **(a)** RNA A-form double helix represented in a simplified version showing only the backbone P atoms and lines connecting the base pairs across the helical axis. The main parameters (rise, inclination, axis and twist) and their values are shown in the figure. Eye symbol on helix side-view defines end-view. **(b)** Simplified schematic end-view of double helix with arrow-end symbols for 5' and 3' ends. **(c)** Antiparallel double-crossover with odd number of half turns between crossovers. Helices and junctions are numbered. Number of base pairs between upper and lower double helix is shown. *Eye-symbol* shows relation to end-view in RNA-AO. **(d)** End-view schematic representation of the two junctions. **(e)** Antiparallel double-crossover with even number of half turns between crossovers. Helices and junctions are numbered. Number of base pairs between upper and lower double helix is shown. *Eye-symbol* shows relation to end-view. **(f)** End-view schematic representation of the two junctions in RNA-AE

To construct DX molecules it is sufficient to know the positions of the backbone phosphorus (P) atoms, since the proximity of two P atoms on two different helices indicate the possibility to make a crossover. To make it easy to calculate the position of P atoms we have made a simplified P-helix model that is described by only four parameters (rise, inclination and axis and twist angles) [5] (Fig. 2a). In the P helix model the A-form helix has a large negative inclination that causes the 3' end to be pointing out from

the end of the helix and the 5' end to be recessed (Fig. 2a). The end-view of the helix is useful when considering the different types of crossovers possible (parallel and antiparallel) and can be shown in a simplified schematic view as seen in Fig. 2b.

The inclination of the base pairs causes the DX molecules to behave differently from the DX molecules constructed using DNA double helices. The antiparallel DX with odd number of half turns between crossovers (AO) have the inclinations opposed, resulting in an asymmetric double helix length on each side of the DX (Fig. 2c). To calculate the optimal crossover we use the axis angle parameter, since the DX happens from the two different strands of the helix. The end-view of the two junctions show that the shallow and deep groove are projecting to each side of the tile (Fig. 2d).

The antiparallel DX with an even number of half turns between crossovers (AE) it is simpler to calculate the optimal position of crossovers. In this case the helical periodicity of 11 base pairs of the A-form double helix identifies the possible crossover distances as a multiple of 11. Figure 2e shows a DX-AE of 22 base pairs. The end-view of the two junctions show that the grooves point to the same side at the two crossovers.

The calculations can be extended by linking more than two helices together by DXes. This leads to an offset between crossovers with a number of base pairs in between, which we call the dovetail seam. In this case the number of base pairs between the crossovers on adjacent helices determine if the helices are positioned in a plane or bends out from or into the plane (for more details see [5]). Changing distances between crossovers that does not fit the optimal distances can also be used to induce curvature of the helices as it has been done in the DNA origami field [6].

1.3 Outline of the Major Procedures in the Protocol

Designing an RNA origami structure requires several steps that are greatly facilitated by computer software and algorithms.

The process begins by constructing a 3D model to assure that the structure you are designing is feasible concerning geometry and strain (Fig. 3a). First double helices are aligned correctly to allow crossovers to be made. Tertiary motifs are extracted from databases and added to the double helix scaffold. Software and scripts are used to merge the motifs together into a single chain, followed by strain minimization to visualize and evaluate the quality of the final 3D model.

The second major procedure deals with the construction of a 2D blueprint to describe the strand path and base pairs of the 3D model (Fig. 3b). The 2D blueprint is used to introduce sequence constraints that define important primary, secondary and tertiary motifs. The 2D blueprint further constitutes a computer-readable format that can be analyzed by custom-made scripts and formatted for use in other analysis, prediction and design programs.

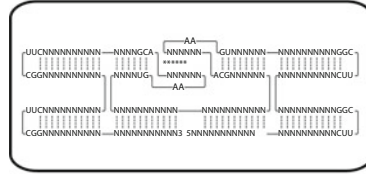
A. Create a 3D model

1. Find 3D motifs
2. Align the motifs
3. Ligate the PDB file
4. Refine the structure



B. Write the 2D structure

1. Write the secondary structure
2. Incorporate sequence restrictions
3. Trace the structure
4. Output a NUPACK code



C. Design the sequence

1. Design sequences
2. Evaluate the folding
3. Design primers
4. Order template and primers

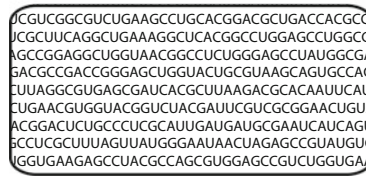


Fig. 3 Workflow for RNA origami design. The design process can be divided into 3 tasks: (1) creating a 3D model, (2) converting the 3D model to a secondary structure (3) designing the sequence. This tutorial describes the modeling, data editing and calculation steps that are required to complete each of these tasks

The third step is the design of sequences that are compatible with the designed structure (Fig. 3c). In this protocol we use the *NUPACK* design algorithm to obtain sequences that fold into the desired structure. We further analyze the folding properties using several prediction algorithms. Finally we give guidelines for designing primers for amplifying the template and directions for ordering your first RNA origami structure.

2 Materials

All actions described in this protocol are performed in *OS X (version 10.11.3)*. Other operating systems might use other shortcuts or need additional programs. Look in the user guide of the programs for instructions on other platforms.

2.1 Hardware

1. A computer.
2. A mouse (3D modeling is possible using a touchpad, but more cumbersome).

2.2 *Swiss-Pdb Viewer*

Although *Swiss-PdbViewer* is mainly used in regards to three-dimensional protein models it also handles nucleotides and has a user-friendly interface connecting the 3D model to its sequence.

1. Download and install the most recent version of *Swiss-PdbViewer* (<http://spdbv.vital-it.ch>). On this website you can also find the user guide, Tips & Tricks and tutorials etc. This tutorial was made with version 4.1.

2.3 *Assemble2* and *UCSF Chimera*

The programs *Assemble2* and *UCSF Chimera* can be used both separately and as a combined package. It is important that they are installed in the proper order for them to be connected correctly. *Assemble2* handles the visualization and manipulation of the secondary structure while *Chimera* handles the three-dimensional view.

1. Download and install the current production release of *Chimera* (www.cgl.ucsf.edu/chimera). On this website you can also find the user guide and tutorials etc. This tutorial was made with version 1.10.1 of *Chimera*.
2. Install the latest version of *Java* (<http://java.com/download/>). This tutorial was made with version 8 update 73 of *Java*.
3. Download and install the latest stable release of *Assemble2* (www.bioinformatics.org/assemble). On this website you can also find the manual with tutorials etc. This tutorial was made with version 1.1 of *Assemble2*.
4. Open *Assemble2* and write the path of the *Chimera* executable in the popup window. This ensures that *Chimera* launches with *Assemble2*. If *Chimera* is not launched when reopening *Assemble2* look in the tutorial *How to install Assemble2?* on the *Assemble2* website for guidelines.
5. The final step to setup the “communication channel” between *Chimera* and *Assemble2* is to activate the *Read Standard Input* in *Chimera* (**Tools > Utilities > ReadStdin**) (see **Note 1** for adding *ReadStdin* to *Favorites*).

2.4 *Perl Scripts*

Two *Perl* scripts have been developed as helpful tools that speed up the design process. After the 3D motifs have been aligned to form the final 3D model the **ligate.pl** *Perl* script is used to thread the correct strand path through the structure. It reads a PDB file from a defined 5'-nucleotide and connects all the nucleotides of the different motifs into one model. The script has the syntax (**perl ligate.pl input.pdb > output.pdb**). The **trace.pl** *Perl* script is used to trace through the secondary structure and create a *NUPACK* code, which is used for the sequence design. It has the syntax (**perl trace.pl input.txt > output.txt**).

1. *Perl* is included in *OS X*, but *Windows* users have to download and install *Perl* (www.perl.org).
2. *Menlo* is the preferred font for the text editor (*TextEdit* in *OSX* and *NotePad* in *Windows*) to display the special characters in the output of the **trace.pl** *Perl* script. Download and install the

Menlo font and select it in your text editor. Alternatively, use the *Deja Vu Sans Mono* font.

- The two *Perl* scripts can be downloaded here (www.andersen-lab.dk). Save the *Perl* scripts in the directory you will be working in.

3 Methods

As an example structure to present a step-by-step protocol for designing an RNA origami we demonstrate the design process of a structure similar to the 2H-AE tile presented by Geary et al. [4]. The structure consists of two double helices connected by an anti-parallel double crossover with an even number of half turns between the crossovers, and hence the name 2H-AE.

The standard A-form RNA double helices connected by a double crossover make up the fundamental framework of the structure (Fig. 4). The kissing loop, positioned between the two crossovers, coaxially stacks the double helices and makes it possible to thread a single strand of RNA through the whole structure. At each end of the double helices a UUCG tetra loop is placed to provide stability. To reduce the stability of the DNA template and thereby help ease the synthesis and the PCR, G-U wobble pairs are inserted in stems longer

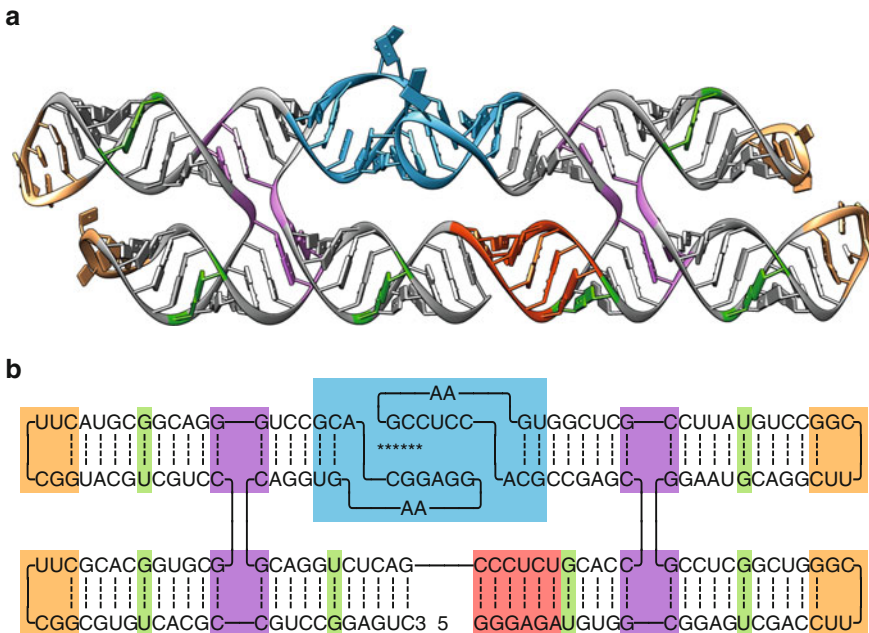


Fig. 4 The final 3D model and 2D blueprint of the 2H-AE RNA origami structure. Side view of the 3D model (**a**) and 2D blueprint (**b**) of the 2H-AE RNA origami with the sequence and structural elements of the A-form RNA double helices (*grey*), immobilized crossovers (*magenta*), kissing-loop (*blue*), UUCG tetra-loops (*orange*), G-U wobble pairs (*green*), and the T7 RNA polymerase promoter sequence (*red*)

than eight base pairs. The T7 polymerase leader sequence is incorporated at the 5'-end to provide a proper transcription initiation.

3.1 Creating a 3D Model

The 3D motifs needed to create the 2H-AE RNA origami (Fig. 4) are:

- An A-form RNA double helix.
- A 180° kissing loop.
- A UUCG tetra loop.

First we obtain the individual motifs, then we align them with respect to each other and finally we ligate the motifs together and refine the 3D model.

3.1.1 Generating a Standard A-Form RNA Double Helix

The fundamental unit upon which all the rest of the motifs are placed is the standard A-form RNA double helix. This section demonstrates how to create a double helix with a specific length and sequence.

1. Go to the *make-na server* website (<http://structure.usc.edu/make-na/server.html>) and name the duplex **Helix**. Select **A** as *Helix Type* and choose **RNA** for both *Top* and *Bottom* strands.
2. Type in a sequence of G, C, A and U with the desired length. The complementary strand will be made automatically. Here we make a 44 base pair double helix (four helix turns) by inputting the sequence **GAUGCGAUGCGAUGCGAUGACGCGUAUGCAUGCGAUCGAGCUAU**.
3. Press **make NA** and save the file *Helix.pdb* in your working directory with the *Perl* scripts. The output is an RNA double helix with two strands called chain *A* and chain *B*, which each have nucleotides with numbers from 1 to 44 (see **Note 2** for more information on PDB files). Alternatively, you can make the double helix in the program *Assemble2* (see **Note 3**).

3.1.2 Acquiring 3D Motifs

As mentioned in the introduction there are several websites where it is possible to search for specific 3D RNA motifs. This section demonstrates how to find a 180° kissing loop.

1. Go to *Search* on the *RNA junction* website (<https://rnajunction.ncifcrf.gov>), select **kissing-loop** as *Structure type*, set *Angle range* to **175–185** and press **Begin Search**.
2. Choose entry no. 13070, which is the same used in Geary et al. [4], and click on *PDB*, which leads to the *Research Collaboratory for Structural Bioinformatics Protein Data Bank (RCSB PDB)* website.
3. Under *Download Files* choose *PDB Format (Text)*. Move the file to your working directory. Rename and change the file extension to ‘.pdb’ (**KL_8B8R.pdb**). The output is a kissing-loop

with two strands called chain *A* and chain *B*, which each have nucleotides numbered from 1 to 23 (see **Note 2** for more information on PDB files).

3.1.3 Extracting an RNA Motif from a Larger Structure

Sometimes the motifs needed to build the desired RNA origami are not available as a separate PDB file, but only as part of a larger structure. This section demonstrates how to extract a small 3D motif (UUCG tetra-loop) from a larger PDB file (*PDB_id: 1F7Y*) using *Swiss-PdbViewer* (see Fig. 5).

1. Search for **1F7Y** on the *RCSB PDB* website (www.rcsb.org/). Under *Download Files* choose *PDB Format (Text)*. Move the file to your working directory. Rename and change the file extension to '.pdb' (**UUCG_1F7Y.pdb**).
2. Open the file in *Swiss-PdbViewer*, close potential warnings and close the input log. Open the *Control Panel* and *Layers Info* (**Wind > Control Panel** and **Wind > Layers Info**).
3. It is possible to hide parts of the 3D motif to create a better overview and make the 3D modeling easier. To hide all the amino acids and ions first locate them by scrolling down the list in the *Control Panel*. Remove the check mark in the *show* column next to the individual amino acids and ions you want to hide (see **Note 4** for more info on the controls in *Swiss-PdbViewer*).
4. Rename the UUCG tetra-loop and the connecting double helix, i.e., the nucleotides G30 to U39, by selecting the nucleotides in the *Control Panel*. Click on G30 and then click U39

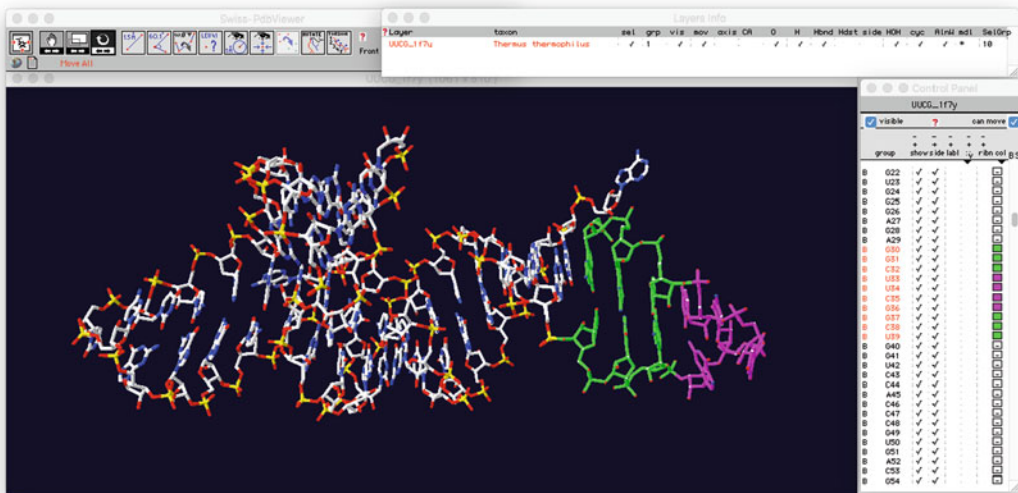


Fig. 5 Extracting an RNA motif from a larger structure using *Swiss-PdbViewer*. The nucleotides of the UUCG tetra-loop (*magenta*) and connecting double helix (*green*) are selected (marked *red*) in the *Control Panel* at the right. The selection is renumbered and saved as a separate motif

while holding down **shift**. Rename the selected nucleotides (**Edit > Rename Current Layer...**) by inputting *Layer Name: UUCG*, *Rename Chain of Selected Groups: A*, and *Renumber Selected Groups from: 1*.

5. Extract the 10 nucleotide tetra-loop motif by saving it (**File > Save > Selected Residues Of Current Layer...**) in your working directory and naming it with the file extension `‘.pdb’` (**UUCG.pdb**). You can now close *Swiss Pdb-Viewer*.

3.1.4 Positioning the Double Helices for a Double Crossover Using Chimera

The central part of the 2H-AE RNA origami is the double-crossover motif. This section demonstrates how to position two double helices correctly for a double crossover using only the command line in *Chimera*. During the steps in 3.1.4 it is important **not** to interact with the 3D view during the protocol, because the commands will not work properly if the 3D view is rotated manually. The *x*-axis (pointing right), *y*-axis (pointing up) and *z*-axis (pointing out of the screen) are static, so if the model is rotated manually the position in regards to the coordinate system will change. It is possible to arrange double helices and motifs by hand in both *Chimera* and *Swiss-PdbViewer* (see **Note 5** for Tips & Tricks on 3D modeling by hand), but for novices it is much easier and faster using the command line.

To create an antiparallel double crossover it is important that the strands that are connected by the crossovers are running in opposite directions. This protocol positions two identical double helices in such a way that the crossovers connect chain A on one double helix to chain B on the other double helix. The P atoms in the crossovers are positioned close to each other, but the nucleotides in the crossovers are not connected until later in the protocol. We color the structures to make it easier to see that the commands are correct and that we are aligning the motifs correctly.

1. Open *Chimera* and open the panels *Side View* (**Tools > Viewing Controls > Side View**), *Model Panel* (**Tool > General Controls > Model Panel**) and *Command Line* (**Tool > General Controls > Command Line**). It can be helpful to set often-used tools to open automatically or add them to *Favorites* (see **Note 1**).
2. Open *Helix.pdb* (**File > Open...**) in *Chimera*. You will see it added to the *Model Panel* with the model ID number 0. Remember that the commands in the protocol will not work if you manually manipulate the 3D view. Rename it in *Model Panel* by scrolling down, selecting **rename...** and writing **Helix 1**. Then click **OK**.
3. Repeat **step 2**, but rename the double helix **Helix 2**. You will see it added to the *Model Panel* with the model ID number 1.

4. Change the representation of the two double helices to see all the atoms and bonds. Write **select** in the *command line* to select all the atoms and press **Enter** (all commands in *Chimera* are executed by pressing **Enter**, which will not be mentioned in the remaining method). Open the *Nucleotides* panel (**Tools > Depiction > Nucleotides**) and select *Show backbone as: atoms & bonds* and select *Show side (sugar/base) as: atoms & bonds*. Then click **OK** and use the command **~select** to deselect all.
5. Color the two double helices, specific nucleotides and atoms to easily identify the eight nucleotides that are involved in the double crossover, and the four P atoms used to align the double helices correctly. Use the command **color grey** to paint all the atoms grey. Color the nucleotides *11*, *12*, *33*, and *34* on chain *A* in *Helix 1* yellow by using the command **color yellow #0:11-12.A,33-34.A** (see **Note 6** for the syntax of *Chimera* commands). Color the P atom on nucleotide *12* and *34* red with the command **color red #0:12.A,34.A@P**. Do the same for *Helix 2*, but hide *Helix 1* to see the coloring, since the double helices are still overlapping. To hide *Helix 1*, go to the *Model Panel* and remove the check mark in the *S* (for Show) box next to *Helix 1*. Color the nucleotides *11*, *12*, *33*, and *34* on chain *B* in *Helix 2* yellow by using the command **color yellow #1:11-12.B,33-34.B**. Color the two P atoms red with the command **color red #1:12.B,34.B@P**. Show *Helix 1* again with a check mark in the *S* box in the *Model Panel*.
6. Positioning the helical axis of the two double helices in the same plane (the current z-y plane) will make the manipulation of the two double helices easier using the command line. To get a symmetrical and unstrained double crossover we also position the P atoms of the crossovers in that plane. Use the command **turn z -17** to rotate both double helices so that a line from the center of the double helices to the P on *Helix 1* is vertical and pointing down, because we want to position *Helix 2* below *Helix 1* (Fig. 6a).
7. Now we can use the geometric parameters of the standard A-form double helix from previously published work [5] to position the two double helices for a double crossover. The angle between the P on chain *A* in *Helix 1* and the P on chain *B* in *Helix 2* is calculated as:

$$\text{Axis} - \text{Twist} = 139.9^\circ - 32.73^\circ = 107.17^\circ$$
 Rotate *Helix 2* so that a line from the center of the double helices to the P on chain *B* in *Helix 2* is vertical and pointing up. The position is 180° around the helical axis from the P on chain *A* in *Helix 1*, so we have to rotate *Helix 2*:

$$180^\circ - 107.17^\circ = 72.83^\circ$$
 Use the command **turn z 72.83 model #1** to perform the rotation and see the yellow nucleotides both in the top and on the bottom of the double helices in the *Side View*.

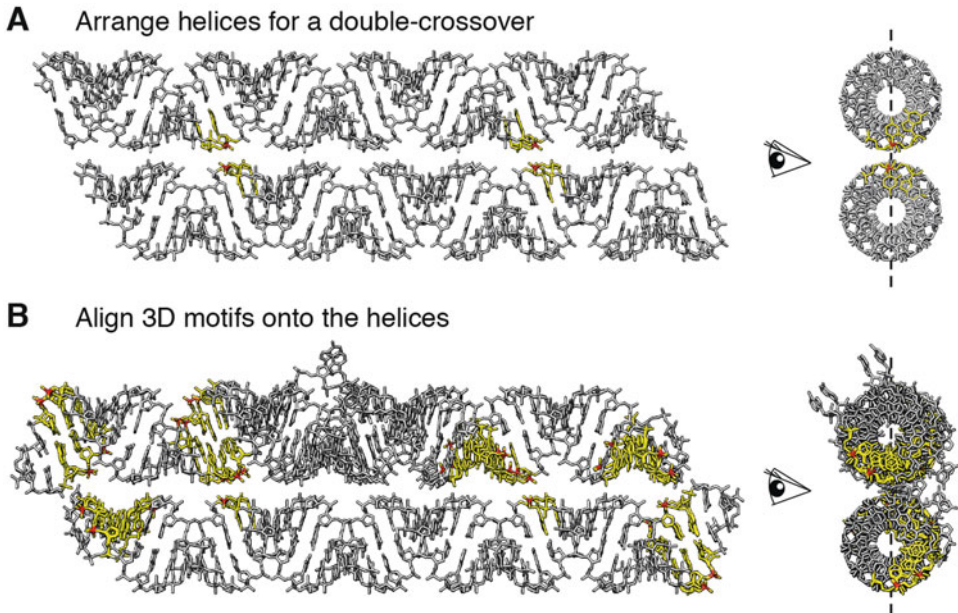


Fig. 6 Arranging double helices and aligning 3D motifs onto them. Two double helices correctly positioned for a double-crossover (**a**) with four tetra loops and a kissing loop aligned onto them (**b**). Eye symbol on helix side-view defines end-view. The P atoms (*red*) and connecting nucleotides (*yellow*) are used to position the two double helices correctly for a double crossover. The P atoms are in the same plane as the helical axes (**a, right**) and directly above and below each other along the helical axes (**a, left**). A tetra loop is aligned at each end of the double helices and a kissing loop is aligned on the top double helix between the two crossovers (**b**)

8. Separate the two double helices by translating *Helix 2* downwards so that it is parallel with *Helix 1* by using the command **move y -22 model #1**. The separating distance will influence the double crossover and empirical data from modeling reveals an optimal distance around 2 Å, and the double helix itself is 20 Å, resulting in 22 Å in the command.
9. Rotate both double helices to better view the position of the colored nucleotides. We rotate around the *y*-axis with the command **turn y 90** and click **View All** in the *Side View* panel to scale the view and include all displayed atoms.
10. The distance measured parallel to the double helix axis (now the *x*-axis) between the P on chain *A* in *Helix 1* and the P on chain *B* in *Helix 2* can be calculated from the geometric parameters presented in the introduction as:

$$\text{Rise} - \text{Inclination} = 2.81 \text{ \AA} - (-7.45 \text{ \AA}) = 10.26 \text{ \AA}.$$
 To translate *Helix 2* to the proper position for the double crossover use the command **move x 10.26 model #1**.
11. Click **View All** in the *Side View* panel, save your work (**File > Save Session As...**) and name it **1_2H-AE_helices.py**.

3.1.5 Arranging the Tetra-Loop Motifs on the Double Helices Using Chimera

Next we position the four tetra-loops onto the ends of the two double helices. This operation is made simple by the *match* command, which fits a selection of atoms from one model to a selection of atoms on another model. To achieve a realistic model we recommend that at least a couple of base pairs overlap when connecting two motifs. If fewer base pairs overlap it can be difficult to fit the motifs properly and undesired bends or kinks where the base stacking is not modeled correctly can occur. While it is possible to arrange the motifs on the double helix by hand the *match* command makes it a lot quicker. Again we color the structures to make it easier to see that the commands are correct and that the motifs are aligned correctly.

1. Continue to have the *I_2H-AE_helices.py*-session open, containing the aligned *Helix 1* and *Helix 2*. Load four tetra-loops into *Chimera* by opening (**File > Open...**) *UUCG.pdb* four times. You will see them added to the *Model Panel* with the model ID numbers 2-5. Click **View All** in the *Side View* panel to see all the motifs.
2. Rename the first tetra loop in the *Model Panel* by scrolling down, selecting **rename...** and writing **Loop 1**. Then click **OK**. Repeat for the other three tetra loops and rename the second **Loop 2** etc.
3. The representation of the tetra loop might not need to be changed to see all the atoms and bonds, but the protocol is as in **step 4** in Subheading 3.1.4. Use the command **select #2,3,4,5** to select all four tetra loops. Open the *Nucleotides* panel (**Tools > Depiction > Nucleotides**) and select *Show backbone as: atoms & bonds* and select *Show side (sugar/base) as: atoms & bonds*. Then click **OK** and use the command **~select** to deselect all.
4. Color the six nucleotides and the four P atoms used to align the tetra-loop correctly with the double helices. First use the command **color grey #2,3,4,5** to paint all the tetra loops grey. Color the nucleotides 1-3 and 8-10 in *Loop 1-4* yellow by using the command **color yellow #2,3,4,5:1-3,8-10**. Color the P atom on nucleotide 2, 3, 9, and 10 in *Loop 1-4* red with the command **color red #2,3,4,5:2-3,9-10@P**. Color the corresponding nucleotides and P atoms in *Helix 1* and *Helix 2* with the commands **color yellow #0,1:1-3,42-44** and **color red #0,1:2-3,43-44@P**.
5. To align the tetra loop onto the end of the double helices we use the *match* command. The *match* command fits the specified atoms in one model to the specified atoms in another model. The first atom in the first model is fitted to the first atom in the second model etc. (see **Note 6** for the syntax of *Chimera* commands). Use the command **match #2:2-3,9-10@P**

#0:43-44.B,2-3.A@P to align *Loop 1* to one end of *Helix 1* and the command **match #3:2-3,9-10@P #0:43-44.A,2-3.B@P** to align *Loop 2* to the other end of *Helix 1*. In the same way the commands **match #4:2-3,9-10@P #1:43-44.B,2-3.A@P** and **match #5:2-3,9-10@P #1:43-44.A,2-3.B@P** aligns *Loop 3* and *Loop 4* to the ends of *Helix 2*.

6. Click **View All** in the *Side View* panel, save your work (**File > Save Session As...**) and name it **2_2H-AE_loops.py**.

3.1.6 Arranging the Kissing-Loop Motif on the Double Helix Using Chimera

Due to the deviation from standard A-form double helix of the kissing-loop motif the positioning is a bit more difficult. While it is possible to arrange the motifs on the double helix by hand in *Chimera* or *Swiss-PdbViewer* the command line in *Chimera* makes it a lot quicker.

We start by aligning one side of the kissing loop in the same procedure as for the tetra loop. Once the kissing loop is aligned on one side we can determine the nucleotides to align it to on both side at the same time to get the best alignment. We first align four P atoms on one side of the kissing-loop to four P atoms on the double helix between the crossovers. Remember the kissing-loop has a chain A and B each with nucleotides 1–23. We start by aligning 2–3, 22–23 on chain A. The kissing-loop is to be incorporated on *Helix 1* somewhere between the two crossovers. The length of the kissing-loop motif almost spans the full length between the crossovers, which restricts the number of possible positions. See the final position of the kissing-loop in Fig. 6b.

1. Continue to have the *2_2H-AE_loops.py*-session open, containing the aligned *Helix 1* and *Helix 2* and all four tetra-loops. Load the kissing-loop into *Chimera* by opening (**File > Open...**) *KL_8B8R.pdb*. You will see it added to the *Model Panel* with the model ID number 6. Click **View All** in the *Side View* panel to see all the motifs.
2. Rename the kissing-loop in the *Model Panel* by scrolling down, selecting **rename...** and writing **KL**. Then click **OK**.
3. The PDB file of the kissing-loop contains multiple ions, which are not needed for the modeling and can be removed with the command **show #6:1-23**, which shows only the nucleotides 1–23 on both chains.
4. Change the representation of the kissing-loop with the same protocol as in **step 4** in Subheading 3.1.4. Use the command **select #6** to select the kissing-loop. Open the *Nucleotides* panel (**Tools > Depiction > Nucleotides**) and select *Show backbone as: atoms & bonds* and select *Show side (sugar/base) as: atoms & bonds*. Then click **OK** and use the command **~select** to deselect all.

5. Color the three outermost base pairs on each side of the kissing-loop and the eight P atoms used to align the kissing-loop correctly onto the double helix. First use the command **color grey #6** to paint the whole kissing-loop grey. Color the nucleotides *1-3* and *21-23* on chain *A* and *B* in *KL* yellow by using the command **color yellow #6:1-3,21-23**. Color the P on nucleotide *2*, *3*, *22*, and *23* on chain *A* and *B* in *KL* red with the command **color red #6:2-3,22-23@P**.
6. We first color the nucleotides and P in *Helix 1* where we will align one side of the kissing-loop, specifically the nucleotides *11-13* on chain *A* and *32-34* on chain *B* in *Helix 1* and the four P atoms that connects them. Use the commands **color yellow #0:11-13.A,32-34.B** to color the nucleotides and **color red #0:12-13.A,33-34.B@P** to color the P atoms.
7. Align one side of the kissing-loop to *Helix 1*, specifically the nucleotides *2*, *3*, *22*, and *23* on chain *A* in *KL* is aligned with the nucleotides *11-13* on chain *A* and *32-34* on chain *B* in *Helix 1*, using the command **match #6:2-3.A,22-23.A@P #0:12-13.A,33-34.B@P**.
8. To align the other side of the kissing-loop we choose the nucleotides in the double helix that fits the best (by hovering the cursor over a nucleotide a small box with the model number, chain, nucleotide, and atom info will appear). To find the nucleotides for the best fit it can be beneficial to move the kissing-loop by hand (see **Note 5** for Tips & Tricks for 3D manipulation by hand). Empirical modeling data shows that the best fit with the lowest RMSD is obtained with the command **match #6:2-3.A,22-23.A,2-3.B,22-23.B@P #0:12-13.A,33-34.B,13-14.B,32-33.A@P**. It aligns the kissing-loop to the double helix in a position between the crossovers, with six base pairs from one of the crossovers to the kissing-loop and seven base pairs from the other crossover to the kissing-loop.
9. Click **View All** in the *Side View* panel, save your work (**File > Save Session As...**) and name it **3_2H-AE_KL.py**. The next steps are performed in *Swiss-PdbViewer*, which does not read the '.py'-format. Save the *Chimera* session as PDB files (**Save > Save PDB...**) and name them **3_2H-AE_\$name.pdb**, select all the models in *Save models:* and select *Save multiple models in multiple files* in your working directory. Close *Chimera*.

3.1.7 Merging and Ligating the PDB File

Here we use *Swiss-PdbViewer* to merge the selected nucleotides of the different motif into one layer. We hide the overlapping base pairs so only the ones that are to make up the final structure are shown, define the crossovers by renaming the nucleotides chain names, merging the motifs into a single structure, define the 5'-end and use the **ligate.pl** *Perl* script to thread the correct strand path.

1. Open *3_2H-AE_Helix 1.pdb* and the six other PDB files named *3_2H-AE_* in *Swiss-PdbViewer*, close potential warnings and the input log. Open the *Control Panel* and *Layers Info* (**Wind > Control Panel** and **Wind > Layers Info**).
2. Hide overlapping base pairs by removing the check mark in the *show* column in the *Control Panel*, so only the nucleotides making up the final model are shown.
 - (a) For the UUCG tetra-loops only show the four nucleotides loop and the G–C base pair next to the loop and hide the two other base pairs. Select **3_2H-AE_Loop 1** in *Layers Info* and remove the check mark next to nucleotide **1–2** and **9–10** in the *show* column in the *Control Panel*. Repeat the process for the three other tetra-loops.
 - (b) The outermost base pair in both ends of the two double helices are also hidden, so that no nucleotides are overlapping. Select **3_2H-AE_Helix 1** in *Layers Info* and remove the check mark in the *show* column next to nucleotide **1** and **44** on both chain **A** and **B**. Do the same for *Helix 2*.
 - (c) For the kissing-loop we hide the two outermost base pairs on each side of the loop. Select **3_2H-AE_KL** in *Layers Info* and remove the check mark in the *show* column next to the nucleotides **1–2** and **22–23** on both chain **A** and **B**.
 - (d) The base pairs on the central part of the corresponding double helix (*Helix 1*), which the kissing-loop is going to replace, are also hidden, so that no nucleotides are overlapping. Select **3_2H-AE_Helix 1** in *Layers Info* and remove the check mark in the *show* column next to the nucleotides **13–31** on chain **A** and the nucleotides **14–32** on chain **B**.

The base pairing of the merged structure might be disrupted if the merging pattern is a sticky-end, but is kept intact if a blunt-end merging pattern is created (Fig. 7a). It is important to hide or show base pairs and not single nucleotides, since this will determine the merging pattern between two motifs.

3. Prepare the structure for ligation by indicating the double-crossover. The ligation script reads the structure from a specified 5'-end and searches for the next P atom on that chain. If a P atom is not found within a distance threshold the search continues on other chains. This feature is used to direct the strand path to another strand using chain names. When the nucleotide pair that are to connect to each other in a crossover from one double helix to another have the same chain name (e.g., *X*) and the two other connecting nucleotides in the crossover have a different chain name (e.g., *Y*), the script will connect the nucleotides on different strands with the same

chain name rather than continue along the helix to a nucleotide with a different chain name. This feature can also be used to circumvent two motifs unintentionally ligating (*see Note 7*). Rename the chains of the four pairs of nucleotides in the crossovers, i.e., A11-B34, A12-B33, A33-B12, and A34-B11 (the nucleotides colored in **step 5** in Subheading 3.1.4). Select one nucleotide at a time in *Control Panel* and *Rename Chain of Selected Groups*: (**Edit > Rename Current Layer...**). The chain names of the four pairs of nucleotides could be renamed e.g., X, Y, Z, and Q (see example in the insert in Fig. 7).

4. In *Control Panel* select all the **shown** nucleotides for each layer and merge the selections (**Edit > Create Merged Layer from Selection (by column)**). To see that all the nucleotides have been merged properly hide all other layers than the new *_merge_* layer by removing the check mark in the *vis* column in *Layers Info*.

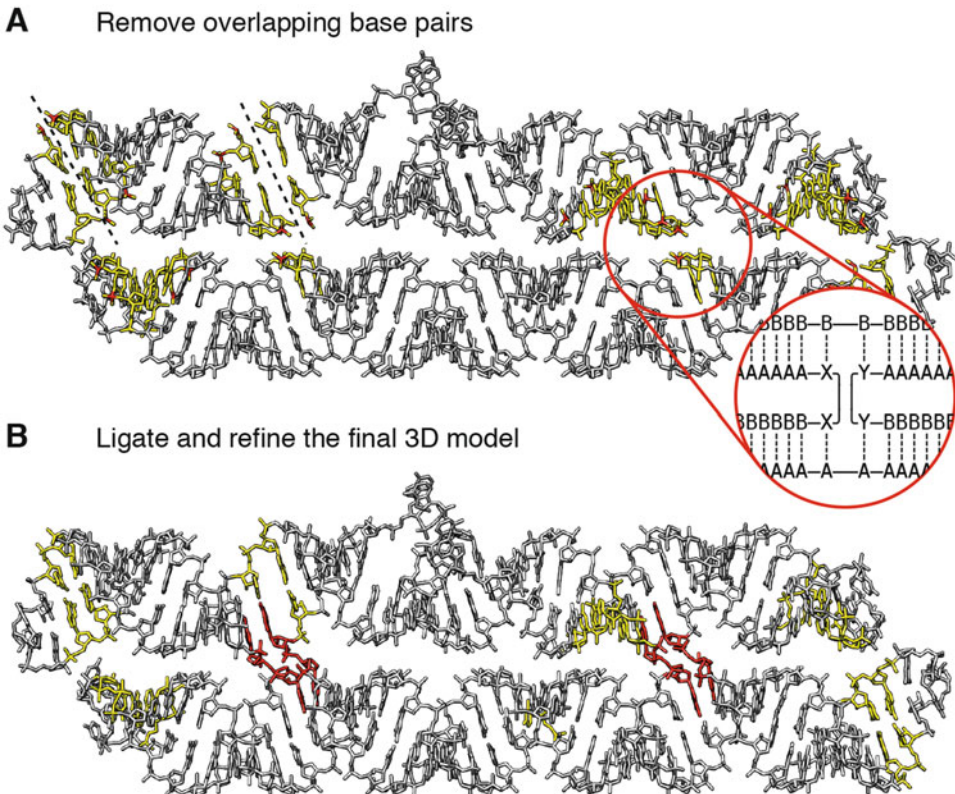


Fig. 7 Connecting the 3D motifs and refining the 3D model. Overlapping base pairs are removed, so that only the nucleotides for the final model remain (**a**). The merging pattern should always be blunt end and not sticky end. Examples of blunt end merging points are shown in dotted lines. The insert shows an example of chain names for the nucleotides in the crossover that guide the *ligate.pl Perl* script to form the correct strand path. The refined 3D model (**b**) with merged crossovers (*red*) and merged nucleotides (*yellow*) at the blunt end merging points

5. Renumber the nucleotides by selecting **_merge_** in *Layers Info* and selecting all nucleotides in *Control Panel*, then (**Edit > Rename Current Layer...**) and *Renumber Selected Groups from: 2*.
6. Specify the 5'-end of the structure, which we choose to be on chain *A* in *Helix 2* midway between the crossovers, i.e., nucleotide *A23*. Select **Helix 2** in *Layers Info*, unhide it by adding the check mark in the *vis* column, and color the nucleotide **A23** in *Control Panel* for easy recognition. Rotate the structure to a position where the colored nucleotide is easily visible. Hide *Helix 2* and select the corresponding nucleotide in the **_merge_** structure using the **Pick atom** tool (Fig. 9) in the *Toolbar* and click on the nucleotide in the 3D view. See that it is selected in *Control Panel* and (**Edit > Rename Current Layer...**) *Renumber Selected Groups from: 1*.
7. Save the project (**File > Save > Project (all layers)...**) as **4_2H-AE_project.pdb**. Select the **_merge_** layer in *Layers Info* and save the structure (**File > Save > Current Layer...**) as **4_2H-AE_merged.pdb** and close *Swiss-PdbViewer*.
8. To ligate the structure open a *Terminal* (in *Windows* open *Perl (command line)*) and change directory to the folder containing your model *4_2H-AE_merged.pdb* and the *Perl* script *ligate.pl* by writing **cd** and the path of the folder (*see Note 8*). Write the following command to run the ligate script and output a new PDB file named *5_2H-AE_ligated.pdb* (**perl ligate.pl 4_2H-AE_merged.pdb > 5_2H-AE_ligated.pdb**) and press **Enter**.
9. Open *5_2H-AE_ligated.pdb* in *Chimera* to see that the strand path has been made correctly (*see Note 7* if the strand path is incorrect).

3.1.8 Refining and Evaluating the 3D Model

The final step of the 3D model design process is to refine the structure and evaluate if further iteration of the 3D modeling is needed or if we can proceed with the secondary structure and sequence design.

1. Open *Assemble2* and remember to connect *Chimera* with the *ReadStdin* (**Tools > Utilities > ReadStdin**) if it is not done automatically. Open *5_2H-AE_ligated.pdb* in *Assemble2* (**File > Load > RNA Tertiary Structure... > from a PDB file**). A secondary structure is shown in *Assemble2* and the 3D model is shown in *Chimera*.
2. Select the whole secondary structure by clicking the 5'-nucleotide, then **shift-click** on the 3'-nucleotide.
3. Refine the selected nucleotides by clicking the **gears** symbol in *Assemble2* and choose 10 iterations (*see Note 9*). The iteration process can be monitored in the *Terminal* with iteration number, number of deviating distances and the global deviation. When the refinement is finished a second structure appears in *Chimera*.

4. Save the refined model as **6_2H-AE_refined.pdb** from *Chimera* (**Actions > Write PDB...**) and make sure to choose only the refined model under *Save models*. The 3D model is complete, but should be evaluated before proceeding with the sequence design.
5. There are several ways to evaluate the quality of the 3D model.
 - (a) Open *6_2H-AE_refined.pdb* in *Assemble2* (**File > Load > RNA Tertiary Structure... > from a PDB file**) and confirm that all the base pairs in the secondary structure are still intact.
 - (b) Open *6_2H-AE_refined.pdb* in *Swiss-PdbViewer* and inspect the distances between neighboring base pairs at the ligation sites to look for bonds and angles that deviate from normality. Also inspect the two crossovers to see that they are not entangled.

If the structure quality is poor, iterate the design process by going back to an earlier version of the model and manipulate the trouble area using the tools presented in the sections above and in Subheading 4.

3.2 Converting the 3D Model to a Secondary Structure

After the 3D model has been refined and evaluated to be of an acceptable quality the secondary structure is the focus of the remaining design process. The **trace.pl** *Perl* script is used to make the handling of the structure-to-sequence process easier. First a secondary structure blueprint is made by rewriting the structure from *Assemble2*, then sequence restraints such as the sequence of the kissing-loop are implemented in the blueprint and finally the *Perl* script outputs a code, which can be used to design the sequence in *NUPACK*.

3.2.1 Create a Blueprint from the Secondary Structure

This is a rather tedious task where the current design process has not been automated yet. The basic procedure is to copy the secondary structure from *Assemble2* into a text file.

1. Open *6_2H-AE_refined.pdb* in *Assemble2* (**File > Load > RNA Tertiary Structure... > from a PDB file**), enlarge the 2D view of *Assemble2* and close *Chimera*, which will not be needed for this procedure.
2. Arrange the secondary structure in *Assemble2* to look like the secondary structure in Fig. 8a. To manipulate the secondary structure, select the section of the structure you want to manipulate by clicking on the 5'-end of the desired section and **shift**-click on the 3'-end of the section (*see Note 10* for selection in *Assemble2*). Press **alt/option** while left-clicking to rotate the selection or **alt/option** while right-clicking to move the selection.

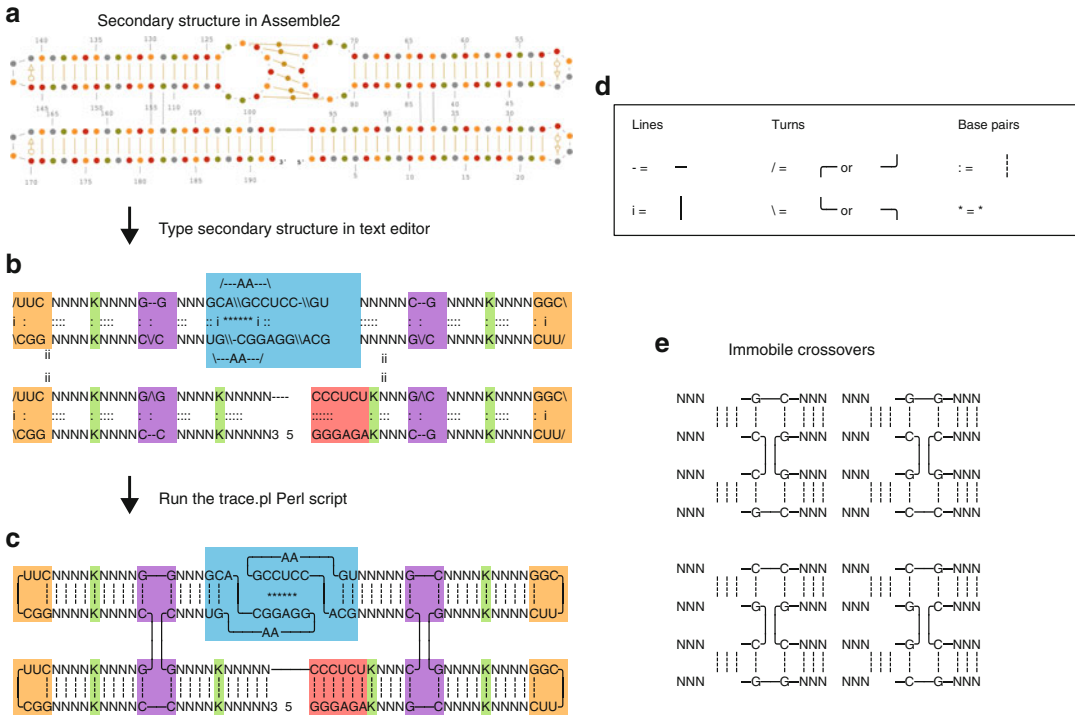


Fig. 8 Creating the 2D blueprint. *Assemble2* shows the secondary structure (a) of the 3D model. The secondary structure is copied to a text file (b) by typing it using the characters in (d). After the sequence constraints, e.g., immobilized crossovers (e), have been added the *trace.pl* Perl script can output a blueprint with a refined secondary structure (c)

3. Open a new *TextEdit* file (*NotePad* in *Windows*) and type the secondary structure from *Assemble2* by hand. Only specific sequences to be incorporated in the structure, e.g., the UUCG tetra-loops, are specified in the secondary structure blueprint file. The unspecified sequences, i.e., double helices, are written with N. See Fig. 8d for a cheat sheet for typing the secondary structure in *TextEdit*.

3.2.2 Implement Sequence Constraints

The sequence of the 3D model is not the final sequence, but only serves as a guide for the proper three-dimensional structure. The final sequence is designed using *NUPACK*. Specific sequence constraints are implemented to insure proper transcription initiation and trouble-free DNA synthesis.

1. At the 5'-end of the structure the consensus sequence of the +1 to +6 of the T7 RNA polymerase is incorporated [7]. Both the promoter (*GGGAGA*) and its complementary sequence (*UCUCCC*) are specified in the secondary structure (red nucleotides in Fig. 8b).

2. The base pairing sequence of the natural HIV DIS kissing-loop is *GCGCGC*, but multiple different sequences have previously been used in RNA nanotechnology [4, 8, 9]. Pick one of the kissing-loop sequences from the previous papers.
3. Because the crossovers are stacked Holliday junctions they have the possibility to branch migrate if there are sequence complementarities on the different double helices near the crossovers. G–C pairs are positioned strategically on all four sides of the crossovers to immobilize the double-crossover in a static position. There are four different configurations to immobilize a crossover (Fig. 8c).
4. To reduce secondary structure in the DNA template, which can interfere with the synthesis of the DNA, a G–U wobble pair is incorporated for every eight base pairs of double helix. The letter **K** specifies G–U wobbles and during the sequence design *NUPACK* will incorporate either G–U or U–G pairs at these positions (green nucleotides in Fig. 8b).
5. Convert the *TextEdit* file to plain text (**Format > Make Plain Text**), which can be read by the *Perl* script. Add spaces around the structure, so that each of the four sides of the structure has at least one row or column of spaces around it. Save the file (**File > Save**) as *7_2H-AE_raw.txt*.

3.2.3 Trace the Blueprint and Get a Design Code for *NUPACK*

1. To create a code for the sequence design in *NUPACK* open a *Terminal* (in *Windows* open *Perl (command line)*) and change directory to the folder containing the *7_2H-AE_raw.txt* and the *Perl* script *trace.pl* by writing **cd** and the path of the folder (see **Note 8**). Run the *Perl* script (**perl trace.pl 7_2H-AE_raw.txt > 8_2H-AE_nupack.txt**).
2. The file *8_2H-AE_nupack.txt* contains a refined version of the blueprint (as in Fig. 8c) and a description of the trace, i.e., where the 5'-end is found, if the structure was successfully traced, how many nucleotides are in the blueprint and how many nucleotides were found between the 5'-end and 3'-end, which should be the same. The file also provides an output of the sequence and the structure in dot-bracket notation, which is useful for illustrations of the arc-diagram (see **Note 11**). At the bottom of the file is the *NUPACK* code.

3.3 Sequence Design and Evaluation

The final part of the design process is the sequence design. Here we use *NUPACK*, which is available online and has a user-friendly interface that allows you to both design and analyze sequences. The *trace.pl* *Perl* script outputs a *NUPACK* code, which is used by *NUPACK* to design a sequence that will fold into the designed secondary structure. To obtain a sequence with the proper quality multiple repetitions of the steps in this section might be necessary.

3.3.1 Designing Sequences

1. Open *NUPACK* (www.nupack.org/) in your web browser and click the **Design** tab.
2. Copy-paste the *NUPACK* code from the bottom of *8_2H-AE_nupack.txt* into the *Target structure* box on the *NUPACK* design page.
3. Press update to see the secondary structure in *Preview*. You can change the parameters in *Target structure* (see **Note 12**), but we recommend that you use the standard settings.
4. Click **Design** at the bottom of the page to start the sequence design. *NUPACK* will output the designs as a list of sequences with calculated normalized ensemble defects (NEDs).

3.3.2 Evaluating the Folding of Different Sequences

The calculated NED from *NUPACK* is the first parameter used to evaluate and compare the sequences. The lower the NED the better compliance with the structure. GC content is also a parameter and although not the most critical factor it should be kept low not to cause difficulties with the PCR. To further evaluate the folding of a particular sequence *mFold* provides a user-friendly output with more structure information about the suboptimal folded structures, which can be minimized. This step becomes more important when you design bigger structures.

1. Make an *Excel* sheet with the columns **Design Name**, **Sequence #**, **NED**, **GC %**, **ΔG** , **2nd ΔG** and **Sequence**.
2. Choose around 10 sequence outputs with low normalized ensemble defect (obtained from multiple *NUPACK* design runs), copy the sequences to the excel sheet, give them a name and sequence number and write their NED.
3. To fill out the rest of the information in the *Excel* sheet perform **steps 4** and **5** for each of the ten sequences.
4. Open *NUPACK* (www.nupack.org) and select **Analysis**. Copy-paste the sequence into the *strand1* box in *Strand species*. Use the default settings (*Nucleic acid type: RNA*, *Temperature: 37 °C*, *Number of strand species: 1*, *Maximum complex size: 1*) and press **Analyze**. The result will give you the predicted secondary structure. Press **To Utilities** at the bottom, which will give you more information in the *Details* box, e.g., the percentages of each nucleotide, which you can use to fill out the *GC %* column in the *Excel* sheet.
5. Open *mFold* (<http://unafold.rna.albany.edu/?q=mfold/RNA-Folding-Form>) and copy-paste the sequence into the appropriate box and press **Fold RNA** at the bottom. On the result page under *View Individual Structures* you get a list of the folded structure(s) each with their own ΔG . Fill in the information in the *Excel* sheet with ΔG for structure 1 and *2nd ΔG* for structure 2 of the outputted structures. Preferably you should only

get a single structure. If multiple structures are outputted the fewer the better and the bigger difference in ΔG between structure 1 and structure 2 the better. By modifying the sequence it is often possible to remove undesired suboptimal folds (*see* Subheading 3.3.3).

6. From the overview in the *Excel* sheet you can choose the optimal sequence candidate from your sequence pool. The best sequence is the one that has a combination of low normalized ensemble defect, not too high GC content ($\leq 65\%$), a low ΔG from only one structure fold in *mFold* or a big difference between ΔG and *2nd* ΔG .

3.3.3 Optimizing the Folding of a Sequence

If the output from *mFold* gives multiple structures the suboptimal structures can often be removed by subtle changes in the sequence, e.g., changing a G–C pair to a C–G pair can remove unwanted off-target structures and still promote folding of the correct structure. Here is a short protocol for optimizing the desired fold of your designed structure.

1. Print the secondary structure outputs from *mFold* and identify nucleotides that base pair differently in the designed structure fold and the off-target structure fold. If some of the nucleotides are part of the constrained nucleotides, e.g., the T7 leader, immobilized crossovers, tetra-loops, or the kissing-loop (*see* Subheading 3.2.2), they cannot be changed, but the rest can be manipulated to obtain a better fold.
2. Identify a strong undesired secondary structure in the off-target fold, e.g., a stem of three or more G–C pairs, and mark the same nucleotides in both the target and off-target fold.
3. Change a base pair, e.g., G–C to C–G, in the target fold that will disrupt the strong undesired secondary structure in the off-target fold. Changing G–C pairs to A–U pairs can also be attempted and will decrease the GC content.
4. Iterate this process by submitting the new sequence to *mFold* and continue if it compares favorably to the former sequence. It is not always possible to remove all the undesired suboptimal folds, but this process will create a bigger difference in ΔG between the desired fold and the off-target folds, which gives a higher probability of folding the designed structure.

3.3.4 Designing Primers

Depending on what application is intended for your RNA origami structure you will have to transcribe it from either a PCR product or a plasmid. If the RNA origami is to be made by run-off transcription from a PCR product the reverse primer will have to bind to the 3'-end of your structure. The sequence design of the structure might have to be iterated if the reverse primer contains undesired secondary structure or can form primer dimers.

1. Convert your chosen RNA sequence to DNA and attach the T7 promoter sequence **CTAATACGACTCACTATA** to the 5'-end. The underlined nucleotide is not part of the promoter but have been shown to increase the transcription [10].
2. Use the T7 promoter and the 5'-end of the sequence to create the forward primer from or add another sequence upstream of the T7 promoter to use as primer site.
3. Use the **reverse compliment** of the 3'-end of the sequence to create the reverse primer. It might be necessary to add a T7 terminator if the structure is to be incorporated into a plasmid, but this is not covered in this protocol.
4. Go to the *NEB Tm Calculator* website (<http://tmcalculator.neb.com/>) and select the PCR kit you prefer to use. Copy-paste the first 30 nucleotides from the 5'-end into the *Primer 1* box and the reverse complement of the last 30 nucleotides from the 3'-end into the *Primer 2* box. Delete one nucleotide at a time from the 3'-end of the primers until the annealing temperatures are within the recommended temperature range.

4 Notes

1. We recommend adding often-used tools to *Favorites* in *Chimera* and setting certain panels to open automatically (especially *ReadStdin* is recommended to make *Auto Start*, to secure the connection to *Assemble2*). Go to (**Favorites > Preferences...**) and check mark both the *Auto Start* and *In Favorites* boxes for **Command Line**, **Model Panel**, **Side View** and **ReadStdin**, and also check mark the *In Favorites* box for **Sequence** and **Nucleotides**.
2. It is possible to order or manipulate a PDB file directly in a text editor. Some PDB files have a lot of information that is not important for the 3D motif, e.g., authors, source and remarks. The information about the 3D motif is stored in the rows that start with ATOM. Each row has all the information about that particular atom in the following columns; atom serial number, atom name, nucleotide, chain name, nucleotide number, x-coordinate, y-coordinate, and z-coordinate. For more information see the PDB file format documentation (www.wwpdb.org/documentation/file-format).
3. To make a standard A-form RNA double helix in *Assemble2* you can make a fasta-file with the full sequence of both strands in the double helix and put a UUCG tetra-loop between the two strands. The example below is for a 10 bp double helix.
>helix
CGAUGCGAUCUUCGGAUCGCAUCG

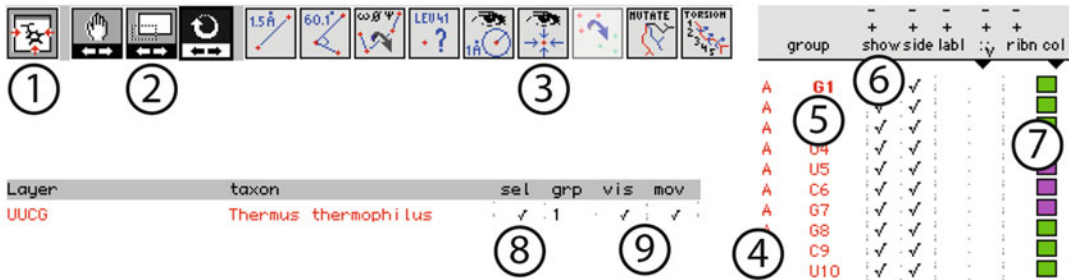


Fig. 9 The controls in *Swiss-PdbViewer*. The Toolbar (1–3), Control panel (4–7) and Layers info (8, 9) are the main controls. (1) Center the view on all shown layers. (2) Translate, zoom or rotate. (3) Pick atom and center of rotation. (4) Chain name. (5) Nucleotide number. (6) Hide a single nucleotide by removing the check mark in the *show* column. (7) Change the color of a nucleotide. (8) Select a layer by putting a check mark in the *sel* column. (9) Only the layers with a check mark in the *vis* and *mov* columns are visible and movable, respectively

Save the text-file as *.fasta* and open it in *Assemble2* (**File > Load > RNA Molecule(s)**). Chose a secondary fold in the *1: 2D Folds* menu at the bottom and see the secondary structure in the main view panel. Select the double helix by clicking on the first nucleotide 3 times. Click on the **hammer** symbol to generate the 3D fold and see the 3D model in *Chimera*. Save the PDB file from *Assemble2* (**File > Export > 3D model as PDB file**).

- The most often used controls in *Swiss-PdbViewer* are found in the *Toolbar*, *Layers Info*, and *Control Panel* (Fig. 9). It is possible to change between translate, zoom, and rotate by selecting it in the *Toolbar* (2 in Fig. 9) or with the Tab key. When using a mouse and rotation is selected the left mouse button rotates, the right mouse button translates and left + right mouse button zooms. The rotation can be locked to only rotate around one axis at a time, which makes it easier to manipulate motifs by hand in 3D. The control, alt/option and command keys lock the rotation around the *x* (pointing to the right), *y* (pointing up), and *z*-axis (pointing out of the screen), respectively. The center of rotation can be selected to be either a specific atom or nucleotide. With the center on atom tool (3 in Fig. 9) in the *Toolbar* a single atom is chosen as the center of rotation by clicking on the atom in the 3D view, while a nucleotide can be chosen as center of rotation in the *Control Panel* by option-clicking (alt/option + left click) on the nucleotide (5 in Fig. 9). By removing or adding a check mark in the *show* column in the *Control Panel* (6 in Fig. 9) nucleotides can be hidden or shown, respectively. Multiple nucleotides can be selected by clicking on the nucleotide name and dragging or by using the standard shortcut keys *command* and *shift*. It is also possible to select all nucleotides in the same chain simply by clicking on the chain name in the *Control Panel* (4 in

Fig. 9). When multiple nucleotides are selected (shown in red in the *Control Panel*) they can be shown or hidden with the + or – above the *show* column. Nucleotides can be colored by clicking (and dragging) the box in the *col* column (7 in Fig. 9) the *Control Panel*. Entire layers can be shown or hidden by adding or removing a check mark in the *vis* column in the *Layers Info* (9 in Fig. 9). Clicking the centering button in the *Toolbar* (1 in Fig. 9) centers all visible layers and changes the center of rotation. Selecting a subset of layers by adding or removing check marks in the *sel* column in *Layers Info* (8 in Fig. 9) and make the selection of layers to move a lot easier. Only layers with a check mark in the *mov* column in *Layers Info* (9 in Fig. 9) are movable. Clicking on *mov* check marks only the layers selected in the *sel* column, while right clicking on any of the check marks in the *mov* column removes all check marks in that column. More information about *Swiss-PdbViewer* can be found on the website <http://spdbv.vital-it.ch>.

5. Tips & Tricks on 3D modeling by hand in both *Chimera* and *Swiss-PdbViewer*.
 - (a) When manipulating 3D models by hand we recommend first choosing which motif/layer is the static model to which the rest is aligned and stick to that decision.
 - (b) Only manipulate the static model if you manipulate all the rest of the motifs at the same time, so that the position of the motifs relative to the static model is only changed when manipulating one of the motifs.
 - (c) Focus on one motif at a time.
 - (d) Go from big to small manipulations, i.e., start by positioning the motif approximately at the desired position simply by translating it multiple times from different directions, then rotate the motif (is made easier by locking the axis *see Note 3*) to roughly fit the desired position and iterate between translating and rotating with smaller and smaller manipulations.
 - (e) It can be beneficial to pick a specific center of rotation to aid the positioning of a motif. We recommend choosing a P to align and using that as a center of rotation for the subsequent manipulations after first positioning it correctly.
 - (f) Iterations between manipulating the individual motif and rotating all the motifs (including the static model) help to keep an overview of the three-dimensionality of the position.
6. Syntax of commands in Chimera. The command to fit two selections is **match** and the first model is fitted to the second model, which is static. The terminology is; ‘#’ = model number, ‘.’ = residue number(s), ‘.’ = chain, ‘@’ = atom. The order of the nucleo-


#2:2@P is fitted to #0:43.B@P

 match #2:2-3,9-10@P #0:43-44.B,2-3.A@P

Fig. 10 Syntax of the command line in Chimera. The command *match* in *Chimera* aligns a tetra-loop (model #2) onto the end of a double helix (model #0) by aligning the first atom specified in the first model (#2:2@P) to the first atom in the second model (#0:43.B@P), which is the static model

tides is critical because *Chimera* fits the first P in model #1 to the first P in model #0 ect. (Fig. 10). For more information on using the command line in *Chimera* see *Chimera's User Guide*, which also has a *Chimera Quick Reference Guide*.

7. If the ligating script does not thread the structure with the correct strand path it might be due to motifs positioned close to each other, i.e., that a phosphate in one motif is closer to the end of the threading strand than the next phosphate in the current motif. Naming the chains of the two motifs differently can circumvent this failure in strand path.

The ligate script basically reads the strand from the number 1 nucleotide and finds the nearest phosphate of the next nucleotide. It orders the PDB file with ascending nucleotide numbers from 1 to the last nucleotide. This can be done manually by numbering the nucleotides in the desired order in *Swiss-PdbViewer* and rearranging the PDB file in a text editor, but the process is quite tedious.

For the ligate script to work properly the following steps should be followed to prepare the PDB file for ligation. (1) There should be no overlapping nucleotides, (2) All nucleotides should have a different nucleotide number (only one nucleotide with number 1), (3) the strand path can be directed by chain name, i.e., the ligate script looks for the next nucleotide with the same chain name first and only switches chain name if the distance goes above the threshold (this is used to create the crossovers).

8. The *Perl* scripts are run in the *Terminal* in *OS X*. Both the input file and the script need to be in the same folder for the script to work. You choose the directory in the *Terminal* by writing `cd /Users/...` and the rest of the folder path. Another trick is to open the folder in *Finder* and only write `cd` (remember a space after) and the drag and drop the small folder name from the top of the *Finder* window to the *Terminal*.
9. It might be necessary to run more than 10 iteration of refinement in *Assemble2* to get to zero deviations, although it is not always possible to remove all the deviations. Keep in mind that it is merely a model and the goal is to see a trend of descending

deviations, which indicates that the bond lengths and distances between atoms in the model are within normal parameters and that the model is a fair estimation of a native structure.

10. Selection in *Assemble2* works by clicking on the nucleotide once to select the nucleotide, twice to select the base pair and three times to select the double helix that nucleotide is in. If a nucleotide is in a single-stranded region the second click will select the whole single-stranded region. By **control**-clicking you can select individual nucleotides not connected to each other. To select a stretch of nucleotides click on the 5'-nucleotide of the stretch and **alt/option**-click on the 3'-nucleotide of the stretch. Rotation or translation of a selection of nucleotides is performed by pressing the **alt/option**-key while left- or right-clicking, respectively.
11. Similar 3D designs with different strand paths will have a difference in the order of co-transcriptional folding, which is easily visualized in an arc-diagram. The output from the *Perl* script *trace.pl* can be used to create an arc-diagram using the online program *R-chie* (www.e-rna.org/r-chie). Go to **Create a Plot** on the *R-chie* website and copy-paste the dot-bracket structure from the section *Output: The sequence and structure* in the file *9_2H-AE_nupack.txt* into the *Secondary Input Structure* box. Set the *Grouping Rule* to **Dot-bracket bracket type**, select the *Color Palette* of your choice and press **Plot**. The arc-diagram of the 2H-AE RNA origami (Fig. 11) shows the co-transcriptional folding order of the structure as well as the pseudoknot base pairs of the kissing loop.
12. The following list are the parameters in the *NUPACK* code that can change the output of designed sequences [11]:
 - (a) *temperature[C]* (default: **37.0**) can be changed to fit the conditions your particular RNA origami structure is to be used in. Lowering the temperature will theoretically lower the GC content of the designs, because the double helices need a lower amount of energy to form.

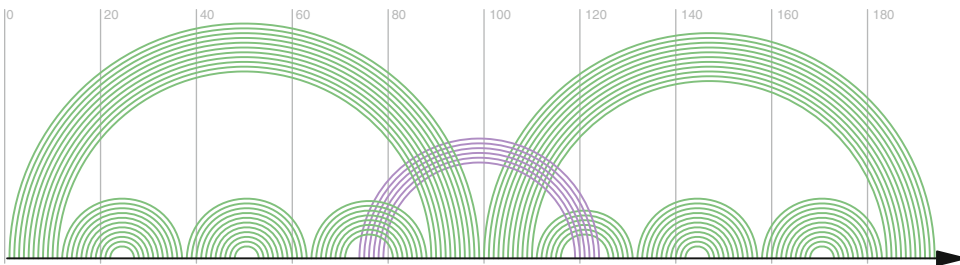


Fig. 11 Arc-diagram of the 2H-AE RNA origami. The diagram shows the co-transcriptional folding order of the structure reading from the 5'-end (left) to 3'-end (right). The pseudoknot base pairs of the kissing-loop are shown in *purple* and the regular base pairs of the rest of the structure are shown in *green*

- (b) *trials* (default: **4**) can be set between 1 and 10 and the higher number will output more sequences.
- (c) *dangles* (default: **some**) can be set to none, some or all and changes the way dangle energies are incorporated into the energy calculations.
- (d) *prevent* (default: **AAAA, CCCC, GGGG, UUUU, KKKKKK, MMMMMM, RRRRRR, SSSSSS, WWWWWW, YYYYYY**) is set to prevent long repetitive or similar sequences. The prevent sequences does not affect the prespecified nucleotides of the design, but only the sequence that *NUPACK* designs.

Acknowledgement

This work was supported by a Sapere Aude Starting Grant from the Danish Council for Independent Research (DFR-0602-01772) and the Centre for DNA Nanotechnology (<http://cdna.au.dk/>) funded by the Danish National Research Foundation (DNRF81).

References

1. Jaeger L, Chworos A (2006) The architectonics of programmable RNA and DNA nanostructures. *Curr Opin Struct Biol* 16: 531–543
2. Fu TJ, Seeman NC (1993) DNA double-crossover molecules. *Biochemistry* 32: 3211–3220
3. Grabow WW, Jaeger L (2014) RNA self-assembly and RNA nanotechnology. *Acc Chem Res* 47:1871–1880
4. Geary C, Rothmund PW, Andersen ES (2014) A single-stranded architecture for cotranscriptional folding of RNA nanostructures. *Science* 345:799–804
5. Geary C, Andersen ES (2014) Design principles for single-stranded RNA origami structures. *Lecture notes in computer science: DNA computing and molecular programming (DNA20)*
6. Dietz H, Douglas SM, Shih WM (2009) Folding DNA into twisted and curved nanoscale shapes. *Science* 325:725–730
7. Ikeda RA, Richardson CC (1986) Interactions of the RNA polymerase of bacteriophage T7 with its promoter during binding and initiation of transcription. *Proc Natl Acad Sci U S A* 83:3614–3618
8. Grabow WW et al (2011) Self-assembling RNA nanorings based on RNAI/II inverse kissing complexes. *Nano Lett* 11:878–887
9. Severcan I et al (2010) A polyhedron made of tRNAs. *Nat Chem* 2:772–779
10. Baklanov MM, Golikova LN, Malygin EG (1996) Effect on DNA transcription of nucleotide sequences upstream to T7 promoter. *Nucleic Acids Res* 24:3659–3660
11. Afonin KA et al (2010) In vitro assembly of cubic RNA-based scaffolds designed in silico. *Nat Nanotechnol* 5:676–682

Assembling RNA Nanoparticles

Shou-Jun Xiao

Abstract

RNA nanoparticles are designed and self-assembled according to noncanonical interactions of naturally conserved RNA motifs and/or canonical Watson–Crick base-pairing interactions, which have potential applications in gene therapy and nanomedicine. These artificially engineered nanoparticles are mainly synthesized from in vitro transcribed RNAs, purified by denaturing and native polyacrylamide gel electrophoresis (PAGE), and characterized with native PAGE, AFM, and TEM technologies. The protocols of in vitro transcription, denaturing and native PAGE, and RNA nanoparticle self-assembly are described in detail.

Key words RNA nanoparticles, Motif, Self-assembly, In vitro transcription, PAGE

1 Introduction

RNA, as mentioned in many textbooks, plays a key role in reproduction and replication of cellular activities. Two types of RNAs are mostly known, messenger RNA (mRNA) and transfer RNA (tRNA) [1]. Not limited to the two RNAs, over the past few decades, scientists have discovered new RNA species possessing diverse functions, such as antisenses (related to effects of RNA interference), aptamers (oligonucleotides or peptides for binding to a specific target molecule), riboswitches for allosteric sensing, ribozymes for enzymatic catalysis, as well as gene regulators. Besides the fundamental scientific challenges, RNA interference (RNAi) is making a great progress as a gene therapy treatment of various diseases through the exogenous delivery of short synthetic RNA duplexes (the so-called small-interfering RNAs, which are often abbreviated as siRNAs or micro-RNAs) into cells [2]. RNA therapeutics includes the use of RNAs possessing a single function or multiple functions with synergistic effects, to fight against all kinds of viruses and diseases. That is why RNA has attracted great interest among scientists.

RNA is made up of four different nucleotides: adenine (A), cytosine (C), guanine (G), and uracil (U), whereas DNA contains thymine (T) rather than U. The well-known single-stranded

structure of RNA is its clover-leaf shape (or precisely an upside down letter L), which is a rigid structure. Different from the linear double helix structures of DNA by means of canonical Watson–Crick base-pairing, RNA exhibits richer chemical, structural, and functional diversities, for example the noncanonical kissing loop interactions.

RNA nanoparticles via programmed self-assembly by means of canonical Watson–Crick base pairing and noncanonical kissing loop interactions have attracted enormous interest because they are challenges both for fundamental RNA nanostructures and for potential biomedical applications. These engineered nanoparticles include the following features: (1) programmable folding and self-assembly to precise tertiary structure, (2) multiple biological functionalities such as ribozymes, riboswitches, RNAi, editing, splicing, and inherent translation and transcription, (3) biocompatibility, (4) relatively low immune response, (5) relatively lower degradation than linear strands by means of nanoparticulate sheltering in biological environment, and (6) relatively lower cost and ease of production. RNA self-assembly generally refers to the spontaneous process by which a preexisting RNA sequence or several associated sequences form an organized structure consisting of a specific network via local noncovalent interactions (i.e., hydrogen bonding, base stacking, and loop-loop interactions between distant nucleotide sites). Scientists have known that recurrent structural motifs (or modules) specify localized organization of conserved or semiconserved nucleotides in natural RNAs. These conserved structural motifs are routinely integrated together to code for specifically localized folding. These specified tertiary structures coordinate together to perform specific operations including intermolecular recognition, catalytic reaction, and/or mechanical functions in nature.

Generally, the folding design for RNA nanoparticles can be classified into three strategies: RNA architectonics [3–6], single-stranded RNA origami [7], and RNA–DNA hybrid self-assembly [8]. In the first RNA architectonics, the thermodynamically stable RNA motifs including internal, multibranching, and kissing loops, extracted from X-ray and/or NMR resolved structures of natural RNA molecules, are recombined into novel RNA nano-assemblies through computer modeling. Obviously the assembly process is thermodynamically controlled. The RNA motifs will be pre-folded before the formation of the final RNA nanoparticles by linking strands. The second strategy, single-stranded RNA origami, is inspired by DNA origami: a known encoded single-stranded RNA can be transcribed from its DNA template, then a combined folding strategy by means of noncanonical kissing loop interactions and canonical Watson–Crick base-pairing to form motifs including crossover Holliday junctions and linkers will form many kinds of nanostructures. The single-stranded RNA origami strategy takes

the advantage of both thermodynamically and kinetically controlled assembly processes. Both of RNA architectonics and single-stranded RNA origami can be executed in step-by-step reactions or in one-pot reaction during the *in vitro* transcription process, which is named as the cotranscriptional assembly. The third strategy, RNA–DNA hybrid assembly, takes use of the canonical Watson–Crick base-pairing between RNA and DNA to fabricate nanostructures. As it is well-known, DNA double helices are in B-form, whereas RNA double helices are in A-form. The hybrid RNA–DNA helices are more presented in A-form than B-form. The RNA–DNA hybrid structures can be used to release the sense RNA for gene regulation and other functionalities. The third strategy is designed to avoid stable intramolecular motifs and rely on canonical base-pairing but not on structural or tertiary interactions. A perfect RNA nanoparticle experiment sometimes needs several theoretical modeling/experimental folding cycles, for feedback between the computational modeling and the realistic folding experiment.

1.1 Design of RNA Nanoparticles

The design of RNA nanoparticles with multiple oligos or a single-stranded RNA is the first and the most important step. The design complexity is out of the scale of this protocol guidance and will not be described in detail here. However, a brief introduction of the design of RNA nanoparticles is given below:

1.1.1 Choice of Motifs

According to a research purpose, thermodynamically stable tertiary RNA motifs (RNA motifs documented as reoccurring base-interactions and tertiary structures may not necessarily adhere to standard Watson–Crick helical base pairs) must be searched in a database (there are many motif databases such as nucleic acid database (NDB) [9], Structural Classification of RNA (SCOR) [10], and Protein Data Bank (PDB) [11]). A key component of the database for RNA nanotechnology is its ability to search for junctions that have specified angle ranges between adjoined helices. The junction angles between helices and the geometry of kissing loop interactions are often key parameters for RNA nanoparticle design. After designing a structure, the motifs, including junctions, involved in a RNA nanoparticle will be synthesized, identified, and characterized.

1.1.2 2D and 3D RNA Nanostructures' Design

To generate 2D and 3D RNA nanostructures, scientists have developed a number of software programs such as NanoTiler [12], RNA2D3D [13], and NUPACK [14] that help organize, join, and model RNA motifs and linkers in a 3D coordinate system. The carefully designed nanostructures will be checked with experimental results and this feedback between the computation and the experiment will be repeated until the final nanostructure is optimized.

1.2 RNA Synthesis

For RNA architectonic nanotechnology, RNA oligos are often used, whereas the RNA origami or single-stranded RNA assembly requires a much longer RNA strand with thousands of ribonucleotides. Although RNA oligos can be chemically synthesized by solid-phase synthesis (most of companies provide less than 30 nt due to the high cost for longer oligos), the much higher price for each base of RNA (10 more times) than DNA is definitely the obstacle for scientists to work in the field of RNA nanotechnology. In fact, RNA oligos are significantly more difficult to synthesize than DNA ones, mainly because the efficiency of coupling each new ribonucleotide is several percents lower than coupling a new deoxyribonucleotide during the solid-phase synthesis, and the overall coupling efficiency for longer oligos will drop dramatically. Considering the expense, only the short RNA oligos less than 30 nt could be ordered from a commercial company. Another convenient approach to synthesize RNA in a laboratory is the *in vitro* transcription, which is one of the main approaches for large scale RNA production. Although RNA oligos longer than 10 nt can be easily prepared by *in vitro* transcription, still people prefer to synthesize RNAs longer than 20 nt by *in vitro* transcription in preparative scale from their corresponding DNA templates. However unlike the *in vitro* PCR to amplify DNA exponentially, the yield of RNA is much variable, depending on reaction parameters such as the RNA polymerase, the length of RNA, the incubation time, and the incubation temperature. Especially for the RNA size, the longer the RNA is, the less efficiently the *in vitro* transcription works. The most common used transcription polymerases to catalyze the *in vitro* transcription are T7 and SP6, where in this protocol T7 RNA polymerase will be adopted. A well-prepared T7 *in vitro* transcription experiment can produce RNA 10–20-folds of its double-stranded DNA template. Nowadays much higher yields up to 150–200-folds have been claimed by some companies, we will still stick to the traditional T7 *in vitro* transcription with an expected yield of around 10–20-folds.

1.2.1 Preparation of DNA Templates

As the *in vitro* transcription is the most convenient technology to prepare pure RNA strands for RNA nanotechnology, we briefly introduce the principle of *in vitro* transcription first: a linear double-stranded DNA template is recognized by a phage RNA polymerase specifically at the 18-bp promoter sequence (5'-TAATACGACTCACTATAG for T7, 5'-ATTTAGGTGACTACTATAG for SP6), then transcription is initiated precisely at the 18th nucleotide of guanosine. To terminate the transcription correctly on a template, the linear double-stranded DNA template must have blunt ends or 5'-protruding ends. Otherwise, DNA templates containing 3'-protruding ends will produce spurious transcripts due to nonspecific initiation. The DNA templates for *in vitro* transcription can be obtained from chemical synthesis of oligonucleotides, PCR products, and linearized plasmids (run-off transcription), which are briefly described below.

1. *Preparing DNA template using oligodeoxynucleotide annealing.* If the RNA to be transcribed is less than 100 bp, this approach is practical only. Two strands of DNA oligonucleotides are designed and ordered from a company: a short sense strand containing only the promoter sequence and a long antisense strand consisting of the complementary DNA template to be transcribed and the complementary promoter sequence at the 3'-end. Upon annealing, the promoter region becomes double-stranded, whereas the template region is a single-stranded anti-sense sequence [15].
2. *Preparing DNA template using PCR.* For some reasons, the reaction efficiency of in vitro transcription from the oligodeoxynucleotide annealing template is not stable. People like to design the oligodeoxynucleotides for PCR amplification and then use PCR products as the DNA templates for in vitro transcription. If the DNA template does not contain a T7/SP6 promoter sequence, a sense primer should be designed that locates the T7 promoter sequence at the 5'-end of the template. Thus the T7 promoter sequence will be added to the 5'-end of the sense template and its complementary promoter sequence to the 3'-end of the antisense DNA template via PCR. To avoid generating double-stranded DNA templates with 3'-overhangs, high fidelity enzymes, while not the non-proofreading polymerases, should be used.
3. *Plasmid construction and amplification to prepare DNA template.* A plasmid vector with a T7 promoter sequence positioned upstream of the transcription start site will be used. To this vector, a DNA template for transcription either from chemical synthesis or from PCR is inserted into the polylinker region, which is between two restriction enzyme cleavage sites. For a "run-off" transcription, restriction enzymes are used to cleave the plasmid at the restriction enzyme cleavage sites that are downstream of the DNA template, thus generating linear double-stranded DNAs with blunt ends or 5'-overhangs for polymerase to run off [16].

For all the above three approaches to generate linearized DNA templates, although some recipes do not need purification of DNAs, we still suggest to use the polyacrylamide gel electrophoresis, abbreviated as PAGE, to purify the DNA templates for in vitro transcription [17]. The purity of DNA template has a great impact on RNA transcription.

1.2.2 Modification of RNA to Increasing Its Chemical Stability

The 2'-OH in the RNA pentose ring renders RNA easy to be degraded by ribonucleases, especially RNase. The phosphodiester bond is also vulnerable to base degradation. The easy degradation of RNA is one of the most challenging obstacles for many biomedical applications, since most RNAs will be degraded and lose their bioactivity during transportation before they arrive in the

targeting region. To improve the RNA's chemical stability, construction of static and rigid nanoparticles such as nanorings is one strategy. The rigid RNA nanoparticles increase the resistance of RNA to nuclease cleavage through physical package. When the diceable siRNAs substrates are installed and embedded within the RNA nanoparticles, they can still play their role of gene regulation after delivery to the cells. Circularization of RNA is another strategy which protects RNA molecules from attack of their both 5'- and 3'-ends by the ubiquitous ribonucleases. The most common strategy to enhance the stability of RNA/RNA duplex is 2'-F chemical modification of the pentose ring by means of protecting the phosphate backbone from nuclease cleavage [4]. Importantly, the incorporation of chemically modified nucleotides produces RNA having similar properties to natural unmodified RNA, in some cases [5]. The capability of 2'-F modified RNAs to direct self-assembly and to retain functional activity has been shown in the case of the packed RNA (pRNA), while in the case of siRNAs, their biological efficacy is still far from matching the structural and functional complexity of natural responsive structural elements such as the ribosome, large ribozymes, and riboswitches.

2 Materials

All materials and equipments in the RNA experiments should be sterilized. The sterile water should be from an Ultra Pure water system such as Milli-Q or Barnstead. All solutions should be RNase-free, i.e., made with 0.05% DEPC (diethylpyrocarbonate) water. Wearing mouth mask and latex-gloves is a must for RNA operation, since any improper operation could lead to RNA degradation.

To run a RNA nanoparticle experiment for rudimentary characterization of electrophoresis analysis and imaging (AFM or EM), a final concentration of 0.1–1.0 μM of each RNA strand (the requirement of different concentrations depends on the packed geometry of nanoparticles) in the assembly solution with a volume of 20–50 μl is needed. That is to say, 5–50 pmol of each RNA strand is generally consumed in one experiment. To ensure that research findings are robust, an experiment should be run multiple times. To guarantee the reproducibility of RNA nanoparticle assemblies, 10 folds of the RNA sets should be prepared in one batch of the *in vitro* transcription. For a thorough RNA nanoparticle experiment with possible repeating assemblies of ten times, 500 pmol (it is about 10 μg for a single stranded 50 nt RNA) RNA should be produced in one batch of *in vitro* transcription. Considering the 10–20-folds of RNA can be transcribed, 50 pmol DNA templates (about 1.6 μg for a double stranded 50 nt DNA template) in a volume of 100 μl solution (corresponding to 0.5 μM) are appropriate for one-pot of *in vitro* transcription.

In this protocol, we focus on the lab scale and the necessary lab protocols to synthesize RNA nanoparticles for rudimentary characterization. The large scale production for biomedical applications can be scaled up proportionally according to the application of RNA nanoparticles.

2.1 Reagents

DNA template from linearized plasmid, PCR, or oligodeoxynucleotides

T7 RNA polymerase at 20 U/ μ l, RQ1 RNase-Free DNase (1 U/ μ l), inorganic pyrophosphatase (0.1 U/ μ l), UltraPure DEPC (diethylpyrocarbonate) treated water, 1 M Tris-HCl (pH 7.5) buffer, T4 RNA ligase, α -[32 P]-ATP (250 μ Ci/mol), UltraPure™ phenol-chloroform-isoamyl alcohol (25:24:1, v/v), glycerol, sodium acetate anhydrous, sodium dodecyl sulfate BioUltra (SDS), spermidine, DTT, EDTA, boric acid, acrylamide-bisacrylamide (37.5:1, wt/wt), 30%, urea, xylene cyanol, bromophenol blue, ammonium persulfate (APS), tetramethylethylenediamine (TEMED), magnesium acetate tetrahydrate, manganese(II) chloride tetrahydrate BioUltra, Whatman chromatography paper.

2.2 Equipment

Microcentrifuge for 0.5 and 1.5 ml tubes, vortex mixer, programmable incubator and/or heating blocks, vertical electrophoresis apparatus for high-resolution PAGE, gel dryer, phosphorimaging instrument and screen, freezer (-20 °C) and 4 °C refrigerator, access to UV spectrophotometer (for single stranded RNA, 1 OD₂₆₀=40 ng/ μ l), Access to AFM and TEM, phosphorimaging instrument (e.g., Typhoon, GE Healthcare), ImageQuant (GE Healthcare).

2.3 Reagent Setup for In Vitro Transcription

10 \times Transcription buffer: 500 mM Tris-HCl, pH 7.5, 250 mM MgCl₂, 50 mM MnCl₂, 100 mM dithiothreitol (DTT), 20 mM spermidine. This buffer can be stored at -20 °C for 1 year.

10 \times NTPs: 50 mM each of ATP, CTP, GTP, and UTP. This solution can be stored at -20 °C for 6 months.

2.4 Reagent Setup for PAGE

10 \times TBE buffer-Mg²⁺: 1 M Tris, 1 M boric acid, 20 mM EDTA, 20 mM Mg(OAc)₂, pH 8.3. This buffer can be stored up to 6 months at room temperature.

2 \times urea-loading buffer: Mix 60% (v/v) glycerol and 2 \times TBE-Mg²⁺ buffer (pH 8.3) containing 16 M urea. This buffer can be stored at room temperature for 1 year.

2 \times Native PAGE loading buffer: Mix 60% (v/v) glycerol and 2 \times TBE-Mg²⁺ buffer (pH 8.3). This buffer can be stored at room temperature for 1 year.

Running dye: 0.05% (w/v) bromophenol blue and 0.05% (w/v) xylene cyanol in 1 \times TBE buffer.

2.5 Reagent Setup for RNA Nanoparticle Assembly

10× RNA nanoparticle assembly buffer: Dissolve 0.2 M NaCl in 10× TBE-Mg²⁺ buffer (pH 8.3). This buffer can be stored at room temperature for 2–3 months.

AFM imaging buffer: 1× TBE-Mg²⁺ (pH 8.3), 50 mM KCl, 50 mM NaCl. This buffer can be stored at room temperature for 1 year.

3 Method

3.1 In Vitro Transcription

3.1.1 In Vitro Transcription of A Single DNA Template

1. Add the following reagents to a 1.5 ml microcentrifuge tube: 10 μ l 10× transcription buffer, 10 μ l 10× NTPs, 5 μ l inorganic pyrophosphatase (0.1 U/ μ l): 0.005 U/ μ l final concentration, 10 μ l DNA template (5 μ M: 0.5 μ M final concentration, 5 μ l T7 RNA polymerase (20 U/ μ l): 1 U/ μ l final concentration, H₂O used to dilute the reaction volume to 100 μ l.
2. Incubate the reaction at 37 °C for 2 h.
3. Add 10 μ l RQ1 RNase-Free DNase (5 U per μ g DNA) in order to digest the DNA templates and incubated at 37 °C for 30 min.
4. Add 100 μ l 50 mM Tris-HCl (pH 7.5) buffer containing 0.6 mM NaOAc, 4 mM EDTA, and 0.5% sodium dodecyl sulfate (SDS) to stop the reaction (*see Note 1*).
5. Add 400 μ l 25:24:1 phenol-chloroform-isoamyl alcohol and vortex for 2 min.
6. Centrifuge the mixture 5 min at 10,000×*g*, 4 °C, and transfer the upper aqueous phase to a new microcentrifuge tube.
7. Add 600 μ l of 100% ethanol and store at -20 °C for 30 min.
8. Take out the tube and centrifuge immediately for 10 min at 16,000×*g*, 4 °C.
9. After centrifugation, observe a white pellet near the bottom of the tube. Discard the supernatant and rinse the white pellet twice with 90% ethanol which is stored at -20 °C. Allow the white pellet air-dry or speed vacuum-dry. Store the RNA pellets at -20 °C.

3.1.2 In Vitro Cotranscription of Multiple DNA Templates and Cotranscriptional Assembly

1. Typically, add the following reagents to a 1.5 ml microcentrifuge tube: 10 μ l 10× transcription buffer, 10 μ l 10× NTPs, 5 μ l inorganic pyrophosphatase (0.1 U/ μ l): 0.005 U/ μ l final concentration, equal moles of all DNA templates (5 μ M): each with 10 μ l to a final concentration of all DNA templates at 0.5 μ M, 5 μ l T7 RNA polymerase (20 U/ μ l): 1 U/ μ l final concentration, H₂O used to dilute the reaction volume to 100 μ l; incubate the reaction at 37 °C for 10–60 min. The completed reaction can be purified with native PAGE after 10 μ l RQ1 RNase-free DNase digestion of DNA templates at

37 °C for 15 min by following **steps 5–9** in Subheading **3.4**, or diluted with AFM imaging buffer five times and immediately imaged with AFM.

2. The above cotranscription protocol can also be used for synthesis of multiple RNA strands with equal scaled-up moles of their corresponding DNA templates. Purification of each RNA can be carried out with the denaturing PAGE by following **steps 6–19** in Subheading **3.2**, after RQ1 RNase-free DNase (scaling-up according to the amount of DNA templates at 5 U/ μ g) digestion of DNA templates in the completed cotranscription solution. To separate each RNA from others, distinguishable migration bands in the denaturing PAGE gel which are determined by the molecular size or the tertiary structure, are a preliminary requirement for cotranscription of mixed DNA templates.

3.1.3 ³²P Radiolabeling for Gel Analysis

In Subheadings **3.1.1** or **3.1.2**, add additional α -[³²P] ATP to a final concentration of 10 μ Ci/ml for RNA body-labeling. Purification for ³²P-labeled RNAs can follow the steps in Subheadings **3.1.1** or **3.1.2** respectively. The dried PAGE gel will be imaged in a phosphorimaging instrument such as Typhoon and analyzed with software such as ImageQuant.

3.1.4 In Vitro Transcription of 2'-F-modified RNA

To reach a specific purpose, 2'-F-modified dCTP and/or dUTP (each at 5 mM final, Trilink) replace CTP and/or UTP, and use the mutant Y639F T7 RNA polymerase instead of T7 RNA polymerase for in vitro transcription in Subheadings **3.1.1** and **3.1.2**. All other steps are the same as for the unmodified RNA.

3.2 Denaturing PAGE (or Called Urea-PAGE) for RNA Purification

1. Purification gels are 1.5-mm thick and often utilize a comb with multiple wells (each well with the dimension of 10 mm \times 10 mm \times 1.5 mm). Using a vertical electrophoresis system with a glass plate size (w \times h) 18 \times 16 cm (*see Note 2*).
2. Using the denaturing PAGE (or urea-PAGE) to purify RNA (*see Note 3*).
3. Fill the lower reservoir of the electrophoresis apparatus with 1x TBE-Mg²⁺, place the gel into the lower tank and avoid the formation of air bubbles at the gel bottom. Clamp and seal the gel to the upper tank. Fill the upper reservoir with 1x TBE-Mg²⁺ so that the wells are covered.
4. Pre-run the gel for 30 min at electric field strength of 20 V/cm (constant voltage) to get rid of any small molecular contamination in the gel. An environmental temperature of around 10 °C should be monitored to avoid over-heating of the glass plate (*see Note 4*).
5. After the pre-run, disconnect the gel apparatus from the power supply and rinse the wells of the urea-PAGE gel with 1 \times TBE-Mg²⁺ to remove any residual urea (*see Note 5*).

6. Using 150 μl urea-loading buffer to dissolve the RNA pellet prepared from the *in vitro* transcription, denature RNA at 95 $^{\circ}\text{C}$ for 2 min and snap cool the solution on ice.
7. Load the denatured RNA solution into 3 wells in the middle, each with 50 μl , using the gel-loading capillary pipette tip (*see Note 6*). Load the running dyes on empty wells besides the sample well to monitor migration.
8. Immediately reconnect the gel apparatus to the power supply and set the power at a constant 20 V/cm. Running time of the gel depends on the size of the oligonucleotide. The gel should be run until the positions of the running dye(s) indicate that the oligonucleotide has migrated one-half to three-fourths of the way through the gel.
9. Carefully remove the gel from the glass plates using a spatula to peel the gel away from the glass and place it on a single layer of transparent plastic wrap.
10. Place the gel on a fluorescent TLC (thin layer chromatography) plate and image the gel by a UV lamp (set at 254 nm) about 15 cm above the gel. The RNA will absorb the light and cast a shadow onto the TLC plate.
11. Using a permanent black marker to trace the oligonucleotide bands on the gel and turn the UV lamp off. Do this quickly, as the UV light will damage the RNA.
12. Cut the oligonucleotide bands out of the gel using a clean razor, transfer them into a 1.5 ml microcentrifuge tube.
13. Air-dry or blow-dry the gel slabs and then mash the gels by a spatula or flattened glass rod (*see Note 7*).
14. Add 800 μl 1 \times TBE-Mg²⁺ for every 500 μl of gel slab and elute on a rotary shaker overnight at room temperature.
15. Centrifuge the tube 6 min at 1000 $\times g$, room temperature, to pellet the gel sediments. Use a syringe to move the clear supernatant into a fresh 15-ml centrifuge tube. Then add 300 μl 1 \times TBE-Mg²⁺ to the remaining gels, stir for 5 min, centrifuge for 6 min at 1000 $\times g$, room temperature, and move the clear supernatant with a syringe into the 15-ml centrifuge tube. Finally filter off any remaining gels into the 15-ml centrifuge tube by passing the suspension through an 0.2 μm filter.
16. Concentrate the sample by extracting against 1 volume n-butanol. Remove the upper butanol layer and repeat until the volume of the lower aqueous layer is 200 μl .
17. Transfer the 200 μl solution to a 1.5-ml eppie tube. Add 20 μl of 3 M sodium acetate to a final concentration of \sim 0.3 M (pH 5.5). Add 3 \times volume absolute ethanol (\sim 700 μl) to the eppie tube, then place the tube 30 min at -20 $^{\circ}\text{C}$.

18. Take out the tube and centrifuge immediately for 10 min at $16,000\times g$, $4\text{ }^{\circ}\text{C}$.
19. After centrifugation, observe a white pellet near the bottom of the tube. Discard the supernatant and rinse the white pellet twice with 90% ethanol (stored at $-20\text{ }^{\circ}\text{C}$). Allow the white pellet air-dry or speed vacuum-dry. Store the purified RNA pellets at $-20\text{ }^{\circ}\text{C}$ (RNA can be stored for half a year in this way). If RNA will be used in 2 months, resolve the dried RNA in 0.05% DEPC-treated TE, pH 7.5 aqueous solution, aliquot them to $50\text{ }\mu\text{l}$ at $5\text{ }\mu\text{M}$, and store the aliquots at $-20\text{ }^{\circ}\text{C}$.

3.3 Assembling RNA Nanoparticles

As RNA nanoparticles can be designed with the noncanonical and canonical interactions, and RNA is much easier to be degraded than DNA, therefore each RNA nanoparticle requires an optimization of the assembly protocol. The step-by-step RNA nanoparticle production includes the following steps: (1) synthesis of individual strands, generally by *in vitro* transcription, (2) purification of RNA strands by urea PAGE, (3) thermal assembly of RNA nanoparticles, and (4) further purification of RNA nanoparticles by native PAGE gel. A newly developed cotranscriptional RNA assembly approach can finish the nanoparticle assembly during the *in vitro* transcription procedure, thus the step-wise approach can be integrated into one-pot reaction. The cotranscriptional assembly ignores the laborious purification steps of individual RNA and renders the RNA nanoparticle synthesis much easier and more powerful. However the step-by-step assembly is more useful in the optimization procedure for designing and constructing an ideal nanoparticle between the computer modeling and experimental folding cycles. Either of the following three protocols can be adopted to assemble RNA nanoparticles.

1. *Assembly of RNA nanoparticles from multiple purified RNA strands.* Dissolve all RNA strands in $90\text{ }\mu\text{l}$ water with equal moles ($\sim 100\text{ pmol}$) in a microcentrifuge tube (0.5 ml), incubate the mixture in a heat block at $95\text{ }^{\circ}\text{C}$ for 2–3 min, snap cool to a designed temperature between 4 and $45\text{ }^{\circ}\text{C}$ immediately, add $10\text{ }\mu\text{l}$ of $10\times$ RNA nanoparticle assembly buffer to $100\text{ }\mu\text{l}$ total volume (the final concentration of each RNA is $1\text{ }\mu\text{M}$), and incubate at a temperature between 30 and $45\text{ }^{\circ}\text{C}$ for 10–45 min to form RNA nanoparticles.
2. *Assembly of RNA/DNA hybrid nanoparticles from multiple purified RNA and DNA strands.* Dissolve all RNA and DNA strands in $100\text{ }\mu\text{l}$ $1\times$ RNA nanoparticle assembly buffer with equal moles (final concentration at $1\text{ }\mu\text{M}$) in a microcentrifuge tube (0.5 ml), incubate the mixture from 80 to $4\text{ }^{\circ}\text{C}$ by slowly cool it at a rate of around $1\text{ }^{\circ}\text{C}/\text{min}$.

3. *Cotranscriptional assembly of RNA nanoparticles.* Typically, add the following reagents to a 1.5 ml microcentrifuge tube: 10 μ l 10 \times transcription buffer, 10 μ l 10 \times NTPs, 5 μ l inorganic pyrophosphatase (0.1 U/ μ l): 0.005 U/ μ l final concentration, equal moles of all DNA templates (5 μ M): each with 10 μ l to a final sum concentration of all DNA templates at 0.5 μ M, 5 μ l T7 RNA polymerase (20 U/ μ l): 1 U/ μ l final concentration, H₂O used to dilute the reaction volume to 100 μ l; incubate the reaction at 37 °C for 10–60 min. The completed reaction can be purified with native PAGE after 10 μ l RNase-free DNase (5 U/ μ g) digestion of DNA templates at 37 °C for 15 min by following **steps 5–9** in Subheading **3.4**, or diluted with AFM imaging buffer five times and immediately imaged with AFM (*see* **Note 8**).

3.4 Native PAGE for Purification and Characterization of RNA Nanoparticles

1. Purification gels are 0.75 mm thick and often utilize a comb with multiple wells (each well with the dimension of 10 mm \times 10 mm \times 0.75 mm) (*see* **Note 9**). Using a vertical electrophoresis system with a glass plate size (w \times h) 18 \times 30 cm.
2. Using the 7% native PAGE to purify assembled RNA nanoparticles (*see* **Note 10**).
3. Fill the lower reservoir of the electrophoresis apparatus with 1 \times TBE-Mg²⁺, place the gel into the lower tank and avoid the formation of air bubbles at the gel bottom. Clamp and seal the gel to the upper tank. Fill the upper reservoir with 1 \times TBE-Mg²⁺ so that the wells are covered.
4. Pre-run the gel for 30 min at electric field strength of 10 V/cm (constant voltage) to get rid of any small molecular contamination in the gel (*see* **Note 5**).
5. After the pre-run, disconnect the gel apparatus from the power supply and rinse the wells of the native PAGE gel with 1 \times TBE-Mg²⁺ to remove any residues.
6. Mix 2 \times native PAGE loading buffer with the assembly solution (1 μ M final RNA concentration) together at equal volume.
7. Load 2–60 μ l of the above solution into each well, using the gel-loading capillary pipette tip. Load the running dyes on empty wells besides the sample wells to monitor migration (*see* **Note 11**).
8. Immediately reconnect the gel apparatus to the power supply and set a constant voltage at 10 V/cm at 4 °C. Run the gel for 3 h for the best. The gel should be run until the positions of the running dye(s) indicate that the oligonucleotide has migrated one-half to three-fourths of the way through the gel (*see* **Note 4**).
9. Carefully remove the gel from the glass plates using a spatula to peel the gel away from the glass and place it on a Whatman chromatography paper and dry the gel on a gel dryer.

10. (a) If RNA nanoparticles are visible under the UV lamp, extract the RNA nanoparticles from the gel as described in **steps 10–19** of Subheading **3.2**.
- (b) If RNA nanoparticles are not visible under the UV lamp, stain the gel in a SYBR staining solution according to manufacturer's guide and image the gel in Typhoon or a similar instrument at its corresponding wavelength. Recover the RNA nanoparticles from the gel as described in **steps 10–19** of Subheading **3.2**.
- (c) If RNA nanoparticles are ^{32}P radiolabeled, expose the dried gel overnight to a phosphorimaging screen, then scan it using a phosphorimaging instrument (Storm, Typhoon or similar) and quantify bands using two-dimensional densitometry software (ImageQuant or similar).

3.5 AFM Imaging

AFM imaging must be carried out immediately after completion of RNA nanoparticles' assemblies. Generally, drop 3–5 μl of an RNA assembly solution on a freshly cleaved mica and let it stay for 2–3 min, then add 100 μl AFM imaging buffer and image it under the aqueous media.

4 Notes

1. **Steps 4–6** in Subheading **3.1.1** are going to remove proteins including polymerases from the aqueous phase. Since the DNA templates are purified, **steps 4–9** can also be omitted. A convenient approach is: directly add an equal volume of 2 \times Urea loading buffer to stop the *in vitro* transcription reaction after **step 3** in Subheading **3.1.1**, and immediately go to **step 6** in Subheading **3.2** for denaturing PAGE purification.
2. Oligonucleotides less than 50 nt can be separated with this plate size, while longer oligonucleotides should be separated with a larger plate in the vertical size such as 30 cm.
3. Generally oligonucleotides less than 25 nt are purified using a 20% polyacrylamide gel. Longer oligonucleotides require a lower percentage of acrylamide as in Table **1**.

Preparation of the gel plate: For a 20% denaturing acrylamide gel of 18 cm \times 16 cm \times 1.5 mm, 50 ml of gel solution is sufficient, made by mixing the following: 24.0 g urea (8 M final), 5 ml 10 \times TBE-Mg $^{2+}$ buffer, 25 ml 40% acrylamide-bisacrylamide (37.5:1, wt/wt) for high resolution, H $_2$ O to 50 ml final. Add 300 μl 10% (wt/vol) APS and 40 μl TEMED (to induce gel polymerization), mix soon, and immediately pour the solution into the gel plate for polymerization into a gel. Acrylamide and bisacrylamide are hazardous. Use appropriate safety precautions and laboratory apparel.

4. Over-heating of the glass plate easily occurs, especially for the native gel electrophoresis, if the environmental temperature is at room temperature (25 °C). Over-heating can result in the breakage of the glass plate and thus the failure of the PAGE experiment. An environmental temperature from 4 to 10 °C can be easily realized in a cooling room of 4 °C, or a 2–8 °C fridge, or just sitting the whole sealed gel device in an ice water bath.
5. Pre-run and rinsing can eliminate some contaminations during the gel preparation.
6. Around 2 µg RNA in a 10 mm × 1.5 mm (wide × thick) well is required to cast a clear UV shadow. The longer the oligonucleotide is in the in vitro transcription, the less full-length product will be obtained.
7. After air-dry or blow-dry the gel slabs, the gel slabs are crispy and easy to be mashed by a spatula or a glass rod. If the gel slabs are not dried, they are slippery and difficult to be mashed.
8. Three approaches are adopted here for RNA nanoparticle assembly. The first approach is preferred for RNA nanoparticles involving the kissing loop interactions: (a) prefolding of noncanonical structures in water by denaturing at 95 °C for a few minutes, then snap-cooling to a designed temperature (between 4 and 45 °C) immediately, (b) add the assembly buffer and incubate at a temperature between 30 and 45 °C for 10–45 min to form RNA nanoparticles by canonical Watson–Crick base-pairing. The second approach is preferred for RNA nanoparticles (including RNA/DNA nanoparticles) designed only with canonical Watson–Crick base-pairing. It is similar to the self-assembling of DNA nanostructures by a slow temperature decrease from 80 °C at a rate of around 1 °C/min. The third approach is the cotranscriptional assembly, which means the RNA nanoparticle assembly occurs during the transcription procedure. In this approach, RNA can be a single strand transcribed from a DNA template or multiple strands

Table 1
Choice of the acrylamide concentration for oligonucleotide size (nt)

Oligonucleotide size (nt)	Polyacrylamide concentration (%)
<25	20
25–50	15
50–90	12
>90	8

transcribed from a mixture of their corresponding DNA templates in designed stoichiometric ratios. The one-pot cotranscriptional assembly is powerful for scaling-up production of RNA nanoparticles, which could be used in RNA therapeutics. For beginners, 100 pmol RNA in an assembly solution of 100 μ l is a good start for necessary characterizations including native PAGE, AFM, or TEM imaging.

9. The amount of RNAs used in the nanoparticle assembly (50–100 pmol) is in the analytical scale, thus a 0.75 mm thick gel in the native PAGE is more sensitive for UV shadowing. Since a RNA nanoparticle is of much larger molecular weight, a 7% native PAGE gel is suggested for analysis.
10. Preparation of the gel plate: For a 7% denaturing acrylamide gel of 18 cm \times 30 cm \times 0.75 mm, 50 ml of gel solution is sufficient, made by mixing the following: 5 ml 10 \times TBE-Mg²⁺ buffer, 8.75 ml 40% acrylamide–bisacrylamide (37.5:1, wt/wt) for high resolution, H₂O to 50 ml final. Add 300 μ l 10% (wt/vol) APS and 40 μ l TEMED (to induce gel polymerization), mix soon, and immediately pour the solution into the gel plate for polymerization into a gel. Acrylamide and bisacrylamide are hazardous. Use appropriate safety precautions and laboratory apparel.
11. For cotranscriptional assembly, the nanoparticles can be directly imaged with AFM or TEM.
12. Depending on different analysis methods, the corresponding volume of the assembly solution is loaded. The most commonly used methods are ³²P radiolabeling and SYBR staining, where ³²P radiolabeling is the most sensitive method down to 60 fg RNA [18], and SYBR staining can detect 100 pg RNA [19]. If using the UV shadowing method, at least 1 μ g RNA in a single well of 10 mm \times 0.75 mm (wide \times thick) is required to cast a clear UV shadow.

References

1. Krebs JE, Goldstein ES, Kilpatrick ST (2014) *Lewin's genes XI*, Jones & Bartlett Learning, Boston
2. Davis ME, Zuckerman JE, Choi CHJ, Seligson D, Tolcher A, Alabi CA, Yen Y, Heidel JD, Ribas A (2010) Evidence of RNAi in humans from systemically administered siRNA via targeted nanoparticles. *Nature* 464:1067–1070
3. Chworos A, Severcan I, Koyfman AY, Weinkam P, Oroudjev E, Hansma H, Jaeger L (2004) Building programmable jigsaw puzzles with RNA. *Science* 306:2068–2072
4. Afonin KA, Bindewald E, Yaghoobian AJ, Voss N, Jacovetty E, Shapiro BA, Jaeger L (2010) In vitro assembly of cubic RNA-based scaffolds designed in silico. *Nat Nanotechnol* 5: 676–682
5. Shu D, Shu Y, Haque F, Abdelmawla S, Guo P (2011) Thermodynamically stable RNA three-way junctions as platform for constructing multi-functional nanoparticles for delivery of therapeutics. *Nat Nanotechnol* 6:658–667
6. Grasbow GW, Jaeger L (2014) RNA self-assembly and RNA nanotechnology. *Acc Chem Res* 47:1871–1880

7. Geary C, Rothmund PWK, Andersen ES (2014) A single-stranded architecture for cotranscriptional folding of RNA nanostructures. *Science* 345:799–804
8. Ko SH, Su M, Zhang C, Ribbe AE, Jiang W, Mao C (2010) Synergistic self-assembly of RNA and DNA molecules. *Nat Chem* 2: 1050–1055
9. Berman HM, Gelbin A, Westbrook J (1996) Nucleic acid crystallography: a view from the nucleic acid database. *Prog Biophys Mol Biol* 66:255–288
10. Klosterman PS et al (2002) SCOR: a structural classification of RNA database. *Nucleic Acids Res* 30:392–394
11. Berman HM et al (2000) The protein data bank. *Nucleic Acids Res* 28:235–242
12. Bindewald E et al (2008) Computational strategies for the automated design of RNA nanoscale structures from building blocks using NanoTiler. *J Mol Graph Model* 27:299–308
13. Martinez HM, Maizel JV Jr, Shapiro BA (2008) RNA2D3D: a program for generating, viewing, and comparing 3-dimensional models of RNA. *J Biomol Struct Dyn* 25:669–683
14. Zadeh JN, Steenberg CD, Bois JS, Wolfe BR, Pierce MB, Khan AR, Dirks RM, Pierce NA (2011) NUPACK: analysis and design of nucleic acid systems. *J Comput Chem* 32: 170–173
15. Milligan JF, Groebe DR, Witherell GW, Uhlenbeck OC (1987) Oligoribonucleotide synthesis using T7 RNA polymerase and synthetic DNA templates. *Nucleic Acids Res* 15:8783–8798
16. Schenborn ET, Mierendorf RC Jr (1985) A novel transcription property of SP6 and T7 RNA polymerases: dependence on template structure. *Nucleic Acids Res* 13:6223–6236
17. Andrus A (2000) Polyacrylamide gel electrophoresis (PAGE) of synthetic nucleic acids. *Curr Protoc Nucleic Acid Chem* 10.4.1–10.4.10
18. Huang C, Yu, YT (2013) Synthesis and labeling of RNA in vitro. *Curr Protoc Mol Biol*. Unit 4.15
19. Tuma RS, Beaudet MP, Jin X, Jones LJ, Cheung CY, Yue S, Singer VL (1999) Characterization of SYBR gold nucleic acid gel stain: a dye optimized for use with 300-nm ultraviolet transilluminators. *Anal Biochem* 268:278–288

Part II

Applications of DNA Structures

DNA Functionalization of Nanoparticles

Fang Lu and Oleg Gang

Abstract

DNA-nanoparticle conjugates are hybrid nanoscale objects that integrate different types of DNA molecules and inorganic nanoparticles with a typical architecture of a DNA shell around an inorganic core. Such incorporation provides particles with unique properties of DNA, addressability and recognition, but, at the same time, allows exploiting the properties of the particle's inorganic core. Thus, these hybrid nano-objects are advantageous for rational fabrication of functional materials and for biomedical applications. Here, we describe several established DNA functionalization procedures for different types of surface ligands and nanoparticle core materials.

Key words DNA, Nanoparticle, Conjugate, Surfaces, Functionalization

1 Introduction

Decorating inorganic nanoscale components with DNA molecules opens new opportunities for building nanomaterials for novel applications in sensing, gene delivery, optical and energy fields. DNA based platform also provides a flexibility and versatility for building complex structures from nanoparticles using DNA programmable interparticle interactions. The DNA-nanoparticle conjugate is a sort of nanomaterial biocomposites, and they are enable bridging biological systems and nanomaterials. The groups of Mirkin [1] and Alivisatos [2] first introduced the functionalization of nanomaterials with DNA oligonucleotides for gold nanoparticle (NP) systems in the pioneering papers in 1996. Mirkin et al. [1] synthesized 13-nm gold nanoparticles (Au NPs) and attached the surface with alkyl-thiol modified DNA strands. Alivisatos and coworkers [2] attached alkyl-thiol modified DNA strand to 1.4 nm Au NPs with a single maleimide group. A variety of strategies for functionalization of NP of different core materials with DNA have been developed over the years.

The choice of NP functionalization strategy generally depends on the combination of factors, including NP surface chemistry, the

intrinsic NP core material and the NP synthesis procedure, the nature of NP surface ligands, the available functional groups, and the desired conjugation between NP and DNA, which might depend on a particular application. In general, based on the ligands used for the particle stabilization, NPs can be divided into two classes, according to the hydrophilic and hydrophobic property of surface ligands. For hydrophilic NPs with the functional groups of ligands and the ligand-NP interactions, DNA can be attached to the surface of NPs or to the ligand shell either directly or by using intermediaries (e.g., cross-linking molecules)-mediated reactions. On the other hand, various types of nanomaterials ranging from metal, semiconductor to carbon are synthesized with hydrophobic surface, which has to be chemically modified into hydrophilic one for further DNA functionalization. The chemical modification usually involves replacing or attaching the original hydrophobic ligands with hydrophilic or amphipathic compounds, which can provide additional “handles” that can act as sites for the subsequent DNA functionalization. Depending on the functional group available on the surface of particles and their density, different types of chemical modified DNA oligonucleotides have been exploited for covalent conjugation reactions such as carboxyl-to-amine [3–5] and thiol-to-amine [6]. Recently, a new class of methods based on click-chemistry also has been developed for attaching DNA onto surfaces of various types of NPs, including quantum dot (QD), iron oxide, gold, and platinum [7, 8]. According to the DNA functionalization procedures, we introduce the two main well-established strategies: the direct replacement and functional group grafting, and the subsequent conjugation method.

2 Materials

All solutions are prepared with ultrapure water (18 M Ω cm) using, for example, a Millipore system and analytical grade reagents.

1. Citrate-capped gold nanoparticles (AuNPs). Concentration of nanoparticles can be quantified using the absorbance value at the surface plasmonic resonance (SPR) maximum in UV–Vis absorption spectra with molar extinction coefficients, as provided by a vendor or verified independently.
2. Thiol-modified oligonucleotides in their oxidized form (disulfide).
3. Dithiothreitol (DTT), NAP-5 columns (Sephadex G-25 DNA grade).
4. Cetyltrimethylammonium bromide (CTAB).
5. 10 mM phosphate buffer: 10 mM sodium phosphate, pH = 7.4.

3 Methods

3.1 Direct Replacement Method

The replacement approach is applicable for NPs with weakly surface-bound ligands, wherein DNA directly replaces the original ligands via dative bonds. Well-known examples include Au-thiol (-SH, also called sulfhydryl groups) chemisorption. For the Au-thiol dative bonds, the sulfur atom of a thiol contributes a pair of electrons to the empty orbitals of gold atom on the NP surface [9]. Due to fair stability (typical on the order of 100 kJ/mol [10]), the thiol-metal bonds have been utilized for the functionalization of various types of metal materials, including Au [1, 11–15], Ag [16, 17], and Pt [18] nanoparticles, with alkyl-thiol modified DNA strands. All steps of procedures are performed at room temperature unless otherwise noted.

3.1.1 Functionalize Citrate-Capped Au Nanoparticles with Thiol-Modified DNA [11, 19]

1. Dissolve the lyophilized oligonucleotides (100–300 nmol) in 0.3 mL of a 100-mM DTT solution in purified water or buffer.
2. Keep the reducing reaction for one hour. To remove the DTT, the reduced DNA is loaded on a freshly purified sephadex column (G-25) and eluted with 2.5 mL of 10 mM phosphate buffer (pH=7.4). The final volume of purified DNA should be 0.3–0.5 mL (*see Note 1*).
3. The DNA is quantified using UV–Vis analysis using the known extinction coefficient.
4. Add the fresh reduced DNA to the solutions of Au nanoparticles (3 nmol DNA per mL of Au NPs, *see Note 2*) and incubate for ~4 h with gentle mixing.
5. Stepwise add 1% sodium dodecyl sulfate (SDS) (*see Note 3*), 1 M phosphate buffer (pH=7.4) and 2.0 M sodium chloride (NaCl) to the nanoparticle solution, followed by 10 s of sonication and approximately 30 min of incubation between each salt addition. Specifically, solutions are brought to 0.05, 0.1, 0.2, 0.3, 0.4, and 0.5 M NaCl sequentially. The final salt concentration is 0.5 M NaCl, 10 mM phosphate buffer, and 0.01% SDS.
6. After the final salt concentration is reached, the solution is allowed to incubate for ~16 h with gentle mixing to achieve maximum DNA loading.

To remove the excess, unbound DNA from the solution, the mixture is centrifuged (*see Note 4*), the supernatant is removed and the pellet is resuspended in washing buffer (0.01% SDS, 10 mM phosphate buffer, pH=7.4) (*see Note 3*). This process was repeated three times. The final resuspension typically occurs in 50–100 mL to allow for a concentrated solution of particles in 0.5 M phosphate buffered saline (PBS) buffer (0.5 M NaCl, 10 mM phosphate buffer, pH=7.4) for further uses (*see Notes 5 and 6*).

3.1.2 *Functionalize Cetyltrimethylammonium Bromide (CTAB) or Cetylpyridinium Chloride (CPC)-Capped Au NPs with Thiol-Modified DNA [20, 21]*

1. To coat thiol-modified DNA on NPs surface, CPC-capped Au NPs have to be transferred to CTAB firstly. To realize that, the CPC-capped Au NPs (e.g., 500–1000 μL) are centrifuged twice (20 min, 1500 rcf) and resuspended in water to remove excess CPC surfactant.
2. The resulting particle solution is then brought to 0.05 M CTAB using a concentrated CTAB solution (0.2 M).
3. After allowing approximately 30 min for the particles to incubate in the CTAB solution, they become CTAB-capped Au NPs.
4. CTAB-capped Au NPs in 0.05 M CTAB are spun down twice (20 min, 850 rcf) and resuspended in Ultrapure (18.2 M Ω cm) water.
5. Thiolated DNA just freshly reduced (*see Note 1*) is immediately added to the colloidal solution (3 OD at 260 nm of DNA per mL of nanoparticle colloid, *see Note 2*). Irreversible particle aggregation is only observed if more than 20–30 min are allowed between the final resuspension in water and the addition of thiolated DNA.
6. Allow 1–3 h for thiolated DNAs to react with the gold surface.
7. Particle suspensions are brought to 0.01% SDS (SDS) (*see Note 3*) and 0.01 M sodium phosphate and allowed to sit for 30 min to 1 h.
8. The colloidal particle solutions are then slowly treated with NaCl to allow for electrostatic screening between neighboring DNA strands and denser surface coverage of oligonucleotides. Specifically, solutions are brought to 0.05, 0.1, 0.2, 0.3, 0.4, and 0.5 M NaCl sequentially with approximately 30 min between each salt addition, better with 10 s sonication.
9. After reaching the final salt concentration, particles are allowed to sit \sim 12 h to achieve maximum DNA loading.
10. In order to remove unreacted oligonucleotides from solution, particle suspensions are centrifuged (*see Note 4*), the supernatant is removed, and the pellet is resuspended in 0.01% SDS three times.
11. The final resuspension typically occurs in 50–100 μL to allow for a concentrated solution of particles. Sodium phosphate and NaCl are added to bring the final suspension to 0.01 and 0.5 M sodium phosphate and NaCl, respectively (*see Notes 5 and 6*).

3.1.3 *Functionalize CTAB or CPC-Capped Silver (Ag) NPs with Thiol-Modified DNA [22]*

1. The CPC-capped Au NPs (e.g., 500–1000 μL) are spun down twice (30 min, 850 rcf) and resuspended in water to remove excess surfactant.

2. An aliquot of fresh thiolated DNA solution (*see Note 1*) is added to 1 mL aliquot of freshly dispersed NP solutions (~2 OD at 260 nm of DNA for per mL of nanoparticles, *see Note 2*).
3. Incubate for 3 h to allow thiolated DNAs to react with the Ag surface.
4. Particle suspensions are brought to 0.01 % sodium dodecyl sulfate (SDS) and 10 mM sodium phosphate by adding 1 % SDS and 1 M sodium phosphate (*see Note 3*).
5. Allow to sit for ~12 h.
6. The colloidal nanoparticle solutions are then slowly treated with NaCl to bring NaCl concentration of the solution to 0.5 M slowly by adding aliquots of 3 M NaCl 8–10 times with 30–60 min interval for incubation.
7. After reaching the final NaCl concentration, particles are allowed to sit 12–18 h to achieve maximum DNA loading.
8. To remove the excess, unbound DNA from the solution, the mixture is centrifuged (*see Note 4*), the supernatant is removed, and the pellet is resuspended in washing buffer (0.01 % SDS + 10 mM phosphate buffer, pH = 7.4) three times. The final pellet is typically resuspended in 50–100 μL to get a concentrated solution of particles.
9. Sodium phosphate and NaCl are added to bring the final suspension to get expected concentrations of sodium phosphate and NaCl, respectively (*see Notes 5 and 6*).

3.2 Functional Group Grafting and Subsequent Conjugation Method [5]

This method is useful for the NPs whose surfaces are capped by strong-bound surfactants, such as (poly-vinyl-pyrrolidone) PVP, TOPO (trioctylphosphine oxide), oleic acid (OA), which either lack of functional groups for conjugation or cannot be simply displaced by using direct replacement or non-covalent attachment approaches.

The strategy for nanoparticles (other than Au) functionalization with DNA included three steps: carboxylic group grafting, streptavidin conjugation, and biotinylated-DNA attachment. In the first step, short mercapto acid ligands, such as mercaptoundecanoic acid, and amphiphilic polymers, such as PEG carboxylic acid lipid, are adopted for hydrophilic and hydrophobic nanoparticles respectively. The subsequent two steps rely on the 1-Ethyl-3-(3-dimethylaminopropyl) carbodiimide (EDC crosslinker)-assisted chemistry and on the specific and strong streptavidin–biotin binding (association constant $2.5 \times 10^{15} \text{ M}^{-1}$). We use streptavidin–biotin–DNA, rather than amine-terminated DNA, in order to achieve a higher grafting density of DNA, owing to the abundant amine groups on STV and four binding sites for biotin.

3.2.1 Functionalization of Nanoparticles with Carboxylic Group

Ligand-exchange for hydrophilic nanoparticles: The PVP capped on the surface of shaped Pd nanoparticles is replaced with 11-mercapto-undecanoic acid (MUA) by a ligand-exchange process.

1. Adjust the pH value of the freshly prepared PVP-capped Pd nanoparticles in aqueous solution to ~9 by phosphate buffer, which contains ~0.01 % Tween 20.
2. Then, excess MUA (with mole ratio ~105 times to Pd nanoparticles) in ethanol is mixed with the above solution.
3. The mixture is incubated at 90 °C for 6 h with brief sonication.
4. Finally, after a purification procedure (*see Note 4*), the MA-capped Pd nanoparticles are well dispersed in phosphate buffer with pH at 6–9.

3.2.2 Amphiphilic Polymers Attachment for Hydrophobic Nanoparticles

1. FeO or QD dispersed in toluene are first mixed with amphiphilic polymers, such as lipid-PEG carboxylic acid (DSPEPEG (2000) Carboxylic Acid, Avanti Polar Lipids), which have hydrophobic chains interacting with ligands on the nanoparticles and carboxylic acid group for further functionalization.
2. Then the mixture is incubated for 2–4 h at room temperature.
3. After complete evaporation of the organic solvent, the residual solid is purified by a centrifugation-wash cycle procedure, where the particles are washed three times by borate buffer with pH 7–9.
4. After purification, the nanoparticles are dispersed in borate buffer with pH at 7–9.

3.2.3 Conjugation of Nanoparticles with Streptavidin

The as-prepared carboxylic group-capped nanoparticles are conjugated with streptavidin by formation of an amide bond between carboxylic groups on the nanoparticles, provided by the ligand, and primary amine groups of streptavidin through EDC-assisted chemistry.

1. Typically, concentrated nanoparticles are first diluted by pH = ~7 phosphate buffer.
2. Then, the solution is mixed with fresh prepared EDC (0.5 mg/mL), *N*-hydroxysulfosuccinimide (NHSS, 0.5 mg/mL) and streptavidin. The quantity of streptavidin is 40–100 times that of the nanoparticles.
3. The mixture is allowed to incubate at room temperature for 2 h.
4. After purification, the nanoparticles are dispersed in phosphate buffer.

3.2.4 Functionalization of Nanoparticles with Biotinylated- DNA

The as-prepared streptavidin capped nanoparticles are easily coupled with biotinylated-DNA because of the strong and specific affinity of biotin to streptavidin.

1. The streptavidin-capped nanoparticles are mixed with excess biotinylated-DNA (*see Note 2*) and incubated for several hours at room temperature.
2. After the remove of excess DNA by purification (*see Note 4*), the nanoparticles are dispersed in phosphate buffer to bring the final suspension to get expected concentrations (*see Notes 5 and 6*).

4 Notes

1. Once treated with reducing procedure, any oligonucleotide that is not used immediately should be stored frozen. Over time, the oligonucleotides will oxidize and the reducing procedure will need to be repeated prior to coupling.
2. For the amount of DNA added to nanoparticle solution, the molar ratio of DNA to nanoparticle must be at least 10 times of maximum DNAs amount loaded on per particle, which depends on the particle size. For example, for 10 nm spherical nanoparticles, the number of single-stranded DNAs bound to each particle is roughly 60, and the molar ratio of the reduced DNA to nanoparticle must be at least about 600.
3. Adding SDS to stabilize nanoparticles during functionalization procedure is essential for large-sized particles, e.g., the ones with diameters more than 20 nm; but for the particles with diameters of 5–15 nm, adding SDS is substitutive.
4. When removing the excess, unbound DNA from the solution, the mixture must be centrifuged. Setting centrifuge speed depends on the particle sizes. For example, 1 mL of 10 nm nanoparticles requires at least 1-h centrifugation at 15,000 rpm and large-sized particles can be spun down using less time at lower speeds.
5. To ensure the particle quality for further applications, freshly functionalized nanoparticles must be stored at 4 °C and used as soon as possible.
6. The formation of DNA shell for nanoparticles can be probed by the dynamic light scattering (DLS) method, as shown in the Fig. 1. Also, the circular dichroism (CD) spectrometry method, can be utilized for probing the state of DNA molecules on the surface of plasmonic particles, as shown in the Fig. 2 for silver nanocubes [22]. The stability of the nanoparticle core, before and after functionalization can be evaluated using the transmission electron microscopy (TEM).

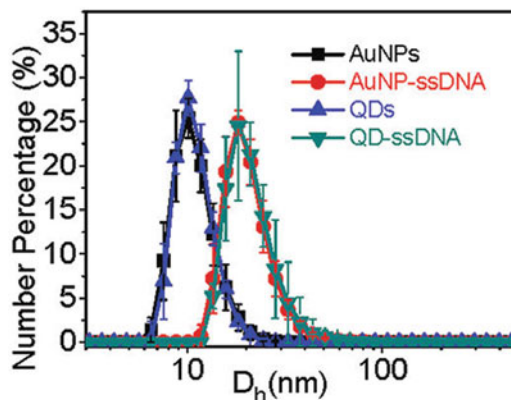


Fig. 1 Dynamic light scattering (DLS) data for bare Au NPs, bare QDs, AuNP-DNA conjugates, and QD-DNA conjugates. It demonstrates that functionalizing with DNA results in the formation of DNA shell (the core is 10 nm AuNP or QD) for nanoparticles, and a hydrodynamic diameter is increasing to about 20 nm. Reprinted with permission from ref. [13]. Copyright 2011 American Chemical Society

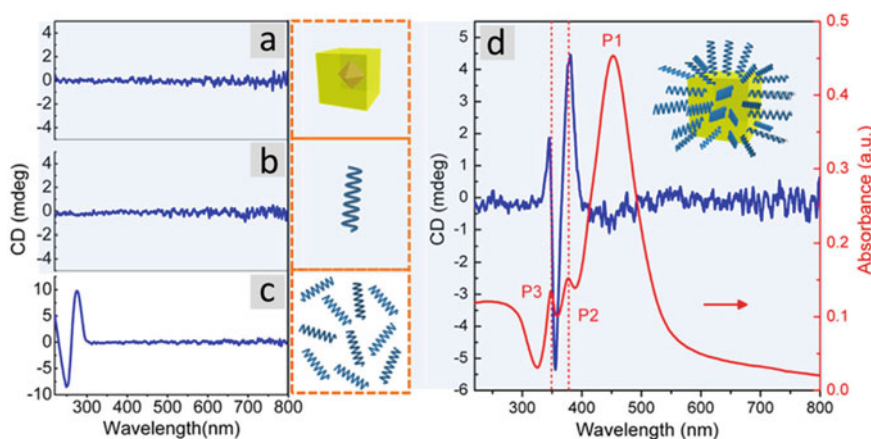


Fig. 2 Circular dichroism (CD) spectra for 0.18 nM bare Ag nanocubes (a), 0.1 μM ssDNA (b), 20 μM ssDNA (c), and 0.18 nM ssDNA-functionalized Ag nanocubes (d). The bare Ag nanocubes without DNA modification shows no CD signal in (a). Natural chirality from little amount of DNA at 0.1 μM concentration cannot be presented in the CD spectrum (b). A thick specimen of ssDNA (20 μM) exhibits the characteristic bisignated CD peaks with maxima at 249 and 275 nm, respectively (c). However, ssDNA-functionalized Ag nanocubes exhibit novel plasmon-induced CD bands (blue curve in d) related to two of UV absorption bands of Ag nanocubes, which is an evidence for Ag nanocube-DNA conjugates. Red curve in d is an UV-Vis absorption spectrum of ssDNA-functionalized Ag nanocubes. Reprinted with permission from ref. [22]. Copyright 2013 American Chemical Society

References

1. Mirkin CA, Letsinger RL, Mucic RC et al (1996) A DNA-based method for rationally assembling nanoparticles into macroscopic materials. *Nature* 382:607–609
2. Alivisatos AP, Johnsson KP, Peng XG et al (1996) Organization of “nanocrystal molecules” using DNA. *Nature* 382:609–611
3. Maye MM, Nykypanchuk D, Van Der Lelie D et al (2007) DNA-regulated micro- and nanoparticle assembly. *Small* 3:1678–1682
4. Sun DZ, Gang O (2013) DNA-functionalized quantum dots: fabrication, structural, and physicochemical properties. *Langmuir* 29: 7038–7046

5. Zhang YG, Lu F, Yager KG et al (2013) A general strategy for the DNA-mediated self-assembly of functional nanoparticles into heterogeneous systems. *Nat Nanotechnol* 8:865–872
6. Parak WJ, Gerion D, Zanchet D et al (2002) Conjugation of DNA to silanized colloidal semiconductor nanocrystalline quantum dots. *Chem Mater* 14:2113–2119
7. Heuer-Jungemann A, Kirkwood R, El-Sagheer AH et al (2013) Copper-free click chemistry as an emerging tool for the programmed ligation of DNA-functionalised gold nanoparticles. *Nanoscale* 5:7209–7212
8. Zhang C, Macfarlane RJ, Young KL et al (2013) A general approach to DNA-programmable atom equivalents. *Nat Mater* 12:741–746
9. Sapsford KE, Algar WR, Berti L et al (2013) Functionalizing nanoparticles with biological molecules: developing chemistries that facilitate nanotechnology. *Chem Rev* 113:1904–2074
10. Daniel MC, Astruc D (2004) Gold nanoparticles: assembly, supramolecular chemistry, quantum-size-related properties, and applications toward biology, catalysis, and nanotechnology. *Chem Rev* 104:293–346
11. Hurst SJ, Lytton-Jean AKR, Mirkin CA (2006) Maximizing DNA loading on a range of gold nanoparticle sizes. *Anal Chem* 78:8313–8318
12. Nykypanchuk D, Maye MM, Van Der Lelie D et al (2008) DNA-guided crystallization of colloidal nanoparticles. *Nature* 451:549–552
13. Sun DZ, Gang O (2011) Binary heterogeneous superlattices assembled from quantum dots and gold nanoparticles with DNA. *J Am Chem Soc* 133:5252–5254
14. Vial S, Nykypanchuk D, Yager KG et al (2013) Linear mesostructures in DNA-nanorod self-assembly. *ACS Nano* 7:5437–5445
15. Xiong HM, Van Der Lelie D, Gang O (2008) DNA linker-mediated crystallization of nanocolloids. *J Am Chem Soc* 130:2442–2443
16. Lee JS, Lytton-Jean AKR, Hurst SJ et al (2007) Silver nanoparticle-oligonucleotide conjugates based on DNA with triple cyclic disulfide moieties. *Nano Lett* 7:2112–2115
17. Tokareva I, Hutter E (2004) Hybridization of oligonucleotide-modified silver and gold nanoparticles in aqueous dispersions and on gold films. *J Am Chem Soc* 126:15784–15789
18. Polsky R, Gill R, Kaganovsky L et al (2006) Nucleic acid-functionalized Pt nanoparticles: catalytic labels for the amplified electrochemical detection of biomolecules. *Anal Chem* 78:2268–2271
19. Maye MM, Nykypanchuk D, Van Der Lelie D et al (2006) A simple method for kinetic control of DNA-induced nanoparticle assembly. *J Am Chem Soc* 128:14020–14021
20. Jones MR, Macfarlane RJ, Lee B et al (2010) DNA-nanoparticle superlattices formed from anisotropic building blocks. *Nat Mater* 9:913–917
21. Lu F, Yager KG, Zhang YG et al (2015) Superlattices assembled through shape-induced directional binding. *Nat Commun* 6:6912
22. Lu F, Tian Y, Liu M et al (2013) Discrete nanocubes as plasmonic reporters of molecular chirality. *Nano Lett* 13:3145–3151

Purification Techniques for Three-Dimensional DNA Nanostructures

Travis A. Meyer

Abstract

Separation of self-assembled three-dimensional nanostructures from excess staple strands, misfolded structures, or unattached functional elements is critical for downstream applications. Numerous purification techniques exist, with varying yields, purities, and hetero-element compatibilities. In this chapter, we focus on three such techniques—agarose gel electrophoresis, ultrafiltration, and polymeric bead pull-down—which together satisfy requirements for a range of applications.

Key words Purification, DNA nanotechnology, Three-dimensional DNA nanostructures, Agarose gel electrophoresis, Ultrafiltration, Polymeric bead pull-down

1 Introduction

The final crude product following the bottom-up self-assembly of three-dimensional DNA nanostructures contains many different molecular species—from the desired, properly folded nanostructure to misfolded/aggregated structures and excess free DNA oligonucleotides. For the majority of downstream applications, it is ideal (or even necessary) to selectively isolate the desired product from the initial mixture. This is especially true when functionalization of the DNA nanostructure is the next step, as excess oligonucleotides and misfolded structures can competitively inhibit heteroelement incorporation [1]. In this chapter, we describe three different purification techniques which together satisfy a range of different requirements.

The first, agarose gel electrophoresis, is the broadest and most specific, and the one traditionally used for a majority of 3D DNA nanostructure purification [2–7]. This technique separates species via size, shape, and charge, and is based on the molecular process of sieving. When an electric potential is applied across an agarose gel, charged species such as DNA migrate through pores in the gel—the smaller or more compact the molecule, the more quickly

it moves through the gel. Agarose gel electrophoresis can be used for separation from excess DNA oligonucleotides, misfolded or aggregated structures (including dimers, trimers, and other oligomers), and heteroelements. However, agarose gel electrophoresis is limited by low yields, lack of scalability, and incapability with very large nanostructures or certain heteroelements. Furthermore, residual agarose fragments and DNA-intercalating dyes contaminate the final product. While the primary method of recovering DNA nanostructures from the gel involves excision of the bands of interest and crushing the gel, other groups have developed alternative recovery methods such as electroelution to improve yields [8].

The second, ultrafiltration, has also been used extensively for 3D DNA nanostructure purification [9–14]. This technique is much more limited than agarose gel electrophoresis, but has several distinct benefits. Ultrafiltration works by using an external force, typically centrifugation, to drive the movement of solvent and select solutes across a semi-permeable membrane. With the choice of a membrane with an appropriate molecular weight cutoff (for large 3D DNA nanostructures, typically 100 kDa), DNA nanostructures can be separated from smaller species, including free DNA oligonucleotides and a small subset of heteroelements. However, ultrafiltration cannot be used to purify desired products from aggregates, higher order structures, or large heteroelements. This technique typically provides substantially higher yields than agarose gel electrophoresis, and is easily scalable to facilitate the purification of large amounts of nanostructures in a relatively short amount of time. It should be noted that more sensitive nanostructures can be damaged by the ultrafiltration process.

The final technique, polymeric bead pull-down, satisfies a much smaller but still important range of requirements. This technique works by specifically and reversibly attaching DNA nanostructures to a much larger element, such as a latex bead. Thus, techniques that can be used to isolate these large beads, such as relatively low-speed centrifugation, can be used to isolate the attached DNA nanostructures from other unattached species. Following successive washing steps, the DNA nanostructure can be separated from the polymeric beads using toe-hold mediated strand displacement. This technique is a modified version of a purification strategy originally published by Shaw et al. [15] and also shows similarity to an affinity-tagged purification technique established by Numajiri et al. [16]. Unfortunately, polymeric bead pull-down cannot be used to purify nanostructure products from free DNA oligonucleotides or misfolded/aggregated structures (as these species will also contain the tag needed for hybridization to the beads), and thus requires a previous purification step such as agarose gel electrophoresis or ultrafiltration.

However, polymeric bead pull-down is especially useful for the purification of DNA nanostructure–heteroelement conjugates from free heteroelements—particularly species which are incompatible with the gel electrophoresis environment, prevent movement of the DNA nanostructure–heteroelement conjugate into the gel, or with species that are too large to be separated by ultrafiltration. Even for DNA nanostructure–heteroelement conjugates which can be resolved easily during agarose gel electrophoresis (such as DNA nanostructures functionalized with gold nanoparticles), the polymeric bead pull-down method can provide substantially higher yields than electrophoresis.

For a general rule of thumb, our lab chooses to use these different techniques to satisfy different requirements, namely:

- Agarose Gel Electrophoresis.
 - For the analysis of newly designed structures or annealing protocols, before the absence of aggregates or dimers/oligomers has been validated.
 - For analysis techniques requiring small volumes/low concentrations (such as transmission electron microscopy or atomic force microscopy).
- Ultrafiltration.
 - After a design/annealing protocol has been verified to produce the correct DNA nanostructure in high yields.
 - When large quantities of DNA nanostructures are needed (e.g., In vitro or in vivo experiments).
- Polymeric Bead Pull-Down.
 - When specific heteroelements used to functionalize DNA nanostructures are incompatible with agarose gel electrophoresis.
 - When large quantities or high concentrations of functionalized DNA nanostructures are needed.

It should be noted that a variety of other purification techniques have been described in the literature, each with their own unique benefits and limitations. These include free flow electrophoresis (FFE) [17], precipitation following PEG crowding [18, 19], rate-zonal centrifugation [20], size-exclusion chromatography (SEC) [21], and fast protein liquid chromatography (FPLC) [15]. We highly encourage readers to investigate these techniques to see if they satisfy requirements for specific applications. The work by Shaw et al. is especially insightful, as they directly compare several of these techniques for the purification of functionalized DNA nanostructures.

2 Materials

2.1 *Technique 1:* *Agarose Gel* *Electrophoresis*

1. Gel and Running buffer: 0.5× TBE/Mg. 44.5 mM Tris, 44.5 mM boric acid, 1 mM EDTA, 10 mM MgCl₂, pH 8 (*see Note 1*).
2. Agarose—Choose molecular biology grade, low EEO agarose with a gel temperature near 37 °C at 1.5%, a melting temperature near 88 °C at 1.5%, and a gel strength above 1200 g/cm² at 1%.
3. Ethidium bromide—10 mg/mL in deionized water.
4. DNA gel loading dye (6×)—Containing either glycerol or Ficoll.
5. Razor blade.
6. Plastic pestle.
7. Freeze 'N Squeeze DNA Gel Extraction Spin Column.
8. UV transilluminator.
9. Electrophoresis chamber and power supply.
10. Centrifuge.

2.2 *Technique 2:* *Ultrafiltration*

1. 1× TE/Mg Buffer: 5 mM Tris, 1 mM EDTA, 10 mM MgCl₂, pH 8 (*see Note 2*).
2. Amicon Ultra Regenerated Cellulose 100 kDa cutoff filter.
3. Centrifuge.

2.3 *Technique 3:* *Polymeric Bead* *Pull-Down*

1. 0.5× TBE/Mg Buffer (*see Note 3*)—*see* Subheading 2.1, step 1.
2. poly(T)-conjugated poly(Styrene) Beads—We have used both Oligotex and GenElute beads successfully (*see Notes 4 and 5*).
3. Centrifuge.
4. Pluronic F-127.
5. 3'-poly(A) Containing “Anchor” Oligonucleotides.
6. “Releasing” Oligonucleotides.
7. 37 °C Incubator or Oven.

3 Methods

3.1 *Technique 1:* *Agarose Gel* *Electrophoresis*

1. Prepare 1.5% agarose gel by adding 1.8 g agarose to 120 mL of Gel and Running buffer and microwave on high until agarose is dissolved (*see Note 6*). Add 6 μL of 10 mg/mL ethidium bromide for a final concentration of 0.05%.
2. Wash electrophoresis chamber thoroughly with deionized water. Place gel tray into chamber so that the rubber gaskets

form a tight seal with the chamber walls. Add in a well comb into the appropriate slots. Pour hot agarose-ethidium bromide solution into gel tray and let sit until gel sets (approximately 45 min—the gel will turn translucent and feel firm to the touch when set).

- Carefully remove well comb, making sure to not damage the wells. Remove gel tray from the electrophoresis chamber and rotate 90°, so that rubber gaskets are perpendicular to side of chamber with electrodes (*see Note 7*). Fill the chamber with Gel-Running buffer until the solution covers the top of the gel.
- Add 1 volume equivalent of DNA Gel Loading Dye to 5 equivalents of crude DNA nanostructure mixture. Carefully pipette this solution into the appropriate number of wells (*see Notes 8 and 9*). A marker can also be added, such as a 1 kb DNA ladder or pure scaffold strand solution (for DNA origami)
- Turn on the power supply, and run the gel for approximately 1–2 h at 2.5 V/cm (*see Note 10*).
- Remove gel from electrophoresis chamber and place on UV transilluminator. Under illumination, use razor blade to excise bands of interest. (Warning: UV light can be damaging to eyes and skin. Make sure to wear proper protective gear before using a UV transilluminator). Transfer bands to 1.5 mL plastic tube (*see Note 11*).
- Using a plastic pestle, crush the excised bands inside the plastic tube. Centrifuge for a couple seconds to pellet all liquid and gel fragments. Using a razor blade or scissors, cut off the bottom of the plastic tube containing the crushed gel, and transfer to upper chamber of Freeze ‘N Squeeze DNA Gel Purification spin columns (*see Note 12*).
- Centrifuge at 2000×*g* for 15 min. Purified DNA nanostructure can be removed from the collection tube and stored at 4 °C until needed.

3.2 Technique 2: Ultrafiltration

- Pre-wet cutoff filter by adding 500 μL 1× TE/Mg buffer and centrifuging at 2800×*g* for 3 min (*see Note 13*).
- Add crude DNA nanostructure mixture into upper chamber of cutoff filter and fill to 500 μL with 1× TE/Mg buffer. Centrifuge at 2800 rcf for 3 min (*see Note 14*).
- Remove the flow-through and refill upper chamber to 500 μL with 1× TE/Mg buffer. Centrifuge as in **step 2**.
- Repeat **step 3** approximately 3–4 times (*see Note 15*). At this point, the retention volume containing the purified product can be removed from the upper chamber and stored at 4 °C until needed.

**3.3 Technique 3:
Polymeric Bead
Pull-Down**

1. Use a 3D DNA nanostructure design tool (such as caDNAo) to place several unique “anchor” strands (*see* **Notes 16** and **17**). These strands should contain three unique domains—a ~20-nt “anchoring” domain complementary to a ssDNA region in the nanostructure (i.e., scaffold strand in DNA origami), a ~10-nt toehold domain, and a 25-nt poly(A) domain. The poly(A) domain should be placed on the 3'-end of the oligonucleotide.
2. Design releasing strands which are complementary to the toehold domain and the “anchoring” domain (*see* **Note 18**).
3. Include an excess of poly(A) containing strands in the crude strand mixture prior to annealing.
4. After annealing, purify the product for excess staple strands using either agarose gel electrophoresis (technique 1—Subheadings **2.1** and **3.1**) or ultrafiltration (technique 2—Subheadings **2.2** and **3.2**) (*see* **Note 19**).
5. Follow appropriate protocol for conjugating heteroelements to DNA nanostructure.
6. Add 1 mL of 5% Pluronic F-127 to 1.5 mL plastic tubes and let sit for 4 or more hours (*see* **Note 20**). The number of tubes should be the same as the number of samples to be purified. After incubation, the tubes should be washed with copious amounts of deionized water.
7. Add 5 μ L of poly(T)-containing poly(styrene) beads to 500 μ L of 0.5 \times TBE/Mg buffer, vortex, and then centrifuge at max speed for 2 min (*see* **Note 21**). Remove supernatant, and resuspend in 500 μ L of buffer.
8. Centrifuge for a second time at max speed for 2 min and remove supernatant.
9. Add mixture of purified DNA nanostructure and excess heteroelements and mix thoroughly by pipetting up and down. Leave overnight in a rotary mixer or other mixing device.
10. Centrifuge at max speed for 2 min and remove the supernatant (*see* **Note 22**). Resuspend the polymeric beads in 100 μ L of buffer.
11. Repeat **step 10** two more times (*see* **Note 23**). Final resuspension volume should be tailored to ideal downstream concentration.
12. Add 1000-fold excess of releasing strands, and incubate at 37 °C overnight with some form of agitation.
13. Centrifuge at max speed for 2 min and remove supernatant containing purified product. Store at 4 °C until needed.

4 Notes

1. Our lab typically prepares a 20 L working solution of $0.5\times$ TBE + Mg as we frequently run agarose gels for multiple purposes (and the running buffer solution is not recyclable due to precipitation of the magnesium salts during electrophoresis). A $10\times$ solution is prepared in 1 L (890 mM Tris-HCl, 890 mM Boric Acid, 20 mM EDTA, 200 mM MgCl_2) and diluted down to 20 L before use. If the specific DNA structure/application is sensitive to boric acid, acetic acid can be used instead (TAE/Mg buffer).
2. This buffer should ideally be identical to the buffer used during the annealing/assembly of the DNA nanostructure (the buffer provided here is simply what we primarily use for the assembly procedure). You can tailor this buffer to fit your individual structure/application.
3. This buffer is used because it is traditionally the buffer of the purified DNA nanostructures following agarose gel electrophoresis. If you have used another buffer for initial purification of the DNA nanostructures prior to this step (or have used a specific buffer during the heteroelement incorporation step), that buffer should be used in place of $0.5\times$ TBE/Mg buffer.
4. These products are traditionally used (and marketed) for mRNA purification, but we have found that they work just as well for capturing DNA strands with 3'-poly(A) tails. We have found that cellulose beads lead to significant non-specific adsorption, and thus only poly(styrene) beads should be used.
5. In the original work in which this technique is based on, the authors use poly(T) coated magnetic beads and use magnetic fields rather than centrifugation for separation. While we have found that centrifugation of polymeric beads works well and obviates the need for specialized magnetic trays, the use of these magnetic beads is beneficial if the DNA nanostructure and/or heteroelements are sensitive to centrifugation.
6. The percentage of the agarose gel can be altered depending on the application—higher percentages typically lead to increased band separation, but slower migration overall. While 1.5% works well for typical DNA origami formed from the p7560 scaffold, you should try several different percentages (between 0.5 and 3%) if 1.5% leads to sub-optimal resolution. The total volume of agarose-buffer needed depends on the size of gel to be cast. We have found that 120 mL works well for 12 cm \times 14 cm gel trays. Smaller volumes will need to be used when using smaller gel trays.
7. The specific protocol for assembling the electrophoresis chamber varies between different products—the example given

here is for Thermo Scientific Owl EasyCast gel chambers. Refer to the user manual provided with your specific chamber before assembly.

8. The amount of sample that can be loaded into each well depends on the dimensions of the well comb and the total volume of the gel. For example, we typically load 30 μL of sample into wells formed from 1.5 mm \times 4 mm teeth with 120 mL gel volume in a 12 cm \times 14 cm gel tray, and load 60 μL into wells formed by 1.5 mm \times 7 mm teeth.
9. We have found that roughly 200 ng of DNA is needed in each well to facilitate easy band identification on the UV transilluminator with the naked eye. While pure dsDNA (for example, from PCR reactions) can be seen at \sim 50 ng, the presence of excess staples, misfolded structures, aggregates, etc. means that the actual amount of true product is lower.
10. Using a 24.5 cm long electrophoresis chamber, we typically set the voltage to 60 V. Higher voltages are inadvisable, as high temperatures generated due to resistive heating can lead to alterations to the DNA nanostructure or the gel. If a smaller chamber is being used, or the designed nanostructure is especially temperature sensitive, lower voltages are recommended. It is also feasible to place the entire chamber in an external ice-water bath or cold room to minimize resistive heating for temperature-sensitive structures/applications.
11. Try to use as small a volume of gel as possible per tube. The more gel you put into a single tube, the lower the yield—the increased gel volume acts as a barrier to hinder movement of the product through the filter.
12. If a larger volume of gel was placed into the tube, it can be difficult or impossible to place the cutoff tip of the tube into the upper chamber of the Freeze 'N Squeeze spin column and close the lid. If this is the case, try to wedge the tube tip into the upper chamber and then centrifuge for approximately 5 seconds on a small tabletop centrifuge. This should be enough to transfer the liquid and gel debris into the upper chamber of the spin column. The empty tip bottom can now be removed and the lid closed.
13. Pre-wetting the filter helps improve yield by minimizing the amount of sample that is absorbed by the filter. The use of blocking reagents (such as Pluronic F127) can also be used to prevent non-specific adsorption and improve yields [15]. Filtration rates can vary from batch to batch, and thus the centrifugation time can be extended past 3 min in order to achieve a 20–30 μL retention volume.
14. As with pre-wetting, centrifugation times can be extended beyond 3 min if retention volume is greater than 20–30 μL .

Higher centrifugation speeds are not recommended, as this can damage three-dimensional DNA nanostructures.

15. In order to verify that sufficient purification has occurred, a small portion of the concentrated product can be analyzed using agarose gel electrophoresis (*see* Subheading 3.1). Resuspension and centrifugation steps should be repeated until the presence of staple strands is no longer visible using a gel imaging system. Oftentimes different batches of tubes will require more or less rounds of centrifugation.
16. The majority of 3D DNA nanostructure designs utilize single-stranded overhangs or loops at the end of helices in order to minimize oligomerization or aggregation due to base-stacking effects. We have found this feature provides an ideal location for incorporating the poly(A)-containing strands needed for polymeric bead pull-down purification.
17. In general, the more poly(A) containing sequences you include, the higher the final yield will be. In our lab, we have compared structures containing either 1 or 4 poly(A) strands, and the structures containing 4 strands consistently result in higher yields. However, the incorporation of only 1 strand does work, particularly if design constraints make it difficult to include more than one strand. These strands should ideally be placed near each other on the edge of the nanostructure.
18. There should be the same number of releasing strands as anchoring strands, as each releasing strand will be different. While the region complementary to the toe-hold domain will be the same, the region complementary to the “anchor” domain will be different for each “anchor” strand.
19. Excess staple strands must be removed prior to purification using the polymeric bead pull-down method as excess poly(A)-containing “anchor” strands can bind to the poly(T) poly(styrene) beads, outcompeting the DNA nanostructure and decreasing yield. As such, the polymeric bead pull-down method should only be used for purifying pure 3D DNA nanostructures from excess heteroelements, such as nanoparticles and proteins.
20. We have found that pre-incubation of 1.5 mL plastic tubes with a concentrated solution of non-ionic surfactants like Pluronic F-127 can help prevent non-specific adsorption of the poly(T)-containing poly(styrene) beads, which can significantly improve yields. We typically add the blocking solution to the tubes the night before, and then wash extensively with deionized water prior to adding the poly(styrene) beads.
21. The exact amount of polymeric beads added should be tailored based on the binding capacity of the beads and the amount of DNA nanostructure to be purified. In general, we have found that 5 μ L of Oligotex beads is sufficient for purification of

100 μL of a 5 nM DNA origami solution (0.5 pmol), but smaller quantities of beads can be used.

22. We recommend that you save this supernatant the first time you try a purification and analyze this sample (via agarose gel electrophoresis, atomic force microscopy, transmission electron microscopy, etc.) to ensure that no trace of DNA nanostructure is present.
23. The number of centrifugation steps needed is highly dependent on the kind of heteroelement used and the degree of purity needed. It is recommended to save all supernatants and analysis for presence of heteroelements in order to determine the optimum number of centrifugation steps for a specific application.

References

1. Saccà B, Niemeyer CM (2012) DNA origami: the art of folding DNA. *Angew Chem Int Ed Engl* 51:58–66. doi:10.1002/anie.201105846
2. Douglas SM, Dietz H, Liedl T et al (2009) Self-assembly of DNA into nanoscale three-dimensional shapes. *Nature* 459:414–418. doi:10.1038/nature08016
3. Wei B, Dai M, Yin P (2012) Complex shapes self-assembled from single-stranded DNA tiles. *Nature* 485:623–626. doi:10.1038/nature11075
4. Ke Y, Ong LL, Shih WM, Yin P (2012) Three-dimensional structures self-assembled from DNA bricks. *Science* 338:1177–1183. doi:10.1126/science.1227268
5. Castro CE, Kilchherr F, Kim DN et al (2011) A primer to scaffolded DNA origami. *Nat Methods* 8:221–229. doi:10.1038/nmeth.1570
6. Ke Y, Douglas SM, Liu M et al (2009) Multilayer DNA origami packed on a square lattice. *J Am Chem Soc* 131:15903–15908. doi:10.1021/ja906381y
7. Douglas SM, Marblestone AH, Teerapittayanon S et al (2009) Rapid prototyping of 3D DNA-origami shapes with caDNAo. *Nucleic Acids Res* 37:5001–5006. doi:10.1093/nar/gkp436
8. Bellot G, McClintock MA, Lin C, Shih WM (2011) Recovery of intact DNA nanostructures after agarose gel-based separation. *Nat Methods* 8:192–194. doi:10.1038/nmeth0311-192
9. Kuzuya A, Sakai Y, Yamazaki T et al (2011) Nanomechanical DNA origami “single-molecule beacons” directly imaged by atomic force microscopy. *Nat Commun* 2:449. doi:10.1038/ncomms1452
10. Pilo-Pais M, Watson AM, Demers S et al (2014) SERS plasmonic enhancement using DNA origami-based complex metallic nanostructures. *Nano Lett* 14:2099–2104. doi:10.1021/nl5003069
11. Ke Y, Lindsay S, Chang Y et al (2008) Self-assembled water-soluble nucleic acid probe tiles for label-free RNA hybridization assays. *Science* 319:180–183. doi:10.1126/science.1150082
12. Gu H, Chao J, Xiao SJ, Seeman NC (2010) A proximity-based programmable DNA nanoscale assembly line. *Nature* 465:202–205. doi:10.1038/nature09026
13. Sobczak JP, Martin TG, Gerling T, Dietz H (2012) Rapid folding of DNA into nanoscale shapes at constant temperature. *Science* 338:1458–1461. doi:10.1126/science.1229919
14. Douglas SM, Bachelet I, Church GM (2012) A logic-gated nanorobot for targeted transport of molecular payloads. *Science* 335:831–834. doi:10.1126/science.1214081
15. Shaw A, Benson E, Högberg B (2015) Purification of functionalized DNA origami nanostructures. *ACS Nano* 9:4968–4975. doi:10.1021/nn507035g
16. Numajiri K, Yamazaki T, Kimura M et al (2010) Discrete and active enzyme nanoarrays on DNA origami scaffolds purified by affinity tag separation. *J Am Chem Soc* 132:9937–9939. doi:10.1021/ja104702q
17. Timm C, Niemeyer CM (2015) Assembly and purification of enzyme-functionalized DNA origami structures. *Angew Chem Int Ed Engl* 54:6745–6750. doi:10.1002/anie.201500175
18. Stahl E, Martin TG, Praetorius F, Dietz H (2014) Facile and scalable preparation of pure

- and dense DNA origami solutions. *Angew Chem Int Ed Engl* 53:12735–12740. doi:[10.1002/anie.201405991](https://doi.org/10.1002/anie.201405991)
19. Douglas SM, Chou JJ, Shih WM (2007) DNA-nanotube-induced alignment of membrane proteins for NMR structure determination. *Proc Natl Acad Sci U S A* 104:6644–6648. doi:[10.1073/pnas.0700930104](https://doi.org/10.1073/pnas.0700930104)
 20. Lin C, Perrault SD, Kwak M et al (2013) Purification of DNA-origami nanostructures by rate-zonal centrifugation. *Nucleic Acids Res* 41:e40. doi:[10.1093/nar/gks1070](https://doi.org/10.1093/nar/gks1070)
 21. Wickham SFJ, Endo M, Katsuda Y et al (2011) Direct observation of stepwise movement of a synthetic molecular transporter. *Nat Nanotechnol* 6:166–169. doi:[10.1038/nnano.2010.284](https://doi.org/10.1038/nnano.2010.284)

Chapter 9

DNA Nanostructure as Smart Carriers for Drug Delivery

Xiangyuan Ouyang, Jie Chao, Shao Su, and Chunhai Fan

Abstract

Self-assembled DNA nanostructures have recently emerged as a type of drug delivery carriers due to their suitable sizes, well-defined nanoscale shapes, precise spatial addressability, and excellent biocompatibility. Here, we describe practical procedures in detail for the design and construction of DNA nanostructures with different width and patterns by long rolling circle amplification (RCA) strands and a few short staples, and provide practical guidance and troubleshooting advice for delivering CpG immunostimulatory drugs with these RCA based DNA nanostructures.

Key words DNA nanostructures, Rolling circle amplification, Drug delivery, CpG immunostimulatory drugs

1 Introduction

Delivery carriers are of importance in nanomedicine because they can transport multiple functional agents including guiding agents for targeting to specific cells or tissues, imaging agents for diagnosis, and drugs for therapy. An ideal carrier for drug delivery should be nontoxic, easy to load agents and able to control drug release. Previously reported drug delivery carriers include cationic dendric polymers, liposomes, gold nanoparticles (AuNPs), mesoporous silica nanoparticles, quantum dots, and carbon nanomaterials [1–10]. DNA nanostructures have recently been employed as drug delivery carriers because of their well-defined sizes, synthesis convenience and potential to control drug release. For example, Turberfield's and our groups found that DNA tetrahedral could efficiently deliver cytosine-phosphate-guanosine (CpG) oligonucleotides into macrophage-like RAW264.7 cells and stimulate significant immune responses [10, 11]. Compared with DNA tetrahedral, DNA origami-based compacted nanostructures offer greater flexibility in design and functionality and probably higher stability in cells [12, 13]. Liedl and coworkers utilized hollow 30-helix DNA origami nanotubes for the delivery of immune-activating CpGs into freshly isolated spleen cells that targeted the

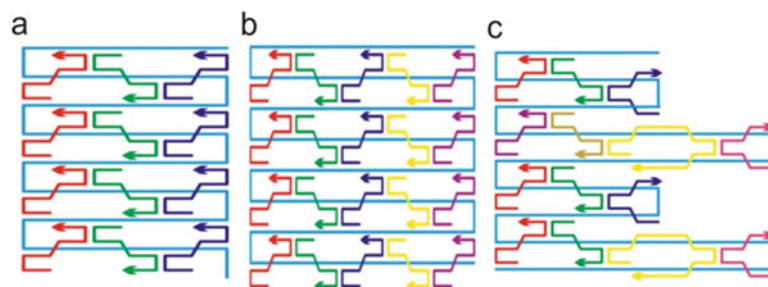


Fig. 1 Schematic illustration of the folding pathway of the single-stranded RCA product to form DNR-1 (a), DNR-2 (b), and DNR-3 (c) (reproduced from ref. [20] with permission from Elsevier)

endosome [12]. Another elegant example is that an autonomous DNA nanorobot can transport molecular payloads to cellular surfaces through an aptamers-lock mechanism [14].

To date, three methods were developed to obtain complex DNA nanostructures. The first one involves DNA tiles that utilize the helical turn of DNA to form crossovers between two or more double strands within its structure [15]. The second method to obtain rigid DNA nanostructures relies on the origami principle, in which a long scaffold strand (usually a virus M13mp18 genomic DNA of approximately 7 kb) is folded by hundreds of short auxiliary strands into a well-defined shape [16]. Combining the concept of DNA tiles and DNA origami, Yin's group employed single-stranded tiles with concatenated sticky ends to form two and three-dimensional canvas [17, 18]. Nevertheless, these DNA nanostructures were constructed from hundreds of oligonucleotides with deliberately designed sequences. Here, we demonstrate that long rolling circle amplification (RCA) strands can be folded into large nanostructures by using only several short staple strands.

Firstly we took place M13 by RCA strands as the scaffold and obtained a large amount of long scaffold ssDNA with different periodic unit by rolling circle amplification. Then they were folded back and forth in different width and patterns, rectangle with width of 16 nm (DNR-1) and 27 nm (DNR-2), and jagged shape (DNR-3), as illustrated in Fig. 1. Furthermore we tested the ability of these nanostructures to cross the plasma membrane and enter cells by confocal fluorescence microscopy and evaluated their potential as delivery carriers for CpG immunostimulatory drugs by enzyme-linked immunosorbent assay (ELISA).

2 Materials

All solutions are prepared with ultrapure water (18 M Ω cm) from a Millipore system (Milli-Q synthesis A10) and analytical grade reagents.

2.1 Scaffold ss-DNA Synthesis

1. *E. Coli* DNA ligase buffer (10×): 300 mM tris-HCl (pH 8.0 at 25 °C), 40 mM MgCl₂, 100 mM (NH₄)₂SO₄, 12 mM EDTA, 1 mM NAD (*see Note 1*). Leave one aliquot at 4 °C for current use and store remaining aliquots at -20 °C.
2. Phi29 DNA polymerase reaction buffer (10×): 330 mM tris-acetate (pH 7.5 at 25 °C), 100 mM Mg-acetate, 660 mM K-acetate, 1% (v/v) Tween 20, 10 mM dithiothreitol (DTT) (*see Note 2*). Leave one aliquot at 4 °C for current use and store remaining aliquots at -20 °C.
3. T4 DNA polymerase reaction buffer (5×): 335 mM tris-HCl (pH 8.8 at 25 °C), 33 mM MgCl₂, 5 mM DTT, 84 mM (NH₄)₂SO₄. Leave one aliquot at 4 °C for current use and store remaining aliquots at -20 °C.
4. *E. Coli* DNA ligase. Leave one aliquot at 4 °C for current use and store remaining aliquots at -20 °C (*see Note 3*).
5. Phi29 DNA polymerase. Leave one aliquot at 4 °C for current use and store remaining aliquots at -20 °C.
6. T4 DNA polymerase. Leave one aliquot at 4 °C for current use and store remaining aliquots at -20 °C.
7. dNTP mixture (*see Note 4*). Leave one aliquot at 4 °C for current use and store remaining aliquots at -20 °C.
8. Phosphorylated linear DNA and ligation template (Table 1) (*see Note 5*). Leave one aliquot at 4 °C for current use and store remaining aliquots at -20 °C.
9. Thermomixer comfort.
10. Gel extraction kit.

2.2 DNA Nanostructures Construction

1. TAE/Mg²⁺ buffer (10×): 400 mM tris (pH 7.6), 200 mM acetic acid, 20 mM EDTA, and 125 mM magnesium acetate (*see Note 6*). Prepare and store at room temperature.
2. Scaffold ss-DNA. Store at -20 °C.
3. DNA staple strands (Table 2 and Table 3). Store at -20 °C.
4. PCR machine.

2.3 Cell Cultures

1. RAW264.7 macrophage-like cells.
2. Cell culture medium: Dulbecco's modified Eagle's medium (DMEM) supplemented with 10% heat-inactivated fetal bovine serum, 0.15% NaHCO₃, 100 units/mL penicillin, 100 mg/mL streptomycin, and 2 mM L-glutamine (*see Note 7*). Store at 4 °C.

2.4 Cytokine Assays

1. Anti-Mouse TNF-α pair (*see Note 8*). Store at 4 °C.
2. Phosphate buffer solution (1×): 10 mM Na₂HPO₄, 2 mM KH₂PO₄, 37 mM NaCl, and 2.7 mM KCl (pH 7.4). Store at 4 °C.

Table 1
Phosphorylated DNA and ligation template sequences used in this work

Oligo DNA	Sequence (5'-3')
DNR-1-circle	PO ₃ -TATGC CCAGC CCTGT AAGAT GAAGA TAGCG CACAA TGGTC GGATT CTCAA CTGGT ATTCT CAACT CGTAT TCTCA ACTCG TCTCT GCCCT GACTT C
DNR-1-primer	CAGGG CTGGG CATAG AAGTC AGGGC AGAG
DNR-2-circle1	PO ₃ -TAACTCTTGGGACTGGCAGCTTCAACCATGACCGATTATCGGATGGGCACATTCGCAGGTCTGACAGGACGGATT GATTGG
DNR-2-circle2	PO ₃ -CACAAATGGTCGGACAAGGTACGCATATACTCGAATCCTATTCTCAAGTGTCTCTGATCTGACTTCTATGTCCAGC CCTG
DNR-2-primer1	TACCTTGTCCGACCAATTGTGCCAATCAATCCGTCCTGTCA
DNR-2-primer2	GCTGCCAGTCCCAAGAGTTACAGGGCTGGACATAGAAAGTC
DNR-3-circle1	PO ₃ -TAACTCTTGGGACTGGCAGCTTCAACCATGACCGATTATCGGATGGGCACATTCGCAGGTCTGATAGACGGGATTGA TTGG
DNR-3-circle2	PO ₃ -GAAATCTTATACGCCCTCCGGGAGCCTACGATACATGCCCGGTTCAATCTGCATGAGTGATGTCTTCATTCAAAGCCC GTATTAAAGCCGAAAGATAGCC
DNR-3-circle3	PO ₃ -CACAAATGGTCGGACAAGGTACGCATATACTCGAATCCTATTCTCAAGTGTCTCTGATCTGACTTCTATGTCCAG CCCTG
DNR-3-primer1	CCGGAGGGTATAAGATTTCCCAATCAATCCGTCCTATCA
DNR-3-primer2	TACCTTGTCCGACCAATTGTGGGCTATCTTCGGCTTAATAC
DNR-3-primer3	GCTGCCAGTCCCAAGAGTTACAGGGCTGGACATAGAAAGTC

Table 2
DNA staple strands sequences used in this work

Oligo DNA	Sequence (5'-3')
DNR-1-staple1	CAGCCCTG TAAGATGA AGATAGCG TCTATGCC
DNR-1-staple2	CCCTGACT CACAATGG TCGGATTC CGTCTCTG
DNR-1-staple3	TCTCAACT TCAACTCG TATTCTCA ACTCGTAT
DNR-2-staple1	CAGCCCTGTAACTCTTGGGACTGGTCTATGTC
DNR-2-staple2	ATCTGACTCAGCTTCACCATGACCCGTCTCTG
DNR-2-staple3	TCTCAAGTGATTATCGGATGGGCAAATCCTAT
DNR-2-staple4	TATACTCGCATTTCGCAGGTCTGACGGTACGCA
DNR-2-staple5	TCGGACAAAGGACGGATTGATTGGCACAATGG
DNR-3-staple1	ATACGCCTTAACTCTTGGGACTGGTCTATGTC
DNR-3-staple2	ATCTGACTCAGCTTCACCATGACCAGGACGGA
DNR-3-staple3	CATTCGCAGGTCTGATGATTATCGGATGGGCA
DNR-3-staple4	CAGCCCTGCCGGCGAGCCTACGATGAAATCTT
DNR-3-staple5	TTGATTGGACATGCCCGGTTTCATCCGTCTCTG
DNR-3-staple6	TCTCAAGTTGCATGAGTGATGTCTTCATTCAAG CCCGTATGGTACGCATATACTCGAATCCTAT
DNR-3-staple7	CACAATGGTCGGACAATAAGCCGAAGATAGCG

Table 3
DNA strands sequences used in cell experiments

Oligo DNA	Sequence (5'-3')
DNR-1-staple1-20A	CAGCCCTGTAAGATGAAGATAGCGTCTATGCCAAAAAAAAAAAA AAAAAAAAA
DNR-1-staple2-20A	CCCTGACTCACAATGGTCGGATTCCGTCTCTGAAAAAAAAAAAA AAAAAAAAA
DNR-1-staple3-20A	TCTCAACTTCAACTCGTATTCTCAACTCGTATAAAAAAAAAAAAA AAAAAAAAA
CPG-20 T	TCC ATG ACG TTC CTG ACG TTTTTTTTTTT TTTTTTTTTT
DNR-1-staple2-TAMRA	TAMRA-CCCTGACTCACAATGGTCGGATTCCGTCTCTG

- 24-Well culture plates.
- Modified DNA staples and CpG immunostimulatory oligodeoxynucleotide (*see* **Note 9**). Store at -20°C .
- Multiskan FC.

3 Methods

3.1 Design of RCA-Based DNA Nanostructures

1. The first step proceeds by folding a single long scaffold strand. In this work we employ M13 by RCA strands as the scaffold. The linear RCA scaffold (celeste line) is folded back and forth in a raster fill pattern (Fig. 1), each line of which contained odd number of half-turns (1 turn \approx 10.67 bases, 3.6 nm in length) (*see Note 10*).
2. Create staple strands complementary to RCA scaffold. The staples (denoted as different colors in Fig. 1) spanned three helical domains of the linear scaffold (*see Note 11*). The space between adjacent crossovers is 1.5-turn long. The staple strands not only fold each periodic unit of the scaffold DNA but also connect adjacent units (*see Note 12*).
3. Nucleotide sequences of the RCA scaffold strands and staples are designed using SEQUIN (*see Note 13*) [19], which is a software tool for generating de novo DNA sequences for DNA self-assembly. The sequence design tool assigns DNA sequences on the basis of sequence symmetry minimization.

3.2 Scaffold ssDNA Preparation Process

1. 10 μ L phosphorylated linear DNA (100 μ M) and 10 μ L ligation template (100 μ M) are mixed and incubated at 90 $^{\circ}$ C for 3 min (*see Note 14*) (step a in Fig. 2).
2. *E. coli* DNA ligase and *E. coli* ligase buffer are added when the solution has been cooled to room temperature. The mixture is incubated at 25 $^{\circ}$ C for 16 h (step a in Fig. 2).
3. The ligase is inactivated by heating at 65 $^{\circ}$ C for 10 min.
4. The ligated circular DNA is then treated with T4 DNA polymerase at 37 $^{\circ}$ C for 16 h (*see Note 15*) (step b in Fig. 2).
5. The polymerase is inactivated by heating at 85 $^{\circ}$ C for 10 min.
6. The production is purified by 10% PAGE and redispersed in water, and 4 μ M 50 μ L of the circular DNA template is obtained (*see Note 16*).
7. 50 μ L of RCA reaction buffer supplemented with 5 units phi29 DNA polymerase and 1 mM dNTP mixture is added to 6 μ L of 4 μ M circular DNA template and 6 μ L of 4 μ M primer which is amplified at 30 $^{\circ}$ C in 30 min (*see Note 17*) (step c and d in Fig. 2).
8. The polymerase is inactivated by heating at 65 $^{\circ}$ C for 10 min.
9. The generated ssDNA is purified by ethanol precipitation and stored at -20 $^{\circ}$ C to be used as scaffold ss-DNA (*see Note 18*).

3.3 Assembling and Characterization

1. The scaffold ssDNA and staple strands are mixed to a volume of 20 μ L in 1 \times TAE/Mg²⁺ buffer (*see Note 19*).

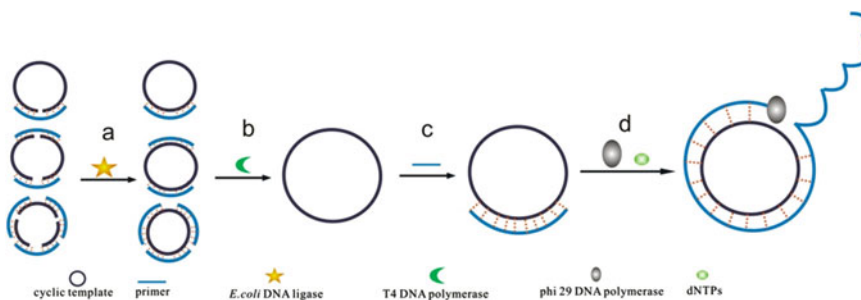


Fig. 2 Preparation of long, single-stranded scaffold DNA by RCA (reproduced from ref. [20] with permission from Elsevier)

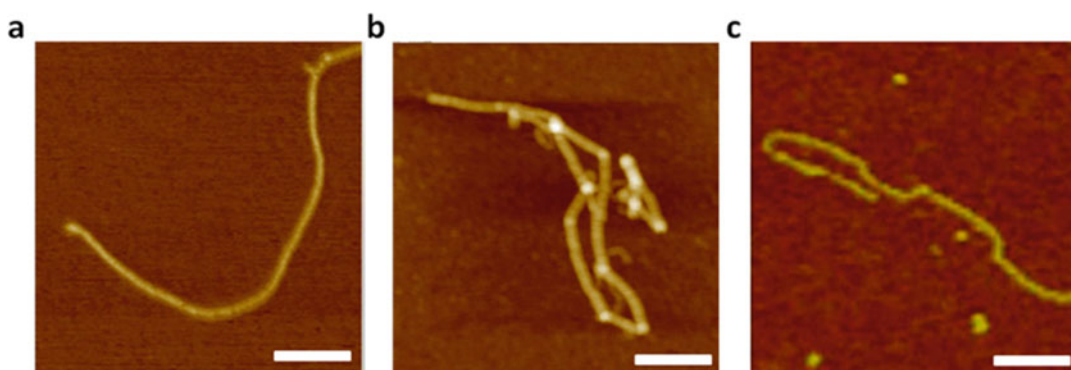


Fig. 3 AFM images of DNR-1 (a), DNR-2 (b) and DNR-3 (c). Scale bars were 200 nm (reproduced from ref. [20] with permission from Elsevier)

2. The sample is cooled from 95 to 4 °C in a PCR machine at a rate of 1 °C/min for ~1.5 h, and stored at 4 °C before AFM imaging (*see Note 20*).
3. 2 μL of samples is deposited onto freshly cleaved mica, and left to adsorb to the surface for 2 min, rinsed with Milli-Q water and dried up immediately with nitrogen. Then they are mounted on a J scanner of the MultiMode 8 AFM.
4. Adjust the AFM parameters, such as gain, setpoint, and scanning speed to get a clear image (Fig. 3). Imaging is performed in tapping mode in air.

3.4 Cellular Uptake Assay

1. RAW264.7 cells are grown in Dulbecco's modified Eagle's medium (DMEM) cell culture medium at 37 °C in humidified air containing 5% CO₂. And they are seeded in a 35 mm glass bottom dish at a density of 2×10^5 cells/mL and incubated at 37 °C for 12 h.
2. Then they are washed twice with phosphate buffer (PBS). For imaging, one of staple strands is modified with a fluorophore (TAMRA) at the 5' end. The TAMRA-DNR-1, and single- or

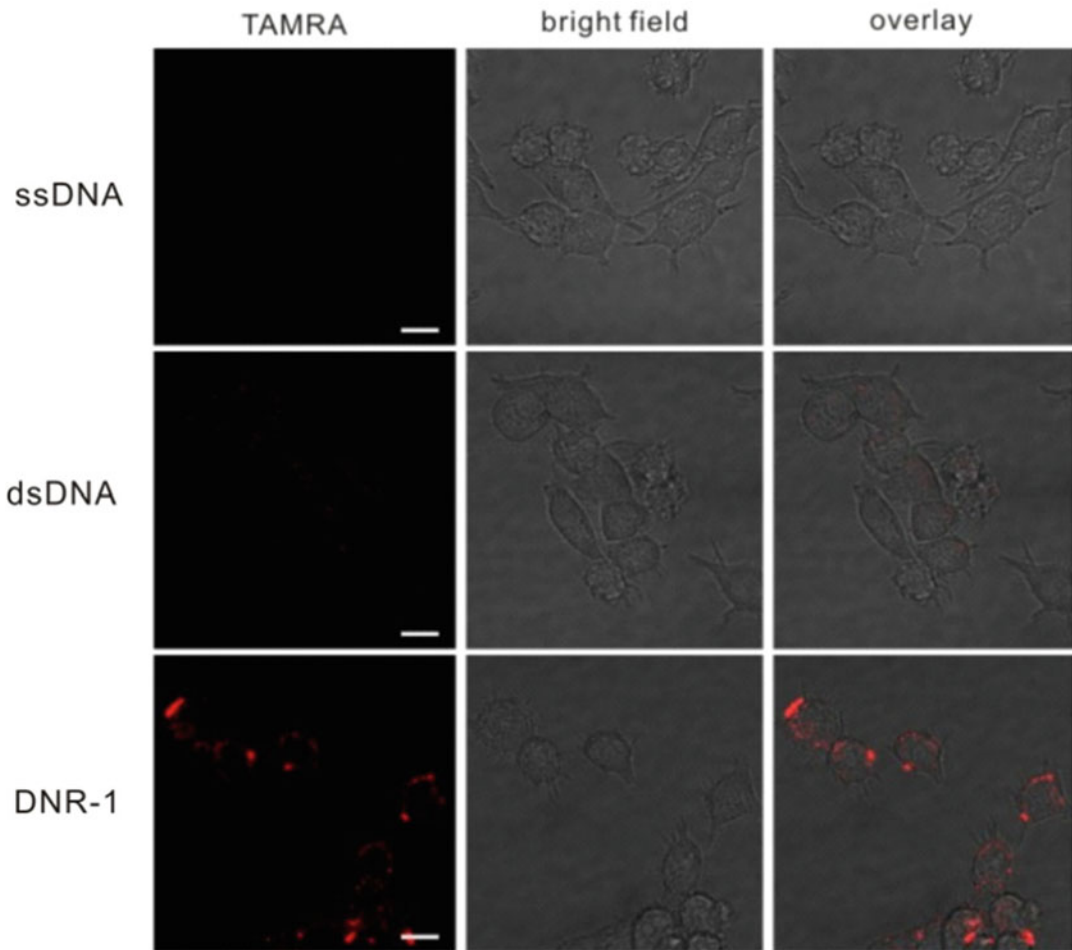


Fig. 4 Confocal microscopic images for intracellular localization of TAMRA-labeled ss- or ds-ODNs and TAMRA-DNR-1. Scale bars: 10 μm (reproduced from ref. [20] with permission from Elsevier)

double-stranded TAMRA-DNA are incubated with macrophage-like RAW264.7 cells for 4 h at 37 °C. After that, cells are washed twice with PBS and fresh clean medium is then added in.

- Images of these living cells are then obtained using a laser confocal microscope (Fig. 4). Wavelength set is 561 nm excitation/570–650 nm emission.

3.5 Cytokine Assays

- RAW 264.7 cells are seeded on 24-well culture plates at a density of 5×10^5 cells/mL and cultured for 24 h at 37 °C before treatment.
- Cells are washed twice with 0.5 mL of PBS. Then, the RCA-based DNA nanostructures bearing CpG oligodeoxynucleotides (ODNs) of certain concentration are diluted with fresh medium

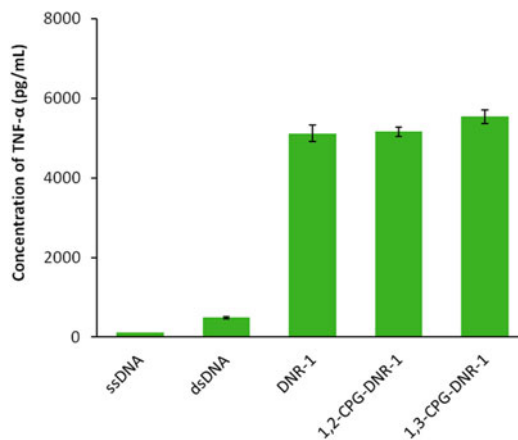


Fig. 5 The release of TNF- α from RAW264.7 cells stimulated by different DNRs with CpG ODNs. Error bars represent standard deviation (SD) of four independent measurements (reproduced from ref. [20] with permission from Elsevier)

and then added to cells. The cells are incubated at 37 °C for 8 h. The supernatants are collected and stored at -80 °C until use.

3. The levels of TNF- α in the supernatants are determined by enzyme-linked immunosorbent assay (ELISA) using antibody pairs specific to these cytokines (Fig. 5).

4 Notes

1. NAD⁺ (nicotinamide adenine dinucleotide) is required as a cofactor, in contrast to other ligases which use rATP.
2. The presence of active reducing reagent in the reaction buffer is critical for this enzyme. While the reaction buffer supplied with the enzyme contains DTT, older buffer stocks or stocks that have been repeatedly frozen and thawed should be supplemented with 1 mM DTT to obtain maximal activity.
3. Employ box filled with ice to keep *E. Coli* DNA ligase, phi29 DNA polymerase, and T4 DNA polymerase active.
4. dNTP mixture can be diluted using sterile Milli-Q water or sterile TE (10 mM tris-HCl, 1 mM EDTA pH 7.5).
5. Centrifuge the DNA samples at 12,000 $\times g$ for 3 min and dissolve them in Milli-Q water by gently swirling mixture.
6. Dilute 2 μ L of 10 \times TAE/Mg²⁺ buffer to 13 μ L with Milli-Q water and add 5 μ L of the DNA strands.
7. Dulbecco's Modified Eagle Medium can be stored at 4 °C in the dark for at least 1 year.
8. For testing mouse TNF- α in supernatant, the purified anti-mouse TNF alpha antibody is useful as the capture antibody in a sandwich

ELISA assay, when used in conjunction with the biotinylated anti-mouse TNF alpha antibody as the detecting antibody.

9. The staple strands are extended with 20 adenine bases, which were complementary to 20 thymine bases extended from the CpG oligodeoxynucleotide.
10. Each line of DNR-1 contained 48 bases that corresponded to 4.5 turns, and each line of DNR-2 contained 80 bases that corresponded to 7.5 turns. The design of DNR-3 followed that of DNR-1 and DNR-2, and its folding pathway showed the 4.5-turn spacing and 7.5-turn spacing alternately.
11. Three of the DNR-3's staples only spanned two helical domains of the linear scaffold.
12. Each periodic unit of DNR-1 was folded with three staple strands to form a rectangle. Similar to DNR-1, DNR-2 was folded with five staples. A jagged shape (DNR-3) was folded with seven staples.
13. A computer program called SEQUIN has been developed by Seeman to assign sequences for the design of nucleic acid secondary structure. A general rule of sequence design is to minimize sequence symmetry in the branched structure to avoid possible undesired pairing between participating strands and mobility of the junction points.
14. Given the technical difficulty synthesizing DNA strands with lengths exceeding 100 bases, we obtained 160 and 256-base circle DNA templates by ligating two and three short DNA strands.
15. T4 DNA polymerase synthesizes DNA on a 5'–3' direction. The enzyme also has 3'–5' exonuclease activity on single-stranded and double-stranded DNA. In the presence of dNTPs, T4 DNA polymerase 3'–5' exonuclease activity is inhibited and the polymerase activity predominates. Thus, caution should be taken to avoid introduction of dNTPs in this step.
16. The first step is to cut out the band of the circular DNA mechanically with a razor blade. It is important to trim the band of all excess gel material, because the purity and dilution of the recovered DNA are greatly affected by the volume of the initial gel slice. The slice may be soaked briefly in water to remove gel buffer and SYBR gold, prior to recovery of the DNA. Then the circular DNA was excised from the gel with gel extraction kit.
17. Precisely controlling the amplification time of RCA process and the ratio of scaffold/staple is crucial for the length of DNA nanostructures. We obtained high yield of DNR-1 with ~100 nm in length under the RCA conditions of 5 min amplification time and a scaffold–staple ratio of 1:20. Similarly,

~500-nm-long DNR-1 were obtained using amplification time of 10 min and the scaffold–staple ratios of 1:100; and ~1- μ m-long DNR-1 using 30-min and 1:500, respectively.

18. Do not overdry DNA, because it is difficult to dissolve overdried DNA. Add buffer or Milli-Q water just after disappearance of milky-white color of the pellet.
19. Keep staples excessive to make the nanostructures well-folded.
20. Storage at 4 °C for a period of 1 week will result in aggregation of nanostructures.

Acknowledgements

We appreciate financial support from the Ministry of Science and Technology of China (2012CB932600) and the National Science Foundation of China (91127037, 91123037, and 90913014).

References

1. Pack DW, Hoffman AS, Pun S, Stayton PS (2005) Design and development of polymers for gene delivery. *Nat Rev Drug Discov* 4:581–593
2. Al-Jamal WT, Kostarelos K (2011) Liposomes: from a clinically established drug delivery system to a nanoparticle platform for theranostic nanomedicine. *Acc Chem Res* 44:1094–1104
3. De M, Ghosh PS, Rotello VM (2008) Applications of nanoparticles in biology. *Adv Mater* 20:4225–4241
4. Mintzer MA, Simanek EE (2009) Nonviral vectors for gene delivery. *Chem Rev* 109:259–302
5. Rosenholm JM, Peuhu E, Eriksson JE, Sahlgren C, Linden M (2009) Targeted intracellular delivery of hydrophobic agents using mesoporous hybrid silica nanoparticles as carrier systems. *Nano Lett* 9:3308–3311
6. Ruan G, Agrawal A, Marcus AI, Nie S (2007) Imaging and tracking of tat peptide-conjugated quantum dots in living cells: new insights into nanoparticle uptake, intracellular transport, and vesicle shedding. *J Am Chem Soc* 129:14759–14766
7. Huang X, Yin Z, Wu S, Qi X, He Q, Zhang Q, Yan Q, Boey F, Zhang H (2011) Graphene-based materials: synthesis, characterization, properties, and applications. *Small* 7:1876–1902
8. Lee JH, Yigit MV, Mazumdar D, Lu Y (2010) Molecular diagnostic and drug delivery agents based on aptamer-nanomaterial conjugates. *Adv Drug Deliv Rev* 62:592–605
9. Welsher K, Liu Z, Sherlock SP, Robinson JT, Chen Z, Daranciang D, Dai H (2009) A route to brightly fluorescent carbon nanotubes for near-infrared imaging in mice. *Nat Nanotechnol* 4:773–780
10. Walsh AS, Yin HF, Erben CM, Wood MJA, Turberfield AJ (2011) DNA cage delivery to mammalian cells. *ACS Nano* 5:5427–5432
11. Li J, Pei H, Zhu B, Liang L, Wei M, He Y, Chen N, Li D, Huang Q, Fan C (2011) Self-assembled multivalent DNA nanostructures for noninvasive intracellular delivery of immunostimulatory CpG oligonucleotides. *ACS Nano* 5:8783–8789
12. Schueller VJ, Heidegger S, Sandholzer N, Nickels PC, Suhartha NA, Endres S, Bourquin C, Liedl T (2011) Cellular immunostimulation by CpG-sequence-coated DNA origami structures. *ACS Nano* 5:9696–9702
13. Jiang Q, Song C, Nangreave J, Liu X, Lin L, Qiu D, Wang Z-G, Zou G, Liang X, Yan H, Ding B (2012) DNA origami as a carrier for circumvention of drug resistance. *J Am Chem Soc* 134:13396–13403
14. Douglas SM, Bachelet I, Church GM (2012) A logic-gated nanorobot for targeted transport of molecular payloads. *Science* 335:831–834
15. Winfree E, Liu F, Wenzler LA, Seeman NC (1998) Design and self-assembly of two-dimensional DNA crystals. *Nature* 394:539–544
16. Rothmund PWK (2006) Folding DNA to create nanoscale shapes and patterns. *Nature* 440:297–302

17. Wei B, Dai M, Yin P (2012) Complex shapes self-assembled from single-stranded DNA tiles. *Nature* 485:623–626
18. Ke Y, Ong LL, Shih WM, Yin P (2012) Three-dimensional structures self-assembled from DNA bricks. *Science* 338:1177–1183
19. Seeman NC (1990) Denovo design of sequences for nucleic-acid structural-engineering. *J Biomol Struct Dyn* 8:573–581
20. Ouyang X, Li J, Liu H, Zhao B, Yan J, He D, Fan C, Chao J (2014) Self-assembly of DNA-based drug delivery nanocarriers with rolling circle amplification. *Methods* 67:198–204

DNA G-Quadruplex-Based Assay of Enzyme Activity

Zhuoliang Liu, Kaiyu He, Wang Li, Xin Liu, Xiahong Xu, Zhou Nie,
and Shouzhao Yao

Abstract

DNA G-quadruplexes are special three-dimensional (3D) DNA nanostructures formed by specific G-rich DNA sequences. These 3D DNA nanostructures can bind with hemin and significantly improve the intrinsic peroxidase activity of hemin. Besides this function, they also enhance the fluorescence intensity of some G-quadruplex-specific dyes. Owing to these features, G-quadruplexes possess several superiorities in the detection of enzymes involved in nucleic acid metabolism, including facile probe fabrication without labeling, simple detection process without washing or separation steps, rapid observation by naked eyes, and easy integration with nucleic acid amplification strategies to amplify signals. Herein, we describe two strategies for label-free detection of enzyme activity based on DNA G-quadruplexes. To increase sensitivity, template-dependent and template-independent DNA amplifications were introduced for the amplification of G-rich DNA sequences. DNA methyltransferase and terminal deoxynucleotidyl transferase were detected as two model analytes, respectively.

Key words G-quadruplex, Enzyme activity, DNazyme, Thioflavin T, Colorimetric, Label-free, Methyltransferase, Terminal deoxynucleotidyl transferase

1 Introduction

DNA can fold into a variety of alternative structures other than the canonical Watson-Crick duplex. Among these noncanonical DNA nanostructures, the G-quadruplex, a four-stranded topology, is of great interest owing to its roles in key biological processes such as the maintenance of telomeres and regulation of gene transcription. DNA G-quadruplexes are three-dimensional nucleic acid nanostructures formed by specific repetitive G-rich DNA sequences [1]. As shown in Fig. 1, in these G-rich DNA sequences, four guanine bases form a G-quartet *via* Hoogsteen base pairings, then two or more G-quartets stack upon each other to form a G-quadruplex structure, and the intervening sequences are extruded as single-strand loops. This 3D DNA nanostructure is stabilized by monovalent cations that occupy the central cavities between the stacks, neutralizing the electrostatic repulsion of inwardly pointing

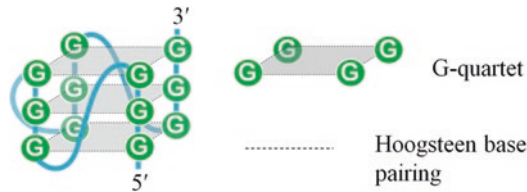


Fig. 1 G-quadruplexes are built from the stacking of successive G-quartets. The G-quartet is a cyclic square planar alignment of four guanines interacted *via* Hoogsteen base pairing

guanine oxygens. Subsequent studies suggested that DNA G-quadruplex structures form not only within one strand (intramolecular) but also between multiple strands (intermolecular). These 3D DNA nanostructures can be extremely stable, and their stabilities depend on many factors, including the length and composition of the DNA sequence, the size of the loops between the guanines, strand stoichiometry and alignment, and the nature of binding cations [2].

Interest in DNA G-quadruplex has increased enormously in recent years due to its peroxidase-mimicking DNAzyme character after binding to hemin (iron(III)-protoporphyrin IX), the cofactor of natural HRP [3]. The docking between hemin and G-quadruplex creates micro-environment profitable for significantly improving the intrinsic peroxidase activity of hemin, capable of efficiently catalyzing the oxidation of various substrates in the presence of H_2O_2 . This catalytic activity has been employed as a signal producer to detect various targets, including metal ions, small molecules, nucleic acids, proteins, and living cells [4–7]. Besides the peroxidase function, some small fluorogenic molecules, such as thioflavin T (ThT), have been discovered to selectively bind to G-quadruplexes resulting in a great fluorescence enhancement [8] and have inspired the exploitation of a series of G-quadruplex-based fluorescent sensors [9–11]. Owing to these features, G-quadruplexes possess several superiorities in the detection of enzymes involved in nucleic acid metabolism, including facile probe fabrication without labeling, rapid observation by naked eyes, and easy integration with various nucleic acid amplification strategies to increase sensitivity [12–14]. Most DNA G-quadruplex-based sensors were designed on the basis of target-dependent formation of G-quadruplexes, which then were utilized to generate colorimetric or fluorescent signals. Generally, the interaction between target and probe causes the release of one G-quadruplex DNA sequence. Therefore, if a target-dependent amplification of G-quadruplex DNA sequence is introduced, the sensitivities of the sensors will certainly be greatly increased. To date, several amplification strategies for G-rich DNA sequences have been reported. These amplification techniques can be grouped into those template-required (strand displacement

amplification (SDA), rolling circle amplification (RCA)) [15], and template-independent (terminal deoxynucleotidyl transferase (TdT)-catalyzed DNA tailing reaction) DNA synthesis [14].

Usually, a C-rich DNA template is applied in the amplification of G-rich DNA sequences using SDA. In this enrichment method, the template consists of three regions. The first region is complementary to a DNA primer, which is located at the 3' end. The third region has a C-rich sequence, locating at the 5' end. The second region is located between the first and the third regions. When this second region forms a duplex in the presence of the complementary strand, the complementary strand can be cleaved into two parts by the nicking endonuclease at a specialized nicking site. By the cooperation of nicking enzyme and polymerase, target-triggered continuous cycles of polymerase extension, nicking enzyme cleavage, and replicated strand release will generate numerous copies of G-rich sequences. Besides this template-required amplification strategy, G-rich DNA sequences can also be synthesized without a template by employing a unique DNA polymerase named TdT, which catalyzes the addition of deoxyribonucleoside triphosphates (dNTPs) to the 3' hydroxyl terminus of a DNA primer. In this amplification, by using a dGTP-rich dNTP pool, a randomly arrayed G-rich sequence, which has been demonstrated to be capable of forming G-quadruplex [14], could be obtained by TdT polymerization using a dGTP-rich dNTP pool.

In this protocol, we describe two strategies for label-free detection of enzymes involved in DNA metabolism based on DNA G-quadruplexes. To amplify the signal, template-required SDA and template-independent TdT-catalyzed DNA tailing reaction were employed for the amplification of G-rich DNA sequences, respectively. DNA methyltransferase (MTase) and terminal deoxynucleotidyl transferase were detected as two model analytes, respectively. DNA MTase catalyzes the DNA methylation process which results in the covalent addition of a methyl group to the target cytosine or adenine in the specific DNA sequences [16]. DNA methylation has a central role in the epigenetic control of mammalian gene expression during development and is required for X inactivation, genomic imprinting, and silencing of retroviral elements [17, 18]. In recent years, studies on cancer pathology have proved that aberrant DNA methylation is a new generation of cancer biomarkers and DNA MTase is a potential target in anticancer therapy [19, 20]. The other model analyte, TdT, is a special polymerase that catalyzes the incorporation of deoxynucleotides at the 3' hydroxyl terminus of DNA primer without a template [21]. The pathological significance of TdT has been proved by that the TdT activity in blast cell acts as an important biomarker to identify leukemia [22]. Alterations in TdT activity and/or its expression level may play a significant role in the initiation and progression of various cancers as well as in the response of the cancers to

chemotherapy. Moreover, TdT is widely used as a molecular biology tool for labeling DNA end, rapid amplification of cDNA ends (RACE), and apoptosis cell detection by the TdT-mediated dUTP-biotin nick end labeling (TUNEL) [23–26]. Therefore, it is significant to develop facile methods to monitor the activities of these enzymes.

For the highly sensitive detection of MTase activity, a methylation-responsive DNA machine is designed to amplify G-rich DNA sequences *via* SDA. The mechanism of the DNA machine is depicted in Fig. 2a. This machine is a hybrid containing two single-stranded DNA (ssDNA): one is used as the methylation-responsive probe named DNA-Mac1 and the other is the template for amplification named DNA-Mac2. DNA-Mac2 consists of three regions. Region I is complementary to part of DNA-Mac1. Region II has a nicking site for nicking endonuclease Nt.BbvC I when it forms a duplex. Region III is used as a template for polymerizing G-rich DNA sequence that will form G-quadruplex. DNA-Mac1 is a hairpin DNA containing three segments, which can be methylated and cleaved by the Dam MTase/DpnI coupling reaction. One (segment B) is an 18 base-pair duplex stem with methylation-responsive sequence in the middle, tethering a 5 bases loop. Another part (segment A) can hybridize with a 13-base part of region I of DNA-Mac2, yielding a complete DNA machine. The third one (segment C) is an unpaired four “T” bases sequence at the elongation of the 3′ terminus, which serves as a block to prohibit the undesired replication initiated at the 3′ end of DNA-Mac1. When segment B is not methylated, DNA-Mac2 is blocked by DNA-Mac1 to prevent it from forming an active machine. In the presence of the Dam MTase, segment B is methylated and cleaved by DpnI sequentially, resulting in the fragmentation of DNA-Mac1 into three parts. Two parts, a new hairpin and a small ssDNA fragment, are released. The third part, an ssDNA containing segment A, hybridizes with region I of DNA-Mac2, switching on the DNA machine. Then, the replication of the track (regions II and III of DNA-Mac2) is initiated in the presence of polymerase and dNTPs mixture. Since the replicated strand in region II includes the nicking site for Nt.BbvC I, the cleavage of region II by nicking enzyme restarts the replication by polymerase to produce a secondary DNAzyme to replace the original one. Thus, plenty of G-quadruplex-forming sequences are produced. Subsequently, with the coordination of hemin, the G-quadruplex-hemin DNAzyme catalyzes the oxidation of 2,2′-amino-di(2-ethylbenzothiazoline sulfonic acid-6) ammonium salt (ABTS²⁻) by H₂O₂ to produce the colored product ABTS^{•-} ($\lambda_{\max} = 415 \text{ nm}$, $\epsilon = 3.6 \times 10^4 \text{ M}^{-1} \text{ cm}^{-1}$). This strategy will be easily extended to analyze endonuclease activity through proper DNA probe design, which will contribute to the future application of G-quadruplex-based technologies to the enzyme activity analysis for therapeutic purposes.

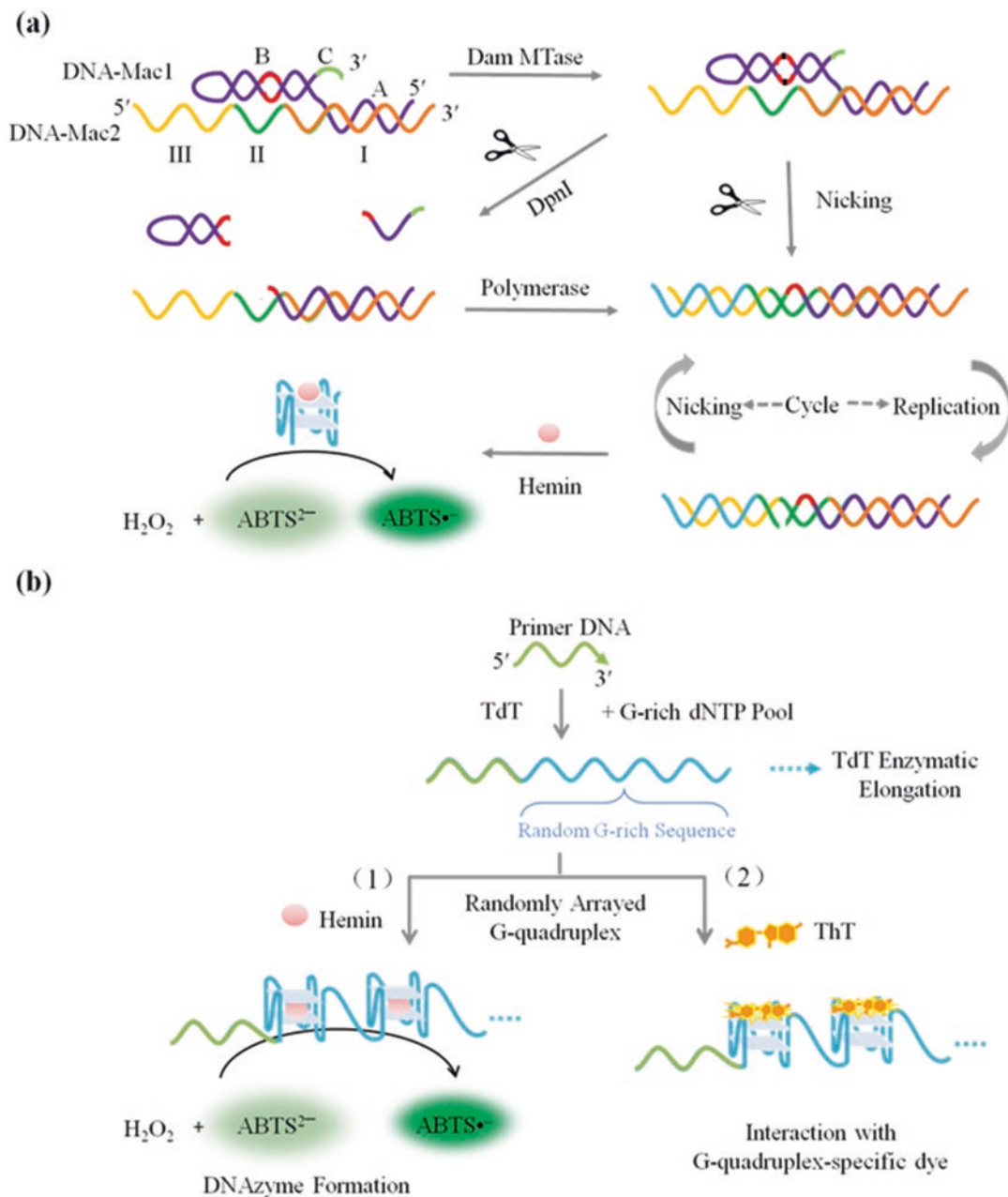


Fig. 2 (a) Schematic diagram of the Dam MTase activity assay using methylation-responsive DNA-based machine. Adapted with permission from ref. [12]. Copyright 2010 American Chemical Society. (b) Schematic presentation of the preparation of TdT-generated G-quadruplexes and its derivative colorimetric (1) and fluorescent (2) assays of TdT activity. Adapted from ref. [14] with permission from The Royal Society of Chemistry

To detect TdT activity, a 14-base ssDNA is used as a primer probe to synthesize randomly arrayed G-rich DNA sequence by employing G-rich dNTP pool as depicted in Fig. 2b. This long and random G-rich sequence forms multiple and consecutive G-quadruplexes, which are then coordinated with hemin or ThT to

produce colorimetric or fluorescent signals, respectively. It presents a facile strategy for label-free detection of TdT activity with high sensitivity and colorimetric readout. Due to the quick binding interaction between ThT and G-quadruplex to form a stable fluorescent complex, it is feasible to monitor the activity of TdT in real time, which is seldom seen in current enzyme assays based on DNA G-quadruplex. Unlike conventional DNAzyme-related assays based on the DNA probes containing the specific DNAzyme sequence, this TdT-generated DNAzyme provides a novel methodology to develop biosensors without considering the sequence of DNAzyme in the probe design, which remarkably simplifies the design process and shortens the probe sequence. Moreover, the use of a TdT-generated randomly arrayed G-quadruplex as a signal producer will improve the TdT-related biosensing applications, such as DNA labeling and apoptosis assay, which generally require modified nucleotides and a tedious multi-step procedure. This sensing system can be readily extended to a great variety of targets, such as metal ions, small molecules, transcription factors, enzymes, and even cancer cells, by integrating the cognate DNA recognition element with nuclease-mediated activation of TdT-generated DNA G-quadruplex.

In conclusion, DNA G-quadruplexes have shown exceptional promise and potential, as well as versatility, for applications in biochemical analysis of critical enzymes in DNA metabolism. It allows for a facile preparation and detection process: the DNA probe does not require the labor-intensive and expensive chemical modification; the detection is simple and without washing or separation steps, and the results can be visualized by the naked eyes without sophisticated instrumentation. Moreover, combining with nucleic acid *in vitro* amplification, the sensitivity can be further enhanced (*see Note 21*). Specialists involved in DNA G-quadruplex and peroxidase-mimic DNAzyme will learn how the following protocol can be applied to their studies, whether in molecular biology or chemistry. General readers from a broad spectrum of disciplines will also appreciate an introduction to this unique 3D DNA nanostructure for biosensing.

2 Materials (*See Note 1*)

All samples and solutions were prepared using ultrapure water with an electric resistance of 18.25 M Ω •cm obtained from a Millipore filtration system. Chemicals and reagents: DNA oligonucleotides, 2,2'-amino-di(2-ethyl-benzothiazoline sulfonic acid-6) ammonium salt (ABTS²⁻), deoxyadenosine triphosphate (dATP), deoxythymidine triphosphate (dTTP), deoxyguanosine triphosphate (dGTP), dNTPs mixture, 4-(2-hydroxyethyl) piperazine-1-ethanesulfonic acid sodium salt (HEPES) and 2-(4-morpholino) ethanesulfonic acid (MES), hemin, ThT, DNA adenine methylation (Dam) MTase, Nt.BbvC I, Klenow fragment (3'-5'-exo-), DpnI, S-adenosylmethionine (SAM), and TdT.

2.1 DNA Oligos

Oligonucleotides: Different regions of DNA probes are indicated with different fonts and colors. They are coloured in the same way as in Fig. 2.

ssDNA for assembly the DNA machine employed in Dam MTase activity assay (*see Note 2*):

DNA-Mac1, 5'-CATCACGTACGTGACGAGATCAAGGTCTGACTTTTTGTCAGACCTTGATCTCGTTTT-3'.

DNA-Mac1 consists of three segments (from 5' to 3'): segment A (in italics) can hybridize with a 13-base part of region I of DNA-Mac2; segment B is an 18 base-pair duplex stem (underlined) of the hairpin with methylation-responsive sequence (GATC) in the middle, linked by a 5 bases loop (five "T" bases); segment C (four "T" bases, in bold), which serves as a block to prohibit the undesired replication initiated at the 3' end of DNA-Mac1.

DNA-Mac2, 5'-CCCAACCCGCCCTACCCGCTGAGGTCTCGTACGTACGTGATG-3'.

DNA-Mac2 is composed of three regions (from 3' to 5'): region I (in italics) is complementary to part of DNA-Mac1; region II (the 7-nt domain, in bold) can be recognized by nicking endonuclease Nt.BbvC I when it forms a double strand; region III (underlined) is used as a template for polymerizing G-rich DNA sequence that will form G-quadruplex.

DNA primer for TdT activity assay (*see Note 3*):

5'-AATACAACCTCTCA-3'.

2.2 Buffer Solutions

1. Annealing buffer: 100 mM Tris-HCl (pH 7.5), 1 M NaCl, 10 mM EDTA.
2. Methylase buffer: 50 mM NaCl, 10 mM Tris-HCl, 10 mM MgCl₂, pH 7.5 (*see Note 4*).
3. HEPES solution: 25 mM HEPES (*see Note 5*), 200 mM NaCl, 20 mM KCl (*see Note 6*), 0.05% (v/v) TritonX-100 (*see Note 7*), pH 5.2 (*see Note 8*).
4. TdT reaction buffer: 0.2 M Potassium cacodylate (*see Note 9*), 0.025 M Tris, 0.01% (v/v) Triton X-100, 1 mM CoCl₂ (*see Note 10*), pH 7.2.
5. MES-Tris buffer: 100 mM 2.5× MES-Tris, 50 mM KCl, and 0.05% (v/v) Triton X-100, pH 5.5.
6. Tris-HCl buffer: 50 mM Tris-HCl, 50 mM KCl, pH 7.2.
7. Stock solution of hemin: 1 mM Hemin in DMSO. Store it at room temperature protected from light (*see Note 11*).
8. ThT solution: 100 μM ThT in water.
9. ABTS²⁻ solution: 20 mM ABTS²⁻ in water (*see Note 12*).
10. H₂O₂ solution: 20 mM H₂O₂ in water (*see Note 13*).

2.3 Equipment

1. DU 800 UV/Visible Spectrophotometer (Beckman Coulter, USA).
2. QuantaMaster™ fluorescence spectrophotometer (PTI, Canada).
3. Digital Dry Bath (Bio-Rad, USA).
4. Digital camera (Canon, Japan).

3 Methods

3.1 Colorimetric Assay of Dam MTase Activity Using Methylation-Responsive DNA Machine (See Note 14)

1. Determine the concentration of DNA-Mac1 and DNA-Mac2 by preparing duplicate dilutions and measuring the absorbance value at 260 nm (A_{260}), respectively. Calculate the concentration of DNA:

$$C (\text{mol} / \text{L}) = \frac{0.033A_{260}}{\text{MW}} \times F$$

where MW is the molar mass (g/mol) of DNA strand, and F is the dilution factor.

2. Add DNA-Mac1 and DNA-Mac2 in 1× annealing buffer and mix. The final concentration of the hybrid is 10 μM.
3. Bring the mixed oligonucleotide solution to 65 °C by placing the tube in a 65 °C (or higher) digital dry bath. Maintain the solution at 65 °C for 10 min.
4. Remove the solution from the digital dry bath and allow it to cool slowly to room temperature for 1–2 h.
5. Store the hybrid at 4 °C as a stock solution for further use.
6. Set up the following reaction at room temperature in a 600 μL Eppendorf tube and add the reagents in order as they are listed in Table 1.

Table 1
Colorimetric assay of Dam MTase activity

Components	Amount	Final concentration
10× Methylase buffer	1.0 μL	1×
The hybrid of DNA-Mac1 and DNA-Mac2	10 pmol	1.0 μM
dNTPs	5.0 nmol	0.5 mM
SAM	800 pmol	80 μM
DpnI	4.0 U	400 U/mL
Nt.BbvC I	4.0 U	400 U/mL
Klenow fragment	2.0 U	200 U/mL
Dam MTase	0–4.0 U	0–400 U/mL
Water to a final volume of	Up to 10 μL	Total volume

- Mix gently and spin down for a few seconds to collect the reaction mixture at the bottom of the tube.
- Incubate the mixture at 37 °C for 2 h.
- Add 2.0 μL of 10 μM hemin, 20 μL of 10 \times HEPES solution, and 128 μL of H_2O , mix, and incubate the resulting solution at 37 °C for 30 min.
- Add 20 μL of 20 mM ABTS²⁻ (*see Note 15*) and 20 μL of 20 mM H_2O_2 (*see Note 16*) separately (*see Note 17*).
- Mix the solution and monitor immediately the absorption spectra at 415 nm in 2.5 min.
- Calculate the absorbance change (ΔAbs) in 2.5 min and plot ΔAbs vs. [Dam MTase] (U/mL) (Fig. 3).
- If necessary, capture the results using a digital camera (*see Note 8*).

3.2 Colorimetric Assay of TdT Activity Using Random G-rich DNA Sequence (See Note 18)

Part I: Evaluate the effect of the dNTP composition on the activity of randomly synthesized G-quadruplex DNAzyme.

- Set up the following reaction (Table 2) at room temperature in a 200 μL Eppendorf tube. Use different compositions of dNTP including various combinations of dGTP (percentage ranging from 50 to 100%), dATP (percentage ranging from 0 to 50%) and dTTP (percentage ranging from 0 to 50%) (*see Note 19*).
- Mix gently and spin down for a few seconds to collect the reaction mixture at the bottom of the tube.
- Incubate the mixture at 37 °C for 2 h.
- Terminate the DNA tailing reaction by heating the solution at 75 °C for 10 min.
- Add 21 μL of H_2O , 32 μL of 2 \times MES-Tris buffer, and 1 μL of 10 μM hemin, mix, and incubate the resulting solution at 37 °C for 30 min.
- Add 8 μL of 20 mM ABTS²⁻, mix, and transfer the solution to a cuvette to record the absorbance change. After 20 s, add 8 μL of 20 mM H_2O_2 and mix the solution with a pipette within 10 s to initiate the color reaction. Continue to monitor the absorption spectra at 415 nm in 4.0 min immediately.
- Calculate the initial reaction rate ν from the absorbance change at 415 nm during initial 60 s to evaluate the catalytic activities of TdT polymerization products as a function of different compositions of three-component substrate pool (dGTP + dATP + dTTP).
- Determine the optimal content of nucleotide substrate pool for TdT-generated DNAzyme (Fig. 4).

Part II: Colorimetric detection of the TdT activity.

- Conduct the reaction following steps 1–6 except using the optimal content of nucleotide substrate pool (60% dGTP + 40%

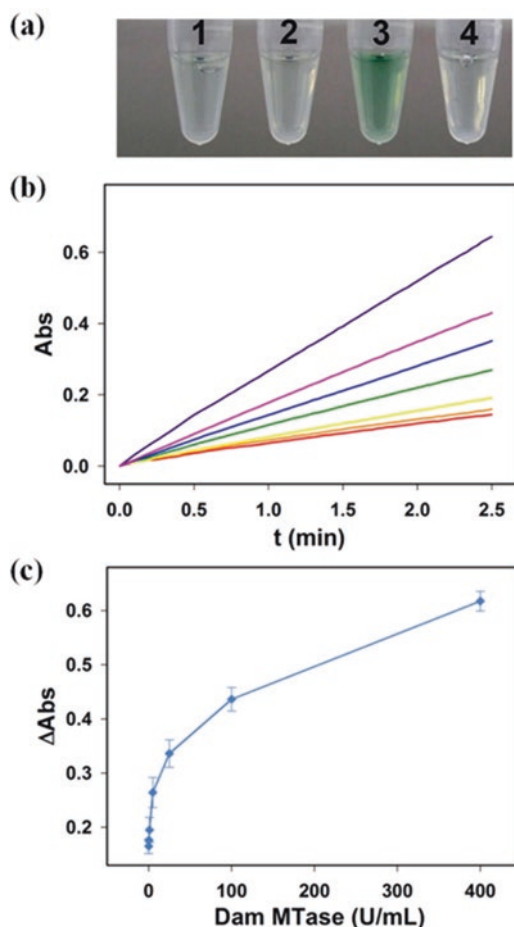


Fig. 3 Assay of Dam MTase activity by DNA-based machines. **(a)** The visualization analysis of Dam MTase activity: (1) treated without Dam MTase or DpnI; (2) treated with DpnI but without Dam MTase; (3) treated with both Dam MTase and DpnI; (4) treated with EcoRI MTase and DpnI. **(b)** The time-dependent absorbance changes upon analyzing Dam MTase. The curves from bottom to top were obtained with different concentrations of Dam MTase: 0, 0.25, 1, 5, 25, 100, and 400 U/mL, respectively. **(c)** The absorbance change (Δ Abs) in 2.5 min is plotted as a function of the Dam MTase concentration. Reproduced from ref. [12] with permission from The American Chemical Society

Table 2
Colorimetric assay of TdT activity

Components	Amount	Final concentration
10× TdT reaction buffer	1.0 μ L	1 ×
DNA primer	10 pmol	1.0 μ M
dNTPs	10 nmol	1.0 mM
TdT	4.0 U	400 U/mL
Water to a final volume of	Up to 10 μ L	Total volume

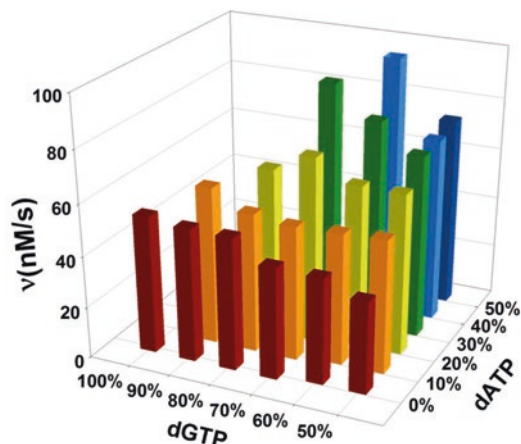


Fig. 4 The catalytic activities of Hemin via binding with TdT polymerization products as a function of different compositions of a three-component substrate pool (dGTP + dATP + dTTP). In all experiments, the TdT reaction mixtures contain DNA primer (0.5 mM) and TdT (4 U). Reproduced from Ref. [14] with permission from The Royal Society of Chemistry

dATP) (Fig. 4) (*see Note 20*) and different amounts of TdT ranging from 0.2 to 8 U to detect TdT enzyme.

10. Calculate ΔAbs in 4.0 min and plot ΔAbs vs. the amount of TdT (U) (Fig. 5).
11. If necessary, capture the results using a digital camera (*see Note 8*).

3.3 Fluorescent Assay of TdT Activity Using Random G-Rich DNA Sequence

Part I: Optimize the composition of the dNTP pool to obtain most suitable G-quadruplex for enhancing the fluorescence intensity of ThT.

1. Set up the following reaction (Table 3) at room temperature in a 200 μL Eppendorf tube. Use different compositions of dNTP including various combinations of dGTP (percentage ranging from 50 to 100%), dATP (percentage ranging from 0 to 50%), and dTTP (percentage ranging from 0 to 50%).
2. Mix gently and spin down for a few seconds to collect the reaction mixture at the bottom of the tube.
3. Incubate the mixture at 37 $^{\circ}\text{C}$ for 2 h.
4. Terminate the DNA tailing reaction by heating the solution at 75 $^{\circ}\text{C}$ for 10 min.
5. Add 38 μL of H_2O , 50 μL of 2 \times Tris-HCl buffer, and 2 μL of 100 μM ThT, mix, and incubate the resulting solution at room temperature for 5 min.
6. Monitor the emission spectra from 445 to 600 nm with excitation at 425 nm.

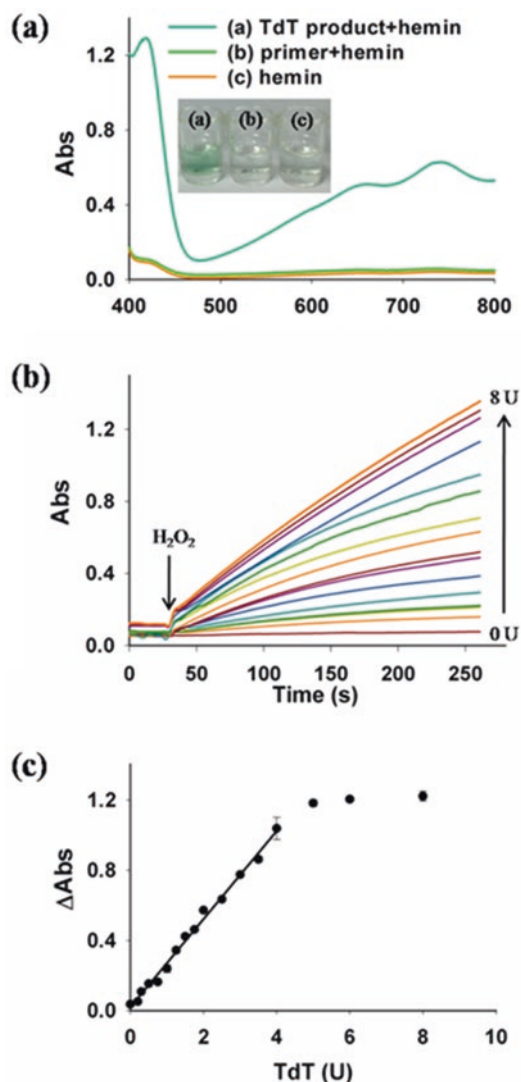


Fig. 5 (a) UV–Vis absorption spectra and photography (inset) to show the DNAzyme activity of TdT-generated G-quadruplexes in the $\text{ABTS}^{2-}\text{-H}_2\text{O}_2$ system. Inset: (a) hemin and TdT polymerization product (dNTP pool: 40 % dATP and 60 % dGTP); (b) hemin and primer; (c) hemin. (b) Time-dependent absorbance changes at 415 nm versus different amounts of TdT. (c) The absorbance change in 4 min is plotted as a function of the amount of TdT. Reproduced from ref. [14] with permission from The Royal Society of Chemistry

Table 3
Fluorescent assay of TdT activity

Components	Amount	Final concentration
10× TdT reaction buffer	1.0 μL	1×
DNA primer	10 pmol	1.0 μM
dNTPs	10 nmol	1.0 mM
TdT	4.0 U	400 U/mL
Water to a final volume of	Up to 10 μL	Total volume

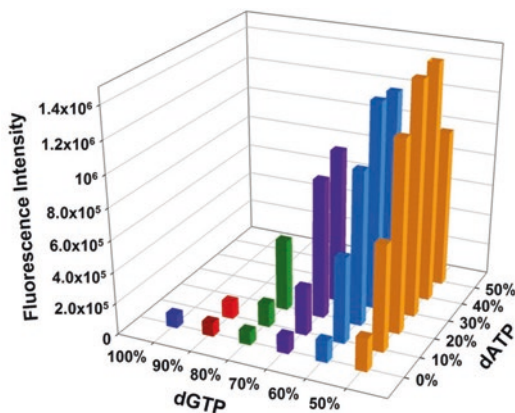


Fig. 6 The ThT fluorescence enhancement *via* binding with TdT polymerization products as a function of different compositions of three-component substrate pool (dGTP + dATP + dTTP). In all experiments, the TdT reaction mixtures contain DNA primer (1 μ M) and TdT (4 U). Reproduced from Ref. [14] with permission from The Royal Society of Chemistry

7. Calculate the ThT fluorescence enhancement to investigate the enhancing effects of TdT polymerization products on the fluorescence intensity of ThT as a function of different compositions of three-component substrate pool (dGTP + dATP + dTTP).
8. Determine the optimal content of nucleotide substrate pool for TdT-generated G-quadruplexes (Fig. 6).

Part II: Fluorescent detection of the activity of TdT.

9. Conduct the reaction following **steps 1–6** except using the optimal content of nucleotide substrate pool (50% dGTP + 40% dATP + 10% dTTP) (Fig. 6) (*see Note 20*) and different amounts of TdT ranging from 0 to 8 U to detect TdT enzyme.
10. Plot the fluorescence intensity of ThT at 485 nm (FL) vs. the amount of TdT (U) (Fig. 7).

3.4 Real-Time Fluorescence Detection of TdT Activity

1. Set up the following reaction at room temperature in a 200 μ L Eppendorf tube (Table 4):
2. Mix gently and spin down for a few seconds to collect the reaction mixture at the bottom of the tube.
3. Transfer the solution to a cuvette quickly and monitor the fluorescence intensity immediately at 485 nm with excitation at 425 nm. Keep the solution at 37 $^{\circ}$ C during the measurement by using a fluorescence spectrophotometer equipped with a temperature controller (Fig 8).

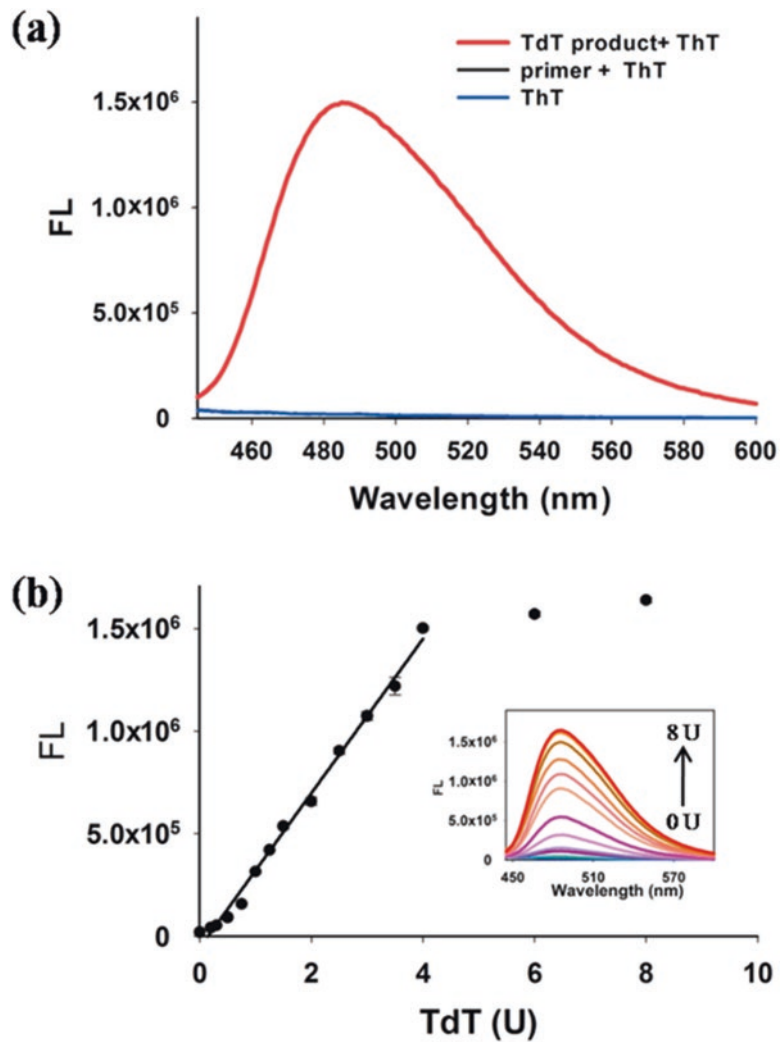


Fig. 7 (a) Fluorescence emission spectra of ThT in the presence of TdT-generated G-quadruplexes (dNTP pool: 50 % dGTP, 40 % dATP and 10 % dTTP). (b) The fluorescence intensity of ThT at 485 nm is plotted as a function of the amount of TdT. The insert figure shows the fluorescence emission variation of ThT *versus* different amounts of TdT. Reproduced from ref. [14] with permission from The Royal Society of Chemistry

Table 4
Real-time fluorescence detection of TdT activity

Components	Amount	Final concentration
10× TdT reaction buffer	10.0 μL	1 ×
DNA primer	100 pmol	1.0 μM
dNTPs (50 % dGTP, 40 % dATP, and 10 % dTTP)	100 nmol	1.0 mM
ThT	2.0 nmol	20 μM
TdT	0–20 U	0–200 U/mL
Water to a final volume of	100 μL	Total volume

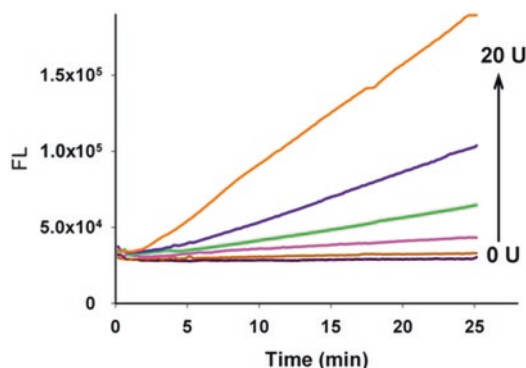


Fig. 8 Real-time detection of TdT activity by the dynamic change of fluorescence intensity at 485 nm with increasing TdT reaction time. Reproduced from ref. [14] with permission from The Royal Society of Chemistry

4 Notes

1. Store enzymes at $-20\text{ }^{\circ}\text{C}$. In order to maintain the full catalytic activity of enzymes, enzyme stock solutions can be aliquoted into several tubes to avoid repeated thawing and freezing manipulation. And enzymes should be put on ice during the process of experimental operation. Similarly, the mixture dNTP solution should also be aliquoted into several packages to avoid repeated freezing and thawing.
2. Pay attention to the direction of each DNA sequence (from 5' to 3'), making sure not to reverse the sequence. The reverse sequences do not assemble the DNA machine. At the 3' terminal of DNA-MacI probe, four non-complementarily additional thymine bases were employed to avoid undesirable polymerization by polymerase. Alternatively, the modification of 3' terminal with chemical groups (such as phosphate group or dideoxynucleotide) are optional approaches to avoid undesirable polymerization.
3. When synthesizing a random G-rich DNA sequence using TdT, ssDNA with chain lengths of three or more nucleotides serves as a favorable primer. In this protocol, the DNA primer chosen for the assay of TdT is a 14-base ssDNA without complicated secondary structure.
4. It is important to note that a high concentration of reducing substances, such as dithiothreitol (DTT) and mercaptoethanol, will reduce the colored product $\text{ABTS}\cdot^-$. Therefore, the reaction buffer and storage buffer for enzymes were prepared without DTT in this protocol.
5. The catalytic activity of G-quadruplex/hemin complex (G-quadruplex DNAzyme) depends on buffer ingredient. Nitrogenous buffers (e.g., MES- NH_4 , MES- NaOH , and HEPES- NH_4) are favorable, whereas oxyanion buffers (e.g.,

$\text{NaH}_2\text{PO}_4\text{-NH}_4$, $\text{NaH}_2\text{PO}_4\text{-NaOH}$, citrate- NH_4 , and HAc- NaAc) appear to prohibit its activity. Therefore, it is strongly recommended to choose nitrogenous buffers, such as MES and HEPES, for the DNAzyme-related experiments.

6. The catalytic activity of G-quadruplex DNAzymes can be influenced by the species and concentration of the cations, such as K^+ and Na^+ . K^+ facilitates the formation of parallel G-quadruplexes whereas the presence of Na^+ causes the formation of antiparallel structures. Because the stabilizing ability of K^+ for G-quadruplexes is much better than that of Na^+ , addition of a small amount of K^+ into a large quantity of Na^+ will lead to obvious changes in G-quadruplex structures (antiparallel \rightarrow mixed parallel/antiparallel, mixed parallel/antiparallel \rightarrow parallel or antiparallel \rightarrow parallel), accompanied by the increase in the catalytic activities of the G-quadruplex/hemin complexes. In addition, the presence of NH_4^+ can improve the performance of G-quadruplex DNAzyme-based sensors. Therefore, according to the various experimental requirements, the suitable species and concentrations of the cations should be considered.
7. Hemin can aggregate to form dimers in aqueous solutions. Such aggregation is detrimental to the interaction between hemin and G-quadruplexes. Triton X-100 can mediate shifts of the dimer-monomer equilibrium towards the monomer. Therefore, the presence of Triton X-100 is crucial to G-quadruplex DNAzyme-based sensors. The optimal Triton X-100 concentration ranges from 0.03 to 0.05% (w/v) [3].
8. In the presence of G-quadruplex DNAzymes, ABTS^{2-} is oxidized by H_2O_2 to the colored product $\text{ABTS}^{\bullet-}$. The free radical product $\text{ABTS}^{\bullet-}$ is not stable in neutral or alkaline solution, and it will quickly decay to a colorless product through disproportionation. This is not benefit for the accumulation of the colorimetric signal and the improvement of the detection sensitivity. It will also affect the use of ABTS^{2-} in visual detection. Therefore, it is suggested that the peroxidation is performed in a weakly acidic buffer with a pH value between 5.0 and 6.5. A buffer with a pH value lower than 5.0 is not recommended, because the catalytic activity becomes lower as the pH value decreases.
9. The potassium cacodylate contained in the reaction buffer for TdT is toxic. Handle it with care and dispose of it in accordance with the relevant laws and regulations.
10. Cobalt is a necessary cofactor of TdT. Metal chelators, ammonium, chloride, iodide, and phosphate ions are the inhibitors of TdT. Therefore, these substances should be avoided when detecting the activity of TdT.

11. Hemin is dissolved in DMSO and kept at room temperature. When the temperature is below 10 °C, hemin will be precipitated.
12. The toxicological properties of this product have not been thoroughly investigated.
13. H₂O₂ solution should be freshly prepared before use.
14. The catalytic activity of DNAzymes with different structures follows the order: parallel > mixed parallel/antiparallel > antiparallel. Therefore, the commonly used DNAzyme sequences are those which can form parallel G-quadruplexes. In this protocol, the methylation-responsive DNA machine synthesize numerous DNA fragments containing one of the commonly used DNAzyme sequences (GGGTAGGGCGGGTTGGG). Generally, G-rich sequences with short loops are inclined to form parallel G-quadruplexes, and those with long loops usually fold into antiparallel G-quadruplexes.
15. The catalytic rate of DNAzyme shows a zero-order dependence on ABTS²⁻ concentration. The recommended concentration is between 0.5 and 2.0 mM, a higher concentration of ABTS²⁻ will result in a higher background.
16. As the H₂O₂ concentration increases, the enzyme activity of G-quadruplex DNAzyme is improved. However, the disproportionation of ABTS^{•-} is accelerated when a high concentration of H₂O₂ is used. To overcome this, a certain amount of adenosine triphosphate (ATP) can be added into the sensing system. The presence of ATP can not only inhibit efficiently the disproportionation of ABTS^{•-}, but also improve the catalytic activity of the G-quadruplex DNAzyme [27].
17. Add drops of H₂O₂ and ABTS²⁻ separately, at different sides of the Eppendorf tubes before spinning them down. This is to minimize any undesirable reactions between the two reagents.
18. Long G-rich sequences could confer hemin with higher catalytic activity than short sequences [28]. The length of the G-rich sequences polymerized by TdT depends on the ratio between the primer and the dNTP. With a fixed constitution of substrate dNTP pool, the smaller the ratio is, the longer the extended sequence is. It would be better to optimize the ratio for excellent experimental results in a certain experiment.
19. The TdT-yielded DNA sequences are nonspecific and nearly random, and their sequence compositions are largely dependent on the constitution of substrate dNTP pool. In order to obtain most suitable G-quadruplexes for improving the peroxidase activity of hemin or enhancing the fluorescence intensity of ThT, the constitution of dNTP substrate pool was

optimized. The previously reported G-quadruplex DNAzymes revealed that the percentage of deoxyguanosine in the typical DNAzyme sequences ranges from 57 to 78%, and deoxycytidine was seldom in these sequences. Therefore, in the polymerization of a random G-rich DNA sequence utilizing TdT, two criteria were followed for constructing a dNTP substrate pool: (1) the proportion of dGTP was more than 50%; (2) dCTP was excluded to avoid the possible cytosine-guanine base pair that forms an undesirable second structure to disturb the formation of G-quadruplexes [14].

20. These optimized results of the dNTP substrate pool in this protocol can be adopted in other research work. Also, readers can optimize the constitution of dNTP substrate pool by themselves according to their own experimental conditions to acquire a most suitable composition for a certain research.
21. This protocol shows sensitive and selective detection of enzymes involved in nucleic acids metabolism based on DNA G-quadruplexes. Figure 3b depicts the time-dependent absorbance changes observed upon analyzing different concentrations of Dam MTase (from 0 to 400 U/mL). The calibration curve (Fig. 3c) indicates that the detection limit of this DNA machine-based method is 0.25 U/mL. Figure 5b shows the time-dependent absorbance changes observed upon using different concentrations of TdT, and the corresponding calibration curve is shown in Fig. 5c. A fairly well linear response is observed in the concentration range of TdT from 0.3 to 4 U with a correlation efficiency of 0.993 and a low detection limit (DL) of 0.0394 U ($S/N=3$). Figure 7 indicates the fluorescent assay results of TdT activity based on TdT-generated long random G-rich sequence. A good linear response is observed in the concentration range of TdT from 0.3 to 4 U with a detection limit of 0.05 U (Fig. 7b). In addition, due to the quick binding interaction between ThT and the G-quadruplex to form a stable fluorescent complex, the activity of TdT can be monitored in real-time (Fig. 8). This protocol is versatile and can be extended to detect other enzymes involved in nucleic acid metabolism with proper DNA sequence design.

Acknowledgments

This work was funded by the National Natural Science Foundation of China (Nos. 21222507, 21175036, 21235002, 21575038, and 21305037), the Foundation for Innovative Research Groups of NSFC (Grant 21221003), and the Natural Science Foundation of Hunan Province (No. 2015JJ1005).

References

1. Huppert JL (2010) Structure, location and interactions of G-quadruplexes. *FEBS J* 277: 3452–3458
2. Bochman ML, Paeschke K, Zakian VA (2012) DNA secondary structures: stability and function of G-quadruplex structures. *Nat Rev Genet* 13:770–780
3. Travascio P, Li Y, Sen D (1998) DNA-enhanced peroxidase activity of a DNA–aptamer–hemin complex. *Chem Biol* 5:505–517
4. Zhu X, Gao X, Liu Q et al (2011) Pb²⁺-introduced activation of horseradish peroxidase (HRP)-mimicking DNAzyme. *Chem Commun* 47:7437–7439
5. Liu B, Zhang B, Chen G et al (2014) An omega-like DNA nanostructure utilized for small molecule introduction to stimulate formation of DNAzyme–aptamer conjugates. *Chem Commun* 50:1900–1902
6. Zheng A, Li J, Wang J et al (2012) Enzyme-free signal amplification in the DNAzyme sensor *via* target-catalyzed hairpin assembly. *Chem Commun* 48:3112–3114
7. Wang F, Lu C, Liu X et al (2014) Amplified and multiplexed detection of DNA using the dendritic rolling circle amplified synthesis of DNAzyme reporter units. *Anal Chem* 86:1614–1621
8. Mohanty J, Barooah N, Dhamodharan V et al (2013) Thioflavin T as an efficient inducer and selective fluorescent sensor for the human telomeric G-quadruplex DNA. *J Am Chem Soc* 135:367–376
9. Peters GM, Skala LP, Plank TN et al (2015) G4-quartet·M⁺ borate hydrogels. *J Am Chem Soc* 137:5819–5827
10. Liu XF, Hua XX, Fan QL et al (2015) Thioflavin T as an efficient G-quadruplex inducer for the highly sensitive detection of thrombin using a new Förster resonance energy transfer system. *ACS Appl Mater Interfaces* 7(30):16458–16465
11. Chen Q, Zuo JF, Chen JF et al (2015) A label-free fluorescent biosensor for ultratrace detection of terbium (III) based on structural conversion of G-quadruplex DNA mediated by ThT and terbium (III). *Biosens Bioelectron* 72:326–331
12. Li W, Liu ZL, Lin H et al (2010) Label-free colorimetric assay for methyltransferase activity based on a novel methylation-responsive DNAzyme strategy. *Anal Chem* 82:1935–1941
13. He KY, Li W, Nie Z et al (2012) Enzyme-regulated activation of DNAzyme: a novel strategy for a label-free colorimetric DNA ligase assay and ligase-based biosensing. *Chem Eur J* 18:3992–3999
14. Liu ZL, Li W, Nie Z et al (2014) Randomly arrayed G-quadruplexes for label-free and real-time assay of enzyme activity. *Chem Commun* 50:6875–6878
15. Kong DM (2013) Factors influencing the performance of G-quadruplex DNAzyme-based sensors. *Methods* 64:199–204
16. Cheng XD, Roberts RJ (2001) AdoMet-dependent methylation, DNA methyltransferases and base flipping. *Nucleic Acids Res* 29:3784–3795
17. Li E (2002) Chromatin modification and epigenetic reprogramming in mammalian development. *Nat Rev Genet* 3:662–673
18. Jaenisch R, Bird A (2003) Epigenetic regulation of gene expression: how the genome integrates intrinsic and environmental signals. *Nat Genet* 33(Suppl):245–254
19. Jones PA, Baylin SB (2002) The fundamental role of epigenetic events in cancer. *Nat Rev Genet* 3:415–428
20. Manel E (2002) CpG island hypermethylation and tumor suppressor genes: a booming present, a brighter future. *Oncogene* 21:5427–5440
21. Coleman MS, Hutton JJ, Simone PD et al (1974) Terminal deoxyribonucleotidyl transferase in human leukemia. *Proc Natl Acad Sci U S A* 71:4404–4408
22. McCaffrey R, Lillquist A, Sallan S et al (1981) Clinical utility of leukemia cell terminal transferase measurements. *Cancer Res* 41:4814–4820
23. Roychoudhury R, Jay E, Wu R (1976) Terminal labeling and addition of homopolymer tracts to duplex DNA fragments by terminal deoxynucleotidyl transferase. *Nucleic Acids Res* 3: 101–116
24. Deng GR, Wu R (1983) Terminal transferase: use in the tailing of DNA and for in vitro mutagenesis. *Methods Enzymol* 100:96–116
25. Schmidt W, Mueller M (1996) Controlled ribonucleotide tailing of cDNA ends (CRTC) by terminal deoxynucleotidyl transferase: a new approach in PCR-mediated analysis of mRNA sequences. *Nucleic Acids Res* 24:1789–1791
26. Gorczyca W, Gong J, Darzynkiewicz Z (1993) Detection of DNA strand breaks in individual apoptotic cells by the in situ terminal deoxynucleotidyl transferase and nick translation assays. *Cancer Res* 53:1945–1951
27. Kong DM, Xu J, Shen HX (2010) Positive effects of ATP on G-Quadruplex-Hemin DNAzyme-mediated reactions. *Anal Chem* 82:6148–6153
28. Stefan L, Denat F, Monchaud D (2011) Deciphering the DNAzyme activity of multimeric quadruplexes: insights into their actual role in the telomerase activity evaluation assay. *J Am Chem Soc* 133:20405–20415

Spatial Organization of Enzyme Cascade on a DNA Origami Nanostructure

Jinglin Fu and Tianran Li

Abstract

Self-assembled DNA nanostructures hold great promise to organize multi-enzyme systems with the precise control of the geometric arrangements. Enzymes modified with single-stranded DNA anchors are assembled onto the DNA origami tiles by hybridizing with the corresponding complementary strands displayed on the surface of the DNA nanostructures. Here, we describe a protocol of assembling a two-enzyme cascade on a discrete, rectangular DNA origami tile, where the distance between enzymes is precisely controlled for investigating the distance-dependent cascade activities.

Key words DNA origami, Enzyme cascade, Protein–DNA conjugation, Denaturing PAGE, AFM

1 Introduction

Over the past few decades, DNA nanostructures have emerged as promising biomaterials with the controlled assembly on the nanoscale [1–3]. Since Seeman’s original proposal of DNA-based “Holliday” junctions [4], various 1D, 2D, and 3D nanostructures have been designed and constructed via the self-assembly of DNA molecules [5–7]. Recent breakthroughs in scaffolded DNA origami [8] and single-stranded DNA bricks [9] have enabled the design and fabrication of sophisticated 3D nanostructures, as well as structures with complex curvatures [10–13]. Macroscopic structures of 2D and 3D crystals are also formed via the rational design of DNA assembly and aggregation [14, 15]. Due to the addressable assembly, DNA nanostructures have been widely used as molecular scaffolds to position elements into diverse geometrical patterns for realizing specific functionalities, such as light-harvesting complex [16], nanoparticle plasmonics [17, 18], high-affinity ligands [19, 20], super-resolved fluorescence imaging [21], and super-molecular networks [22–24].

DNA scaffold-directed assembly holds great promise to organize multi-enzyme systems with the precise control of the geometric

arrangements. Many of the enzymes in biochemical pathways are spatially organized to improve both reaction speed and specificity. Understanding the effect of spatial organization on the enzyme activity in biochemical pathways is not only fundamentally important, but also translates biochemical pathways to non-cellular applications. Recently, several significant progresses have been reported, including the organization of two-enzyme cascade with controlled distance [22, 24, 25], biomimetic “swinging arms” [23], DNA tweezers-actuated enzyme nanoreactors [26, 27], and DNA nanocage-encapsulated proteins [28, 29]. Here, we present a general protocol of assembling a GOx/HRP enzyme cascade on DNA origami nanostructures with the controlled distance between enzymes.

2 Materials

2.1 Chemicals

Glucose oxidase (GOx), horseradish peroxidase (HRP), tris-buffered saline (TBS), dimethyl sulfoxide (DMSO), T-CEP (Tris-(2-carboxyethyl)-phosphine hydrochloride) and Tris base are purchased from Sigma (St. Louis, MO). β -Gal streptavidin conjugates are purchased from Rockland (Gilbertsville, PA). Neutravidin, ABTS (2,2'-azinobis [3-ethylbenzothiazoline-6-sulfonic acid]-diammonium salt), and SPDP (*N*-succinimidyl 3-(2-pyridyldithio)-propionate) are purchased from Pierce (Rockford, IL). M13mp18 single-stranded DNA is purchased from Affymetrix (Santa Clara, CA). Single-stranded oligonucleotides are purchased from Integrated DNA technology (Coralville, Iowa). All buffer solutions are prepared in deionized water (dI H₂O, 18.2 M Ω cm at 25 °C).

2.2 Buffer Solutions

Buffer solutions for DNA origami assembly are prepared using dI H₂O and are stocked at 4 °C in the dark (*see Note 1*).

1. The 50 \times TAE stock solution contains 2 M Tris base, 1 M acetic acid, and 0.1 M EDTA.
2. The 10 \times TAE-Mg²⁺ stock solution contains 0.4 M Tris and 125 mM Mg²⁺. The pH value is adjusted to 8 using NaOH or acetic acid.
3. The 1 \times TAE-Mg²⁺ buffer solution is diluted from 10 \times TAE-Mg²⁺ with the final concentration of 40 mM Tris and 12.5 mM Mg²⁺.
4. The 10 \times TBE stock solution contains 0.89 M Tris, 0.89 M boric acid, and 20 mM EDTA.
5. The 20% denaturing PAGE gel mix (A) is prepared by adding 500 mL of 40% acrylamide solution (19:1 for Ac/Bis, BioRad), 100 mL 10 \times TBE, and 500 g of urea (OmniPur, EMD Millipore) into dI H₂O for a total volume of 1000 mL, with the final concentration of 20% acrylamide, 8.3 M urea, and 1 \times TBE.

6. The 0% denaturing PAGE gel mix (B) is prepared by adding 500 g of urea and 100 mL 10× TBE into dI H₂O for a total volume of 1000 mL, with the final concentration of 8.3 M urea and 1× TBE.
7. The elution buffer contains 500 mM CH₃COONH₄, 10 mM (CH₃COO)₂Mg, and 2 mM EDTA with pH adjusted to 8.

3 Methods

The general method of assembling a GOx/HRP cascade on DNA origami tiles is illustrated in Fig. 1, where DNA-conjugated GOx and HRP are assembled on rectangular DNA origami tiles by hybridizing with the corresponding complementary strands that are displayed on the surface of the origami scaffolds. We present the detailed procedures below, including (1) DNA–enzyme conjugation, (2) assembly of an origami tile, (3) enzyme assembly on DNA origami nanostructures, and (4) activity assay of assembled GOx/HRP cascade on DNA origami tiles.

3.1 Preparation of Denaturing Polyacrylamide Gel Electrophoresis (PAGE) for DNA Purification

The denaturing PAGE solutions (0–20%) are prepared by mixing the two stock solutions of (A) 20% Denature PAGE gel mix, and (B) 0% Denature PAGE gel mix. Stock solutions of (A) and (B) were prepared in TBE buffer. Detailed preparation methods are described in below:

1. Prepare oligonucleotides in dI H₂O with a concentration of 0.5 OD/μL. For 8 μL of DNA sample, add 4 μL of

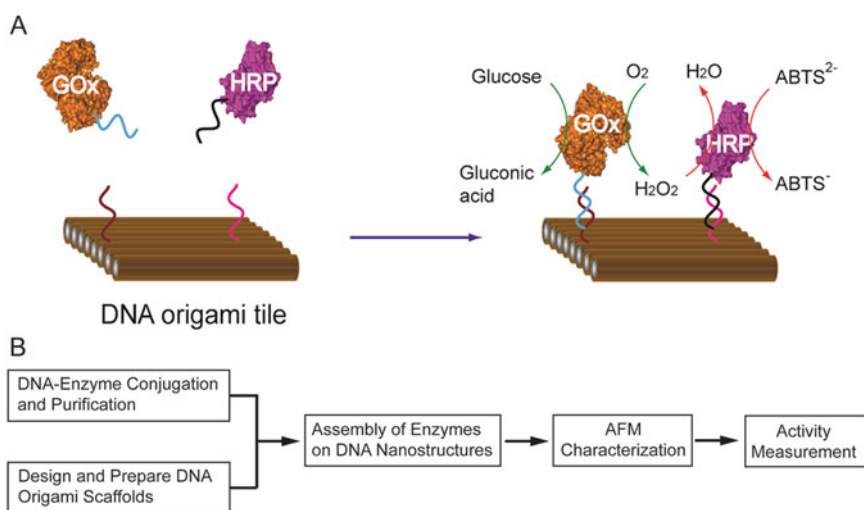


Fig. 1 Co-assembly of an enzyme cascade on a DNA origami template with controlled inter-enzyme distances. (a) The strategy of assembling a GOx/HRP pair on a rectangular DNA origami tile (reproduced from ref. [24] with permission from the American Chemical Society). (b) A general workflow of the methods

bromophenol blue dye and 4 μL of xylene cyanol FF dye. The dyes are used to visually track the electrophoresis movement. Vortex the mixture for 20 s, and spin down at 376 rcf for 30 s. Heat up the mixture to 90 °C for 5 min.

2. Load 15 μL of DNA solution to a single gel well. The gel electrophoresis is run at a constant current of ~30–40 mA for 2–3 h depending on the length of the DNA. The temperature is controlled at ~35 °C using the water circulating bath.
3. After the electrophoresis, the gel is placed on a UV transilluminator in the dark room. With 254 nm UV-light, the DNA band can be visualized without the addition of staining dyes (e.g., ethidium bromide). The DNA band is cut from the gel using a razor blade, followed by chopping down into small pieces. The small pieces of DNA gel is then collected by a centrifugal filter tube (0.22 μm). Then the filter tube is frozen at -20 °C for 1 h, which helps the elution of DNA molecules from the gel.
4. 500 μL of the elution buffer is added into the centrifugal filter, followed by shaking on a rocker for 2 h at room temperature. Alternatively, the filter tube can be incubated at 4 °C overnight. The elution buffer will loosen the gel structure for allowing DNA molecules to migrate out from the gels into solution. The elution buffer is then collected by centrifuging the filter tube at 6010 rcf for 10 min. Discard the waste gel pieces that remain on the top of the filter.
5. 1000 μL of butanol (99.8%) is added into the collected elution buffer, followed by vortexing for 1 min, and spinning down at 376 rcf for 1 min. After centrifuging, discard the upper layer of butanol, which extracts any organic impurities from the DNA sample, such as ethidium bromide and tracking dyes.
6. 1000 μL of ethanol (200 proof) is added into the DNA solution, followed by the incubation at -20 °C for 30 min in order to precipitate DNA molecules. (DNA has the lowest solubility in 70% ethanol.) The solution is then spun down at 9391 rcf for 30 min at 4 °C. Discard the ethanol solution, and repeat the ethanol precipitation one more time.
7. The collected DNA precipitants are dried into solid powder using the vacufuge for 3 h at 30 °C. Then 50 μL of sterile water (DNase- and protease-free with the filtration through 0.2 μm filter and autoclaved) is added into the tube to dissolve the solid DNA. The concentration of purified DNA strands is quantified by the absorbance at 260 nm.

3.2 DNA–Enzyme Conjugation and Purification

SPDP is used to covalently conjugate single-stranded oligonucleotides to the surface of enzymes [23, 24, 26]. As shown in Fig. 2, SPDP first reacts with lysine residues on the enzyme surface, followed by the activation of a pyridyl disulfide group to create a



Fig. 2 Schematic illustration of the SPDP cross-linking chemistry used for the DNA–enzyme conjugation

disulfide bond linkage between a thiol-modified DNA and an enzyme. In an example of demonstration, a GOx is covalently modified with a 5' thiol-modified P-1 anchor strand (P-1: 5'-HS-TTT TTC CCT CCC TCC), and an HRP is covalently modified with another 5' thiol-modified P-2 anchor strand (P-2: 5'-HS-TTT TTG GCT GGC TGG). The detailed conjugation steps are described as following:

1. Enzymes (GOx, 160 kDa; HRP, 44 kDa) are first pre-washed with 50 mM sodium HEPES buffer (pH 7.5) using an Amicon-30 kDa cutoff filter for removing small impurities and primary amine contaminants. The concentration of the enzymes are quantified using UV absorbance at 452 nm for GOx ($\epsilon=28200 \text{ M}^{-1} \text{ cm}^{-1}$) and 403 nm for HRP ($\epsilon=100000 \text{ M}^{-1} \text{ cm}^{-1}$) (*see Note 2*).
2. Prepare 20 mM SPDP stock solution in DMSO. For 1000 μL of 40 μM GOx solution, 10 μL SPDP stock is added into the enzyme solution with a SPDP-to-enzyme ratio of 5 for GOx. For 1000 μL of 40 μM HRP solution, 40 μL of SPDP stock is added with a SPDP-to-enzyme ratio of 20. Then, 100 μL of 1 M NaHCO_3 is added to adjust the pH value of reaction mixture to be ~ 8.5 . The reaction is incubated at room temperature for 1 h in the dark, allowing amine-reactive *N*-hydroxysuccinimide (NHS) esters to react with the lysine residues on the enzyme surface (*see Note 3*).
3. After the first step of reaction, the excess SPDP is removed by the filtration with 50 mM HEPES (pH 7.5) buffer using Amicon-30 kDa cutoff filters, repeating three times.
4. The SPDP modification is evaluated by adding the T-CEP to release pyridine-2-thione (extinction coefficient: $8080 \text{ M}^{-1} \text{ cm}^{-1}$), resulting in an increase of absorbance at 343 nm (*see Note 4*).
5. SPDP-modified enzymes are then incubated with a tenfold excess thiol-modified DNA solution. The reaction mixture is incubated in 50 mM sodium HEPES (pH 7.5) for 1 h at room temperature in dark.
6. After the reaction, the excess DNA molecules are removed by the filtration using Amicon-30 kDa cutoff filters. Wash the DNA–enzyme conjugates once using 50 mM HEPES (pH 7.5)

with 1 M NaCl, and then three times using 50 mM HEPES (pH 7.5). The high salt concentration in the first wash helps to remove DNA molecules that are nonspecifically bound to protein due to the electrostatic interactions (*see Note 6*).

7. The concentration of the DNA-conjugated enzyme is quantified by UV absorbance at 452 nm for GOx and 403 nm for HRP (*see Notes 6 and 7*).

3.3 Design and Assembly of DNA Origami Nanostructures

DNA origami templates are designed using open-access software of Tiamat [30] or CadNano [31]. In this protocol, we used a published rectangular DNA origami with a dimension $\sim 60 \text{ nm} \times 80 \text{ nm}$ [24], which consisted of 226 staple strands and a 7429-nt single-stranded M13mp18 DNA (Fig. 3). In order to assemble enzymes on the surface of a DNA origami tile, the capture strands with the complementary sequences to the anchor strands, are extended from the 3' end of selected staple strands. The assembly and purification of DNA origami nanostructures are performed using the following procedures:

1. Single-stranded staple strands are ordered from IDT without further purification. The capture strands are purified using an 8% denaturing PAGE (*see Note 1*).
2. The 100 μL of 20 nM single-stranded M13mp18 DNA is incubated with a fivefold molar excess of staple stands and a tenfold molar excess of capture strands in $1 \times \text{TAE-Mg}^{2+}$ buffer (pH 8.0) [24] (*see Note 8 and 9*).
3. The reaction mixture is thermally annealed using PCR thermocycler (Eppendorf) from 95 to 4 $^{\circ}\text{C}$ with the temperature gradient as shown in Table 1.

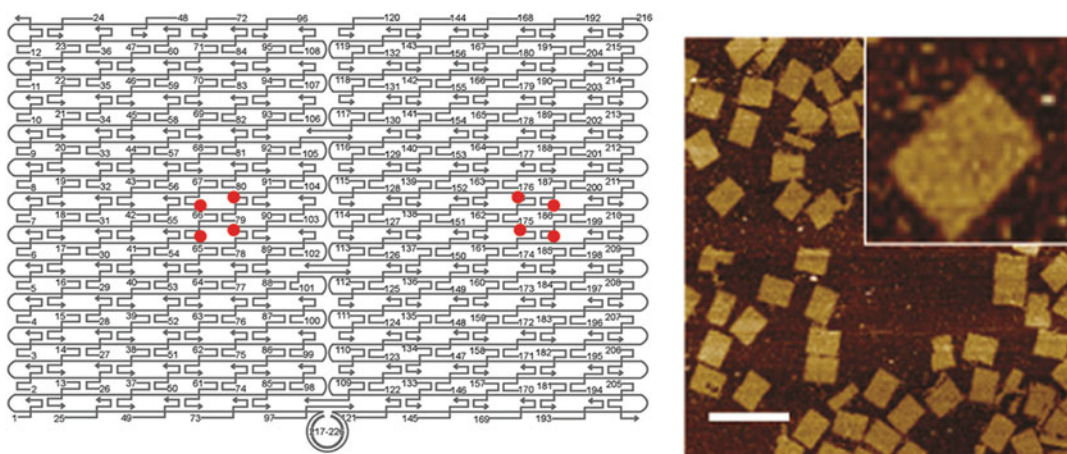


Fig. 3 The design of rectangular DNA origami tile (*left*) and the AFM characterization of the origami structures (*right*) (reproduced from ref. [24] with permission from the American Chemical Society). Scale bar: 100 nm. In order to assemble enzymes on the surface of the origami tile, the capture strands are extended from the 3' end of selected staple strands (label with the *red* color). The distance between the two capture sites are $\sim 45 \text{ nm}$

Table 1
The temperature gradient program for assembling DNA origami structures

Assembly protocol	
Temperature (°C)	Gradient
90	30 s
86–71	1 min/step
70–60	10 min/step
59–30	15 min/step
29–26	10 min/step
25	25 min
4	Hold

- The excess staple and capture strands are removed by the filtration of the origami solution with a 100 kDa Amicon filter using 500 μL , $1\times$ TAE- Mg^{2+} buffer (pH 7.5), repeating three times.
- The purity of the origami tiles is analyzed by agarose gel electrophoresis (2%). The concentration of DNA origami tiles is quantified by the absorbance at 260 nm, assuming an extinction coefficient of $\sim 109,119,009 \text{ M}^{-1} \text{ cm}^{-1}$.

3.4 Assembly and AFM Characterization of Enzymes on DNA Nanostructures

The 100 μL of 10 nM DNA origami solution is incubated with 30 nM GOx-P1 and 30 nM HRP-P2 in $1\times$ TAE- Mg^{2+} buffer (pH 7.5) with an enzyme-to-origami ratio of 3. The reaction mixture is thermally incubated using a PCR thermocycler with a temperature gradient from 37 to 10 $^{\circ}\text{C}$ (*see* **Notes 10** and **11**). The detailed temperature gradient is: 37 $^{\circ}\text{C}$ for 5 min; 36–10 $^{\circ}\text{C}$, 2 min per degree decrease. The solution is then kept at 4 $^{\circ}\text{C}$ for storage. The enzyme-assembled DNA nanostructures are visualized and characterized using AFM in solution, which operation procedures are briefly described as below:

- First, tear off a few layers of mica using a transparent single-side sticky tape. This will generate a smooth and freshly cleaved mica surface.
- Deposit $\sim 2 \mu\text{L}$ of 10 nM DNA origami sample onto a freshly cleaved mica surface and leave it to adsorb for 1 min.
- Add 80 μL of $1\times$ TAE- Mg^{2+} (pH 8) buffer on the top of the DNA sample. It is optional to add 2 μL 100 mM Ni^{2+} to enhance the adsorption of the DNA nanostructures on the mica. Another 40 μL of $1\times$ TAE- Mg^{2+} buffer is added into a liquid cell.
- The sample is scanned using SCANASYST-FLUID + probe under “Scanasyst in fluid” mode.

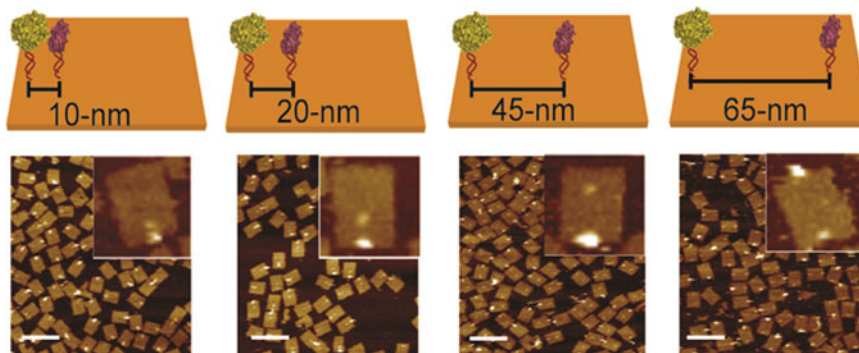


Fig. 4 AFM visualization of the assembly of a GOx/HRP cascade on a rectangular DNA origami tile with the distance ranging from 10, 20, and 45 to 65 nm. Scale bar: 100 nm (reproduced from ref. [24] with permission from the American Chemical Society)

- As shown in Fig. 4, the rectangular DNA origami tiles are clearly identified under AFM imaging. The assembled enzymes are higher than surrounding surface of the origami tile, resulting in bright spots (increased height). Because GOx (~10 nm) is larger than HRP (~5 nm), the brighter and bigger spot is GOx, and the other smaller one is HRP. The average distance between enzymes is measured by AFM imaging (*see Note 12*).

3.5 Activity Assay of the Assembled GOx/HRP Cascade on DNA Origami

Enzyme assay is performed using 96-well microplate reader. The 10 nM GOx/HRP-origami solution is diluted to 1 nM using 1× TBS buffer (pH 7.5) with 1 mM MgCl₂. To initiate the catalytic reaction, 1 nM enzyme solution is incubated with 1 mM glucose and 2 mM ABTS²⁻ in TBS buffer, where GOx first catalyzes the oxidation of glucose to produce H₂O₂, followed by HRP-catalyzed oxidation of ABTS²⁻ to ABTS^{•-}. As shown in Fig. 5a, the activity of the GOx/HRP cascade is determined by monitoring the increase of absorbance at 410 nm. As shown in Fig. 5b, the activity of GOx/HRP cascade is highly sensitive to the distance between enzymes, where a GOx/HRP pair with 10 nm distance exhibits the highest enzyme activity. The enzyme cascade activity quickly decreases with the increase of the distance between the two enzymes from 10 to 20 nm or further. The assay procedures are briefly described as below:

- First prepare 50 μL of 2 nM enzyme-assembled origami tiles in 1× TBS buffer (pH 7.5) with 1 mM MgCl₂. The enzyme solution is transferred into a black, round-bottom 96-well plate.
- Prepare 50 μL substrate solution of 2 mM glucose and 4 mM ABTS²⁻ in TBS buffer. The substrate solution is added into the 96-well plate. The final assay solution is 100 μL, containing 1 nM enzyme, 1 mM glucose, and 2 mM ABTS²⁻.
- Immediately after adding the substrate, the plate is inserted into the microplate reader to start the measurement.

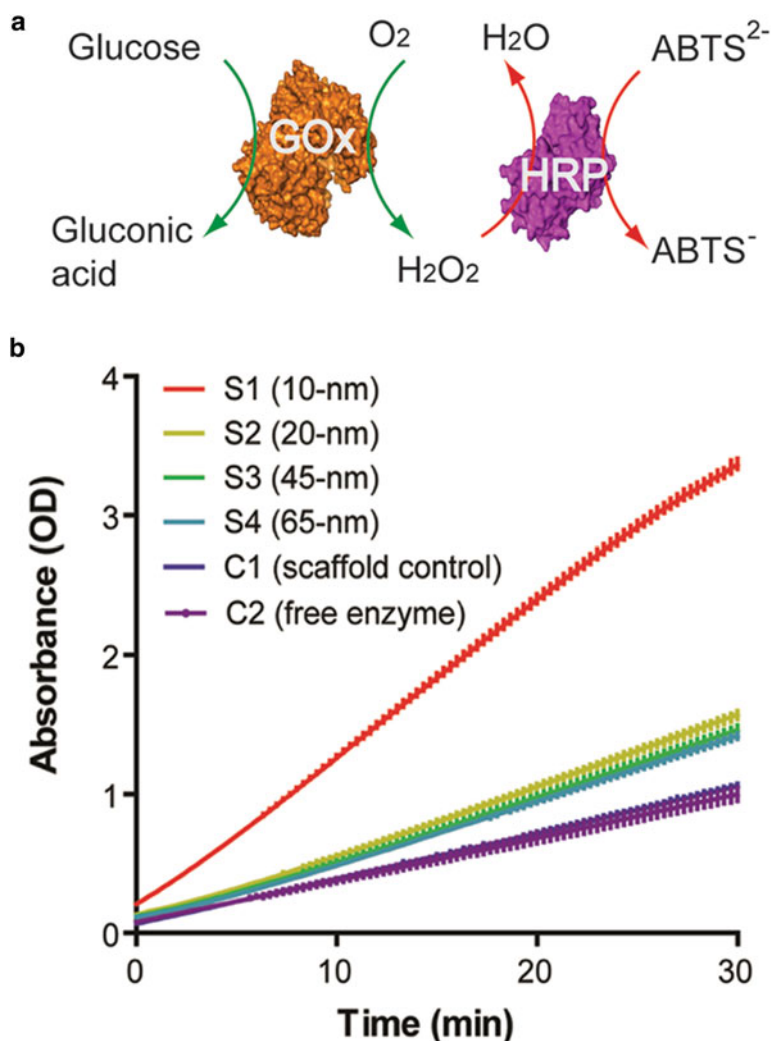


Fig. 5 Distance-dependent activity of a GOx/HRP pair on the DNA origami tile. **(a)** The detection of the cascade activity using a ABTS^{2-} reporter which is oxidized to ABTS^- with an increase of absorbance at 420 nm. **(b)** Plots of product concentration vs. time for a series of DNA nanostructured enzyme cascades with the distance ranging from 10, 20, and 45 to 65 nm, as well as free enzymes (reproduced from ref. [24] with permission from the American Chemical Society)

4 Notes

1. All buffer solutions are filtered using 0.22 μm filter, and then wrapped with Aluminum foil to protect from light to avoid degradation.
2. In the SPDP chemistry, the buffer solutions must be free of primary amines. Buffers like phosphate or HEPES are preferred for running the conjugation. Enzymes are also required

to pre-wash with the buffer to remove any impurities containing primary amines.

3. It is critical to control the pH value (8-8.5) for SPDP modification on enzyme surface. If pH value is lower than 8, the primary amines on the lysine residues are largely protonated, preventing them from reacting with NHS ester. If pH value is higher than 9, NHS ester is quickly hydrolyzed within 20 min [32].
4. Avoid overly labeling enzymes with too many SPDP molecules. If the label ratio of SPDP per enzyme is more than 3, it will significantly damage the activity of enzymes.
5. In the purification of DNA-modified enzymes, the washing buffer with the high concentration of NaCl helps to remove nonspecifically-bound and stacked DNA molecules due to the disruption of the electrostatic interactions between DNA molecules and enzymes.
6. If the measured DNA-to-enzyme ratio is higher than the SPDP-to-enzyme ratio, it indicates the presence of noncovalently-bound DNA molecules. Further purification steps (e.g. ionic-exchanged fast protein liquid chromatography) are required to remove these nonspecific DNA molecules.
7. To purify the DNA-modified enzymes with the exact number of labeled DNA per enzyme, ionic-exchange chromatography may be used as described in the published report [23].
8. Most DNA staple strands received from IDT are not purified for assembling DNA origami. However, capture strands must be purified by denaturing PAGE to avoid any incomplete fragments that are not hybridized with DNA-modified enzymes.
9. The staple strands at the edges of DNA origami (e.g. staple 1-12, and 205-216 in Figure 2) are removed from the structure to reduce the π - π stacking between DNA origami tiles.
10. The hybridization of enzymes to DNA origami tiles cannot be run at temperature higher than 37°C due to the thermal denaturation of enzymes.
11. It is not recommended to vortex the solution of assembled DNA origami nanostructures; instead, the solution can be mixed by pipetting repeatedly.
12. In the AFM imaging, most origami tiles are deposited on the mica surface with the protein decorated side facing up, likely due to the strong interaction (charge or stacking) of the opposite flat side with the mica surface.

Acknowledgement

This work is supported by an Army Research Office MURI subaward to J.F. (parent award: W911NF-12-1-0420), an Army Research Office Young Investigator award (W911NF-14-1-0434) to J.F., and a Cottrell College Science Award to J.F. Authors are grateful to Dr. Ting Zhang for proofreading the manuscript.

References

1. Fu J, Liu M, Liu Y, Yan H (2012) Spatially-interactive biomolecular networks organized by nucleic acid nanostructures. *Acc Chem Res* 45:1215–1226
2. Pinheiro AV, Han D, Shih WM, Yan H (2011) Challenges and opportunities for structural DNA nanotechnology. *Nat Nanotechnol* 6:763–772
3. Seeman NC (2010) Nanomaterials based on DNA. *Ann Rev Biochem* 79:65–87
4. Seeman NC (1982) Nucleic acid junctions and lattices. *J Theor Biol* 99:237–247
5. Chen J, Seeman NC (1991) Synthesis from DNA of a molecule with the connectivity of a cube. *Nature* 350:631–633
6. Kallenbach NR, Ma R-I, Seeman NC (1983) An immobile nucleic acid junction constructed from oligonucleotides. *Nature* 305:829–831
7. Fu TJ, Seeman NC (1993) DNA double-crossover molecules. *Biochemistry* 32:3211–3220
8. Rothmund PWK (2006) Folding DNA to create nanoscale shapes and patterns. *Nature* 440:297–302
9. Ke Y, Ong LL, Shih WM, Yin P (2012) Three-dimensional structures self-assembled from DNA bricks. *Science* 338:1177–1183
10. Andersen ES, Dong M, Nielsen M et al (2009) Self-assembly of a nanoscale DNA box with a controllable lid. *Nature* 459:73–76
11. Han D, Pal S, Nangreave J, Deng Z, Liu Y, Yan H (2011) DNA origami with complex curvatures in three-dimensional space. *Science* 332:342–346
12. Dietz H, Douglas SM, Shih WM (2009) Folding DNA into twisted and curved nanoscale shapes. *Science* 325:725–730
13. Douglas SM, Dietz H, Liedl T, Hogberg B, Graf F, Shih WM (2009) Self-assembly of DNA into nanoscale three-dimensional shapes. *Nature* 459:414–418
14. Ke Y, Ong LL, Sun W, Song J, Dong M, Shih WM, Yin P (2014) DNA brick crystals with prescribed depths. *Nat Chem* 6:994–1002
15. Zheng J, Birktoft JJ, Chen Y, Wang T, Sha R, Constantinou PE, Ginell SL, Mao C, Seeman NC (2009) From molecular to macroscopic via the rational design of a self-assembled 3D DNA crystal. *Nature* 461:74–77
16. Stein IH, Steinhauer C, Tinnefeld P (2011) Single-molecule four-color FRET visualizes energy-transfer paths on DNA origami. *J Am Chem Soc* 133:4193–4195
17. Kuzyk A, Schreiber R, Fan Z, Pardatscher G, Roller E-M, Hogele A, Simmel FC, Govorov AO, Liedl T (2012) DNA-based self-assembly of chiral plasmonic nanostructures with tailored optical response. *Nature* 483:311–314
18. Tan SJ, Campolongo MJ, Luo D, Cheng W (2011) Building plasmonic nanostructures with DNA. *Nat Nanotechnol* 6:268–276
19. Williams BAR, Diehnelt CW, Belcher P, Greving M, Woodbury NW, Johnston SA, Chaput JC (2009) Creating protein affinity reagents by combining peptide ligands on synthetic DNA scaffolds. *J Am Chem Soc* 131:17233–17241
20. Rinker S, Ke Y, Liu Y, Chhabra R, Yan H (2008) Self-assembled DNA nanostructures for distance-dependent multivalent ligand-protein binding. *Nat Nanotechnol* 3:418–422
21. Iinuma R, Ke Y, Jungmann R, Schlichthaerle T, Woehrstein JB, Yin P (2014) Polyhedra self-assembled from DNA tripods and characterized with 3D DNA-PAINT. *Science* 344:65–69
22. Wilner OI, Weizmann Y, Gill R, Lioubashevski O, Freeman R, Willner I (2009) Enzyme cascades activated on topologically programmed DNA scaffolds. *Nat Nanotechnol* 4:249–254
23. Fu J, Yang YR, Johnson-Buck A, Liu M, Liu Y, Walter NG, Woodbury NW, Yan H (2014) Multi-enzyme complexes on DNA scaffolds

- capable of substrate channelling with an artificial swinging arm. *Nat Nanotechnol* 9:531–536
24. Fu J, Liu M, Liu Y, Woodbury NW, Yan H (2012) Interenzyme substrate diffusion for an enzyme cascade organized on spatially addressable DNA nanostructures. *J Am Chem Soc* 134:5516–5519
 25. Erkelenz M, Kuo C-H, Niemeyer CM (2011) DNA-mediated assembly of cytochrome P450 BM3 subdomains. *J Am Chem Soc* 133:16111–16118
 26. Liu M, Fu J, Hejesen C, Yang Y, Woodbury NW, Gothelf K, Liu Y, Yan H (2013) A DNA tweezer-actuated enzyme nanoreactor. *Nat Commun* 4, doi: [10.1038/ncomms3127](https://doi.org/10.1038/ncomms3127)
 27. Xin L, Zhou C, Yang Z, Liu D (2013) Regulation of an enzyme cascade reaction by a DNA machine. *Small* 9:3088–3091
 28. Douglas SM, Bachelet I, Church GM (2012) A logic-gated nanorobot for targeted transport of molecular payloads. *Science* 335:831–834
 29. Linko V, Eerikainen M, Kostianen MA (2015) A modular DNA origami-based enzyme cascade nanoreactor. *Chem Commun* 51:5351–5354
 30. Williams S, Lund K, Lin C, Wonka P, Lindsay S, Yan H (2009) Tiamat: a three-dimensional editing tool for complex DNA structures. In: Goel A, Simmel F, Sosik P (eds) *DNA computing*, vol 5347, *Lecture notes in computer science*. Springer, Heidelberg, pp 90–101
 31. Douglas SM, Marblestone AH, Teerapittayanon S, Vazquez A, Church GM, Shih WM (2009) Rapid prototyping of 3D DNA-origami shapes with caDNAo. *Nucleic Acids Res* 37:5001–5006
 32. Nojima Y, Iguchi K, Suzuki Y, Sato A (2009) The pH-dependent formation of PEGylated bovine lactoferrin by branched polyethylene glycol (PEG)-n-hydroxysuccinimide (NHS) active esters. *Biol Pharm Bull* 32:523–526

Lipid Membrane Encapsulation of a 3D DNA Nano Octahedron

Steven D. Perrault and William M. Shih

Abstract

Structural DNA nanotechnology methods such as DNA origami allow for the synthesis of highly precise nanometer-scale materials (Rothemund, *Nature* 440:297–302, 2006; Douglas et al., *Nature* 459:414–418, 2009). These offer compelling advantages for biomedical applications. Such materials can suffer from structural instability in biological environments due to denaturation and nuclease digestion (Hahn et al., *ACS Nano* 2014; Perrault and Shih, *ACS Nano* 8:5132–5140, 2014). Encapsulation of DNA nanostructures in a lipid membrane compartmentalizes them from their environment and prevents denaturation and nuclease digestion (Perrault and Shih, *ACS Nano* 8:5132–5140, 2014). Here, we describe the encapsulation of a 50 nm DNA nanostructure having the geometry of a wireframe octahedron in a phospholipid membrane containing poly-(ethylene glycol), resulting in biocompatible DNA nanostructures.

Key words DNA, Nanotechnology, Liposome, NanoOctahedron, Vesicle

1 Introduction

Structural DNA nanotechnology methods, such as DNA origami [1, 2], allow researchers to produce nanometer-scale architectures using DNA as a programmable polymer. These materials differ from conventional nanomaterials in the precision of their design and synthesis [3], as well as in their programmed addressability, which allows for near-angstrom organization of functional ligands (*e.g.*, proteins [4], fluorophores [5], and metal particles [6]) on the nanostructures. These unique capabilities have inspired researchers to pursue biomedical application of DNA nanotechnology. Recent demonstrations include a multiplexed barcode having potential as a diagnostic marker [7], a nano-caliper that can mediate cell phenotype [8], and a therapeutic nano-robot [9].

Despite the apparent potential of engineering biomedical devices *via* DNA origami, the sensitivity of these materials to degradation in biological environments is a major challenge. The stability of origami-based DNA nanostructures was systematically

examined in standard tissue culture media, revealing two mechanisms of nanostructure degradation [10]. The nanostructures were found to be sensitive to a physiological, low divalent-cation environment, which caused denaturation of the nanostructures in a design-dependent manner. As well, nucleases present in bovine serum that is used to supplement tissue culture medium was able to fully digest DNA nanostructures within 24 h of incubation. In vivo profiling of DNA nanostructure stability has revealed similar challenges, with rapid degradation and clearance of DNA nanostructures observed within minutes of intravenous injection [11]. These findings provide compelling evidence that protection strategies are needed for DNA nanostructures that are intended for translation into biological environments. Here, we demonstrate a method for membrane encapsulation of a DNA NanoOctahedron. The formulation of the membrane includes poly-(ethylene glycol), provides protection against ionic denaturation and nuclease digestion, and is suitable for in vivo systemic use. The method results in NanoOctahedron that are tightly wrapped by the membrane, having a diameter of ~50 nm. The encapsulated DNA NanoOctahedron therefore provides a platform for development of in vitro and in vivo diagnostic and therapeutic devices.

2 Materials

Prepare all solutions using ultrapure water (prepared by purifying deionized water to attain a sensitivity of 18 M Ω cm at 25 °C) and analytical grade reagents. Prepare and store all materials and solutions at room temperature, unless otherwise specified.

2.1 Folding a Stock Solution of DNA NanoOctahedron

1. Purchased oligonucleotides (Table 1) should be ordered normalized to a concentration of 100 μ M and mixed together to produce three pools, outlined in Table 2. These three pools correspond to “outer handle” (48 oligos), “inner handle” (12 oligos), and “core” (84 oligos).
2. The p7308 single-stranded DNA scaffold can be purchased from Guild BioSciences. Alternatively, the scaffold can be produced *via* recombinant phage [12].
3. 20 \times Folding buffer: 100 mM Tris, 20 mM EDTA.

2.2 Purification of a Stock Solution of Folded DNA NanoOctahedron

1. 15 mL Amicon Ultra Centrifugal Filter 30 K.
2. Filter wash buffer: 1 \times Folding buffer, 0.05 % Tween-20 (V/V).
3. Heavy glycerol buffer: 1 \times Folding buffer, 45 % glycerol (V/V).
4. Light glycerol buffer: 1 \times Folding buffer, 15 % glycerol (V/V).
5. Polyclear open-top centrifuge tubes.
6. Ultracentrifuge Optima XPN-80 and SW-55 Ti rotor.
7. Gradient station.

Table 1
Oligonucleotide list for the DNA NanoOctahedron

#	Sequence	Length
1	CCAGCGAGTTACTTTAGCCGACTAAAGACACTCATCAGCGCTAAATTTTTTCTTCCACACCACACTCCCATCTA	70
2	TTCTTAAACAGGGAGTTAAATAGAAAGGAGCTTTCGATCATCAITTTTTTCTTCCACACCACACTCCCATCTA	70
3	GAAAACACCTTGCTTCTGTCTATCGGGAGTGAAACATTTCCCAITTTTTTCTTCCACACCACACTCCCATCTA	70
4	CCTGCTCGGCAAAATCCCTTATAAATCAAAACAGTTGGTAATAATTTTTTCTTCCACACCACACTCCCATCTA	70
5	ACCGAACATATTGAATAACTTTTTCTCAGAGCCGGAAACCCGTAACAATAATTTTTTCTTCCACACCACACTCCCATCTA	74
6	CTCAGTGCCAGCAGAAATGGTTTTTAGCTACACTTAAATCCGCCACCCCTTTTTTCTTCCACACCACACTCCCATCTA	74
7	GTAGATAITTTGTTTTCACTTTTACAGACAACCAGTACATCAGATAITTTTTTCTTCCACACCACACTCCCATCTA	74
8	GGAAACGCATCGGGTAAAATTTTAAACCGATGCCGACAATAATCATTTTTTTTTCTTCCACACCACACTCCCATCTA	74
9	GGCTTTTTCATTGAATCCCTAGGAATACACAAAATTTGACGATTTTTTCTTCCACACCACACTCCCATCTA	70
10	AAACITTAATAAGAATAAATAGTGAATTAACAAGAGATTAGAGTTTTTCTTCCACACCACACTCCCATCTA	70
11	TTTAGTAAATCACCGAAAAGTTTTTGTATTTGGAATCGGCCTCGAGCCAGTTTTTTTTCTTCCACACCACACTCCCATCTA	74
12	TATCAGAITTTTTAAGAAAATTAACGTCAGTAAATTTGTTGACCCCTTTTTTCTTCCACACCACACTCCCATCTA	70
13	AATTCATTAAAGGTGAATTTTAAAGACTCTCACAATACAAAAGGCTTTTTTCTTCCACACCACACTCCCATCTA	70
14	CATATAACATACTTTTTTATTTTGTATAATTACAITGGGTGGCATCTTTTTTCTTCCACACCACACTCCCATCTA	74
15	ACCCATGATCTAAAAGTTTTTCGGAATAGGGCAAGCCITTAGCGATTTTTTCTTCCACACCACACTCCCATCTA	70
16	AGTACCTTTTTTAAATATGCAGCAAAGCGAGGTCAGACGGGAGATTTTTTCTTCCACACCACACTCCCATCTA	70
17	TTAGAGCTATAATCACCAITTTTTGTACCAAATAAAGCATATAACCGTTTTTTTTCTTCCACACCACACTCCCATCTA	74
18	TCCAGACATCCCATCCCTAAAACAGTAGGGGTAAAGTCCAGTGGTTTTTTTTCTTCCACACCACACTCCCATCTA	70
19	GGCTGTAATTCGAGCATAATTTTCCITTTGACCAAGCITTGAATTAITCTTTTTTCTTCCACACCACACTCCCATCTA	74
20	AAATATGAAACGGAAAATATTTTAAATAGCATTAAGCCCCAACCTAAATTTTTTCTTCCACACCACACTCCCATCTA	74

(continued)

Table 1
(continued)

#	Sequence	Length
21	GCCCCGTATGCGACGCCCAATTTTATCACCCGGGGGAAATAAAGAA CGTTTTTCTTTCACACCACTCCATCTA	74
22	GGAAACCTCACCCAGTGAGATTATCCGGCTCCCGCTTTAATCTGTGTTTTTCTTTTCACACCCACACTCCATCTA	70
23	ACCTCCCACGCTAACGAGCTCATCGAGAGAGGGCGTCAATAGGATTTTTCTTACACCCACACTCCATCTA	70
24	TATCAGGTTGATAATCAGAAAGATTCAAGAGATCTCAATAGAATTTTTCTTTCACACCCACACTCCATCTA	70
25	CGTTTGCCCCCTCAGAGCCAACGTCACCATAGCCCCAAACACCATTTTTTCTTTCACACCCACACTCCATCTA	70
26	AATAAAGGGGACCGCCACTTTTTTGTGTCTACAA CGGGGGGAGAAATTTTTTCTTTCACACCCACACTCCATCTA	74
27	AATCTCACCGCGGGGCCCTTTTGTGCTGAATGGTCAITTTTAACTATAITTTTTTCTTTCACACCCACACTCCATCTA	74
28	TCTGTACCTTATAGGAATCTTTTTAGATAAAGCTAATGGAGTGGCTTTTTTCTTTCACACCCACACTCCATCTA	74
29	CAGAGCCCCACTACAAGAAATTTAAGAGAAAAACATGAATCCAGTAAATTTTTCTTTCACACCCACACTCCATCTA	74
30	TTTTAGTCCATCACTATCGTTTTTAGGGATTTTCAGAGCGGACACTATCATTTTTTCTTTCACACCCACACTCCATCTA	74
31	GTCACGAGACCGTATACGCCAATTCAGGGCCACAGGGAACATCAATTTTTTCTTTCACACCCACACTCCATCTA	70
32	GAACCTACAAAATCAGTAGCTTTTAAAGGTAAAAAAGGGCGCTGATAAAATTTTTTCTTTCACACCCACACTCCATCTA	74
33	ACCGAGAGGTTTTGAATACTTTTTCTGAATATCAATAATATCCAAAAGGTTTTTTTTCTTTCACACCCACACTCCATCTA	74
34	GCACGTAGAATCCTGAGAAAGAAAGCGATGGTTGCTAGCGAGATTTTTTCTTTCACACCCACACTCCATCTA	70
35	GATTTAAGTTGCGTTGTTCTTTTTCCAATAGGGTAATACCCGCGCGGTTTTTTTTCTTTCACACCCACACTCCATCTA	74
36	GAAACGAGTACCAGT CAGGACGCATAGGCTGACGAGCTTATAGTTTTTTTTCTTTCACACCCACACTCCATCTA	70
37	CCGTGGGGGACGACGACATTGTTAAATAACCCGTATGAAAAATTTTTTCTTTCACACCCACACTCCATCTA	70
38	AGTTTTAAGGTGCCGTAAACTTGATATTAGTGTACTAATGCCCCTTTTTTCTTTCACACCCACACTCCATCTA	70
39	AAAGAGAAACAACCCAAAAAGTTTTTATGCGTTTTTAAATTTGTGAGACTGTTTTTTTTCTTTCACACCCACACTCCATCTA	74
40	ATTCTGTATATCAAAAATTAACAACAATCGGAATTAGGTGAATTTTTTCTTTCACACCCACACTCCATCTA	70
41	AGCTTTTTTGAAGCAGAAAGTTTTTACATAAATCATTTTGAAAAGGGGGATTTTTTCTTTCACACCCACACTCCATCTA	74
42	GCGAAAACAATAGGAACGTTTTTTTGCAAATCTATCAAACTAGCCAGCTTTTTTCTTTCACACCCACACTCCATCTA	74

43	GAATGATTGACGTGTAGCGTTTTTTTACCAGACTCATCTTCGAGCITTCAAATTTTTTCTTTCACACCCACACTCCATCTA	74
44	TTAGAGATTGTACATCAAATTTTACTAGCAAAAACAAGAAAAGAAACGGTTTTTTCTTTCACACCCACACTCCATCTA	74
45	AGACAAATGATTCATATTTTTTATCGTAAATGGGATATATAAACACTTTTTTTCTTTCACACCCACACTCCATCTA	74
46	TTGACGGCAGATAGAACCCCTTAGTAATAAGGAAATAATCATAACATTTTTTCTTTCACACCCACACTCCATCTA	70
47	TCTAAAGAAAGGTTATCTAATAAAAACATCGCAGCAACGGGATTTCTTTTTTTCTTTCACACCCACACTCCATCTA	70
48	GGCAAAGGACITTTGCGGGATTAGATACACCAATAACCTACATTTTTTTTTCTTTCACACCCACACTCCATCTA	70
49	ACGGCCACATCTTTGAATAAGGCTTGGCCCTGGCTGAGGTGTAAAATTTATCTACCCAAACTCAC	42
50	TATTCATATGGTTTGGTAGCTATTTTTGAAAGGGTGAGTAATAAATTTATCTACCCAAACTCAC	42
51	CTGTAATCAAAGAAAGGAAAAACGCTCATCATCACTCAATACAAAATTTATCTACCCAAACTCAC	42
52	GTTTGAGAACAAACCCACGGCTGAGAGCCAGCCATTAGCGAACAAAATTTATCTACCCAAACTCAC	42
53	TAAATATGCAAAAAGACAGGGCGGCTACTAAAGGAGCCGAGAAAAATTTATCTACCCAAACTCAC	42
54	TGAATAAAAAATTAATTAAGTTGGGTAACTGCGCAAACAAGCAAAAATTTATCTACCCAAACTCAC	42
55	GCTCCATTTATACCGAACAAAAGTCAGAGGAAAAATGAGAAACGAAAATTTATCTACCCAAACTCAC	42
56	TTTTCTTTTGTGTTGAAAGTACCGACAAAAGCTTAATATAAAGAAAATTTATCTACCCAAACTCAC	42
57	ACCTACCATTTATCATCGGTTTTTATCAGCTTACAACTATCAGCGAAAATTTATCTACCCAAACTCAC	42
58	GGGTGCGACGGGTTAACAGTGCCCGTATAAAAAGAAATTTGCCAAAATTTATCTACCCAAACTCAC	42
59	CGTAAACGTACCGTAGTATTCTAAGAAACGCACAAAGCAAAACAAAATTTATCTACCCAAACTCAC	42
60	CAACATGTTAATGAAATCCAATCGCAAGTATCAAAGCTGAGAAAATTTATCTACCCAAACTCAC	42
61	CAGAGCTTTAGTATAAGTCCCGTGGATTGCCACCTGAAT	39
62	TGTGCTGATCGGTTTCTGTTGCCGGAAAATTTTATGTGAG	39
63	ATTAATCCAATATCTTTAGGAGCACCTGTAAATTTTTTAA	41
64	GAAAGGCGCAAGGCGTTACATTTAACAATTTCAATATCCCTTAG	44
65	CAAGAGTCATTCAGTTCATAATCAAAAATCACCGCCACCCACCCAC	44
66	GCCATTTAAAAATCGTCGCTATTATAATTAACCAGGCTGTGG	41

(continued)

Table 1
(continued)

#	Sequence	Length
67	TACCTTTGCATGGCTAGTACCCGTATATATATACAGAACGGAT	41
68	CTCATATATAGTAAACGGCAATTTTCGGTCAATGAAACTTAGCA	42
69	ATTTTTTGGGAACGAGGGCCGAGACGGTCAAATAAAAAATAGC	41
70	TAAATCCAAACAAAAGATACCCGATAGTTGCATATTCGCTCAGCA	44
71	TTCTTTGCAGAAAGCCCTTATTTCAACGGTTGTAGTGCCCTGA	41
72	AGGCCGGGGCGTTGGGAAGAAAAATCTATTAACACATCGAT	41
73	CAGACCAAAACCAACCCTCAGAGCCGCCAGATGAACCCCTTCAT	41
74	GTTTGACATTTCTGACCTGAAAGCGTAAACGAGTAAATGGTC	41
75	GTAGAAAGATTGCAACTTAGCAAAAATTAAGCAAAAACATTAAAAAT	44
76	ACCAATAAACATTAATTTGCTGAACCTCAAAAAACAGTTTAAATAGA	44
77	CCAACAGTCAATCGTAGTAGCATTAACATTTTCGGCAGATTTA	42
78	TGATAGCTTGTATCGGCCCTCAGGAAGATTAATGCAAAAATAC	41
79	CGAACGACAACAGTGGGCGGATTTGACCCGTACCCGTGCATCCAGCC	44
80	AAATCTTGTTTAGCCCAATTTCTGGAGAATAACATTTCTGG	39
81	CCAGCCAACTCAAAACGCAAAATTAACCCAAAGGATATGACC	39
82	ATTGAGGCATCACCATGTGAGCGAGTAAACCAGCTCAATTCGC	42
83	TTGCGGTTTGCCCATATAACATTTGAGTCAACCCGTCGCTG	39
84	CGCCTGACCACCATGGCTATTAGTCTTCGCACTCTGCCA	39
85	TTCATCGGAACGCAACGTTAATAATTTAAACAACGAAAAGGA	39
86	AATAACCACTAATAGTCTGAAATGGATTATAAGGGACGTGGCAC	44

87	AGCAGCAGTTTTCAITTTGGGCTTGAGATGGATTTTAAATAAAAAC	44
88	AGTATAGACCGTCTTTCCAGAGCCTAATGAGGGTTCGGTACT	41
89	GTACCCGCCCGTCTTTCCAGACGTTGGTATTAAGCCGTT	41
90	TAGCGCCCGTAATCACCCAGTAGCACCCACGTTAGAACTGG	39
91	TTTTAATTTCTTATCCGACACTGAGTTTTCGTCGCCCTCATGAATTT	44
92	CTTACCAGACTTGCTCAITTTCAGGGATATGTATCAGATATA	42
93	AGAAAGTCAATCGTCAITTCCAAAGAACGAGTAAATAGTTAG	39
94	TTAATGCAGTCAATATTTTAAATGCAAGCCATCGGAAAT	39
95	ACCCCGGTCATTTGCAATAAGTTTATTTTGCTTATTAAGAA	42
96	AACTCAAGCCGGATAATCATGGTCAATCCCAATCACAAAGAA	39
97	TCGCCGTGATTAACCTGAAACGACGGCCAGTGTAGCGAGCCCGGGT	44
98	ACATACGCATTAATTAATAAACAAACATGTTTCGTCTGAAATAATC	44
99	CCGGAGACCCGGAGAGACCA GCGCCAAAGACATAITTGATTGGGAA	44
100	GTGAAATTTCTTTACGAGCATGTAGAAAAAGCTGTTCCACACA	41
101	CCAACGCTGGGGCAACAGCTGATTGCTACCAGTTGAGAAT	41
102	GTGTAGGGAATCACCGTCAACCGACTTGATGCCGTGAGAAAAGG	41
103	CGCCATAGAGAATAITCCAGCTGCATTAATGGCGCCAGCCGCCTG	44
104	AAATAATGACGACAGCGTTGGGCTCACTGCACAATTTCTGT	42
105	TAATAATTTAACATTTATACAAATTTCTCCTTCAGGTGGTT	39
106	CTGGCATTAAGAAAGCCCCAAAAACAGGAATACCCACGCAATA	41
107	TGTTAGCCACCACGGCTGAGAGTCTGGAGCTGTCAATTTATAAGC	44
108	AGCGAAAAGGAAAGCAAAATCAGGTCTTTAGAAAATAAATAA	39

(continued)

Table 1
(continued)

#	Sequence	Length
109	CGCTAGCCGTTGTAAGCAAAAAGAAGATGAAAACAATTAACAG	42
110	GATTAAGCCAGACCCGATAITTTAGTTAATTCGTGAAAGCCTG	44
111	CAAGAAAAACGTACAATAATAACGGAAAGATTGCATATGT	39
112	ATAGTCAAAACACCCGGAATCATAATTACTACCCTGTCAAAAA	41
113	AAGAGTCGAAACTAAAGTACGGTGTCTTTAAAGACATCATAG	41
114	TAACTGACAGAGAAITTTATCCCAATCCAATCAGCGACCT	39
115	GTCTGAGGCTGATGCCCTCCTTTTGATAAGAATAATGCTTCAATC	44
116	GGCGTTATTCAAATGAAGCAAACTCCAACGATTGCAACTATT	42
117	GTAATAGACTAGCGGATAGCTTAGAGGAAGTTGTAGCT	39
118	GAAGCCCGAGATAAAGAATACTAAAACTTTTTCAACAGAG	42
119	AGCCTTTAACACCCCTAAGCGGAAACAAAAGGAAATCCTAAAGGA	44
120	TAAACCCATAACGATTATTATACAGGTAAGGCCAGGAACGG	39
121	CAGGAGGCACCCCGGAGGTTTTTGAAGCAITTTTATGTTACAA	44
122	GCAGATATCGTTTACCCTTTCCTCGTTAGAAATTAGACACCGAGTA	44
123	TTAGACTAAGGCCGCTTTTGGGGGATCGGATTTACTCGTAT	41
124	GTTGAGAGAGTGTTTTTATAATCAGTGGAAGATAACTAAT	41
125	AGGAAAGTTCTCAAATGCTTTAAAACAAAACCTGGGGGCGCT	41
126	GAGTGAGTTTTTGACCGTAAAAAGAAAAACAGTTAAGGAAT	41
127	AGGGCGCGCCGCTAAGTTTTGCCAGAGGCTGCGGAAAAACGA	44
128	TACGCCATAACGTGCAGACGACGATAAAAACACAITTCTCATCA	42

129	CTTAATTGGCAAGGGGAAAGCCGGGGTTCAGATCGTCA	39
130	TGCGAATTAATTGTAGATGATGGCAAITTCATGGAAGAAATTCG	44
131	AGGCTTGACAGCTTAACCAACCAAGAGGAGTCGACAAGAAGTA	42
132	GCGTCATAAAGCCATTGACAGGAGGTGGGCGGGGATTAIT	39
133	AGCCTTAATAAATCTAAACAACCTTTCATAAAGGGTTAGA	39
134	TCCTCAITACATGGCAACCCTAATTTCTGAGGATTAGGGTTTTG	44
135	GTTTCCAGAGGCAAAACCCACAAGAAATGAGATAGCTAACCCAGAA	44
136	ACGATTCGGAAAATCCTGTTTGTATGGTTGAGGGCAAAAATAAA	41
137	CAGCAGGGCGCACTAAATCGGAACCCCTCGCTGGTTAGCCCCG	41
138	ACGAAAITTAACGGAAACGAGGGTAGCAAAGTTTCTTACC	39
139	AGATAGGCCCTTGAGCAGTGCAACGTCAAAAAAATCAAAGCCCCC	44
140	CCGAAAATAITTCGGTTTTTGATGATACAGGCACAAAACGGTCCAG	42
141	TGGACTGTTGAGTAGCAAGCGGTCCAAAAGGGGTTTTTTTT	39
142	ATTTCAATTCGTTAACGTACAGATGAAAGGATCGCAAGTC	39
143	GCITTTGAGTGTAAAGCAGATAGCCGAAACAACCGGCTTGAGGAA	41
144	GCTGCTAATCTTGTGAAAGAGGACACCCAGAACCCTCAGA	39

Oligonucleotide sequences are shown with the “outer handle” sequence (oligos 1 to 48), and “inner handle” sequences (oligos 49–60). The remaining oligonucleotides are “core” (84 oligos)

Table 2
Oligonucleotide pool list

Pool	Oligo start	Oligo end
Outer handle	1	48
Inner handle	49	60
Core	61	144

Table 3
Modified oligonucleotide anti-handle sequences

Oligonucleotide	Sequence	Modification
Anti-Outer Handle_Cholesterol	TAGATGGAGTGTGGTGTGAAG-Chol	3' cholesterol-TEG
Anti-Inner Handle_Cy5	GTGAGTTGTGGTAGATAATTT-Cy5	Cy5 or alternative

2.3 Preparation of a Stock Liposome Solution

- 1,2-Di-(9Z-octadecenoyl)-*sn*-glycero-3-phosphocholine (DOPC, 25 mg/mL), 1,2-distearoyl-*sn*-glycero-3-phosphoethanolamine-*N*-[methoxy(polyethylene glycol)-2000] (PEG-2K-PE, 10 mg/mL), and 1,2-dioleoyl-*sn*-glycero-3-phosphoethanolamine-*N*-(lissamine rhodamine B sulfonyl) (rhodamine-PE, 1 mg/mL). Order these products in chloroform at the indicated concentrations.
- Mini-extruder kit, filter supports, and 0.2 μ m PC membranes.

2.4 Producing and Purifying DNA NanoOctahedron with Annealed Lipids and Fluorophores

- Oligonucleotides labeled with fluorophore of choice (*e.g.*, Cy5), and cholesterol-TEG. *See* Table 3.
- Octyl- β -D-glucopyranoside surfactant.
- Light glycerol buffer + 1% OG: Light glycerol buffer, 1% n-octyl- β -D-glucopyranoside (W/V).
- Heavy glycerol buffer + 1% OG: Heavy glycerol buffer, 1% n-octyl- β -D-glucopyranoside (W/V).

2.5 Encapsulation of Annealed DNA NanoOctahedron

- 7000 Molecular weight cutoff Slide-A-Lyzer Dialysis Cassette.
- Bio-Beads SM-2 Absorbent Media.

2.6 Enrichment of Encapsulated DNA NanoOctahedron

- Optiprep Density Gradient Medium.
- 96 Well, black/clear flat-bottom plate.

2.7 Characterization of the Encapsulated DNA NanoOctahedron Product

- PicoGreen double-stranded DNA dye.
- Greiner Bio-One 384-well Fluortrac plates, black.
- Carbon formvar copper grid, 400 mesh.

3 Methods

Carry out all steps of procedures at room temperature unless otherwise noted.

3.1 Folding a Stock Solution of DNA NanoOctahedron

The following protocol will produce 2.4 mL of a 50 nM solution of DNA NanoOctahedron. This folding can be scaled up or down, keeping the stoichiometry of components constant. As little as 800 μL of DNA NanoOctahedron can be folded for encapsulation; however experience has shown that having more material to work with makes the multi-step process, and characterization of the products, easier. This method has been used to fold up to 9600 μL of DNA NanoOctahedron in a 96-well plate.

1. To produce a 2.4 mL folding mixture at a 50 nM scaffold concentration, mix together 148.8 μL of H_2O , 120 μL of 20 \times folding buffer, 67.2 μL of 500 mM MgCl_2 , 1200 μL of p7308 single-stranded DNA scaffold, 432 μL of “Core” oligo pool, 288 μL of “Outer Handle” oligo pool, and 144 μL of “Inner Handle” oligo pool. These calculations assume a 100 μM starting concentration of the individual oligonucleotides, and provide a 10 \times multiple of each oligonucleotide per molecule of scaffold DNA.
2. Mix thoroughly but gently by inversion. Pulse-spin down the solution to collect. Transfer the 2400 μL into 24 \times PCR tubes, 100 μL into each.
3. Place the tubes on a thermal cycler according to the following schedule: 80 $^\circ\text{C}$ for 5 min, decrease to 65 $^\circ\text{C}$ at 5 min/ $^\circ\text{C}$, incubate at 65 $^\circ\text{C}$ for 20 min, decrease to 25 $^\circ\text{C}$ at 20 min/ $^\circ\text{C}$.
4. Re-combine the 100 μL volumes into a single 2400 μL volume.
5. Prepare a 1.5% 0.5 \times TBE agarose gel + 10 mM MgCl_2 gel with SYBR Safe stain added.
6. Mix 10 μL of the folded product with loading buffer (loading buffer must be adjusted to 10 mM MgCl_2), load into a well of the prepared agarose gel, and separate for 2.5 h at 60 V. Image the gel to verify that the folding was successful (Fig. 1, *see Note 1*).

3.2 Purification of a Stock Solution of Folded DNA NanoOctahedron

1. Fill a 15 mL Amicon Ultra Centrifugal Filter 30 K with filter wash buffer. Centrifuge at maximum speed (up to 5000 $\times g$) in a benchtop centrifuge for 15 min to flow the buffer through the filter (*see Note 2*).
2. Discard the flow through and any buffer retained in the upper filter chamber.
3. Concentrate the 2400 μL of product using the Amicon Ultra Centrifugal Filter. Transfer the 2400 μL of product to the filter

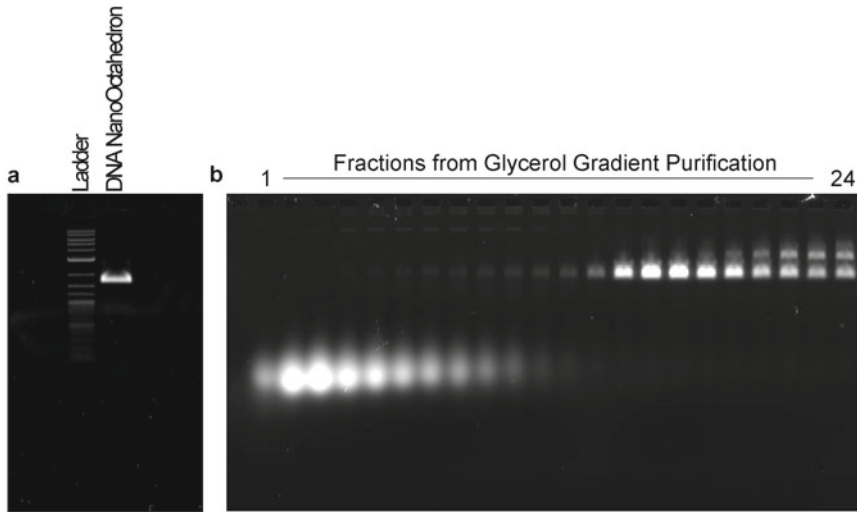


Fig. 1 Folding of the p7308 DNA NanoOctahedron, and purification *via* glycerol gradient ultracentrifugation. (a) An aliquot of the DNA NanoOctahedron folding product was loaded into a 1.5% agarose gel with 0.5× TBE, 1.5% agarose gel with 10 mM MgCl₂ and SYBR Safe, and was separated for 2.5 h at 60 V. The fastest migrating band is excess oligonucleotides from the folding, whereas the slower, sharper band is the primary NanoOctahedron product. (b) A glycerol gradient was prepared, and DNA NanoOctahedron sample was loaded onto the gradient and separated, as described in Subheading 3.2. Obtained fractions were loaded into a 0.5× TBE, 1.5% agarose gel with 10 mM MgCl₂ and SYBR Safe, and separated for 2.5 h at 60 V. Figure adapted in part from Perrault et al. [11]

and centrifuge at maximum speed (or up to $5000\times g$) for 10 min. This should reduce the volume to approximately 1.0 mL. Spin for additional time if the volume is still greater than 1.0 mL.

4. Resuspend the volume retained in the filter thoroughly with a pipette, as it forms a concentration gradient at the bottom of the filter. This improves overall recovery.
5. Transfer the concentrated product from the filter into a microcentrifuge tube. Wash the filter thoroughly with 100 μ L of folding buffer and add to the recovered product volume. Repeat the wash to recover as much product as possible, using a pipette to rinse down the sides of the filter. The total volume should now be approximately 1200 μ L. Add additional folding buffer if necessary. Set aside approximately 20 μ L of concentrated product for agarose gel analysis.
6. Prepare four glycerol gradients in Polyclear open-top centrifuge tubes, using the light glycerol buffer and heavy glycerol buffer, and the gradient station according to the manufacturer's protocol and instrument specifications. We used the following Gradient Station specifications to produce linear gradients: 59 s of rotation, 20 rotations per minute, 85° tilt. If access to a gradient station is not available, see **Note 3**.

7. Use a disposable 1 mL syringe (without needle tip) to remove 500 μL from the top of the gradient.
8. Use a clean disposable 1 mL syringe to transfer 300 μL of the concentrated product to the top of each of the four gradients.
9. Transfer the tubes to the buckets of an SW-55 Ti rotor, and the rotor into the ultracentrifuge. Spin the samples at $367,000\times g$ for 1 h.
10. Carefully retrieve the open-top centrifuge tubes from the rotor. Using the gradient station, fractionate the samples into 24 fractions, in a 96-well plate. If access to a gradient station isn't available, *see Note 3*.
11. Prepare a 1.5% agarose gel with $0.5\times$ TBE, 10 mM MgCl_2 , and SYBR Safe double-stranded DNA stain. Mix 2.5 μL of the concentrated, non-purified sample saved from **step 5**, and 10 μL of each fraction with loading buffer, and load into the gel. Separate for 2.5 h at 60 V. Image the gel to determine which fractions contain the primary product band (Fig. 1).
12. Combine the appropriate fractions containing the separated product band into a microcentrifuge tube.
13. Wash a new 15 mL Amicon Ultra 30 K Centrifugal Filter by filling the upper chamber with filter wash buffer. Centrifuge for 15 min at maximum speed (or $5000\times g$) in a benchtop centrifuge, and discard the flow-through and any filter wash buffer remaining in the upper chamber.
14. Transfer the collected product into the filter. Top up the filter with folding buffer. Centrifuge for 20 min at maximum speed (or $5000\times g$) in a benchtop centrifuge. Top up the upper chamber with folding buffer and repeat the centrifugation. Resuspend the concentrated product with a pipette, and transfer the volume to a microcentrifuge tube. Wash the filter as before, with two volumes of 100 μL folding buffer, to recover as much purified product as possible.
15. Prepare a 1:100 dilution of the sample in folding buffer. Using a spectrophotometer, measure the absorbance of the product at 260 and 280 nm. Use the absorbance at 260 nm and a double-stranded DNA extinction coefficient of 660 g/mol to estimate the molar concentration of the final product ($\text{absorbance}_{260\text{nm}} \div 660 \text{ g/mol} \times 100$ (dilution)).
16. If possible, use negative-stain transmission electron microscopy to image the final product, as a primary method of characterizing that it folded properly. *See* Subheading 3.5 below for details.
17. The stock solution of DNA NanoOctahedron can be stored for at least several months at 4 $^\circ\text{C}$.

3.3 Preparation of a Stock Liposome Solution

This method can be scaled up if very large batches of NanoOctahedron are going to be encapsulated. In that case, the lipid concentration should be kept constant throughout the liposome preparation.

1. To prepare a stock solution of liposomes, use Hamilton syringes to transfer 133.3 μL of DOPC, 63 μL of PEG-2 K-PE, and 47 μL of rhodamine-PE (all in chloroform) to a round-bottom glass test tube.
2. Place the above solution under vacuum overnight to completely remove the chloroform, light protected.
3. The next day, add 300 μL of folding buffer to the lipid film in the tube. Mix vigorously for 1 h, *e.g.*, using an Eppendorf Thermomixer at high rpm.
4. With the vesicle solution still in the glass tube, dip the solution into liquid nitrogen until frozen solid. Transfer to a beaker of room temperature water and allow the solution to thaw. Repeat this freeze-thaw seven times to break up the vesicles.
5. Set up the Mini-Extruder with a 0.2 μm membrane. Fill one of the two extruder syringes with folding buffer. Place both syringes into the extruder and use the folding buffer to ensure that the extruder is sealed, passing the folding buffer back and forth through the extruder. Remove the syringe containing the buffer. Draw back the other syringe to pull as much of the folding buffer out of the extruder as possible. Discard the folding buffer from both syringes.
6. Draw the vesicle solution into one of the extruder syringes. With both syringes in the extruder, pass the vesicle solution back and forth 21 times. This will produce a population of vesicles having an approximate 200 nm diameter. The solution should end up in the opposite syringe to where it started. Remove this and transfer the vesicle solution to a microcentrifuge tube. This stock vesicle solution can be stored for at least 1 month, light protected, at 4 $^{\circ}\text{C}$.

3.4 Producing and Purifying DNA NanoOctahedron with Annealed Lipids and Fluorophores

The following method is for encapsulation of 100 μL of a 20 nM solution of DNA NanoOctahedron. This method can be scaled in concentration and volume. The largest successful batch produced was 1500 μL at 30 nM. Higher concentrations and volumes may be possible. Lower concentrations down to 4 nM have been prepared, although the final concentration of encapsulated DNA NanoOctahedron is low enough that characterization (*e.g.*, *via* transmission electron microscopy) becomes difficult, without experience.

1. Prepare 20 μL of 100 nM DNA NanoOctahedron in 1 \times folding buffer from the stock solution prepared in Subheading 3.2.
2. Produce an annealing master mix by adding these reagents in a PCR tube. Follow the prescribed order to prevent aggregation

and denaturation: 53.0 μL of H_2O , 5.0 μL of 20 \times folding buffer (mix thoroughly), 20.0 μL of 100 nM DNA NanoOctahedron, 2.4 μL of 100 μM Anti-Inner Handle_Cy5 oligonucleotide (Table 3), 10 μL of 1% n-octyl- β -D-glucopyranoside (OG) surfactant, and 9.6 μL of 100 μM Anti-Outer Handle_cholesterol (Table 3). See Note 4 for a theoretical explanation of the encapsulation process.

3. Incubate the sample on a thermal cycler at 35 $^\circ\text{C}$ for 2 h, or overnight.
4. The next day, prepare a single glycerol gradient on the gradient station, as in Subheading 3.2, with light glycerol buffer + 1% OG, and heavy glycerol buffer + 1% OG.
5. Remove 300 μL from the top of the prepared gradient. Layer the 100 μL of annealed sample onto the gradient. Centrifuge for 1 h at 367,000 $\times g$. Fractionate the sample into 24 fractions using the gradient station.
6. Prepare a 1.5% agarose gel with 0.5 \times TBE, 10 mM MgCl_2 , and 0.05% SDS. Load 10 μL of each fraction into the gel. Separate for 2.5 h at 60 V. Image the gel in the fluorophore channel (*e.g.*, Cy5) to determine which fractions contain the annealed product. Note that the presence of SDS in the gel will prevent fluorescence detection *via* SYBR Safe stain.
7. Combine the appropriate fractions into a single sample in a microcentrifuge tube. This annealed product can be stored for at least 1 month, light protected, at 4 $^\circ\text{C}$.

3.5 Encapsulation of Annealed DNA NanoOctahedron

1. Estimate the volume of annealed product from Subheading 3.4, step 7. Add half of this volume of prepared stock liposomes from Subheading 3.3. This will reduce the OG concentration in the annealed product from 1.00 to 0.66%.
2. Incubate for 1 h with gentle mixing.
3. Dilute with twice the total volume with 1 \times folding buffer (*e.g.*, 300 μL of folding buffer added to a 150 μL solution of annealed product and liposomes). This reduces the concentration of OG to 0.33%, below its critical micelle concentration. Transfer the total volume into a 7000 molecular weight cut-off Slide-A-Lyzer Dialysis Cassette. Dialyze the solution for 48 h in 2 L of 1 \times folding buffer, with 2 g of added Bio-Beads SM-2 Absorbent Media, stirring gently.

3.6 Enrichment of Encapsulated DNA NanoOctahedron

1. Prepare a 10 mL isotonic working solution of 54% Optiprep medium for the 60% stock solution by mixing with 0.1 \times volume of 10 \times folding buffer (*e.g.*, 9 mL of 60% Optiprep + 1 mL 10 \times folding buffer).
2. Prepare 2 mL volumes of 28, 18, and 8% Optiprep solution by diluting the 54% working solution with an appropriate volume of 1 \times folding buffer.

3. Prepare ~1.2 mL of 35% Optiprep solution containing the encapsulation product from Subheading 3.5. For example, mix 0.72 mL of 54% Optiprep working solution with 0.3 mL of encapsulation product, and 0.13 mL of 1× folding buffer.
4. Transfer the 1.2 mL volume of 35% Optiprep solution containing encapsulation product into an SW-55 open-top ultracentrifuge tube with a pipette. Using a disposable 1 mL syringe (without needle tip), carefully layer the 28, 18, and then 8% Optiprep solutions on, in succession. Finally, layer 1× folding buffer onto the top of the gradient until the open-top tube is nearly full, leaving an approximate 300 μ L space at the top.
5. Centrifuge at $367,000\times g$ for 16 h at 4 $^{\circ}$ C. The next day, fractionate the sample into 24 fractions in a black-side, clear-bottom 96-well fluorescence plate.
6. Measure the fluorescence of the DNA NanoOctahedron fluorophore (*e.g.*, Cy5) and vesicle rhodamine for the 24 fractions on a fluorescence plate reader. Determine which fractions may contain encapsulated DNA NanoOctahedron *via* the distribution of the two fluorescent channels, which should display overlapping peaks (see example, Fig. 2).

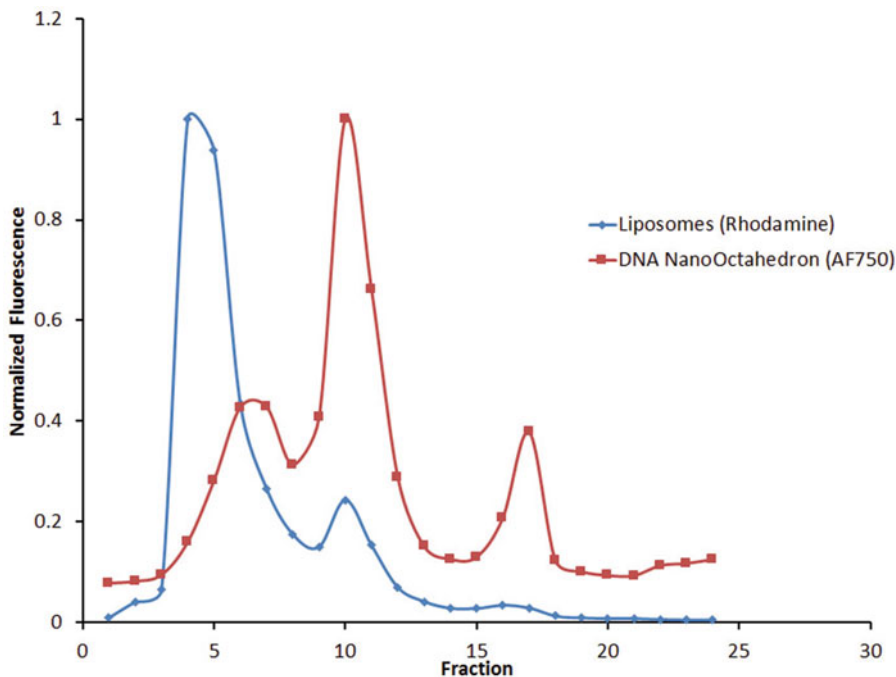


Fig. 2 Example distribution of vesicle and DNA NanoOctahedron after Optiprep gradient float-up. Encapsulated product was separated by equilibrium ultracentrifugation in an Optiprep gradient. The primary peak of liposomes is found towards the top of the gradient in fraction 5. The primary peak of the DNA NanoOctahedron is found in fraction 10. Fractions 9–11 were found to contain the encapsulated DNA NanoOctahedron

7. Dialyze the combined fractions of interest overnight in 1 L of 1× folding buffer using a 7000 molecular weight cutoff Slide-A-Lyzer Dialysis Cassette, or alternative dialysis device, to remove the Optiprep medium and to transfer the product into a buffer solution appropriate for downstream applications (e.g., 1× folding buffer, or PBS adjusted to 10 mM MgCl₂).

3.7 Characterization of the Encapsulated DNA NanoOctahedron Product

Two methods are used to characterize the success of encapsulation, and to determine which fractions contain the product of interest. The PicoGreen dye exclusion assay uses a double-stranded DNA stain that is membrane impermeable, and so cannot access fully encapsulated DNA NanoOctahedron. Staining of a sample in standard buffer (e.g., 1× folding buffer) is compared side by side with the same sample in a buffer containing surfactant to destabilize the membrane. The difference in fluorescence, compared to a standard curve, provides an estimate of the fraction of DNA NanoOctahedron fully encapsulated by a membrane. Yields of ~70% encapsulation are typical. Negative stain transmission electron microscopy is used to obtain single-particle structural data and verify that the NanoOctahedron are encapsulated within a single bilayer membrane.

1. Combined fractions from Subheading 3.6 can be concentrated using a 15 mL Amicon Ultra Centrifugal Filter 30 K MWCO. Note that the filter should be pre-treated with 1× folding buffer WITHOUT Tween-20, as this would solubilize the membrane. After pre-treating the filter, the encapsulated product can be loaded and concentrated by centrifugation at 2000×g.
2. Prepare a standard curve from the stock DNA NanoOctahedron. Prepare 200 μL of 5 μg/mL DNA NanoOctahedron, and then prepare 6× 1:2 dilutions by mixing 100 μL of the buffer used in Subheading 3.6, step 7 (assumed from hereon to be 1× folding buffer) with the DNA NanoOctahedron standards, in succession.
3. Prepare dilutions of the unknown samples from Subheading 3.6. Typically, a 1:5–1:50 dilution of the encapsulated product is appropriate, depending on the initial concentration of DNA NanoOctahedron, and the success of the encapsulation process.
4. Prepare a solution of 1× folding buffer with 1:200 PicoGreen dye added. 30 μL of this solution is needed for each standard curve and unknown sample, plus negative control (e.g., 7 standard curve samples + 3 unknown samples + 1 negative control requires 11 × 30 μL; in this case 400 μL could be prepared to provide excess). A positive control from a previous successful encapsulation run can be useful, if available.

5. Prepare a solution of 1× folding buffer + 1 % OG with 1:200 PicoGreen dye. The same volume is required here as in the previous step.
6. Pipette 10 μL volumes of both PicoGreen solutions into 3× wells of a 384-well black fluorescence plate for each standard, sample, and control to be measured. The presence of OG impacts the overall fluorescence of double-stranded DNA in the samples. Thus, all standards, samples, and controls have to be measured with, and without, 1 % OG present.
7. Add 10 μL of the standards, unknowns, and controls into 3 wells containing 1× folding buffer + PicoGreen, and 3 wells of 1× folding buffer + PicoGreen + 1 % OG. 10 μL of buffer should be used as a negative control.
8. Incubate for 5 min, light protected. Read fluorescence of the PicoGreen on a plate reader with excitation at 480 nm and emission at 520 nm.
9. For analysis, use median values of the three wells for each sample, with and without 1 % OG. Subtract the appropriate background median value for OG-positive and -negative readings from all standards, controls, and samples. Plot median fluorescence versus DNA NanoOctahedron concentration for the standard curve samples. Exclude the highest concentration samples of the standard curve if they are clearly outside of the linear range of detection. Determine the function describing the standard curve samples. Using this function and the median fluorescence values of the unknown samples, determine the estimated DNA NanoOctahedron concentration for all unknown samples in OG-positive and -negative buffer. The percent of encapsulated DNA NanoOctahedron is then obtained by

$$\frac{((\text{OG-positive } (\mu\text{g/mL}) - \text{OG-negative } (\mu\text{g/mL})) / \text{OG-positive } (\mu\text{g/mL}))}{100}$$
10. To prepare samples for negative stain transmission electron microscopy, ensure that the samples were dialyzed in buffer to remove Optiprep medium, which has a high contrast and will make imaging difficult.
11. Transfer 3.5 μL of the sample of interest onto plasma-treated carbon Formvar grids. This method is the same for imaging folded, non-encapsulated DNA NanoOctahedron, or encapsulated product. After 2 min, use filter paper to wick the excess liquid from the grid.
12. Pipette 3.5 μL of 2 % uranyl formate in H₂O (W/V) onto the grid. Incubate for 30 s, and then wick the solution away with filter paper.
13. Imaging can then be carried out using standard electron microscopy methods.

4 Notes

1. The DNA NanoOctahedron folding will typically produce two strongly visible products after separation by agarose gel electrophoresis. The bright, slower migrating band is the well-folded product, whereas the faster and less defined band is excess oligonucleotides. Multimers may also be visible as higher weight molecular weight products migrating more slowly than the primary product band, but these should not be nearly as bright as the primary band. The band can be excised using a scalpel, and the product isolated using Quantum Prep Freeze N Squeeze (Bio-Rad, Waltham, MA, USA). After excising the band, transfer to a microcentrifuge tube. Crush the plug thoroughly, transfer to a Freeze N Squeeze column, and centrifuge at $200 \times g$ for 2 min. The flow-through volume will contain DNA NanoOctahedron that can be imaged *via* negative stain transmission electron microscopy, as described in Subheading 3.7.
2. DNA nanostructures can become adsorbed or entangled with Amicon Filter devices, causing a large degree of material loss. Pre-treating the membrane with buffer containing Tween-20 surfactant greatly reduces nonspecific adsorption.
3. The gradient station allows for highly consistent and rapid production and fractionation of gradients for ultracentrifugation runs. However, if this instrument is not available, it is possible to produce and fractionate successful gradients by hand [13]. Layer an equal volume of 15% glycerol in $1 \times$ folding buffer (V/V) onto 45% glycerol in $1 \times$ folding buffer (V/V) in an open-top ultracentrifuge tube. Cap the tube with a rubber stopper and slowly tilt the tube until lying flat. Incubate for 2 h at room temperature. Slowly return the tube to a vertical position and remove the cap. The gradient can then be used for DNA NanoOctahedron purification. After the centrifugation run, the gradient can be fractionated by hand using a pipette with slow collection of each layer, being careful to remove direct from the top without disturb the remainder of the gradient.
4. Addition of the Anti-Outer Handle_cholesterol to the DNA NanoOctahedron solution would typically cause aggregation of the nanostructures. However, the presence of OG surfactant prevents this by formation of surfactant micelles at the sites of Anti-Outer Handle attachment. Addition of liposomes in Subheading 3.5 causes solubilization of the phospholipid vesicles from the presence of surfactant. Thus, the micelles formed in the annealed DNA NanoOctahedron solution, including those stabilizing the annealed Anti-Outer Handle, will contain a mixture of OG surfactant and phospholipids

from the liposomes. Dialysis of this mixture (Subheading 3.5, step 3) selectively removes the surfactant from the solution, whereas the phospholipids remain. This causes enrichment over time, until the phospholipids dominate and self-assemble into a bilayer membrane around the nanostructure. A more detailed explanation of vesicle reconstitution has been provided by Ollivon et al. [14].

References

1. Rothmund PWK (2006) Folding DNA to create nanoscale shapes and patterns. *Nature* 440:297–302
2. Douglas SM, Dietz H, Liedl T et al (2009) Self-assembly of DNA into nanoscale three-dimensional shapes. *Nature* 459:414–418
3. Castro CE, Kilchherr F, Kim D-N et al (2011) A primer to scaffolded DNA origami. *Nat Methods* 8:221–229
4. Liu Y, Lin C, Li H et al (2005) Aptamer-directed self-assembly of protein arrays on a DNA nanostructure. *Angew Chem* 117:4407–4412
5. Dutta PK, Levenberg S, Loskutov A et al (2014) A DNA-directed light-harvesting/reaction center system. *J Am Chem Soc* 136:16618–16625
6. Chhabra R, Sharma J, Wang H et al (2009) Distance-dependent interactions between gold nanoparticles and fluorescent molecules with DNA as tunable spacers. *Nanotechnology* 20:485201
7. Lin C, Jungmann R, Leifer AM et al (2012) Submicrometre geometrically encoded fluorescent barcodes self-assembled from DNA. *Nat Chem* 4:832–839
8. Shaw A, Lundin V, Petrova E et al (2014) Spatial control of membrane receptor function using ligand nanocalipers. *Nat Methods* 11:841–846
9. Douglas SM, Bachelet I, Church GM (2012) A logic-gated nanorobot for targeted transport of molecular payloads. *Science* 335:831–834
10. Hahn J, Wickham SFJ, Shih WM et al (2014) Addressing the instability of DNA nanostructures in tissue culture. *ACS Nano* 8:8765–8775
11. Perrault SD, Shih WM (2014) Virus-inspired membrane encapsulation of DNA nanostructures to achieve in vivo stability. *ACS Nano* 8:5132–5140
12. Douglas SM, Chou JJ, Shih WM (2007) DNA-nanotube-induced alignment of membrane proteins for NMR structure determination. *Proc Natl Acad Sci* 104:6644–6648
13. Lin C, Perrault SD, Kwak M et al (2013) Purification of DNA-origami nanostructures by rate-zonal centrifugation. *Nucleic Acids Res* 41, e40
14. Ollivon M, Lesieur S, Grabielle-Madlmont C et al (2000) Vesicle reconstitution from lipid-detergent mixed micelles. *Biochim Biophys Acta* 1508:34–50

DNA-PAINT Super-Resolution Imaging for Nucleic Acid Nanostructures

Mingjie Dai

Abstract

Far-field super-resolution fluorescence microscopy has allowed observation of biomolecular and synthetic nanoscale systems with features on the nanometre scale, with chemical specificity and multiplexing capability. DNA-PAINT (DNA-based point accumulation for imaging in nanoscale topography) is a super-resolution method that exploits programmable transient hybridization between short oligonucleotide strands, and allows multiplexed, single-molecule, single-label visualization with down to ~5–10 nm resolution. DNA-PAINT provides a method for structural characterisation of nucleic acid nanostructures with high spatial resolution and single-strand visibility.

Key words DNA-PAINT, Super-resolution imaging, Fluorescence microscopy

1 Introduction

1.1 Overview of DNA-PAINT Super-Resolution Method

Super-resolution fluorescence microscopy has provided an important tool for biologists and nanoscientists, to study single-molecule conformations and dynamics in nanoscale biomolecular and synthetic systems [1, 2]. Recent advances in methods such as STED, SIM, PALM, STORM, and PAINT have allowed optical interrogation of subcellular and nanoscale structures with down to 10–20 nm resolution, allowing direct visualization and quantitation of material defect centers, synthetic nanoscale structures and patterns, cytoskeletal, vesicle and membrane features, single-molecule diffusion and intracellular transport, and so on. In this chapter we discuss a particular implementation of super-resolution microscopy, DNA-PAINT (DNA-based point accumulation for imaging in nanoscale topography), that is particularly suited for single-molecule observation of nucleic acid nanostructures, and detail the design principles, experimental methods, and data analysis procedures for performing experiments with DNA-PAINT.

Traditional characterization methods for observation of nucleic acid nanostructures, in a single-molecule fashion, have mostly relied on atomic force microscopy (AFM) and electron microscopy (EM). While providing immensely useful information regarding nanostructure assembly quality and integral structural features, these methods have their limitations. Compared with AFM, EM provides an efficient method for observation of a large sample area, but it operates under non-biological conditions, and does not allow visualization of single nucleic acid strand components due to lack of contrast, and therefore is not sufficient for interrogation of features such as assembly defects. On top of that, both methods lack chemical (strand) specificity and are limited to single-channel images output of electron density and surface topography graphs, respectively.

DNA-PAINT fluorescence microscopy provides an alternative method for interrogation of nucleic acid nanostructures, that allows single-strand visibility and multiplexed detection with high specificity, and operates in biocompatible environment. DNA-PAINT method falls into the family of stochastic localization microscopy (also called single-molecule localisation microscopy, or SMLM) of the recent fluorescence super-resolution microscopy methods. In brief, super-resolution visualization is achieved by temporally separating nearby target fluorescence emission via stochastic switching of each target between a fluorescence on-state and an off-state, and determining their respective positions with sub-diffraction-limit precision [3]. These methods include PALM (photo-activated localization microscopy) [4, 5], STORM (stochastic optical reconstruction microscopy) [6, 7], and PAINT (point accumulation for imaging in nanoscale topography) [8] and their many variants, and mostly differ from each other in the way that stochastic single-molecule switching is achieved.

Methods based on the PAINT principle rely on diffusion and stochastic transient binding of a fluorophore-conjugated affinity probe that is specific to the imaging target. When bound to the target, the fluorophore transiently stays and produces an apparent bright blinking spot on the recorded camera frame. The relative brightness (or blinking signal-to-noise ratio) of the spot is determined by the accumulated photon emission from the binding relative to background generated from the unbound, freely diffusing probes, and can be dramatically enhanced by placing the sample under total internal reflection (TIR) illumination setup. After the first introduction of the PAINT principle [8], several variants were published with different affinity probes (including DNA-PAINT, uPAINT, BALM, *see refs.* [9–11]). Jungmann et al. [9] first noticed that transient binding between short oligonucleotide strands could be used as such affinity probes to produce blinking patterns suitable for super-resolution imaging (DNA-PAINT). In detail, a short oligonucleotide strand (the “docking strand”) is labelled on the

molecular target of interest, and a complementary sequence (the “imager strand”) is labelled with a fluorophore and used as the affinity probe (Fig. 1a). The method has quickly found application in studying nucleic acid nanostructure conformations and defects, single-molecule binding kinetics and detection of nucleic acid substrates [12, 13].

The method was further developed by Jungmann et al. [14] for multiplexed cellular imaging, Jungmann et al. [15] to quantitative target counting, and Dai et al. [16] to ultra-high-resolution discrete molecular imaging (DMI). In detail, Jungmann et al. [14] generalized the original method to multiplexed, 3D, cellular imaging with orthogonal DNA binding sequences, astigmatism-based 3D point spread function (PSF) detection, and antibody-conjugated DNA strands as target probes. Jungmann et al. [15] developed the method for producing quantitative target counting in a resolution-limited image area. Dai et al. [16] further developed the method to 5 nm resolution, multiplexed single-target imaging via the discrete molecular imaging framework and stringent stage drift correction control. Figure 1b–d illustrates the multiplexing capability, single-target detectability, and high-resolution imaging with DNA-PAINT. In this chapter, we focus on the application of DNA-PAINT as a method for interrogating the self-assembly and molecular arrangements in nucleic acid nanostructures, and discuss the principles for obtaining high-resolution, high-quality images on these nanostructures.

1.2 General Principle for High-Quality and High-Resolution Imaging

In general, the imaging quality and resolution of SMLM microscopy method are determined by a few factors (or technical requirements, *see* Fig. 2) [16]: (1) high localization precision (of single-molecule blinking events), (2) high target signal-to-noise ratio (target SNR in the super-resolved image),¹ (3) low fraction of false localizations (from double-blinking events), and (4) accurate microscope stage drift compensation. Depending on the application, these requirements may be weakened without affecting the imaging results, but all of these requirements are critical for obtaining molecular-resolution single-target imaging, as can be demonstrated by considering a densely packed grid pattern, simulated under different imaging conditions.

The detailed technical discussions of these principles and their characterisation can be found in Dai et al. [16], and are beyond the scope of this method chapter. But it is important to understand the effects of these factors and how they can be achieved in experiments, especially, (1′) high localization precision can be obtained from collecting a large number of photons from single-molecule localization, (2′) high target SNR can be achieved by collecting a large

¹Not to be confused with blinking SNR, which is calculated in a single recorded frame.

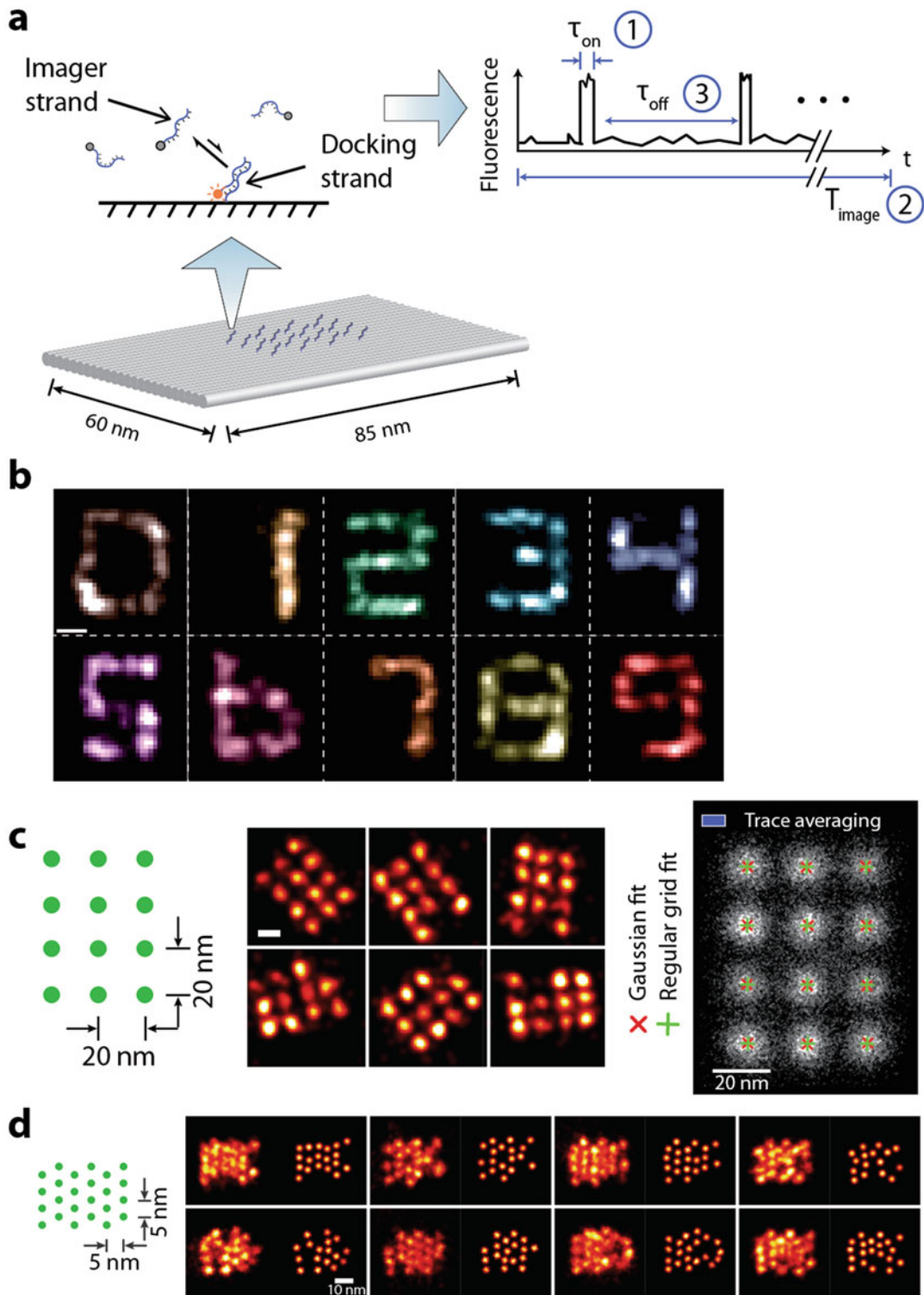


Fig. 1 Principle and examples of DNA-PAINT. (a) Illustration of DNA-PAINT principle: transient binding between a docking strand and dye-conjugated imager strands (**top left**) generates a single-molecule blinking time trace (**top right**), illustrated on a synthetic DNA origami nanostructure, where each cylinder represents a DNA

number of blinking events from individual single targets, and (3') low fraction of false localizations can be achieved by using a low blinking on-off duty cycle. These properties can be controlled by tuning the single-molecule blinking kinetics of the affinity probes (in our case, the oligonucleotide probe), and will be referred to in the design and experimental method sections below.

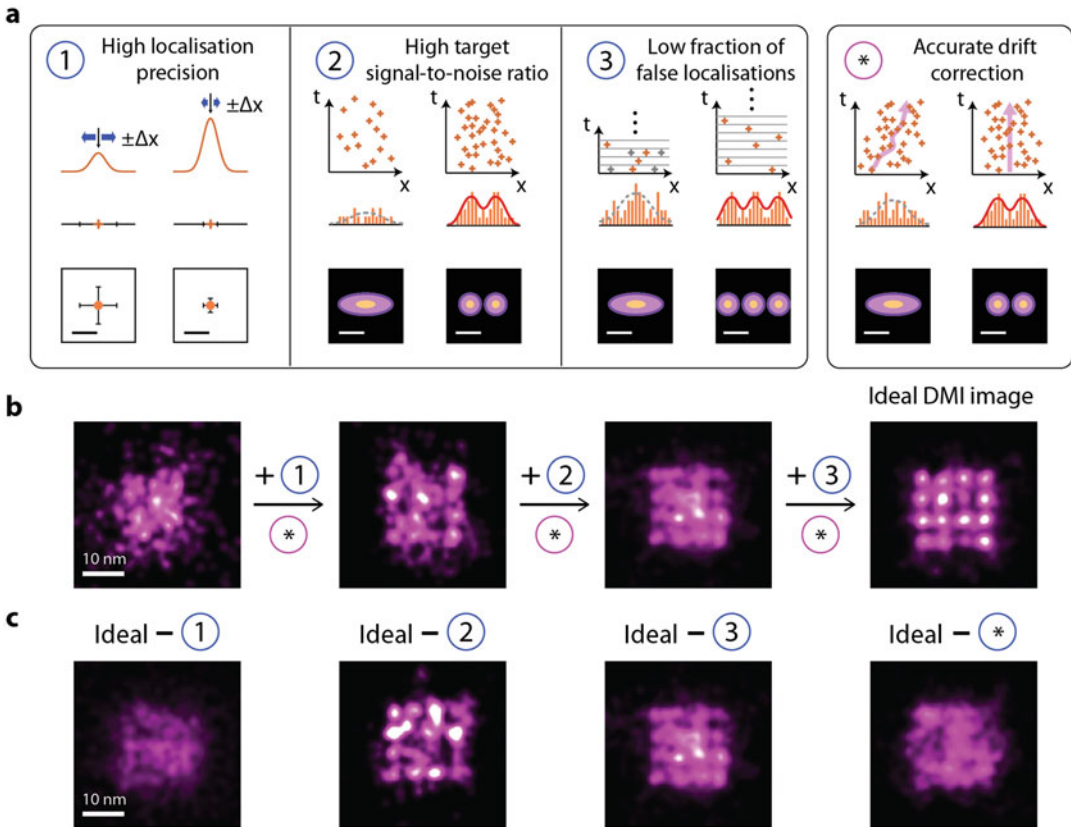


Fig. 2 Technical requirements for achieving discrete molecular imaging. (a) Each panel outlines one technical requirement, and depicts schematically the effect on imaging quality before (left column) and after (right column) the requirement is satisfied. (b–c) Simulations of imaging effects of the technical requirements for a 4×4 regular array structure, under increasingly better imaging conditions without stage drift (b), or under non-ideal imaging conditions with one of the four requirements unsatisfied (c). Figure adapted and reprinted with permission from Dai et al. [16]

Fig. 1 (continued) double helix (bottom). (b) Pseudo-colored, 10-round multiplexed exchange-PAINT images of ten different origamis displaying digits 0–9 in one sample. Image obtained using only one fluorophore (Cy3b) through ten imaging-washing cycles. Scale bar: 25 nm. (c) Design schematics of a 3×4 square grid with 20 nm point-to-point spacing on a DNA origami nanostructure (left), representative DNA-PAINT super-resolution images of the 20 nm grid structure (middle), and single-particle average ($N = 700$) for structural studies. (d) Design schematic of triangular grid with 5 nm spacing (left) and discrete molecular imaging (DMI, right). For each representative single-molecule image, the fluorescent super-resolution image (left) and the automatically fitted image (right) are shown. Figure adapted and reprinted with permission from Jungmann et al. and Dai et al. [14, 16]

1.3 Design of DNA-PAINT Imaging Probes

The binding and blinking kinetics of the imaging probe determines the single-molecule blinking events at the imaging target that are critical for obtaining high-quality super-resolution images, as mentioned above. In brief, imaging probe need to be designed with an appropriate binding strength (free energy) and high binding specificity, and with a photostable fluorophore, to allow for a large number of photons collected (principle 1' above). Since a photostable fluorophore (such as cy3b, atto655, or atto647n dyes) could usually be predetermined and is suitable for a range of imaging probes and applications, the process of designing imaging probe generally consists of designing an appropriate probe binding sequence (the docking and imager strands) and deciding on target anchoring sites.

The principle for designing sequences with appropriate binding strength is to aim at a characteristic binding on-time that would both give the highest blinking SNR, and to match the recording frame time. The single-strand diffusion time scale (the time it takes a single-stranded oligonucleotide to diffuse out of a diffraction-limited area on the surface) and probe binding on-time are both buffer dependent. Under typical buffer conditions for nucleic acid nanostructures (10 mM Mg²⁺) the single-strand diffusion time is around 30–50 ms, and it is recommended to design probes with on-time between 0.5 and 1 s. Nucleic acid binding energy calculation packages such as NUPACK [17] could be used to help design sequences with desired binding strength. Probes with 8–9 nt in length, 50% GC content, and no secondary structure typically give a binding free energy of –10 to –11 kcal/mol (at 25 °C, 10 mM Mg²⁺, 50 mM Na⁺), and achieve an optimized binding on-time, as well as allowing enough coding space for multiplexed imaging applications.

After the binding sequence is decided, the docking strand is typically designed by extending the target nucleic acid strand (such as a staple in DNA origami, a strand in DNA tile or brick-based structure) with a short linker (one or two thymine bases) and the docking sequence. It is recommended to extend the target strand from the 3'-end, since current synthetic nucleic acid chemistry using phosphoramidite extends in the 3'-to-5' direction, and therefore 3' extensions has a lower truncation percentage. In conjunction, it is recommended to label the fluorophore on the 3'-end of the imager strand. Other factors that need to be considered include potential secondary structures on the docking strand, especially between the docking sequence and any unprotected single-stranded sequence nearby. If the docking sequence is to be placed within a loop, steric hindrance would also play a role, and a spacer size of at least 8 nt (such as 8 thymine bases, on each side) is recommended to maximally expose the docking sequence and preserve the binding on-time (data not shown).

1.4 Design of Nucleic Acid Structure Surface Fixation

Nucleic acid nanostructures will need to be fixed to the glass surface for microscopy imaging. Biotin-streptavidin-biotin linkage is a recommended method that is both easy to implement and provide clean and stable surface fixation. There are two strategies for biotin anchoring to the nanostructure, either direct conjugation of biotin (with a linker of 3–6 thymine bases) to a subset of the strands in the nanostructure before the assembly or indirect labeling via a common, stable handle sequence (typically 15 nt or longer), which results in a longer linker spacing and thus less stable attachment, but provides a significantly more economic option. For stable attachment, at least six biotin anchors per nanostructure on a flat (non-twisted) surface, and separated at least 10 nm from each other, are recommended (data not shown).

2 Materials

2.1 Chemicals

For DNA nanostructure synthesis, all unmodified and biotin-modified DNA oligonucleotides can be ordered from IDT (Integrated DNA Technologies). For DNA-PAINT imaging probes, fluorophore-conjugated oligonucleotide used as DNA-PAINT imaging probes could be either purchased commercially (Bio-Synthesis Inc.) or conjugated in-house (see protocol below). All imaging buffers should be prepared with ultrapure water and filtered with 0.22 μm filter before use. Biotin-conjugated BSA, streptavidin, oxygen-scavenging buffers, DNA imager strands, and synthetic DNA nanostructures should be stored at $-20\text{ }^{\circ}\text{C}$.

2.2 Buffers for Nanostructure Surface Fixation

1. Immobilization buffer: 10 mM Tris-HCl, 100 mM NaCl, 0.1% (v/v) Tween 20, pH 8.0.
2. Biotinylated BSA solution: 1.0 mg/ml solution of biotin-conjugated BSA (A8549, Sigma Aldrich) in immobilization buffer.
3. Streptavidin solution: 0.5 mg/ml solution of streptavidin (S-888, Invitrogen) in immobilization buffer.

2.3 DNA-PAINT Imaging Buffers

DNA-PAINT imaging can be performed in a few different buffer choices, depending on application and requirements on imaging quality. The *imaging solution* is prepared by diluting the imager strand to desired concentration (typically between ~ 1 – 20 nM) in the *imaging buffer* of choice. The optimal imager concentration depends on the detailed properties of the sample, especially the density of DNA-PAINT imaging targets. Without prior knowledge, it is recommended to start imaging with ~ 5 nM, and adjust iteratively to optimize the imaging quality depending on the results.

1. Imaging buffer B: For regular imaging of DNA and RNA nanostructures.

Buffer components: 10 mM Tris-HCl, 10 mM MgCl₂, 1 mM EDTA, 0.1 % Tween 20, pH 8.0. Depending on application, MgCl₂ concentration can be adjusted to be compatible with nanostructure stability or to tune DNA-PAINT blinking kinetics.

2. Imaging buffer TP: With oxygen-scavenging and redox system, for high-performance imaging of DNA and RNA nanostructures (*see Note 1*).

Buffer components: 10 mM Tris-HCl, 10 mM MgCl₂, 1 mM EDTA, 0.1 % Tween 20, 10 nM PCD (protocatechuate-3,4-dioxygenase), 2.5 mM PCA (protocatechuic acid), 1 mM trolox, pH 8.0.

- 2.1. Prepare 100× PCD stock solution (1 μM) in 50% glycerol, 50 mM KCl, 1 mM EDTA, and 100 mM Tris-HCl, pH 8.0; prepare 40× PCA stock solution (100 mM) in ultrapure water and adjust pH to 9.0 with NaOH; prepare 100× trolox stock solution (100 mM) by first dissolving in 100% methanol (430 μl per 100 mg of trolox) and bring the volume up with ultrapure water; adjust pH to 9.0 with NaOH.

- 2.2. Prepare buffer TP from buffer B and concentrated stock solutions for each additional component from above. Add 100 μl of 2× imaging buffer B; add 2 μl of 100× trolox, 5 μl of 40× PCA, and 2 μl of 100× PCD, and appropriate volume of imager strand solution; and bring the total volume up to 200 μl. Pipette up and down gently to mix well, and incubate for 10 min before use (*see Note 2*).

3 Methods

3.1 Fluorophore-Labeled Oligonucleotide as DNA-PAINT Imager Strands

For commercially ordered imager strands, resuspend the sample in ultrapure water to 100 μM and store at -20 °C.

For in-house production of imager strands, follow the protocol below. Order 3' (or 5') amino-modified DNA oligonucleotide from IDT, and NHS-ester-modified organic fluorophores from GE (cy3b NHS ester) or Sigma Aldrich (atto655 NHS ester and atto647n NHS ester).

1. Conjugation

- 1.1. Prepare 3' (or 5') amino-modified DNA oligonucleotide in ultrapure water at 1 mM concentration, prepare NHS ester-modified fluorophore (e.g., cy3b, atto655,

- atto647n) in DMSO at 20 mg/ml, and prepare 1 M NaHCO₃ buffer at pH 8.0.
- 1.2. Prepare conjugation reaction solution by adding 20 μ l amino-modified DNA solution, 2 μ l NaHCO₃ buffer, and 4 μ l fluorophore NHS-ester solution in order, and gently vortex to mix.
 - 1.3. Incubate the conjugation solution on shaker and protected from light for 2 h (room temperature).
2. Column purification.
- 2.1. Pre-wash size-exclusion column (GE NAP-5) with 2 ml ultrapure water four times.
 - 2.2. Bring total volume of conjugation solution to 100 μ l and add to column, and add more ultrapure water (~3 ml) to finish collection. Collect every three droplets to a separate well on a microplate.
 - 2.3. Determine peak position and width with fluorescence plate reader (optional), and combine and collect the wells with brightest signals (typically 3–4 wells close to the beginning).
 - 2.4. Freeze the sample with liquid nitrogen, cover with aluminum foil, and lyophilize overnight.
3. HPLC purification.
- 3.1. Prepare HPLC buffer A (0.1 M TEAA, 5% ACN) and HPLC buffer B (0.1 M TEAA, 50% ACN), and resuspend lyophilized sample in 0.1 M TEAA to 50 μ l total volume.
 - 3.2. Pre-wash C18 2.5 μ m column (Xterra MS C18, Waters) and equilibrate with buffer A.
 - 3.3. Set HPLC pumping rate to 1 ml/min, and set linear buffer gradient from 100% HPLC buffer A to 50%:50% HPLC buffer A and B over 30 min. Monitor the elution with absorption at 260 nm (for DNA) and appropriate absorption peak for the fluorophore of interest (e.g., 559 nm for cy3b, 663 nm for atto655 and 644 nm for atto647n), and collect purification product from the sample peak where absorption can be seen at both channels (typically this is the maximum peak at both channels). Collection can be performed either with peak-based automatic collection or by collecting all products in a microplate and manually combining the sample wells.
 - 3.4. Freeze the sample with liquid nitrogen, cover with aluminum foil, and lyophilize overnight.
4. Quantification of conjugation product.
- 4.1. Resuspend the sample with 30 μ l of ultrapure water.

- 4.2. Measure conjugated imager concentration by absorption at the fluorophore's maximum absorption peak.
- 4.3. Optionally, determine the labelling efficiency by measuring the oligonucleotide concentration at 260 nm absorption. Typically a labeling efficiency of >90% is observed.
- 4.4. Resuspend the sample in ultrapure water to 100 μ M and store at -20 °C.

3.2 Sample Preparation for Imaging Nanostructures

1. DNA-PAINT imaging of synthetic nucleic acid nanostructures are carried out in custom-built microscopy flow chamber either on a glass microslide, or on an Ibidi chamber (Ibidi GmbH) for multiplexed imaging with buffer exchange.
 - 1a. Making flow chamber on a glass microslide.
 - 1a.1. Clean glass slide and cover slip surfaces with isopropanol.
 - 1a.2. Build flow chamber by putting down two parallel stripes of double-sided tape on the slide, spaced apart slightly narrower than the width of the cover slip, and then placing the cover slip on the top to form a channel between the cover slip and the glass slide.
 - 1a.3. Press down the cover slip on both sides to make the edges watertight. The finished flow chamber contains a volume of about 20 μ l.
 - 1b. Making flow chamber for multiplexed exchange-PAINT imaging on an Ibidi chamber.
 - 1b.1. Clean a large (24 \times 60 mm) glass cover slip with isopropanol.
 - 1b.2. Open an Ibidi sticky slide (sticky slide VI^{0.4}), remove the protective cover, and position the cover slip on the sticky glue, with the cleaned surface inside (facing the chamber).
 - 1b.3. Press down the cover slip along the boundary of the flow chambers, make sure the chamber is well sealed and watertight (the finished flow chamber contains a volume of about 40 μ l in the middle part).
 - 1b.4. Clean the chamber by placing it inside a UVO cleaner (Jetlight 42) with the lid open, for 5 min.
 - 1b.5. Rinse flow chamber with 100 μ l isopropanol twice, followed by 100 μ l ultrapure water twice.
 - 1b.6. Pre-wash both inlet and outlet tubing with 100 μ l isopropanol twice.
 - 1b.7. Rinse flow chamber with 100 μ l deionized water twice, followed by 100 μ l imaging buffer B twice.

2. Surface immobilization of biotin-labeled nanostructure samples via biotin-streptavidin-biotin linkage. The following protocol is given for microslide-based flow chamber; for Ibidi flow chamber, replace all volumes with 40 μl (instead of 20 μl).
 - 2.1. Dilute biotin-labeled nanostructures in imaging buffer B to desired concentration. Recommended final concentration is 0.1–0.2 nM. For high imaging quality, the optimal concentration will depend on the sample of interest, especially the density of DNA-PAINT imaging targets on the sample structure.
 - 2.2. Rinse flow chamber with 20 μl immobilization buffer twice. Avoid introducing bubbles into the chamber (*see Note 3*).
 - 2.3. Flow in 20 μl of 1 mg/ml biotinylated BSA solution, and incubate for 2 min.
 - 2.4. Rinse flow chamber with 20 μl immobilization buffer twice.
 - 2.5. Flow in 20 μl of 0.5 mg/ml streptavidin solution, and incubate for 2 min.
 - 2.6. Rinse flow chamber with 20 μl immobilization buffer twice.
 - 2.7. Rinse flow chamber with 20 μl imaging buffer B twice.
 - 2.8. Flow in 20 μl of biotin-labeled DNA origami sample solution (~ 0.5 nM, in buffer B), and incubate for 2 min.
 - 2.9. Rinse flow chamber with 20 μl buffer B twice.
 - 2.10. Flow in 20 μl DNA-PAINT imaging solution twice.
 - 2.11. Place the sample on the microscope under live mode (see below), and check the density of blinking spots on the camera. If the density of blinking spots is too high (such that the point spread function (PSF) of neighboring blinking spots are close to each other or almost overlapping), or the number of blinking spots is too low (minimum ~ 50 blinking events in each camera frame), go back to change **step 2.8** and adjust the nanostructure concentration appropriately such that a desired density of blinking spots could be achieved (*see Note 4*).
 - 2.12. (Optional, for multiplexed DNA-PAINT imaging with Ibidi flow chamber only) Connect both inlet and outlet tubings to the Ibidi chamber, and connect outlet to a syringe (5 ml volume). Rinsing and buffer exchange from here onward are performed by feeding the solution from the inlet and pulling on the syringe from the outlet end.

3.3 Single-Molecule DNA-PAINT Super- Resolution Microscopy

The following steps require a well-adjusted microscope, comparable to the setup described in Dai et al. [16]. DNA-PAINT super-resolution fluorescence microscopy of nanostructures is typically performed with total internal reflection (TIR) illumination. Automatic focus lock systems (such as the perfect focus system from Nikon, and the definite focus system from Zeiss) are necessary for maintaining focus over an extended imaging time. Both CCD and CMOS based cameras are suitable for DNA-PAINT imaging.

1. Optimization of imaging conditions and super-resolution movie acquisition.
 - 1.1. Place the microslide or Ibidi flow chamber with nanostructures in DNA-PAINT imaging solution on the microscope stage.
 - 1.2. Turn on the appropriate excitation laser and set the excitation intensity to ~ 0.5 kW/cm². Select appropriate filter modules or cubes for the laser. Set the camera exposure time to ~ 200 ms, and turn on live mode.
 - 1.3. Adjust the microscope focus (coarsely) to the surface with immobilized nanostructures. When focused, bright, diffraction-limited blinking spots of DNA-PAINT imager strands should become visible.
 - 1.4. Adjust the TIR illumination angle to maximize surface illumination while suppressing transmission; in particular, maximize the signal-to-noise ratio between the pixel intensities of the bright blinking spots and the illumination background.
 - 1.5. Adjust camera exposure time in the range of ~ 100 – 500 ms, such that each blinking event ideally lasts ~ 2 – 5 imaging frames. For EMCCD cameras, do not use electron multiplying gain if possible, as this would result in a lowered imaging quality.
 - 1.6. Adjust the microscope focus (finely) to the bright blinking spots; in particular, maximize the pixel intensity of the central (brightest) pixels. When well focused, a sharp, and potentially pixelated image of the point spread function (PSF) could usually be seen for each of the blinking spots.
 - 1.7. Start camera acquisition of ~ 5000 – $20,000$ frames. The optimal length of acquisition depends on the sample properties and desired imaging quality. In particular, longer acquisition allows better target signal-to-noise ratio (tSNR) and higher overall imaging quality.
2. (Optional) Multiplexed DNA-PAINT imaging with buffer exchange. For every additional imaging channel, perform

imaging buffer exchange followed by another super-resolution movie acquisition as in the previous step.

- 2.1. Remove previous imaging buffer by flowing in 400 μl of imaging buffer B and incubate for 2 min.
- 2.2. Introduce new imaging solution by flowing in 200 μl of imaging solution into the chamber and incubate for 2 min.
- 2.3. Adjust microscope and camera settings as necessary, and acquire another super-resolution movie following the procedures described in the previous step.

3.4 Super-Resolution Imaging Data Processing

Super-resolution imaging data processing was generally performed in two steps: (1) spot detection, localization, and filtering and (2) drift correction and super-resolution rendering. We offer a data processing and analysis software suite with graphical user interface (from Dai et al. [16]) for an integrated, easy-to-use data processing. In the following we provide an outline of the key steps and principles of each step in the data analysis, accompanied with instructions in using the custom software for each step.

1. Super-resolution spot detection and single-emitter localization:
 - 1.1a. Spot detection is performed by the principles of background subtraction and Gaussian smoothing, with Gaussian filter size tuned to match the single-molecule blinking PSF size to produce the best sensitivity and specificity for DNA-PAINT super-resolution movies. Single-emitter localization is performed with one of many 2D Gaussian fitting routines, such as a maximum likelihood estimation algorithm from Smith et al. [18].
 - 1.1b. In the DNA-PAINT image analysis software, click “Spot detection and localisation” to open the parameter dialogue box. Enter the acquisition parameters for the movie (movie size, camera pixel size, count to photon conversion factor), and use $\sim 0.25 \times [\text{dye emission maximum wavelength}]$ as the PSF fitting standard deviation.
2. Super-resolution image rendering and drift correction:
 - 2.1a. Super-resolution image rendering is performed by transforming a list of single-molecule localized positions to a 2D histogram with each localization smoothed by a Gaussian function.
 - 2.1b. With the DNA-PAINT image analysis software, click “Load” to open the trace file generated from the previous step. Depending on the desired structural separation, set the sub-pixel resolution to $[\text{camera pixel size}]/20$, such that each display pixel is 20 nm in size, and adjust the display brightness.

- 2.2a. Determine maximally supported imaging resolution from distance between adjacent-frame localizations (DAFL) analysis (*see Note 5*). In DAFL analysis, all pairs of localizations from adjacent imaging frames and spatially close to each other are collected and their 2D distance pooled and their distribution plotted as a histogram. The histogram is fit to a theoretical distribution function to determine the maximally supported imaging resolution.
- 2.2b. With the DNA-PAINT image analysis software, open “Data quality” window, click “Analyse connectivity,” and wait until the analysis is finished and then click “DAFL analysis.” An automatic fitting to the distribution will be performed and the supported resolution will be displayed. Close the window and set the Gaussian smoothing standard deviation to be $1/2.35 \times [\text{maximal supported resolution}]$.
- 2.3a. (Optional, if the drift traces of all nanostructures are overlapping and not separable) Perform DAFL-based drift correction by collecting all pairs of localizations from adjacent imaging frames and close to each other as in the previous step. For every imaging frame, calculate the drift vector by computing the average vector offset from all pairs of localizations that spans the previous and the current frame, and use the vector cumulative sum as the image drift correction trace.
- 2.3b. (Optional, as above) With the DNA-PAINT image analysis software, open “Data quality” window, click “DAFL drift correction,” wait until the analysis is finished, click “Use as drift correction,” and close the window. In the main window, click “Apply” to apply the drift correction.
- 2.4a. Correct for imaging drift by selecting an isolated nanostructure as the drift marker. Extract its blinking time trace over time, and smooth over its time trace as the imaging drift correction.
- 2.4b. With the DNA-PAINT image analysis software, click “Select ROI” to select an isolated nanostructure, and click “Analyse trace” to open trace display window. Enter an appropriate time window (recommended ~500–2000) for the smoothing, click “Calculate,” and wait until calculation finishes. Click “Use as drift correction,” close the window, and click “Apply” in the main window to apply the drift correction.
- 2.5a. Correct for imaging drift by selecting a pool of isolated nanostructures simultaneously, and calculate the photon count-weighted average of their time traces as the imaging drift correction.

2.5b. With the DNA-PAINT image analysis software, first set the sub-pixel resolution to be $\sim 1/3$ – $1/4$ of the structure size, and set a lower intensity threshold to convert the super-resolved image to a binary image mask by setting the “Min density” to ~ 3 – 5 . Click “Select regions” to open another window, and use the structure size filter to select for structures of the correct size range (typically in the range of ~ 5 – 50). Use a combination of binary operations to remove unwanted noise and structures that are very close together, typically by performing a series of 2 – $3\times$ dilation, area filtering, and 2 – $3\times$ erosion in order. Click “Accept” and then “Process,” wait until calculation is finished, and then click “Apply” in the main window to apply drift correction.

3.5 Super-Resolution Image Quality Analysis

- 1.1a. Photon count, localization precision, and image resolution: Photon count is directly reported from single-emitter localization algorithm (*see Note 6*). Localization precision for individual localizations can be determined from two methods, fitting reported uncertainty (FRU) or distance between adjacent-frame localizations (DAFL), *see Note 5*. FRU is typically reported by the single-emitter localization algorithm, such as the reported Cramer-Rao lower bound (CRLB), and DAFL resolution is measured same as in **step 2.2a** above.
- 1.1b. In the DNA-PAINT image analysis software, for FRU localization precision [18], click “Data quality,” select “Localisation precision (nm)” from the drop-down menu, and click “Plot” to show the distribution of localization precision from all fitted localizations. The supported imaging resolution as reported by FRU is equal to $2.35 \times [\text{average localization precision}]$. The procedure for measuring DAFL imaging resolution analysis is the same as described in **step 2.2b** above.
- 1.2a. Number of blinking events and target signal-to-noise ratio (tSNR): These two parameters are analyzed on a target-by-target basis. Number of blinking events per target is analyzed by extracting the blinking time trace for a single imaging target and counting the number of localization bursts through time. Target SNR is calculated by locally plotting a projection histogram of two adjacent imaging targets and analyzing the fitted profile. Here, signal is calculated as the difference in the fitted peak and valley intensity, and noise is calculated as the statistical fluctuation of the fitted peak intensity, assuming Poisson statistics. To make results comparable, histogram bins are taken with width equal to $1/10$ of the separation between the two targets.

- 1.2b. In the DNA-PAINT image analysis software, for the number of blinking events, first click “Select ROI” to select a single imaging target, and click “Analyse trace” to open the trace display window. Click “Analyse” to display the number of blinking events. For target SNR calculation, first click “Select ROI,” select a region including two closely spaced imaging targets, or two clusters of imaging targets, click “Histogram fit,” and open another window. In the new window, re-orient the display so that the two targets or clusters of interest align horizontally, and click “Select ROI” to select an area tightly enclosing all the localizations from the two imaging targets. Set the number of histogram bins to ~20 such that the bin spacing is equal to 1/10 of the target spacing and click “2-peak fit.” The calculated target SNR values will be displayed.
- 1.3a. Blinking kinetics and fraction of false double-blinking localizations. Blinking kinetics are calculated either for a single imaging target, or a group of imaging target (such as all the imaging targets on a single synthetic nanostructure). Characteristic blinking on-time and off-time is separately and similarly calculated, by collecting the fluorescence on duration and off duration for all blinking events, plotting the histogram and fitting to expected distributions, and assuming independent stochastic process. Fraction of false double-blinking localizations is estimated by analyzing the photon count distribution of all localizations, and evaluating the proportion of localizations that has photon count higher than two standard deviation above average (*see Note 6*).
- 1.3b. In the DNA-PAINT image analysis software, for blinking kinetics analysis, first click “Select ROI” and select either one or a group of imaging targets, or an entire nanostructure. Click “Analyse trace” to open the trace display window, and click on “Analyse” to display the on-time and off-time histogram as well as the fitted results. For false double-blinking localizations, click “Data quality” and plot photon count distribution, similar to in **step 3.1b**. The estimated fraction of false localizations will be displayed.

4 Notes

1. Imaging buffer TP with oxygen-scavenging and redox systems helps increase dye brightness and photostability for cy3b and atto647n, but is not compatible with some other fluorophores such as atto655.

2. When preparing imaging buffer TP, mix by gently pipetting up and down, and avoid introduction of any air bubbles. An incubation of 10–20 min after preparation is recommended for the system to reach steady state before use. Sometimes an increase in the number of blinking spots per frame is observed at the beginning (~5–10 min) of the recorded image; this is usually due to incomplete buffer exchange when introducing the imaging solution. Flowing in an excess of imaging solution helps to mitigate the effect.
3. Avoid introducing bubbles into the flow chamber at any stage of the experiment. Air bubbles could not only adversely affect the imaging buffer environment, and also result in incomplete buffer exchange and introduce unwanted friction or blocking inside the Ibidi chambers.
4. During acquisition of super-resolution movies, it is important to maintain a suitable level of number of blinking spots per camera frame. This could be affected by several parameters, including the density of nanostructures, imager strand concentration, and the number of docking targets on the nanostructure sample. When designing the experiment, use an appropriate imager strand concentration to maintain a low false localization fraction, and then adjust nanostructure surface deposition density to maintain a suitable level of blinking spots per frame.
5. Determining the exact supported resolution of a super-resolution rendered image is generally difficult. The traditional method of measuring the full-width at half-maximum (FWHM) value of a single object (such as a labeled microtubule sample) is not ideal, and thus calculated resolution value does not always translate to the ability of reliable separation between two objects (spaced apart by the calculated distance). Here we provide two methods (FRU and DAFL) for estimating the maximal supported resolution. We note that both methods report an optimistic bound of the achievable resolution (i.e., the actual resolution in number is larger than either of those reported by the two methods). Between the two, FRU usually gives a more optimistic evaluation, while DAFL gives a more realistic estimation.
6. Depending on the detailed optical configuration of the microscope, sometimes illumination is not even throughout the entire field of view. Under such circumstances calculations of average photon count and estimated ratio false double-blinking localization will be inaccurate. To overcome the problem, cut out the central region of the super-resolution image (where illumination intensity is highest and the degree of uneven illumination is lowest) and perform photon count statistics calculation on the cut-out region.

References

1. Hell S et al (2015) The 2015 super-resolution microscopy roadmap. *J Phys D Appl Phys* 48:443001
2. Huang B, Bates M, Zhuang X (2009) Super-resolution fluorescence microscopy. *Annu Rev Biochem* 78:993–1016
3. Sahl SJ, Moerner WE (2013) Super-resolution fluorescence imaging with single molecules. *Curr Opin Struct Biol* 23:778–787
4. Betzig E et al (2006) Imaging intracellular fluorescent proteins at nanometer resolution. *Science* 313:1642–1645
5. Hess ST, Girirajan TP, Mason MD (2006) Ultra-high resolution imaging by fluorescence photoactivation localization microscopy. *Biophys J* 91:4258–4272
6. Rust MJ, Bates M, Zhuang X (2006) Sub-diffraction-limit imaging by stochastic optical reconstruction microscopy (STORM). *Nat Methods* 3:793–795
7. Heilemann M et al (2008) Subdiffraction-resolution fluorescence imaging with conventional fluorescent probes. *Angew Chem Int Ed Engl* 47:6172–6176
8. Sharonov A, Hochstrasser RM (2006) Wide-field subdiffraction imaging by accumulated binding of diffusing probes. *Proc Natl Acad Sci U S A* 103:18911–18916
9. Jungmann R et al (2010) Single-molecule kinetics and super-resolution microscopy by fluorescence imaging of transient binding on DNA origami. *Nano Lett* 10:4756–4761
10. Giannone G et al (2010) Dynamic super-resolution imaging of endogenous proteins on living cells at ultra-high density. *Biophys J* 99:1303–1310
11. Schoen I, Ries J, Klotzsch E, Ewers H, Vogel V (2011) Binding-activated localization microscopy of DNA structures. *Nano Lett* 11:4008–4011
12. Johnson-Buck A, Nangreave J, Jiang S, Yan H, Walter NG (2013) Multifactorial modulation of binding and dissociation kinetics on two-dimensional DNA nanostructures. *Nano Lett* 13:2754–2759
13. Johnson-Buck A et al (2013) Super-resolution fingerprinting detects chemical reactions and idiosyncrasies of single DNA pegboards. *Nano Lett* 13:728–733
14. Jungmann R et al (2014) Multiplexed 3D cellular super-resolution imaging with DNA-PAINT and exchange-PAINT. *Nat Methods* 11:313–318
15. Jungmann R et al (2016) Quantitative super-resolution imaging with qPAINT using transient binding analysis. *Nat Methods*. doi:[10.1038/nmeth.3804](https://doi.org/10.1038/nmeth.3804)
16. Dai M, Jungmann R, Yin P (2016) Optical imaging of individual biomolecules in densely packed clusters. *Nat. Nanotech.* doi:[10.1038/nnano.2016.95](https://doi.org/10.1038/nnano.2016.95)
17. Zadeh JN et al (2011) NUPACK: analysis and design of nucleic acid systems. *J Comput Chem* 32:170–173
18. Smith CS, Joseph N, Rieger B, Lidke KA (2010) Fast, single-molecule localization that achieves theoretically minimum uncertainty. *Nat Methods* 7:373–375

Designing DNA Nanotube Liquid Crystals as a Weak-Alignment Medium for NMR Structure Determination of Membrane Proteins

John Min, William M. Shih, and Gaëtan Bellot

Abstract

Thirty percent of the human proteome is composed of membrane proteins that can perform a wide range of cellular functions and communications. They represent the core of modern medicine as the targets of about 50% of all prescription pharmaceuticals. However, elucidating the structure of membrane proteins has represented a constant challenge, even in the modern era. To date, only a few hundred high-resolution structural models of membrane proteins are available. This chapter describes the emergence of DNA nanotechnology as a powerful tool for the structural characterization of membrane protein using solution-state nuclear magnetic resonance (NMR) spectroscopy. Here, we detail the large-scale synthesis of detergent-resistant DNA nanotubes that can be assembled into a dilute liquid crystal to be used as a weak-alignment media in solution NMR structure determination of membrane proteins.

Key words DNA origami, Membrane protein, Nuclear magnetic resonance, Structural biology, Residual dipolar coupling

1 Introduction

Membrane proteins help coordinate pretty much everything a cell does, including signaling, energy generation, transport, and recognition. Today, about 50% of approved therapeutics target human membrane proteins [1, 2]. Given their biological importance, it is surprising that our understanding of membrane proteins molecular mechanisms is still in its infancy. This significant gap in knowledge can be partially attributed to the extreme hydrophobic nature of most membrane protein, as well as the slow pace in the development of structural biological tools to study them. Today, only a few hundred high-resolution structural models of membrane proteins have been deposited into the RCSB Protein Data Bank by X-ray cryptographers and NMR structural biologists. However, recent advances in solution-state NMR spectroscopy are leading to its increased importance in the study of the structure and dynamics of

membrane proteins, especially those with multiple transmembrane-spanning alpha-helices.

One of these recent advances in particular makes possible the accurate measurement of residual dipolar couplings for a wide array of membrane proteins via a new DNA origami technology [3–5]. The residual dipolar couplings method introduced in 2000 involves weak alignment of proteins [6–9]. This alignment is aided by large molecules that form liquid crystals at low concentration, which can provide global orientation restraints that greatly facilitate NMR structure determination and facilitate the *de novo* NMR structure determination of large proteins that cannot be determined using classical NMR techniques [9–14]. A residual dipolar coupling-based refinement approach can be used to resolve the structure of proteins up to 40 kDa in size. However, to do this on membrane proteins you need a weak-alignment medium that is detergent resistant and it has thus far been difficult to obtain such a medium suitable for weak alignment of membrane proteins [15–18]. To remedy this, in the William Shih laboratory, we have developed a new method for a robust, large-scale synthesis of the first detergent-resistant liquid crystals of DNA nanotubes that enable weak alignment of detergent reconstituted membrane proteins [4, 5]. Inspired by the architecture of the well-established phage-based alignment method and facilitated by the magnetic susceptibility anisotropy of DNA, we designed 0.8- μm -long DNA nanotube liquid crystals suitable for high-resolution NMR study of membrane proteins (Fig. 1) [4, 5, 19].

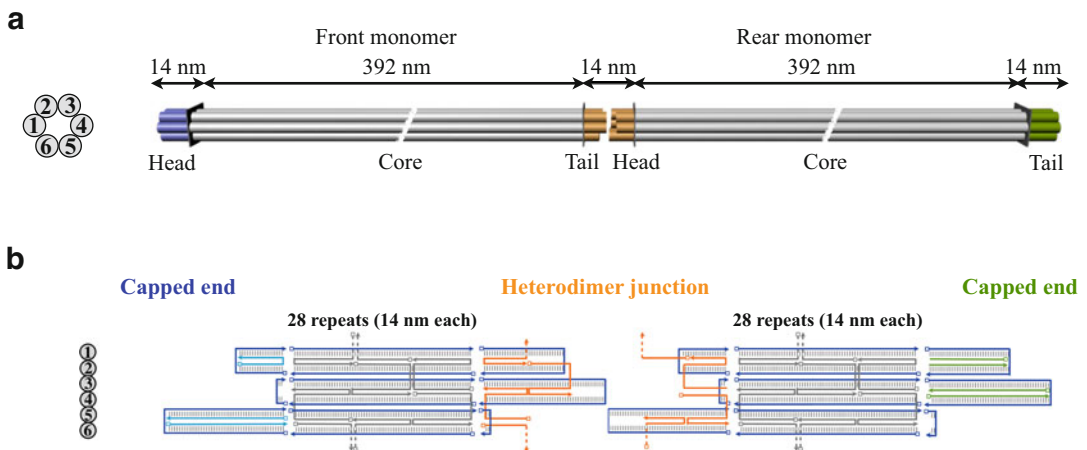


Fig. 1 DNA-nanotube design overview. **(a)** Schematic illustration of the 800-nm-long six-helix bundle heterodimer (not to scale). *Left*, a cross-sectional view. Front monomer with capped head module in *blue*, core module in *grey*, and connector tail module for heterodimerization in *orange*. Rear monomer with capped tail module in *green*, core module in *grey*, and connector head module for heterodimerization in *orange*. **(b)** Design schematics of the DNA six-helix bundle. Scaffold-plus-staple schematic view of the heterodimer junction of front and rear monomer

The emergence of this detergent-resistant liquid crystals has facilitated the accurate measurement of residual dipolar couplings on immunoreceptors, channels, and membrane transporters [20–25]. This detergent-resistant liquid-crystal medium offers a number of properties conducive for membrane protein alignment, including high-yield production, thermal stability, buffer compatibility, and structural programmability. The detailed protocol here describes a method to generalize the use of DNA nanostructures as a detergent-resistant liquid crystal for membrane protein NMR study by offering a user-friendly method for the measurement of membrane protein residual dipolar couplings with a high level of accuracy (Fig. 2).

2 Materials

2.1 Nanomole-Scale Production of M13 Bacteriophage ssDNA Scaffold

1. Luria Broth medium.
2. 2× YT broth capsule microbial medium.
3. Bacto agar.
4. Petri dishes, 100 × 15 mm. All the equipment used for growing cells should be sterilized.
5. Ampicillin sodium salt.
6. Isopropyl β-D-1-thiogalactopyranoside.
7. JM109 bacteria.
8. M13mp18 ssDNA.
9. Shaker incubator, 37 °C.

2.2 Large-Scale Synthesis of DNA Origami Assembly and Agarose Gel Electrophoresis

1. Desalted and lyophilized DNA oligonucleotides.
2. Folding buffer, 20×: Folding buffer contains 100 mM Tris (pH ~8.0), 20 mM EDTA, and 200 mM MgCl₂. Folding buffer can be stored at room temperature for up to 6 months.
3. EDTA.
4. Magnesium chloride hexahydrate, 99.995 %.
5. BioProducts 96-well PCR plate.
6. Aluminum sealing tape for 96-well plates.
7. Disposable multichannel pipettor basins.
8. Gilder fine bar grids.
9. Thermal cycler.
10. UltraPure agarose.

2.3 Nanomole-Scale Purification of DNA Nanotube

1. Qiagen-tip 10000: The maximum DNA binding capacity is 10 mg.
2. Wash buffer QC: Wash buffer QC contains 50 mM MOPS (pH 7.0), 1 M NaCl, and 15% (vol/vol) isopropanol. Wash buffer can be stored at room temperature for up to 6 months.

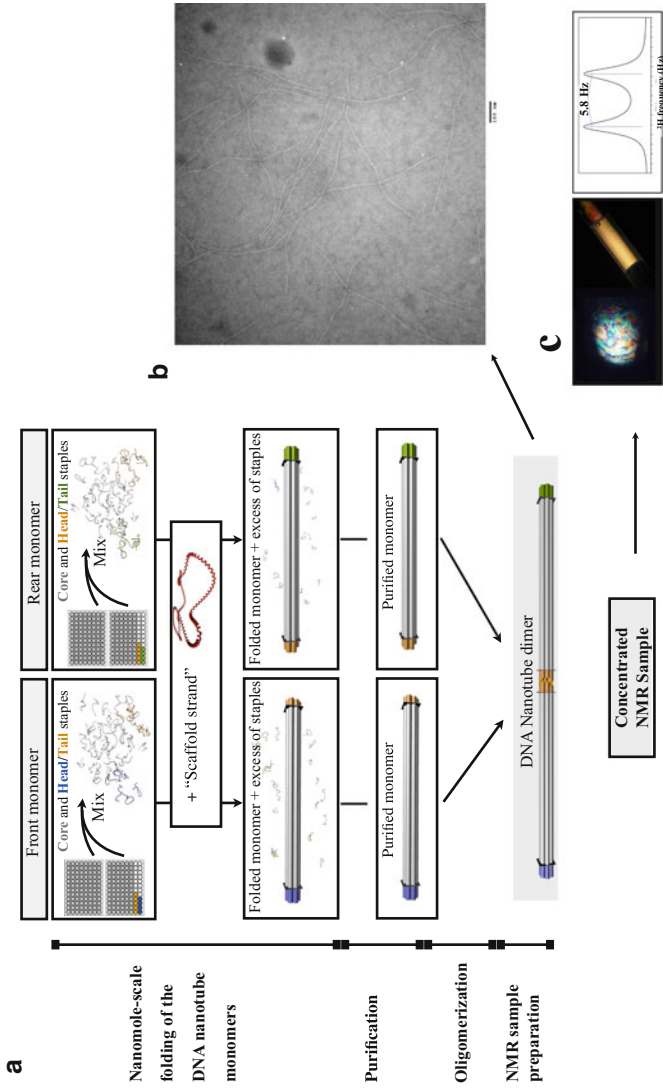


Fig. 2 A flowchart diagram summarizing the steps involved in setting up a large-scale synthesis of the DNA six-helix bundle. **(a)** Step-by-step guide through molecular self-assembly of scaffolded DNA origami nanotube for NMR structure determination of membrane proteins. **(b)** 1 μ l drop solution exhibited birefringence between crossed polarizers by DNA-nanotube heterodimers at 25 mg/ml. 1D NMR spectrum of $2\text{H}_2\text{O}$ at 2H frequency exhibited birefringence 2 mM MgCl_2 , 20 mM Tris-HCl pH 7.5, 100 mM DPC, 90 %/10 % $\text{H}_2\text{O}/\text{D}_2\text{O}$. The 1D spectrum was recorded at 2H frequency of 600 MHz at 25 $^\circ\text{C}$ on a Bruker 600 MHz spectrometer. **(c)** Negative-stain transmission electron micrograph of a purified sample of six-helix bundle heterodimer

3. Elution buffer QF: Elution buffer QF contains 50 mM Tris (pH 8.5), 1.25 M NaCl, and 15% (vol/vol) isopropanol. Elution buffer can be stored at room temperature for up to 6 months.
4. Loading buffer QBT: Loading buffer QBT contains 50 mM MOPS (pH 7.0), 750 mM NaCl, 15% (vol/vol) isopropanol, and 0.15% (vol/vol) Triton X-100. It can be stored at room temperature for up to 6 months. It is highly recommended that all buffers used for chromatography applications be filtered.
5. Centricon-100 concentrators.
6. Sodium phosphate dibasic anhydrous.
7. Sodium phosphate monobasic anhydrous.
8. Polyethylene glycol 8000 (PEG8000).
9. Triton X-100.
10. Sodium chloride.
11. Tris base.
12. MOPS.
13. Glacial acetic acid.
14. Isopropanol.
15. Ethanol, 200 proof.

2.4 Preparation of NMR Protein Samples with DNA Nanotubes and Data Analysis

1. Teflon tube, fluorinated ethylene propylene (FEP).
2. Shigemi NMR tube.
3. Low-DNA-affinity Teflon tube.
4. Microscope with polarizer and rotating analyzer.
5. NMR spectrometer equipped with a triple-resonance probe head [26].
6. NMRPipe and nmrDraw software for processing and analyzing NMR spectra [27–30].

3 Methods

3.1 Nanomole-Scale Folding of the DNA Nanotube Monomers

In order to build six-helix bundle nanotubes of 0.8 μm uniform length, an assembly strategy was conceived to link two unique 0.4 μm six-helix bundle monomers in a head-to-tail fashion (Fig. 1b). For each monomer a 7308-nucleotide (nt) M13-derived single-stranded circle of DNA is used as a “scaffold” and 168 single strands of DNA (of length 42 nt, programmed with complementarity to three separate 14-nt regions of the scaffold) are used as “staples” (Fig. 1b).

11. Each monomer is folded with the p7308 scaffold and unique pools of oligonucleotide staple strands. In a multichannel pipette basin, prepare a 37.8 ml master mix containing the following for each monomer: 120 nM scaffold p7308 (*see Note 1*), 720 nM (average) each staple (*see Note 2*), 20 mM MgCl₂, 1 mM EDTA, and 5 mM Tris (pH 8.0). This volume is intended for 240 folding reactions at 150 µl per reaction and includes a 5% excess to account for pipetting error. *See Notes 3 and 4.*
12. After preparing the master mix, use a multichannel pipette to distribute 150 µl aliquots into 96-well plates.
13. Fill the central 60 wells in each of the four 96-well plates for a total of 240 reactions; *see Note 5.*
14. Seal the plates with aluminum sealing covers for 96-well plates. *See Note 6.*
15. Load the 96-well plates into the thermal cycler and set up the thermal annealing ramp as follows: hold at 80 °C for 5 min, then decrease by 1 °C every 5 min to 65 °C, and then decrease by 1 °C every 40 min to 20 °C. Use a heated lid to minimize evaporation.

3.2 Nanomole-Scale Purification of DNA Nanotube Monomer

1. Pool all 240 completed reactions for each DNA nanotube monomer into a multichannel pipette basin (i.e., one basin for each of the two monomers) and transfer the pooled reactions (37.8 ml) into designated 250 ml Erlenmeyer flasks.
2. Once pooled, bring each sample volume to 100 ml with Buffer QBT. *See Note 7.*
3. Remove 50 µl of each of the two pools for an analytical agarose gel.
4. Column equilibration step: Use one Qiagen-tip 10000 ion-exchange column per monomer. Label each column as rear and front monomer. Equilibrate each column with 75 ml of buffer QBT. Allow the buffer to flow through completely.
5. Column loading step: Apply 100 ml of each monomer to the appropriate column and allow to flow through completely.
6. Column washing step: After the nanotube pools have completely flowed through the column, wash the column six times with 100 ml of buffer QC. Save the washes. *See Note 8.*
7. Nanotubes elution step: Elute each monomer from the column with 100 ml of buffer QF. At this stage, the DNA solution should be homogenous and clear.
8. Remove 50 µl of each of the two eluted samples for an analytical agarose gel.
9. Add MgCl₂ to a final concentration of 25 mM. *See Notes 9 and 10.*

3.3 Heterodimerization of DNA Nanotube Monomers

1. The DNA nanotubes need to be heterodimerized prior to further purification. By using the material that was eluted from the Qiagen-tip 10000 ion-exchange columns, mix equal volumes of the rear and front monomer elutions. *See Notes 11 and 12.*
2. The heterodimerization is performed at 37 °C to improve the kinetics of the reaction. Warm the mixture by incubation in a 37 °C water bath for 15 min.
3. Incubate the mixture at 37 °C for an additional 1 h and 45 min for a total of 2 h at 37 °C. *See Note 13.*
4. Remove 50 µl of the mixture for an analytical agarose gel.

3.4 Concentration of DNA Nanotubes and Formation of DNA Nanotube Liquid Crystals

1. Add 0.25 volumes of 20 % (wt/vol) PEG8000 to the heterodimerized nanotubes.
2. Mix gently and incubate at room temperature for 15 min.
3. Spin down the nanotubes for 30 min at 15,000×g and 4 °C.
4. Carefully decant the supernatant into another bottle. *See Note 14.*
5. Spin the pellet once more for only 1 min at 15,000×g and 4 °C to collect additional supernatant.
6. Carefully remove all remaining supernatant with a pipette.
7. To the nanotube pellet, add sufficient 0.5× folding buffer to achieve a concentration of 3 mg/ml, assuming 80% recovery from the Qiagen-tip ion-exchange columns; this requires ~6 ml of buffer. *See Note 15.*
8. Once the pellet has dissolved, mix the nanotube sample gently and transfer to a 50 ml conical tube.
9. Estimate the concentration of the nanotubes. *See Note 16.*
10. Concentrate the nanotubes to ~30 mg/ml using Centricon-100 concentrator units. Prerinse the Centricon-100 concentrator units by adding 2 ml of water. Spin at 2000×g and 15 °C for 5 min to achieve concentration.
11. Remove excess water by inverting tubes and spinning at 900×g for 2 min.
12. Weigh the Centricon-100 concentrator units, then apply DNA-nanotube samples, and record the mass of the concentrator unit with the DNA nanotubes.
13. Spin the nanotubes in 15-min increments at 1500×g and 15 °C. Estimate the concentration by periodically recording the mass of the concentrators with the DNA nanotubes. The starting concentration of the DNA (3 mg/ml) is ten times lower than the desired concentration (30 mg/ml); therefore, a ten times decrease in the mass of the sample gives a good approximation of the desired concentration. *See Note 17.*

14. When a ten times decrease in sample mass has been achieved, recover DNA by inverting tubes into collection vials and spinning for 3 min, at $1000\times g$, at $20\text{ }^{\circ}\text{C}$. The final total volume will typically be between 1 and 1.5 ml. Concentrated to 30 mg/ml, the nanotube sample will be homogeneous, clear, and viscous. If the DNA nanotube solution does not appear viscous, it is recommended to check the birefringence, as described in **step 15**. If the sample is not birefringent, spin the nanotubes in 15-min increments at $1500\times g$ and $15\text{ }^{\circ}\text{C}$ until the sample appears viscous.
15. Place a $1\text{ }\mu\text{l}$ drop of DNA nanotube liquid crystal solution on a glass microscope slide. Examine the drop at room temperature using a dissecting microscope under normal and crossed polarized light. The nanotubes will appear birefringent between crossed polarizers with characteristic textures of the type shown in Fig. 2c. *See Note 18*.

3.5 Measuring Residual D2O Quadrupole Coupling in the Presence of DNA Nanotubes

1. Add D2O to 250 μl of the DNA nanotube liquid crystal to a final concentration of 10% (vol/vol). Mix slowly by pipetting.
2. Use a low-DNA-affinity Teflon tube to transfer 250 μl of the nanotube sample with 10% D2O into a Shigemi NMR tube. *See Note 19*.
3. Spin down the NMR sample at $500\times g$ and $15\text{ }^{\circ}\text{C}$ for 2 min and add the Shigemi plunger. *See Note 20*.
4. Record 1D NMR spectrum at 2H frequency.
5. Process 1D NMR spectra and measure D2O splittings.

3.6 Preparation of NMR Protein Samples with DNA Nanotubes

1. Prerinse a Centricon-100 concentrator unit.
2. Weigh the Centricon-100 concentrator unit while empty, and then apply 250 μl + 10% of the DNA nanotube sample at a concentration of $\sim 25\text{ mg/ml}$. Weigh the Centricon-100 concentrator unit with the DNA sample.
3. Exchange the DNA nanotubes into the desired protein buffer by diluting the nanotubes twofold with the protein buffer.
4. Mix the twofold-diluted sample slowly by pipetting up and down. Spin the nanotubes in 5-min increments at $1500\times g$, at $15\text{ }^{\circ}\text{C}$.
5. Between each spin, mix the sample slowly by pipetting up and down. Stop the concentration when the columns reach roughly the starting weight.
6. Repeat previous **steps 3–5** three times to achieve sufficient exchange.
7. Once the DNA nanotubes are in the appropriate buffer, an appropriate amount of protein is added to the DNA nanotube solution. The final NMR sample is then prepared by concentrating down

to the appropriate sample volume using a series of 5-min spins at $1500\times g$ and $15\text{ }^{\circ}\text{C}$. See **Note 21**.

8. Recover the NMR sample from the Centricon concentrator unit. See **Notes 22** and **23**.

4 Notes

1. Scaffold: We use a modified bacteriophage M13 genome that is 7308 bp in length, as described previously for DNA origami (<http://www.pnas.org/content/suppl2007/04/02/0700930104.DC1/00930SuppAppendix2.pdf>).

To obtain sufficient quantities of this single-stranded DNA scaffold, production of the bacteriophage that bears the modified 7308 bp genome is progressively scaled-up in a series of steps that yield the “preinoculation” phage, then the “inoculation” phage, and finally the nanomole-scale phage. The inoculation phage is produced in two steps (preinoculation and inoculation) to ensure sufficient quality and quantity.

2. Staples: To generate staples pools, we purchased desalted and lyophilized DNA oligonucleotides in 96-well plates on the 200 nmol scale from Invitrogen. Exact sequences of the oligonucleotide staple strands are listed in supplementary Table 1. Once hydrated, equal volumes of each oligonucleotide are pooled into two groups corresponding to the necessary staple strands for each monomer (Figs. 1a and 2a). For the front monomer, the pool includes core staples, “caps” for the head of the monomer to prevent nonspecific oligomerization, and connector staples for programmed dimerization at the tail of the monomer (Fig. 1). For the rear monomer, the pool includes core staples, caps for the tail of the monomer to prevent nonspecific dimerization, and connector staples for programmed heterodimerization at the head of the monomer (Fig. 1b). Pools are hydrated to achieve an average concentration of $\sim 5\text{ }\mu\text{M}$ per staple strand; individual strand concentrations therefore vary within a range of $\sim 3.5\text{--}6.5\text{ }\mu\text{M}$. Because we are adding a large excess of staple strands compared to scaffold strand, the folding reaction is fairly tolerant of the concentration variations between individual staple strands.
3. In order to prevent evaporation during the folding step, it is highly recommended to leave an empty “border” of wells on each plate. This is because the adhesive used on plate sealing covers rarely form a perfect seal when heated, allowing the boarder wells to evaporate. These border wells will be filled with water, leaving 60 wells per plate for nanotube folding reactions. This is done because the adhesive used on plate sealing covers rarely form a perfect seal when heated, allowing the boarder wells to evaporate.

4. We have observed that the precise magnesium concentration of the folding solution has a dramatic effect on the quality of nanotube folding. Optimal concentrations of MgCl_2 vary with the design of the structure and with the vendor of the oligonucleotide staple strands. For the six-helix bundle nanotube described in this protocol and for staple strands provided as described by Invitrogen, 20 mM MgCl_2 is optimal. Modified nanotubes or nanotubes folded with staple strands purchased from a different vendor may have slightly different optimal concentrations of MgCl_2 . It is highly recommended to use pure magnesium chloride hexahydrate (99.995%) during the folding process. EDTA is added to 1 mM final concentration in the master mix to chelate divalent ion impurities that can compete with magnesium during the folding process.
5. When aliquoting the folding master mix into plates, make sure that there are no air bubbles trapped in the wells, as they could promote the formation of artifacts during folding. Bubbles can be removed after making aliquots by gently pipetting the wells up and down.
6. Ensure that the plates are very well sealed in order to prevent any evaporation during the thermal annealing step.
7. Be sure to mix the samples thoroughly after adding buffer QBT to ensure homogenous distribution of DNA.
8. To improve the efficacy of the column wash step, allow each wash to flow through entirely before applying subsequent washes.
9. The addition of magnesium to the eluted product stabilizes the DNA nanotubes. Some white precipitate may appear during this step but it does not interfere with subsequent steps.
10. The eluted sample can be stored at 4 °C for at least 2 days.
11. After combining the two monomers, be sure to mix the solution by gently swirling the flask.
12. We are assuming that the Qiagen-tip 10000 purification yields roughly equimolar quantities of each monomer, and thus we need to only consider volume. Equimolar amounts of each monomer have to be mixed to form 100% of the heterodimer. If one of the monomers is formed in excess, its amount should be reduced to a stoichiometric quantity before mixing. This can be estimated from the fluorescence intensity of each monomer's band when analyzed via agarose gel electrophoresis.
13. At this point, the heterodimerized mixture can be stored at 4 °C if it is necessary to return to the precipitation at a later time. After few hours at 4 °C the sample can turn turbid. This is a typical behavior of DNA nanostructure stored in buffer QF at 4 °C and does not harm the sample.

14. Save the supernatant in case the nanotube pellet becomes dislodged from the bottle.
15. Do not disturb the pellet initially. Simply add buffer to the tube and allow the buffer to diffuse into the pellet over time. Actively resuspend loose portions of the pellet periodically by swirling. Care should be taken to avoid extremely vigorous mixing at this step. It is highly recommended to let the buffer slowly dissolve the pellet to prevent damage to the nanotubes. This process can easily take one to several hours.
16. The nanotubes can be stored in 0.5× folding buffer at 4 °C for at least 6 days until one is ready to proceed with the concentration step.
17. To prevent damage to the nanotube structure it is recommended that all spins be at speeds less than 2000×*g*. Between 15-min spins, mix the concentrated solution by pipetting up and down gently with a P1000 tip. This will help prevent the buildup of extremely high local concentrations of the nanotubes near the Centricon membrane .
18. DNA nanotubes are very stable and can be stored at 4 °C for at least 12 months.
19. To minimize the loss of DNA, transfer the DNA sample in several steps by pipetting only 40 µl into the NMR tube at a time.
20. At 30 mg/ml, the DNA nanotube liquid crystal solution appears viscous. Despite the viscosity, conventional pipettes or Teflon tube work well to transfer the liquid crystals to an NMR tube. A uniform and bubble-free sample is obtained by slow centrifugation (100–200×*g*) after transferring the sample to the tube, inserting the plunger slowly to the bottom of the tube and pulling the plunger to the desired height.
21. During the course of concentration, a local concentration of both protein and nanotubes around the Centricon membrane may appear. As a consequence, there is a much more favorable environment locally for interaction between the nanotubes and the protein. It is recommended to periodically homogenize the DNA and protein concentration between each spin by pipetting up and down slowly.
22. DNA material may stick to the Centricon membrane. It is possible to recover more than 95% of the DNA sample by inverting tubes into collection vials and spinning for 3 min at 1000×*g* and 20 °C.
23. Store at 4 °C or temperature appropriate for protein of interest.

Acknowledgement

This work was supported by the US National Institutes of Health (NIH) grants 1U54GM094608 to J.J.C., and 1DP2OD004641 and 1U54GM094608 to W.M.S.

References

- Wallin E, von Heijne G (1998) Genome-wide analysis of integral membrane proteins from eubacterial, archaeal and eukaryotic organisms. *Protein Sci* 7:1029–1038
- Landry Y, Gies J (2008) Drugs and their molecular targets: an updated overview. *Fundam Clin Pharmacol* 1:18–22
- Douglas SM et al (2009) Self-assembly of DNA into nanoscale three-dimensional shapes. *Nature* 414:418–459
- Douglas SM, Chou JJ, Shih WM (2007) DNA-nanotube-induced alignment of membrane proteins for NMR structure determination. *Proc Natl Acad Sci U S A* 104:6644–6648
- Bellot G, McClintock MA, Chou JJ, Shih WM (2013) DNA nanotubes for NMR structure determination of membrane proteins. *Nat Protoc* 7:770–778
- Tjandra N, Bax A (1997) Direct measurement of distances and angles in biomolecules by NMR in a dilute liquid crystalline medium. *Science* 278:1111–1114
- Prestegard JH et al (1998) New techniques in structural NMR: anisotropic interactions. *Nat Struct Biol* 5:522–525
- Bax A, Kontaxis G, Tjandra N (2001) Dipolar couplings in macromolecular structure determination. *Meth Enzymol* 127:174–339
- Tolman JR, Flanagan JM, Kennedy MA, Prestegard JH (1995) Nuclear magnetic dipole interactions in field-oriented proteins: information for structure determination in solution. *Proc Natl Acad Sci U S A* 92:9279–9283
- Hansen MR, Mueller L, Pardi A (1998) Tunable alignment of macromolecules by filamentous phage yields dipolar coupling interactions. *Nat Struct Biol* 1065:1074–1075
- Rückert M, Otting G (2000) Alignment of biological macromolecules in novel nonionic liquid crystalline media for NMR experiments. *J Am Chem Soc* 122:7793–7797
- Prosser RS, Losonczy JA, Shivanovskaya IV (1998) Use of a novel aqueous liquid crystalline medium for high-resolution NMR of macromolecules in solution. *J Am Chem Soc* 110:11011–11120
- Fleming K, Gray D, Prasanna S, Matthews S (2000) Cellulose crystallites: a new and robust liquid crystalline medium for the measurement of residual dipolar couplings. *J Am Chem Soc* 122:5224–5225
- Tycko R, Blanco FJ, Ishii Y (2000) Alignment of biopolymers in strained gels: a new way to create detectable dipole-dipole couplings in high-resolution biomolecular NMR. *J Am Chem Soc* 122:9340–9341
- Ma J, Goldberg GI, Tjandra N (2008) Weak alignment of biomacromolecules in collagen gels: an alternative way to yield residual dipolar couplings for NMR measurements. *J Am Chem Soc* 130:16148–16149
- Lorieau J, Yao L, Bax (2008) A liquid crystalline phase of G-tetrad DNA for NMR study of detergent-solubilized proteins. *J Am Chem Soc* 130:7536–7537
- Chou JJ, Gaemers S, Howder B, Louis JM, Bax A (2001) A simple apparatus for generating stretched polyacrylamide gels yielding uniform alignment of proteins and detergent micelles. *J Biomol NMR* 21:377–382
- Jones DH, Opella SJ (2004) Weak alignment of membrane proteins in stressed polyacrylamide gels. *J Magn Reson* 171:258–269
- Zweckstetter M, Bax A (2001) Characterization of molecular alignment in aqueous suspensions of Pfl bacteriophage. *J Biomol NMR* 20:365–377
- Schnell JR, Chou JJ (2008) Structure and mechanism of the M2 proton channel of influenza A virus. *Nature* 451:591–595
- Call ME, Wucherpfennig KW, Chou JJ (2010) The structural basis for intramembrane assembly of an activating immunoreceptor complex. *Nat Immunol* 11:1023–1029
- Berardi MJ, Shih WM, Harrison SC, Chou JJ (2011) Mitochondrial uncoupling protein 2 structure determined by NMR molecular fragment searching. *Nature* 476:109–113
- Wang J, Pielak RM, McClintock MA, Chou JJ (2009) Solution structure and functional analysis of the influenza B proton channel. *Nat Struct Mol Biol* 16:1267–1271

24. Sounier R, Bellot G, Chou JJ (2015) Mapping conformational heterogeneity of mitochondrial nucleotide transporter in uninhibited states. *Angew Chem Int Ed Engl* 54: 2436–2441
25. Sun ZJ, Cheng YK, Mikyung et al (2014) Disruption of helix-capping residues 671 and 674 reveals a role in HIV-1 entry for a specialized hinge segment of the membrane proximal external region of gp41. *J Mol Biol* 426: 1095–1108
26. Flynn PF, Mattiello DL, Hill HDW, Wand AJ (2000) Optimal use of cryogenic probe technology in NMR studies of proteins. *J Am Chem Soc* 122:4823–4824
27. Zweckstetter M (2008) NMR: prediction of molecular alignment from structure using the PALES software. *Nat Protoc* 3:679–690
28. Delaglio F et al (1995) NMRPipe: a multidimensional spectral processing system based on UNIX pipes. *J Biomol NMR* 6:277–293
29. Zweckstetter M, Bax A (2000) Prediction of sterically induced alignment in a dilute liquid crystalline phase: aid to protein structure determination by NMR. *J Am Chem Soc* 122:3791–3792
30. Cornilescu G, Marquardt JL, Ottiger M, Bax A (1998) Validation of protein structure from anisotropic carbonyl chemical shifts in a dilute liquid crystalline phase. *J Am Chem Soc* 120:6836–6837

Direct Nanofabrication Using DNA Nanostructure

Feng Zhou and Haitao Liu

Abstract

Recent advances in DNA nanotechnology make it possible to fabricate arbitrarily shaped 1D, 2D, and 3D DNA nanostructures through controlled folding and/or hierarchical assembly of up to several thousands of unique sequenced DNA strands. Both individual DNA nanostructures and their assembly can be made with almost arbitrarily shaped patterns at a theoretical resolution down to 2 nm. Furthermore, the deposition of DNA nanostructures on a substrate can be made with precise control of their location and orientation, making them ideal templates for bottom-up nanofabrication. However, many fabrication processes require harsh conditions, such as corrosive chemicals and high temperatures. It still remains a challenge to overcome the limited stability of DNA nanostructures during the fabrication process.

This chapter focuses on the proof-of-principle study to directly convert the structural information of DNA nanostructure to various kinds of materials by nanofabrication.

Key words DNA nanostructure, Nanofabrication, SiO₂, Porous carbon material, Self-assembled monolayer, HF etching, Carbonization

1 Introduction

1.1 Structural DNA Nanotechnology

DNA has drawn dramatic attention in material science as structural building blocks in the past several decades. Due to the specificity of base pairing, single-stranded DNA (ssDNA) can recognize another strand with complementary sequence, producing predictable DNA nanostructure. Thanks to the programmability of the DNA hybridization, both arbitrary and robust nanostructure with accurate features and precision of 2–3 nm in dimension can be constructed [1–7] at cost as low as \$6 per m² [8]. The size of an individual 2D and 3D DNA nanostructures can vary from tens of nm to several microns [9–11]. As for the self-assembly of 2D DNA lattice, up to 1 mm in size has been reported [12]. Furthermore, the deposition of DNA on the substrates has been studied to obtain precise control of the location and orientation, which makes it an ideal template for nanofabrication [13–15]. These unique properties of DNA have made it an attractive template for micro- and nanoscale fabrication.

The following sections provide an overview of recent progress in the fabrication of DNA nanostructure.

1.2 DNA Tile-Based Self-Assembly

In 1982, Nadrian Seeman pioneered the proposal of creating a mechanically robust tile structure containing four single-stranded DNA to form a four-way branched junction (also called as tile structure), opening the era of DNA nanotechnology [16]. In this concept, four individual ssDNA associate into a four-arm junction, with complementary portions in a specific pattern to maximize the number of correct base pairs. Since then, many periodic structures, such as 2D lattice arrays, have been assembled using the tile structure as repeating units [17–19]. In 1993, Tsu-Ju Fu and Nadrian Seeman developed the double-crossover DNA tile [20], containing two parallel double-helical domains with individual strands crossing between the domains at crossover points. It was the first mechanically strong DNA structure to form extended 3D nanostructures. Since then, numerous rigid tile structures have been fabricated, such as multi-helix bundles, cross-shaped tiles, or 3- and 5-point stars, and assembled into 3D DNA nanostructures such as nanotubes [21, 22], polyhedra [23, 24], cubes [25], crystals [11], and buckyballs [26].

1.3 DNA Origami

In 2006, Paul Rothemund developed the DNA origami method for the first time. The process involves the folding of a long ssDNA (also called as scaffold strand) aided by hundreds of short synthetic ssDNA (also called as staple strands) [9]. For example, M13mp18, a viral genomic ssDNA and the most widely used scaffold DNA, is mixed with hundreds of staple DNA through a particular design generated by computer programs [27, 28]. Each staple DNA is about 30–50 nucleotides long and specifically designed to complementarily bind to multiple regions of the scaffold strand, folding the specific regions into desired adjacent positions. After mixing, heating and cooling, the various DNA staples hybridize to the desired locations, pulling the long scaffold DNA into a well-defined 2D structure on a scale of 100 nm. By using a larger scaffold strand, DNA nanotechnologist can fabricate a larger DNA nanostructure successfully [10, 29]. In addition to this, 3D nano-robot origami [30] and origami with curvatures [6] were also reported. Moreover, the staples DNA can be modified with multiple functional molecules or particles, such as fluorescent peptide marker [31–33], metal nanoparticles [34–36], and carbon nanotubes [37], making the DNA origami a perfect host for site-specific nano-patterning of desired material.

1.4 Self-Assembly of DNA Single-Stranded Tiles (DNA Bricks)

In 2012, Wei et al. demonstrated the use of DNA single-stranded tiles as the building blocks for construction of complex DNA nanostructures for the first time [38]. In this concept, the DNA building blocks are similar to inter-locking bricks. Each brick is a single-stranded DNA with 42 bases. Every block can connect to

another one if the other block has a sequence of DNA that complements the sequence of the original DNA. In this way, the blocks can self-assemble in areas and form a structure consisting of any number of DNA blocks, such as DNA canvas with 362 blocks. To design a structure, all things need to get done is to withhold the specific blocks before blocks can be self-assembled, such as rectangular ring, alphabetic letters, and eagle head. The same concept was also reported by Mathur et al. in the same year [39].

In addition to the 2D nanostructure, the self-assembly of DNA single-stranded tiles also allows the building of 3-dimensional structures using DNA bricks, as reported by Ke et al. [40]. In this case, each DNA brick is 32 DNA bases long, folding as Lego® brick that has a unique DNA sequence and fits only one location within the block construction. By withholding certain strands before self-assembly, more than 100 different shapes were built. Furthermore, the block structure can be extended to contain any number of DNA bricks, building micro-scale DNA crystals with prescribed depths [41]. This approach is simple, robust, and voxel. It could enable the creation of new nanoscale devices with a wide range of applications [42, 43].

1.5 Self-Assembly Using DNA Nanostructures

The DNA nanostructures, constructed using the methods discussed above, can be modified with particular sticky ends, making them “monomers” for subsequent self-assembly to produce larger structures in micro-scale. In 2010, Endo et al. first reported this method for assembling multiple DNA origami structures by using designed 2D DNA origami rectangles, the so-called DNA jigsaw pieces [44]. Each single DNA jigsaw piece contains concave and convex connectors, which are designed to be shaped and sequenced complementarily as the sticky ends for selective connection. Three to five different DNA jigsaw pieces could be assembled into a desired nanostructure with the correct alignment and uniform orientation. A similar concept was also demonstrated by Woo and Rothmund, to assemble the 2D DNA origami by controlling the geometric arrangement of blunt-end stacking interactions [45].

In addition to 2D nanostructure, large and stiff wireframe DNA polyhedral could be constructed by hierarchical assembly of certain number of three-arm-junction DNA origami tile motif [46]. Each tripod was assembled from scaffold and staple strands DNA to form precisely controlled inter-arm angles and arm lengths. At the end of each tripod, the 30-base strands were designed for connection between two adjacent tripods, serving as sticky ends for inter-monomer connection. Without intermediate purification, the tripods can assemble into the polyhedron. This simple strategy provides general approach for high-yield construction of open wireframe polyhedra.

1.6 Limited Stability of DNA Nanostructures for Nanofabrication of Inorganic Materials

In general, DNA nanostructure is constructed by the hybridization between complementary base sequences to form double-stranded DNA (ds-DNA) at specific location. Thus, the nature of this non-covalent interaction limits the chemical stability of DNA nanostructure, which could unwind and separate into single-stranded DNA (ss-DNA) under certain conditions, or so-called DNA denaturation. Moreover, the DNA nanostructure is made of organic materials, which can degrade under harsh conditions, such as high temperature and oxidative environment. Consequently, most fabrication methods, such as reactive ionic etching and lithography, cannot utilize DNA nanostructure as a direct template because it would not survive the procedure. In conclusion, DNA-based nanofabrication of inorganic materials still faces significant challenges.

The following sections provide a review of DNA structural stabilities under various fabrication conditions (Fig. 1).

1.7 Limited Chemical Stability of DNA Nanostructure

Most of DNA nanostructures are fabricated in aqueous solution with a neutral pH and the presence of certain concentration of buffer. Other than the complementarity of the binding sequences, the ions in buffer solution, such as Mg^{2+} , also play an important role to screen the DNA backbone repulsion, allowing the DNA to self-assemble, and to stabilize the branched junctions of the nanostructure [15]. It is also known that hydrolysis occurs under extreme pH, resulting in denaturation or degradation of ds-DNA [47]. After deposition onto the solid-phase substrate, such as SiO_2 and

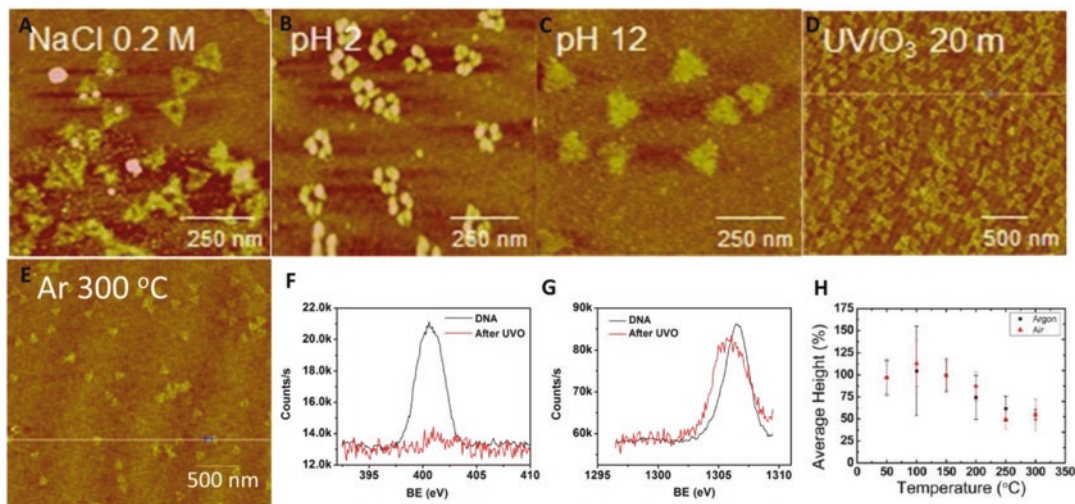


Fig. 1 Limited stability of DNA nanostructures. Deformation of triangular DNA origami in 0.2 M NaCl solution (a), acidic (b) and basic (c) solution. Salt residual structures after UV/O₃ treatment (d) and annealing in Ar at 300 °C for 10 min (e). The XPS results of N1s (f) and Mg2s (g) before and after UV/O₃ treatment proved that the nanostructure after UV/O₃ in d consisted only of salt, with no DNA left. (h) shows that the decomposition of DNA occurred gradually at elevated temperatures. Reprinted with permission from: ref. [48], © 2014 ACS (a–e and h); ref. [51], © 2015 ACS (f and g)

mica, the DNA nanostructures are immobilized onto the surface by electrostatic interaction between the phosphate backbone of DNA, the substrate surface, and absorbed ions as well. The change in composition and pH of the solution can all affect the structural stability of DNA nanostructures.

Recent study showed that after immersing the as-deposited DNA triangles in deionized water, the density of the DNA nanostructures was significantly decreased and the structures were severely damaged due to the desorption of Mg^{2+} [48]. In another experiment, most of DNA triangles deformed into three trapezoidal sides with irregular height after immersion into NaCl solution. The Na^+ is believed to replace the absorbed Mg^{2+} and accumulate on the deformed DNA nanostructures.

In the case of pH, it is reported that the hydrolysis of glycosidic bonds in DNA mainly occurs in acidic pH range [49, 50]. Another report also showed that the as-deposited triangular DNA origami underwent deformation in pH lower than 4 or higher than 12, limiting its usage in wet-etching processes [48].

The DNA nanostructure is also structurally labile under oxidative condition due to its nature of organic molecule. The chemical integrity of dried DNA triangle was devastated after exposure under UV/ O_3 environment for 15 min [48, 51]. DNA nanostructure also can be instantly destroyed under most of O_2 -mediated plasma processes, such as atomic layer deposition (ALD) and dry etching of Si [52]. In summary, the application window for DNA nanostructure is strictly limited by its labile chemical stability.

Tremendous efforts have been made to overcome the limited chemical stability of DNA nanostructure. Metallization is the most widely used approach to preserve DNA nanostructure during DNA-based nanofabrication [2, 35, 36, 43, 53–60]. The resulting metallized nanostructures have been further used as template mask for patterning the underlying substrate, such as shadow nanolithography of silicon by wet etching [59], and as nanopatterning of graphene by O_2 plasma [43]. However, the faithful pattern transfer process cannot be achieved due to the loss of structural information, such as resolution, of DNA nanostructures from the inevitably used metal absorption.

1.8 Thermal Stability of DNA Nanostructure

The construction of DNA nanostructures usually involves annealing and cooling for base sequences to be paired complementarily. At elevated temperature, the hybridization of nucleic acids in ds-DNA is weakened and the structural information of the DNA nanostructure cannot be maintained. In solution, the denaturation temperature of ds-DNA varies from 40 to 100 °C, depending on the base sequence and the buffer composition [61]. After deposition onto the substrate, such as mica and Si, the electrostatic interaction between the phosphate backbone and the substrate provides additional support for DNA nanostructure, promoting the structural

stability. Thermogravimetric analysis (TGA) of salmon DNA film under nitrogen, conducted by Aoi et al., showed that the decomposition bulk DNA started at 230 °C with a residual weight of 53% after heating to 500 °C [62]. In another study, triangular DNA origami thermally decomposed on heating beyond 250 °C in argon, but the triangular features were preserved even after heating at 300 °C [48]. XPS data proved that the remaining triangular structures were from inorganic residue (e.g., magnesium phosphate) after DNA decomposition [51]. Thus, almost all reported DNA-based nanofabrications were either based on solution chemistry or conducted at close to room temperature [2, 8, 35, 36, 42, 51, 53, 54, 57–60, 63, 64]. Work needs to be done to address the limited thermal stability of DNA nanostructure for nanofabrication at high temperature, such as ALD (>150 °C) or carbonization (>500 °C) [65–67].

In summary, given the lack of chemical and thermal stability discussed above, almost all reported DNA-based nanofabrications were either based on solution chemistry or conducted at close to room temperature [2, 8, 35, 36, 42, 51, 53, 54, 57–60, 63, 64]. It still remains a challenge to use DNA nanostructure as a general template for nanofabrication.

To address this challenge, we can either improve the stability of DNA nanostructure or identify and optimize a condition, which is mild to DNA nanostructure and highly selective for the nanofabrication as well. The following section highlights our related researches in addressing this challenge of limited stabilities facing DNA nanostructure based nanofabrication.

2 Nanoscale Patterning of Self-Assembled Monolayers Using DNA Nanostructure Templates

Self-assembled monolayer (SAM) can control and modify the surface properties, such as adhesion, surface potential, and surface chemistry of the substrate. It is widely used in patterning organic solids, molecular electronics, chemical and biological sensing, biomolecule immobilization, and nanofabrication [68–74]. Most of the applications require certain structure of SAM in nanoscale. Current methods, such as dip-pen nanolithography, photolithography and soft lithography to pattern the SAM have difficulty in balancing the scalability, shape selection, resolution, throughput, and cost. Because SAM formation does not require hassle, using DNA nanostructure as the masking template to pattern SAM could potentially offer the best approach among other methods.

Figure 2a shows the strategy to pattern silane SAM with DNA templates by vapor phase deposition [75]. Briefly, DNA nanostructures were deposited on the Si/SiO₂ substrate and subjected to a low-pressure environment. Silane precursor, such as octadecyltri-

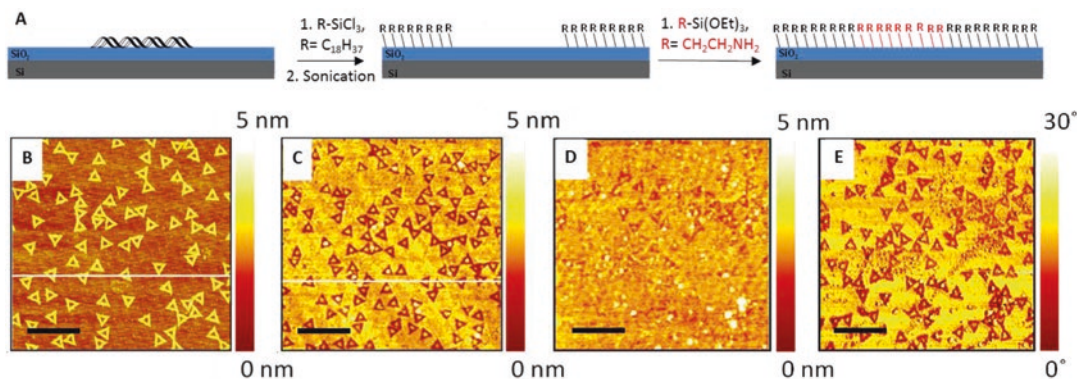


Fig. 2 (a) The cartoon sketch of patterning mixed silane SAMs using a DNA template. DNA nanostructures are deposited on a substrate and exposed to octadecyltrichlorosilane (ODTCS) vapor followed by removal of DNA, resulting in negative tone patterns in the ODTCS SAM. The patterned SAM is then exposed to 3-aminopropyl triethoxy silane (APTES) vapor, resulting in a patterned mixed SAMs. (b) AFM images of DNA nanostructures assembled on a Si substrate. (c) Sample (b) after exposure to ODTCS and after sonication in DI water to remove DNA. (d, e) are the AFM topography and phase images of bilayer silane pattern of APTES and ODTCS. APTES is deposited on the ODTCS pattern substrate at vapor phase resulting in bilayer silane pattern. Scale bar: 500 nm. Reprinted with permission from ref. [79], © 2015 RSC

chlorosilane (ODTCS), could be vaporized from its container and deposited everywhere, on and around the DNA templates on the Si/SiO₂ substrate. Since DNA is anchored on the substrate by electrostatic interaction while SAM could form covalent bond with the substrate, the DNA nanostructures can be lifted off from the substrate on sonication in deionized water, exposing the Si/SiO₂ surface on the bottom and resulting in a negative-tone pattern of silane monolayer. The negative-tone trenches, where the Si/SiO₂ substrate was exposed, could selectively assemble a different silane monolayer, such as 3-aminopropyl triethoxy silane (APTES), by a subsequent vapor or liquid-phase deposition to form a mixed SAM.

Figure 2c shows the negative-tone pattern of the ODTCS on Si/SiO₂ substrate after sonication in DI water. The negative-tone triangular shape is the same as the original DNA nanostructure template. The depth of the trenches, *ca.* 2 nm, is similar to the thickness of the ODTCS monolayer, indicating that the bottom of these trenches exposed the Si/SiO₂ substrate. The ODTCS SAM pattern was then exposed to the APTES vapor, which could selectively deposited on the trenches where SiO₂ was exposed, resulting in the formation of the mixed SAMs patterns with nanoscale resolution. Figures 2d and 3e are AFM topography and phase images after the backfilling. Even though the topography difference is smaller after filling up the trenches with APTES (Fig. 2d), significant contrast could be observed on the phase image due to the different surface chemistry between ODTCS and APTES SAM patterns (Fig. 2d). The backfilling of the APTES also affected the surface wettability by decreasing the water contact angle from 111°

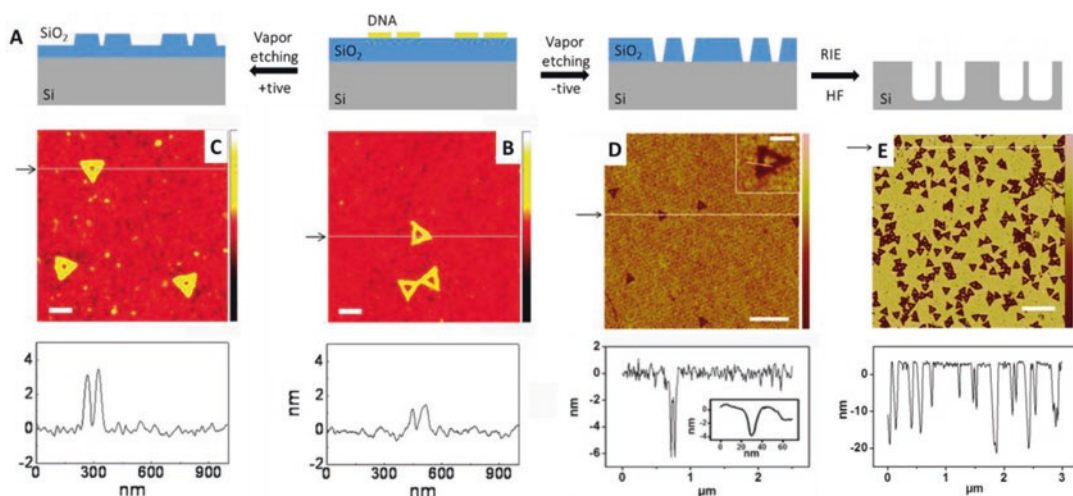


Fig. 3 (a) The cartoon sketch of the DNA-mediated HF etching of SiO₂ and the following patterning on Si by reactive ion etching. AFM images and cross sections of (b) as-deposited DNA triangles; (c) triangular shaped triangular ridges produce by positive-tone pattern transfer at low humidity; (d) triangular trenches produced by negative-tone pattern transfer under optimized condition; (e) triangular patterns on Si of the sample D after subjected to SF₆/O₂ reactive ionic etching and 5% HF solution to remove SiO₂ film. *Arrows* indicate lines of cross section. The color scale bar represents 8 nm in b and c and 10 nm in d and e. The *white* scale bars represent 500 nm, and the scale bar in the inset of D represents 100 nm. Reprinted with permission from: ref. [51] (a, d and e), © 2015 ACS; ref. [83] (b and c), © 2011 ACS

(ODTCS pattern) to 85° (mixed SAM patterns), due to the contribution from the hydrophilic -NH₂ groups of the APTES molecules.

In summary, this patterning method is the first reported approach to form SAM pattern using unmodified DNA nanostructure as masking template. The condition of this vapor phase deposition of SAM will not damage the DNA nanostructure. The DNA nanostructure, even the single layer of closely packed double strands in triangular DNA, is sufficient to block the diffusion of the silane precursor molecule under the DNA template. This easy but robust method could open up new opportunities to use DNA nanostructure as a blocking template for nanofabrication with high resolution.

3 Nanoscale Pattern Transfer from DNA Nanostructure to SiO₂ by Vapor-Phase HF Etching

SiO₂ is one of the most important dielectric materials in Si semiconductor industrial. It can be grown by thermal annealing of Si or by chemical vapor deposition (CVD) on many substrates. It is also an important hard mask materials for semiconductor nanofabrication [76]. The fabrication of pattern structure on SiO₂ can be car-

ried out in wet-, dry-, and vapor-phase processes. The wet etching process often utilizes liquid phase etchant, such as hydrofluoric acid (HF) solution, to etch the exposed SiO₂ surface. In the case of dry etching process, the exposed SiO₂ surface can be removed by the plasma reactive ions, such as F and Cl. Since both methods require harsh conditions, the DNA nanostructure cannot be used as the template in these fabrication processes directly. Vapor-phase etching has been used to faithfully transfer masking patterns into the underlying layers with both isotropic and anisotropic etch methods. Compared to wet and dry etching processes, the vapor-phase etching is favorable in that it offers mild conditions that will not lift off or destroy the DNA nanostructure.

Vapor-phase etching of SiO₂ using HF gas is the reaction between SiO₂ and HF to produce SiF₄ and H₂O:

This reaction occurs after an initiate step by condensation of HF and water on the SiO₂ surface. In the view of this reaction, there are several parameters, such as the amount of HF and isopropanol, the reaction temperature, and etching time, that can affect the etching rate. Basically, the lower the temperature, the longer the time and the higher the pressure of HF would increase the overall etching rate. Since H₂O is produced and accumulated during the reaction, the overall reaction is autocatalytic. Higher vapor pressure of H₂O can usually achieve significant higher etch rates during the reaction. Thus, the difference in the concentration of H₂O would make a big difference in the selectivity of the SiO₂ etching rate.

The DNA can modulate the adsorption of water near its vicinity in nanoscale during the etching due to the difference in H₂O adsorption between on DNA and on SiO₂. On SiO₂, there is always a water monolayer even the relative humidity of H₂O is close to 0. Besides, the amount of absorbed water only increases by 40% when the relative pressure increases from 0 to 0.85 [77]. However DNA shows a much higher response to increases in relative humidity than SiO₂ does [78]. In addition, since the DNA was anchored on SiO₂ based on electro-static interaction of Mg²⁺, the HF ionization efficiency might be higher in this liquid buffer layer [79], which makes a difference in the etching rate of SiO₂. Therefore, the structural information of DNA nanostructure can be transferred to the underlying SiO₂ layer by selective etching.

In 2011, Surwade et al. reported a direct pattern transfer from DNA to SiO₂ using a vapor-phase HF etching process [64]. They found that the DNA nanostructure could modulate the water absorption on SiO₂ locally in nanoscale. At ~50% relative humidity and 25 °C, DNA origami could increase the etching rate of underlying SiO₂, resulting in 1–2 nm deep negative-tone trenches with an average full width at half max (FWHM) of 16.7 nm. At ~34% relative humidity and 30 °C, the 2–3 nm high triangular shaped ridges with a FWHM of 27 nm was obtained (Fig. 3b). This was

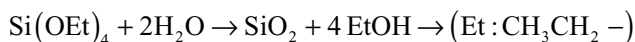
the first proof-of-principle approach to using DNA nanostructure directly in nanofabrication of SiO₂.

In addition, the kinetic behavior of the DNA-mediated HF etching of SiO₂ was investigated by Zhou et al. in 2015 [51]. The parameters, which can affect the selectivity of etching and the outcome of the pattern transfer, include temperature, pressure, relative composition of gas-phase etchants, and etching duration. After systematic study of each parameter, the optimized pattern transfer condition (temperature: 35 °C; etching duration: 20 min; partial pressure: 333 Pa (HF) and 658 Pa (H₂O)) was identified to produce 11 ± 1 nm resolution patterns with a contrast of 6.0 ± 1.5 nm on SiO₂ (Fig. 3d). The as-patterned SiO₂ layer could also be used as a hard mask to produce 18.4 ± 2.7 nm contrast, 19 ± 4 nm resolution features in the underlying Si substrate by plasma etching (Fig. 3e). These results highlight the potential application of DNA nanostructure as a template for general-purpose nanofabrication.

4 Nanoscale Growth and Patterning of Inorganic Oxides Using DNA Nanostructure Templates

Chemical vapor deposition (CVD) is another well-established technique that can produce conformal inorganic coatings at the nanoscale [80]. The thickness of the inorganic coating can be precisely controlled with precision at nanometer by adjusting the reaction time and other deposition parameters. The CVD is vapor-phase process that can be carried out at atmospheric environment at room temperature. This implies the opportunities to utilize DNA nanostructure as template.

In a typical CVD process, SiO₂ is produced by the reaction between Si(OEt)₄ and water [81, 82]:



Whether SiO₂ can be deposited onto a particular substrate or not is largely determined by its ability to adsorb the CVD precursor and water. Given that DNA can modulate the water absorption near its vicinity, the DNA nanostructure can be used as template to facilitate the selective deposition of SiO₂ in the CVD process.

In 2013, Surwade et al. reported a shape-conserving, room-temperature CVD process to convert a DNA nanostructure into an inorganic oxide nanostructure with the same shape [42]. The DNA mediated CVD can produce both positive- and negative-tone SiO₂ nanostructure by changing the CVD conditions. Positive-tone pattern of SiO₂ (width: 37 ± 3 nm; height: 2.6 ± 0.5 nm) was obtained by exposing the as-deposited DNA on Si/SiO₂ substrate (Fig. 4a) to a mixed vapor of Si(OEt)₄ (TEOS), H₂O, *iso*-propanol (IPA), and NH₃ (Fig. 4b). Similar to the case of

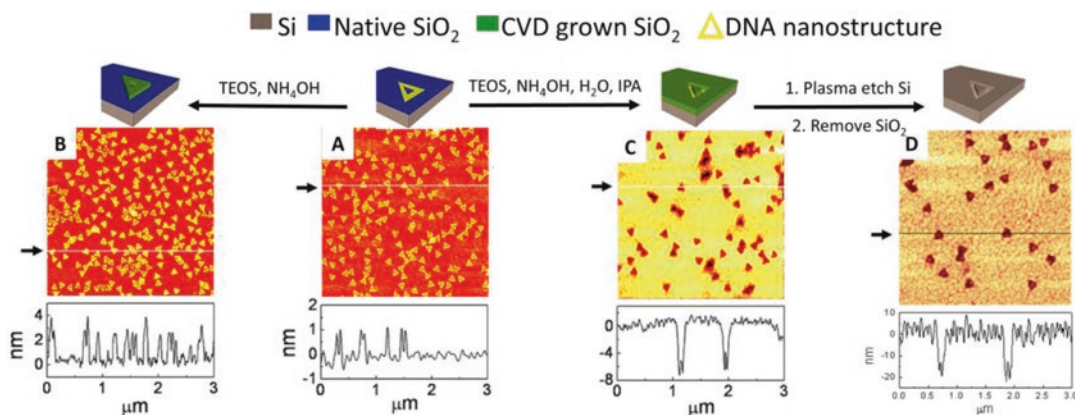


Fig. 4 Cartoon representations (*top*), AFM images (*middle*), and cross sections (*bottom*) are shown for (a) DNA origami triangles deposited on a Si substrate, (b) positive-tone triangular patterns obtained for CVD grown SiO_2 (reaction time 6 h), (c) negative-tone triangular patterns obtained for CVD-grown SiO_2 (reaction time 12 h), and (d) triangular trenches obtained by SF_6/O_2 plasma etching of a Si substrate using a negative-tone CVD-grown SiO_2 as a hard mask. The *arrows* and *lines* indicate the location of the cross section. Reprinted from ref. [42], © 2013 ACS

the negative-tone pattern transfer by DNA mediated etching of SiO_2 [51, 64], more water was absorbed near DNA at high relative humidity while the water absorbed on SiO_2 is passivated by IPA, resulting in more SiO_2 deposited near DNA pattern during the CVD process and the negative-tone afterwards. To reverse this area selectivity of CVD, the IPA and water vials was removed from the reaction chamber and negative-tone triangular structure was obtained with the depth of 7 ± 2 nm and width of 42 ± 5 nm (Fig. 4c). The center void of the triangle template was retained in almost all the structures under both positive-tone and negative-tone conditions, indicating the faithful pattern transfer from DNA nanostructure to SiO_2 by CVD. In addition, the negative pattern of SiO_2 can be used as hard mask to pattern the underlying Si by subsequent plasma etching using SF_6/O_2 . After the plasma etching and the removal of the SiO_2 mask, negative-tone pattern of deeper trenches (depth: 25 ± 2 nm; width: 55 ± 3 nm) was obtained on Si substrate and the central void feature was maintained on almost every structure.

This DNA-mediated CVD method is a highly versatile method for a general-purpose nanofabrication and can also be extended for a wide selection of templates, oxides, and substrate materials. For example, different shaped DNA nanostructures that are fabricated with different methods could always generate both positive- and negative-tone SiO_2 patterns after CVD. In addition, other oxide materials, such as TiO_2 , can be selectively deposited on DNA template on SiO_2 by using $\text{Ti}(\text{O}i\text{Pr})_4$ as precursor to generate positive-tone pattern of TiO_2 . Finally, the selective CVD of oxide is also

compatible to pattern other substrates, such as Au and mica substrates, to generate positive-tone SiO₂ nanostructures. This area-selective DNA-mediated CVD process opens up the possibility to integrate DNA nanotechnology with conventional nanolithography to create high-resolution patterns.

5 Programmably Shaped Carbon Nanostructure from Shape-Conserving Carbonization of DNA

Porous carbon material plays an important role in a wide range of applications, such as aerospace structure, thermal management, and energy storage because of its unique mechanical, thermal, and electrical properties [83–90]. The carbon structure has essential effect on these properties. Therefore, to control the structure becomes the key point to put porous carbon material into application. Currently, uniform-structured porous carbon materials are synthesized using inorganic templates [91–94]. The template can guide an organic precursor, usually a polymer, into the desired structure. The organic-inorganic composite then undergoes a carbonization process at high temperature (typically 500–1000 °C) during which the organic precursor is converted to carbon (amorphous or crystalline). The shape of the inorganic template is transferred to the porous carbon material during carbonization process. Inorganic template controls porous carbon material's structure. However, the inorganic templates can only offer simple structures, such as spheres and rods, limiting the performance for porous carbon materials.

Thanks to the programmability of DNA hybridization, arbitrarily shaped 2D and 3D DNA nanostructures have been made with precise control of size and shape at high resolution [3, 4, 9, 29, 38, 45, 54, 95–100]. These DNA nanostructures are ideal templates for making porous carbon materials to carry out design-based application. It has been reported that DNA can be converted to graphitic structures through carbonization [101, 102]. However, investigation in terms of shape control during DNA carbonization is limited, if there is any. A method to preserve the structural information of DNA nanostructure through carbonization, therefore, is in need.

It is recently reported that the limited thermal stability of DNA nanostructure could be overcome by covering DNA with a protective film (Fig. 5a) [103]. In this case, DNA nanostructure is not only the template, but also the material source for fabrication of carbon nanostructure. The 20 nm Al₂O₃ coating, prepared by ALD, is a perfect protective film for both shape and material preservation of DNA nanostructure at high temperature. Al₂O₃ coating is believed to be a gas diffusion barrier and can prevent or slow down the decomposition products of DNA from escaping and as a

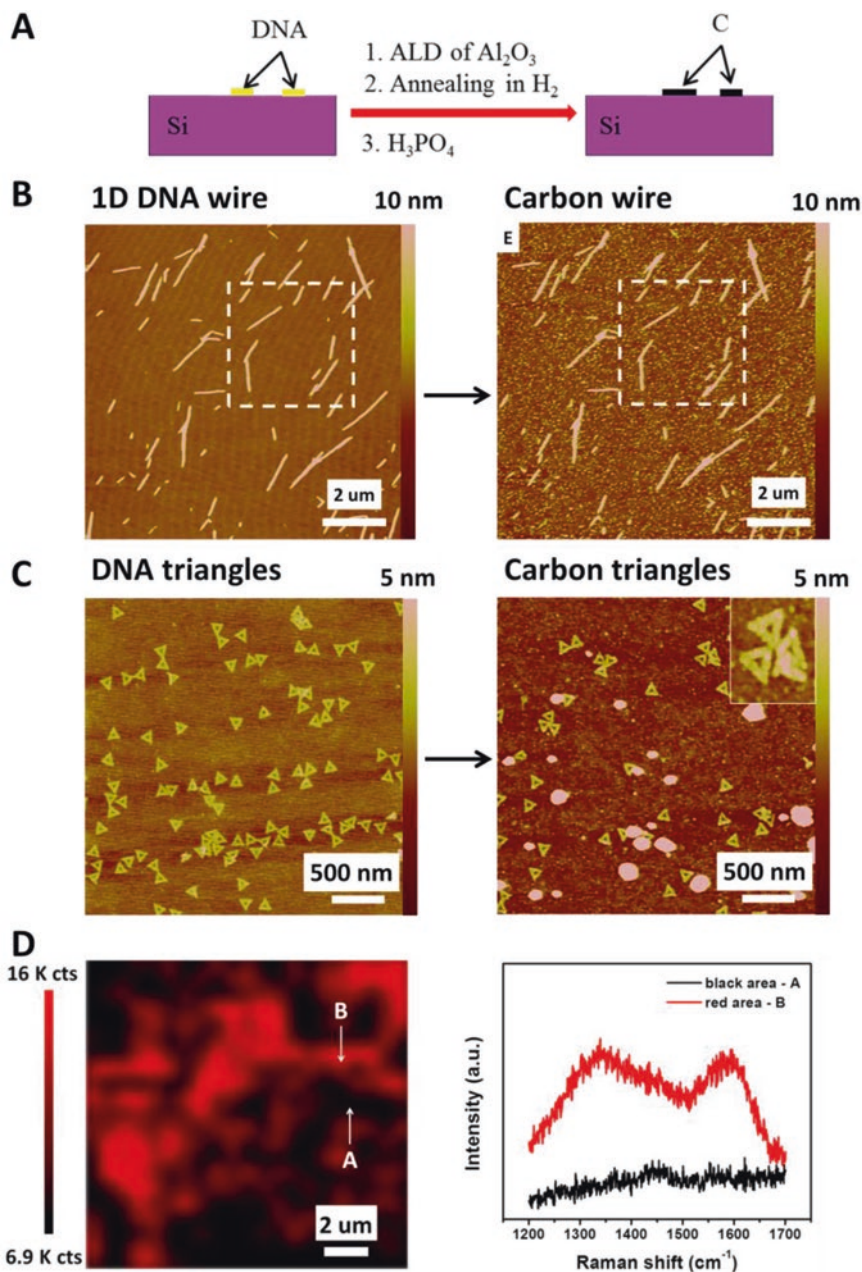


Fig. 5 (a) The cartoon sketch of shape-conserving carbonization of DNA nanostructure. AFM images of the carbonization of 1D DNA crystal (b) and 2D DNA triangles (c). (d) Confocal Raman mapping of annealed 1D DNA crystal at 1611 cm^{-1} and Raman spectra of corresponding spot as indicated by the arrows. Reprinted with permission from ref. [103], © 2015 ACS

result increase the carbonization yield. The 1D (Fig. 5b) and 2D (Fig. 5c) DNA nanostructures in different length scales can be converted to carbon nanostructure with the same shape through high temperature annealing. The resulting carbon nanostructure

was graphitic as can be seen from the Raman spectra and Raman mapping (Fig. 5d). The product is stable to store in ambient environment for over a month and mechanically stable under repeated AFM scanning. However, it is not thermally stable either under laser illumination in air or at 800 °C in H₂. This work showed a new direction to apply the DNA nanostructures as material templates for high-temperature solid-state chemistries.

6 Summary and Outlook

6.1 Summary

In summary, various methods have been reported to address challenges due to the limited stability of DNA nanostructure in direct nanofabrication. The limited chemical stability can be solved by selecting proper conditions for nanofabrication; the poor thermal stability can be solved by covering DNA with a protective film. With these methods, the direct nanofabrication of different nanostructures from 1D, 2D and 3D DNA nanostructures can be achieved. Through a careful manipulation of chemistry, these efforts created a new frontier to using DNA nanostructure for nanoscale fabrication with precise control, high resolution, and extreme complexity.

6.2 Future Perspective

The successful nanofabrication using DNA nanostructure discussed above will undisputedly lead to many new opportunities and innovative applications. The following section lays out the potential DNA based nanofabrication in according with the research discussed in this chapter.

6.3 Nanofabrication Based on Free-Standing 3D DNA Nanostructure

Since the 2D nanofabrication reaches the bottleneck to obtain higher efficiency to generate higher resolution material on the planner surface at a reasonable cost, people have turned to 3D nanofabrication for more opportunities. The fabrication of 3D NAND is able to achieve larger storage volume at lower cost. In addition, many 3D nanostructures have unique properties for designed-based application. For example, a nanoscale carbon-based truss structure could offer a high strength-to-weight ratio [104]. Arrays of 2D nanoscale crosses and 3D coils could offer novel photonic response and energy-absorbing properties, respectively [105, 106]. However, the fabrication of these irregularly shaped nanostructure is extremely challenging using existing approaches.

As discussed in last chapter, recent structural DNA nanotechnology is able to generate arbitrarily-shaped 3D DNA nanostructure with numerous complexities. This could be the resolution. However, DNA nanostructures are generally accepted as soft materials and their applications have long been limited to aqueous environments. As for the 3D DNA nanostructure, such as the

DNA polyhedral, nanopillar, and hierarchical structures, they would deform irreversibly with a threshold force of tens to hundreds of pN in water [24, 34, 107, 108]. Further complications arise when drying the DNA nanostructures. Due to the strong surface tension of water, 3D DNA structure cannot withstand the capillary forces or transverse shear forces; upon drying, these structures inevitably collapse or ruptures [109]. Therefore, the 3D DNA-based nanofabrication has been limited in the solution phase metallization, while many fabrication methods, such as ALD and lithography, are solid-state chemistry in dry environment. If free-standing 3D DNA nanostructure could be produced in dye state, the nanofabrication using 3D DNA nanostructure is freed from solution and leads to a wider range of opportunities. For example, higher strength material can be generated by ALD of ceramic material coated on the free-standing DNA nanostructure. 3D porous carbon material could also be produced from the free-standing 3D DNA nanostructure by shape-conserving carbonization. Furthermore, after self-assembly of various compositions of materials on the 3D DNA nanostructure, the methods discussed allow it to be used as 3D integrated circuits or 3D NAND in dry state.

In summary, the structural DNA nanotechnology provides highly versatile methods for building 1D, 2D, and 3D nanostructures of remarkable complexity, which are ideal templates for design-based nanofabrication. We expect the DNA-based nanofabrication will have a wide range of applications in areas such as nanoelectronics, nanophotonics, mechanical actuation, and energy storage.

References

1. Endo M, Sugiyama H (2009) Chemical approaches to DNA nanotechnology. *Chem Bio Chem* 10:2420–2443
2. Becerril HA, Woolley AT (2009) DNA-templated nanofabrication. *Chem Soc Rev* 38:329–337
3. Dietz H, Douglas SM, Shih WM (2009) Folding DNA into twisted and curved nanoscale shapes. *Science* 325:725–730
4. Douglas SM, Dietz H, Liedl T, Hogberg B, Graf F, Shih WM (2009) Self-assembly of DNA into nanoscale three-dimensional shapes. *Nature* 459:414–418
5. Yang D, Campolongo MJ, Tran TNN, Ruiz RCH, Kahn JS, Luo D (2010) Novel DNA materials and their applications. *Wiley Interdiscip Rev Nanomed Nanobiotechnol* 2:648–669
6. Han D, Pal S, Nangreave J, Deng Z, Liu Y, Yan H (2011) DNA origami with complex curvatures in three-dimensional space. *Science* 332:342–346
7. Pinheiro AV, Han D, Shih WM, Yan H (2011) Challenges and opportunities for structural DNA nanotechnology. *Nat Nanotechnol* 6:763–772
8. Zhang G, Surwade SP, Zhou F, Liu H (2013) DNA nanostructure meets nanofabrication. *Chem Soc Rev* 42:2488–2496
9. Rothemund PWK (2006) Folding DNA to create nanoscale shapes and patterns. *Nature* 440:297–302
10. Yang Y, Han D, Nangreave J, Liu Y, Yan H (2012) DNA origami with double-stranded DNA as a unified scaffold. *ACS Nano*
11. Zheng J, Birktoft JJ, Chen Y, Wang T, Sha R, Constantinou PE et al (2009) From molecular to macroscopic via the rational design of a self-assembled 3D DNA crystal. *Nature* 461:74–77

12. He Y, Chen Y, Liu HP, Ribbe AE, Mao CD (2005) Self-assembly of hexagonal DNA two-dimensional (2D) arrays. *J Am Chem Soc* 127:12202–12203
13. Hung AM, Noh H, Cha JN (2010) Recent advances in DNA-based directed assembly on surfaces. *Nanoscale* 2:2530–2537
14. Gerdon AE, Oh SS, Hsieh K, Ke Y, Yan H, Soh HT (2009) Controlled delivery of DNA origami on patterned surfaces. *Small* 5:1942–1946
15. Kershner RJ, Bozano LD, Micheel CM, Hung AM, Fornof AR, Cha JN et al (2009) Placement and orientation of individual DNA shapes on lithographically patterned surfaces. *Nat Nanotechnol* 4:557–561
16. Seeman NC (1982) Nucleic acid junctions and lattices. *J Theoret Biol* 99:237–247
17. Mao C, Sun W, Seeman NC (1999) Designed two-dimensional DNA Holliday junction arrays visualized by atomic force microscopy. *J Am Chem Soc* 121:5437–5443
18. Fu J, Liu M, Liu Y, Yan H (2012) Spatially-interactive biomolecular networks organized by nucleic acid nanostructures. *Acc Chem Res* 45:1215–1226
19. Yan H, Park SH, Finkelstein G, Reif JH, LaBean TH (2003) DNA-templated self-assembly of protein arrays and highly conductive nanowires. *Science* 301:1882–1884
20. Fu TJ, Seeman NC (1993) DNA double-crossover molecules. *Biochemistry* 32:3211–3220
21. Mathieu F, Liao S, Kopatsch J, Wang T, Mao C, Seeman NC (2005) Six-helix bundles designed from DNA. *Nano Lett* 5:661–665
22. Park SH, Barish R, Li H, Reif JH, Finkelstein G, Yan H et al (2005) Three-helix bundle DNA tiles self-assemble into 2D lattice or 1D templates for silver nanowires. *Nano Lett* 5:693–696
23. Shih WM, Quispe JD, Joyce GF (2004) A 1.7-kilobase single-stranded DNA that folds into a nanoscale octahedron. *Nature* 427:618–621
24. Goodman RP, Schaap IAT, Tardin CF, Erben CM, Berry RM, Schmidt CF et al (2005) Rapid chiral assembly of rigid DNA building blocks for molecular nanofabrication. *Science* 310:1661–1665
25. Chen J, Seeman NC (1991) Synthesis from DNA of a molecule with the connectivity of a cube. *Nature* 350:631–633
26. He Y, Ye T, Su M, Zhang C, Ribbe AE, Jiang W et al (2008) Hierarchical self-assembly of DNA into symmetric supramolecular polyhedra. *Nature* 452:198–201
27. Andersen ES, Dong M, Nielsen MM, Jahn K, Lind-Thomsen A, Mamdouh W et al (2008) DNA origami design of dolphin-shaped structures with flexible tails. *ACS Nano* 2:1213–1218
28. Douglas SM, Marblestone AH, Teerapittayanon S, Vazquez A, Church GM, Shih WM (2009) Rapid prototyping of 3D DNA-origami shapes with caDNA. *Nucleic Acids Res* 37:5001–5006
29. Zhang HL, Chao J, Pan D, Liu HJ, Huang Q, Fan CH (2012) Folding super-sized DNA origami with scaffold strands from long-range PCR. *Chem Commun* 48:6405–6407
30. Douglas SM, Bachelet I, Church GM (2012) A logic-gated nanorobot for targeted transport of molecular payloads. *Science* 335:831–834
31. Lin C, Jungmann R, Leifer AM, Li C, Levner D, Church GM et al (2012) Submicrometre geometrically encoded fluorescent barcodes self-assembled from DNA. *Nat Chem* 4:832–839
32. Jungmann R, Avendano MS, Woehrstein JB, Dai M, Shih WM, Yin P (2014) Multiplexed 3D cellular super-resolution imaging with DNA-PAINT and exchange-PAINT. *Nat Meth* 11:313–318
33. Scheible MB, Ong LL, Woehrstein JB, Jungmann R, Yin P, Simmel FC (2015) A compact DNA cube with side length 10 nm. *Small* 11:5200–5205
34. Sun W, Boulais E, Hakobyan Y, Wang WL, Guan A, Bathe M et al (2014) Casting inorganic structures with DNA molds. *Science* 346
35. Pilo-Pais M, Goldberg S, Samano E, Labean TH, Finkelstein G (2011) Connecting the nanodots: programmable nanofabrication of fused metal shapes on DNA templates. *Nano Lett* 11:3489–3492
36. Liu J, Geng Y, Pound E, Gyawali S, Ashton JR, Hickey J et al (2011) Metallization of branched DNA origami for nanoelectronic circuit fabrication. *ACS Nano* 5:2240–2247
37. Maune HT, S-p H, Barish RD, Bockrath M, Goddard IIA, RothmundPaul WK et al (2010) Self-assembly of carbon nanotubes into two-dimensional geometries using DNA origami templates. *Nat Nano* 5:61–66
38. Wei B, Dai M, Yin P (2012) Complex shapes self-assembled from single-stranded DNA tiles. *Nature* 485:623–626
39. Mathur D, Henderson ER (2013) Complex DNA nanostructures from oligonucleotide ensembles. *ACS Synth Biol* 2:180–185
40. Ke Y, Ong LL, Shih WM, Yin P (2012) Three-dimensional structures self-assembled from DNA bricks. *Science* 338:1177–1183

41. Ke Y, Ong LL, Sun W, Song J, Dong M, Shih WM et al (2014) DNA brick crystals with prescribed depths. *Nat Chem* 6:994–1002
42. Surwade SP, Zhou F, Wei B, Sun W, Powell A, O'Donnell C et al (2013) Nanoscale growth and patterning of inorganic oxides using DNA nanostructure templates. *J Am Chem Soc* 135:6778–6781
43. Jin Z, Sun W, Ke Y, Shih C-J, Paulus GL, Wang QH et al (2013) Metallized DNA nanolithography for encoding and transferring spatial information for graphene patterning. *Nat Commun* 4:1663
44. Endo M, Sugita T, Katsuda Y, Hidaka K, Sugiyama H (2010) Programmed-assembly system using DNA jigsaw pieces. *Chemistry* 16:5362–5368
45. Woo S, Rothmund PW (2011) Programmable molecular recognition based on the geometry of DNA nanostructures. *Nat Chem* 3:620–627
46. Iinuma R, Ke Y, Jungmann R, Schlichthaerle T, Woehrstein JB, Yin P (2014) Polyhedra self-assembled from DNA tripods and characterized with 3D DNA-PAINT. *Science* 344:65–69
47. Gates KS (2009) An overview of chemical processes that damage cellular DNA: spontaneous hydrolysis, alkylation, and reactions with radicals. *Chem Res Toxicol* 22:1747–1760
48. Kim H, Surwade SP, Powell A, O'Donnell C, Liu H (2014) Stability of DNA origami nanostructure under diverse chemical environments. *Chem Mater* 26:5265–5273
49. Lindahl T (1993) Instability and decay of the primary structure of DNA. *Nature* 362:709–715
50. Lindahl T, Nyberg B (1972) Rate of depurination of native deoxyribonucleic acid. *Biochemistry* 11:3610–3618
51. Zhou F, Michael B, Surwade SP, Ricardo KB, Zhao S, Liu H (2015) Mechanistic study of the nanoscale negative-tone pattern transfer from DNA nanostructures to SiO₂. *Chem Mater* 27:1692–1698
52. Mogab CJ, Adams AC, Flamm DL (1978) Plasma etching of Si and SiO₂—the effect of oxygen additions to CF₄ plasmas. *J Appl Phys* 49:3796–3803
53. Braun E, Eichen Y, Sivan U, Ben-Yoseph G (1998) DNA-templated assembly and electrode attachment of a conducting silver wire. *Nature* 391:775–778
54. Schreiber R, Kempter S, Holler S, Schüller V, Schiffels D, Simmel SS et al (2011) DNA origami-templated growth of arbitrarily shaped metal nanoparticles. *Small* 7:1795–1799
55. Tagawa M, Shohda K-I, Fujimoto K, Suyama A (2011) Stabilization of DNA nanostructures by photo-cross-linking. *Soft Matter* 7:10931–10934
56. Kuzyk A, Schreiber R, Fan Z, Pardatscher G, Roller E-M, Hoegel A et al (2012) DNA-based self-assembly of chiral plasmonic nanostructures with tailored optical response. *Nature* 483:311–314
57. Pearson AC, Liu J, Pound E, Uprety B, Woolley AT, Davis RC et al (2012) DNA origami metallized site specifically to form electrically conductive nanowires. *J Phys Chem B* 116:10551–10560
58. Deng Z, Mao C (2004) Molecular lithography with DNA nanostructures. *Angew Chem Int Ed* 43:4068–4070
59. Becerril HA, Woolley AT (2007) DNA shadow nanolithography. *Small* 3:1534–1538
60. He Y, Ye T, Ribbe AE, Mao C (2011) DNA-templated fabrication of two-dimensional metallic nanostructures by thermal evaporation coating. *J Am Chem Soc* 133:1742–1744
61. Khandelwal G, Bhyravabhotla J (2010) A phenomenological model for predicting melting temperatures of DNA sequences. *PLoS One* 5:e12433
62. Aoi K, Takasu A, Okada M (2000) DNA-based polymer hybrids Part 1. Compatibility and physical properties of poly(vinyl alcohol)/DNA sodium salt blend. *Polymer* 41:2847–2853
63. He Y, Liu H, Chen Y, Tian Y, Deng Z, Ko SH et al (2007) DNA-based nanofabrications. *Microsc Res Tech* 70:522–529
64. Surwade SP, Zhao S, Liu H (2011) Molecular lithography through DNA-mediated etching and masking of SiO₂. *J Am Chem Soc* 133:11868–11871
65. Carta G, El Habra N, Crociani L, Rossetto G, Zanella P, Zanella A et al (2007) CVD of MgO thin films from bis(methylcyclopentadienyl) magnesium. *Chem Vapor Deposition* 13:185–189
66. Lim BS, Rahtu A, Gordon RG (2003) Atomic layer deposition of transition metals. *Nat Mater* 2:749–754
67. Niinisto J, Putkonen M, Niinisto L, Stoll SL, Kukli K, Sajavaara T et al (2005) Controlled growth of HfO₂ thin films by atomic layer deposition from cyclopentadienyl-type precursor and water. *J Mater Chem* 15:2271–2275
68. Arya SK, Solanki PR, Datta M, Malhotra BD (2009) Recent advances in self-assembled monolayers based biomolecular electronic devices. *Biosens Bioelectron* 24:2810–2817
69. Gooding JJ, Mearns F, Yang W, Liu J (2003) Self-assembled monolayers into the 21st century: Recent advances and applications. *Electroanalysis* 15:81–96

70. Meiners F, Plettenberg I, Witt J, Vaske B, Lesch A, Brand I et al (2013) Local control of protein binding and cell adhesion by patterned organic thin films. *Anal Bioanal Chem* 405:3673–3691
71. Miozzo L, Yassar A, Horowitz G (2010) Surface engineering for high performance organic electronic devices: the chemical approach. *J Mater Chem* 20:2513–2538
72. Newton L, Slater T, Clark N, Vijayaraghavan A (2013) Self assembled monolayers (SAMs) on metallic surfaces (gold and graphene) for electronic applications. *J Mater Chem C* 1:376–393
73. Wilbur JL, Kumar A, Biebuyck HA, Kim E, Whitesides GM (1996) Microcontact printing of self-assembled monolayers: applications in microfabrication. *Nanotechnology* 7:452–457
74. Zhou Y, Chiu C-W, Liang H (2012) Interfacial structures and properties of organic materials for biosensors: an overview. *Sensors* 12:15036–15062
75. Surwade S, Zhou F, Li Z, Powell A, O'Donnell C, Liu H (2015) Nanoscale patterning of self-assembled monolayers using DNA nanostructure templates. *Chem Commun*
76. Vivien L (2013) *Handbook of silicon photonics*. CRC Press, Taylor and Francis, Boca Raton, p 61
77. Mizushima S (2004) Determination of the amount of gas adsorption on SiO₂/Si(100) surfaces to realize precise mass measurement. *Metrologia* 41:137–144
78. Balkose D, Alp B, Ulku S (2008) Water vapour adsorption on DNA. *J Therm Anal Calorim* 94:695–698
79. Watanabe H, Kitajima H, Honma I, Ona H, Wilhelm RJ, Sophie AJL (1995) Influence of water adsorption/desorption processes on the selectivity of vapor HF etching. *J Electrochem Soc* 142:1332–1340
80. Pierson HO (1999) *Handbook of chemical vapor deposition*, 2nd edn. Noyes, Norwich, NY
81. Ferguson JD, Smith ER, Weimer AW, George SM (2004) ALD of SiO₂ at room temperature using TEOS and H₂O with NH₃ as the catalyst. *J Electrochem Soc* 151:G528–G535
82. Klaus JW, George SM (2000) SiO₂ chemical vapor deposition at room temperature using SiCl₄ and H₂O with an NH₃ catalyst. *J Electrochem Soc* 147:2658–2664
83. Gui XC, Wei JQ, Wang KL, Cao AY, Zhu HW, Jia Y et al (2010) Carbon nanotube sponges. *Adv Mater* 22:617
84. Frackowiak E, Beguin F (2001) Carbon materials for the electrochemical storage of energy in capacitors. *Carbon* 39:937–950
85. Gallego NC, Klett JW (2003) Carbon foams for thermal management. *Carbon* 41:1461–1466
86. Klett J, Hardy R, Romine E, Walls C, Burchell T (2000) High-thermal-conductivity, mesophase-pitch-derived carbon foams: effect of precursor on structure and properties. *Carbon* 38:953–973
87. Zhang LL, Zhao XS (2009) Carbon-based materials as supercapacitor electrodes. *Chem Soc Rev* 38:2520–2531
88. Balandin AA (2011) Thermal properties of graphene and nanostructured carbon materials. *Nat Methods* 10:569–581
89. Ji XL, Lee KT, Nazar LF (2009) A highly ordered nanostructured carbon-sulphur cathode for lithium-sulphur batteries. *Nat Mater* 8:500–506
90. Chesnokov SA, Nalimova VA, Rinzler AG, Smalley RE, Fischer JE (1999) Mechanical energy storage in carbon nanotube springs. *Phys Rev Lett* 82:343–346
91. Sazanov YN, Gribanov AV (2009) Criteria of polymer carbonization. *Russ J Appl Chem* 82:473–482
92. Lee J, Kim J, Hyeon T (2006) Recent progress in the synthesis of porous carbon materials. *Adv Mater* 18:2073–2094
93. Xia YD, Yang ZX, Mokaya R (2010) Templated nanoscale porous carbons. *Nanoscale* 2:639–659
94. Sakintuna B, Yurum Y (2005) Templated porous carbons: a review article. *Ind Eng Chem Res* 44:2893–2902
95. Zhao Z, Liu Y, Yan H (2011) Organizing DNA origami tiles into larger structures using preformed scaffold frames. *Nano Lett* 11:2997–3002
96. Endo M, Sugita T, Rajendran A, Katsuda Y, Emura T, Hidaka K et al (2011) Two-dimensional DNA origami assemblies using a four-way connector. *Chem Commun* 47:3213–3215
97. Castro CE, Kilchherr F, Kim DN, Shiao EL, Wauer T, Wortmann P et al (2011) A primer to scaffolded DNA origami. *Nat Methods* 8:221–229
98. Seeman NC (2010) Nanomaterials based on DNA. *Ann Rev Biochem* 79:65–87
99. Seeman NC (2007) An overview of structural DNA nanotechnology. *Mol Biotechnol* 37:246–257
100. Liu WY, Zhong H, Wang RS, Seeman NC (2011) Crystalline two-dimensional DNA-origami arrays. *Angew Chem Int Edit* 50:264–267
101. Nakao H, Tokonami S, Yamamoto Y, Shiigi H, Takeda Y (2014) Fluorescent carbon nanowires made by pyrolysis of DNA nanofibers and

- plasmon-assisted emission enhancement of their fluorescence. *Chem Commun* 50:11887–11890
102. Sokolov AN, Yap FL, Liu N, Kim K, Ci LJ, Johnson OB et al (2013) Direct growth of aligned graphitic nanoribbons from a DNA template by chemical vapour deposition. *Nat Commun* 4:2402
 103. Zhou F, Sun W, Ricardo KB, Wang D, Shen J, Yin P et al (2016) Programmably-shaped carbon nanostructure from shape-conserving carbonization of DNA. *ACS Nano*
 104. Deb K, Gulati S (2001) Design of truss-structures for minimum weight using genetic algorithms. *Finite Elem Anal Des* 37:447–465
 105. Watts CM, Liu XL, Padilla WJ (2012) Metamaterial electromagnetic wave absorbers. *Adv Mater* 24:Op98–Op120
 106. Gansel JK, Thiel M, Rill MS, Decker M, Bade K, Saile V et al (2009) Gold helix photonic metamaterial as broadband circular polarizer. *Science* 325:1513–1515
 107. Kauert DJ, Kurth T, Liedl T, Seidel R (2011) Direct mechanical measurements reveal the material properties of three-dimensional DNA origami. *Nano Lett* 11:5558–5563
 108. Weizmann Y, Braunschweig AB, Wilner OI, Cheglakov Z, Willner I (2008) A polycatenated DNA scaffold for the one-step assembly of hierarchical nanostructures. *Proc Natl Acad Sci* 105:5289–5294
 109. Smith DM, Schuller V, Forthmann C, Schreiber R, Tinnefeld P, Liedl T (2011) A structurally variable hinged tetrahedron framework from DNA origami. *J Nucleic Acids* 2011:9

Confined Growth of Metal Nanoparticles Within 3D DNA Origami Molds

Wei Sun and Jie Shen

Abstract

Manufacturing prescribed shaped metal nanoparticles promises emerging applications in plasmonics, energy, and disease diagnosis. The key to the shape-controllable synthesis is generating local environments encoded with prescribed geometrical information. Here, we describe a general strategy that uses 3D self-assembled DNA origami as mold to confine the casting growth of metal nanoparticle. By transferring the shape information from DNA cavities to metal nanoparticles, metal nanoparticles with prescribed shapes, dimensions, and surface binding features could be rationally designed and synthesized.

Key words Metal nanoparticle, DNA origami, Confined growth

1 Introduction

Plasmonic metal nanoparticles, such as gold and silver, have been used in plasmonic circuits [1], photovoltaics [2], and high-sensitivity early disease diagnosis [3]. For example, shape-dependent near-field enhancement in plasmonic metal nanoparticles can be used in sensitive label-free detection of disease markers [3–5]. To rationally tune the plasmonic properties tailored to specific applications, it is essential to engineer metal nanoparticles with arbitrarily in silico-designed shapes.

Metal nanoparticles have been manufactured through top-down lithography and bottom-up chemical synthesis. Limited by its spatial resolution (around 10–20 nm) in fabricating 3D features and slow serial processing, top-down lithography (e.g. electron beam lithography) is often used to manufacture prescribed metal nanostructures around 100 nm or larger [1, 6]. Alternatively, using small molecular capping ligands, including amphiphilic surfactants [7], polymers [8], peptides [9], and single-stranded DNAs [10], to tune the energy level of different crystallographic facets, diverse symmetric metal nanoparticles have been synthesized with mono-dispersed dimensions and

tunable surface morphologies. However, *in silico* design of arbitrarily irregular shapes and surface binding properties is still challenging for the bottom-up chemical synthesis.

By encoding 2D/3D geometrical information into 1D linear sequences of the constituent DNAs, DNA self-assembly enables a programmable strategy towards complex prescribed shapes [11]. Particularly, recent inventions of DNA origami [12–14] and DNA bricks [15, 16] provide spatial programmability down to 2 nm. Self-assembled DNA nanostructures have also been used as scaffold to pattern proteins [17], nanoparticles [18], and nanowires [19]. Using metal nanocluster or nanoparticles decorated on the exterior surface of the DNA nanostructures as seeds, metallization has produced diverse metal nanoparticles around DNA nanostructures [20, 21]. However, because the growth at the exterior surface is unconfined, rough surface morphology, uncontrolled dimensions, and multiple grain boundaries are often observed in the metallized DNA nanostructure.

Confining the growth of metal nanoparticles within DNA nanoparticles could address these challenges. Here, we develop a nanocasting strategy to program the 3D metal nanoparticles using self-assembled DNA nanostructures with *in silico*-designed cavities as molds [22]. First, a mechanically stiff open-ended DNA molds is designed using computation software (caDNAo, [23]) and folded following the published 3D DNA origami strategy [13]. Next, 5 nm gold nanoparticles are introduced exclusively at the interior surface of the DNA mold. After that, the open ends of the DNA mold are sealed with DNA lids. Finally, in the presence of metal precursors and reducing agents, the gold seeds grow into metal nanoparticles with shape complementary to the DNA cavities (Fig. 1a).

Using this nanocasting strategy, we synthesized three silver cuboids with prescribed dimensions ranging from 15 to 30 nm, silver prisms with equilateral and right-triangular cross-sections, silver nanoparticle with circular cross-sections, gold cuboid, Y-shaped silver particle, and quantum-dot-silver-quantum-dot composite structure (Fig. 1b).

2 Materials

For DNA origami molds, all the single-stranded DNA oligonucleotides are ordered from IDT (Integrated DNA Technologies) or Bioneer, and kept at $-20\text{ }^{\circ}\text{C}$ before use. NaNO_3 , MgCl_2 , $\text{Mg}(\text{NO}_3)_2$, AgNO_3 , HAuCl_4 , and ascorbic acid are purchased from Sigma Aldrich. Metals, salts, and ascorbic acid are dissolved into ultrapure water with specific concentration (listed in Subheading 3) and frozen at $-20\text{ }^{\circ}\text{C}$ prior to use. 5 nm gold nanoparticles are purchased from Ted Pella.

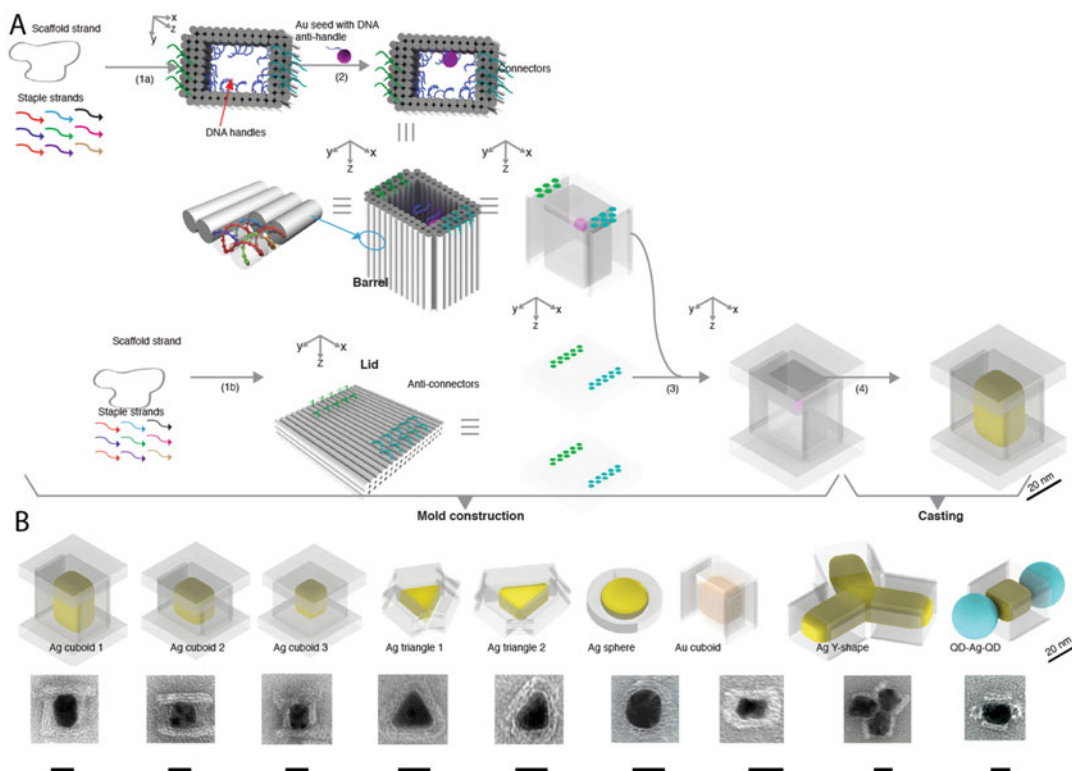


Fig. 1 Nanocasting of metal nanoparticles within programmable DNA molds. (a) Design schematic of the nanocasting strategy. (b) Designs (top) and TEM images (bottom) of the cast metal products. Silver, gold, and quantum dots are depicted as *yellow, orange, and pink* objects. Scale bars are 20 nm [From [22]. Reprinted with permission from AAAS]

2.1 Folding Buffer

120 mM MgCl_2 , 38 mM Tris, and 8 mM EDTA at pH 8.0.

2.2 Gel running buffer for DNA origami molds.

0.5× TBE (45 mM Tris-borate and 1 mM EDTA) and 10 mM $\text{Mg}(\text{NO}_3)_2$ at pH 8.3.

2.2 Uranium Staining Buffer

2% Uranium formate.

3 Methods

3.1 Folding of DNA Origami Molds

Assembly of DNA-origami molds was accomplished following previously reported protocol [13].

1. Pipet 6 μL of DNA staple strand solution (100 μM) from each well on the plates, and mix them into a single 2 mL tube. Final concentration for every staple strand is around 500 nM.
2. Mix 23 μL of scaffold strand (mutated P8064, 200 nM) solution with 46 μL of mixed staple strands solution, 11 μL of double-distilled water, and 12 μL of origami folding buffer within a 200 μL PCR tube. The final concentration in the

reaction solution is: 50 nM scaffold strand, 250 nM each staple strand, 16 mM MgCl₂, 5 mM Tris, and 1 mM EDTA.

3. The reaction solution is put into a thermal cycler, and incubated at 80 °C for 15 min, followed by a fast thermal-annealing ramp from 80 to 65 °C (5 min at each °C) and a slow thermal-annealing ramp from 64 to 24 °C over (105 min at each °C).

3.2 Gel Electrophoresis Purification of DNA Origami Molds

1. Mix 0.9 g of solid agarose gel and 120 mL of 0.5× TBE buffer within a 250 mL beaker.
2. Heat the mixture in a microwave oven for 3 min.
3. 1.2 μL of Mg(NO₃)₂ (1 M) and 6 μL of Sybr Safe are added into the boiled agarose gel solution.
4. Then the agarose gel solution is poured into the gel box, and cooled to room temperature for 1 h.
5. 600 mL of gel running buffer is poured into the gel box.
6. 40 μL of the as-folding products are mixed with 10 μL of glycerol, and loaded into the solidified gel.
7. The electrophoresis is running at 75 V for 3 h incubated in an ice-water bath.
8. The gel band is visualized using Safe Imager 2.0 (Invitrogen; note: dangerous to eyes, needs protection glass). Monomer band is excised using a razor.
9. The monomer DNA origami mold is recovered by pestle crushing, followed by centrifugation for 3 min at 3,381 rcf at room temperature using “Freeze ‘N’ Squeeze” DNA Gel Extraction spin columns (Bio-Rad).
10. Recovered DNA molds are stored at 4 °C for further use.

3.3 5 nm Gold Nanoparticle-DNA Conjugates

1. 20 μL of 2.5 μM phosphine-coated 5 nm gold nanoparticles is mixed with 0.5 μL of 2 M NaNO₃ and 0.65 μL 100 μM thiolated single-stranded DNA (*see Note 2*) in 0.25× TBE buffer. The reaction solution is incubated at room temperature for 36 h in the dark.
2. The reaction solution is loaded into 1% agarose gel containing 0.5× TBE buffer. The electrophoresis was running at 95 V for 1 h in a gel box on an ice-water bath.
3. The purple monomer band is recovered by pestle crushing, followed by centrifugation for 3 min at 9,391 rcf at room temperature using “Freeze ‘N’ Squeeze” DNA Gel Extraction spin columns (Bio-Rad).
4. Recovered gold nanoparticle-DNA conjugates are stored at 4 °C in dark for further use.
5. The sequence for the thiolated DNA is: TATGAGAAGTTAGG AATGTTA-TTTTT-Thiol.

3.4 Decorating 5 nm Gold Nanoparticle Seeds Within DNA Origami Molds

1. Purified DNA molds are mixed with 50 mM NaNO_3 (*see Note 3*) and 10 nM purified 5 nm gold nanoparticle-DNA conjugates, and incubating at 35 °C for 16 h, followed by slowly annealing to 24 °C over 3 h.
2. The reaction buffer is then purified using S300 spin column (GE healthcare) by centrifugation for 2 min at 750 rcf at room temperature to remove excessive 5 nm gold nanoparticle-DNA conjugates (*see Note 5*).
3. For the enclosed DNA molds, DNA lids (folded and purified separately) are mixed with the pre-synthesized seed-decorated DNA origami barrels (stoichiometry *see Note 4*), and incubated at 35 °C for 16 hours, followed by slowly annealing to 24 °C over 3 hours.

3.5 Confined Growth of Metal Nanoparticles

For silver growth:

1. To 5 μL of purified seed-decorated DNA molds, 0.5 μL of 14 mM AgNO_3 and 0.5 μL of 20 mM ascorbic acid (*see Note 1*) are added at room temperature, and pipetted 30 times for mixing.
2. The reaction solution is kept in the dark at room temperature for 4 min to 20 min.

For gold growth:

1. 0.5 μL of 14 mM HAuCl_4 and 0.5 μL of 20 mM ascorbic acid are added to 5 μL of purified seed-decorated DNA molds in 0.5 \times TB buffer at room temperature, and pipetted 30 times for mixing.
2. The reaction solution is kept in the dark at room temperature from 20 min to 2 h.

3.6 Imaging the Sample

3.6.1 Uranium Formate Staining Solution Preparation

1. In a beaker cover by foil, dissolve 60 mg uranium formate (Electron Microscopic Science) into 3 mL boiling water (ultrapure).
2. Wait till the solution is cooled to room temperature.
3. Filter the uranium solution using a syringe equipped with a 0.2 μm syringe filter (Corning).
4. The filtered clear solution is stored within a 10 mL centrifuge tube and covered with foil.
5. Pipet 1 mL clear solution out and added with 5 μL of 5.0 N NaOH for the final staining buffer. Vortex the staining buffer for 15 s, and store it within a 1.5 mL centrifuge tube covered with foil.
6. Before using the staining buffer, centrifuge it at 21,100 rcf for 6 min.

3.6.2 TEM Imaging

1. 3.5 μL of particles are adsorbed onto glow-discharged carbon-coated transmission electron microscopy (TEM) grids for 2 min and then wiped away.

2. The TEM grid is stained using the staining buffer for 45 s, and then wiped away.
3. TEM imaging is performed using an JEOL 1400 operated at 80 keV.
4. High-resolution TEM and electron diffraction are acquired using a JEOL 2010 with FEG operated at 200 keV for unstained nanoparticle sample deposited onto amorphous carbon film.

4 Notes

1. The stability of DNA molds under different ionic conditions.
With 10 mM $\text{Mg}(\text{NO}_3)_2$, DNA molds remain their integrity for at least 1 day in the presence of 1–2 mM reactants (AgNO_3 and ascorbic acid). However, with 10 μM $\text{Mg}(\text{NO}_3)_2$, similar AgNO_3 concentration dissociates DNA molds in 1 min. Higher reactant concentrations (e.g., 20 mM AgNO_3 or 50 mM ascorbic acid) also destabilize the DNA molds, even with 10 mM $\text{Mg}(\text{NO}_3)_2$.
2. Stoichiometry of the 5 nm gold nanoparticle-DNA conjugates.
The presence of dense single-stranded DNAs around gold nanoparticle may affect the quality of subsequent casting growth under weak reducing conditions. To minimize this effect, we set the stoichiometry between single-stranded DNA and 5 nm gold nanoparticle to around 1:1.
3. The stability of the 5 nm gold nanoparticle-DNA conjugates under different ionic conditions.
With 10 mM $\text{Mg}(\text{NO}_3)_2$, low-stoichiometry (1:1) gold nanoparticle-DNA conjugates tend to aggregate at 35 °C. Introducing proper concentration (50 mM) of Na^+ may increase the stability of gold nanoparticle-DNA conjugates. At 35 °C, we do not observe significant aggregation after 19 h.
4. Stoichiometry when forming a closed DNA mold.
Different stoichiometry between the open-ended DNA molds and DNA lids may affect the lid closure yield. We notice that, when the lid-to-mold stoichiometry is increased from 2:1 to 6:1, the lid closure yield slightly increases from 28% to 33%. Additionally, at high lid-to-barrel stoichiometry (6:1), the formation yield for defect structures (e.g. two lids connecting to identical end of the open-ended DNA mold) is around 50%.
5. Purification for the seeds-decorated DNA molds.
We explored using agarose gel electrophoresis to purify the seeds (5 nm gold nanoparticles)-decorated DNA molds. However, agarose gel electrophoresis cannot separate the

closed DNA molds from the defect DNA molds (e.g. open DNA molds with lids connected at both ends). This may be ascribed to either the small mobility difference of distinct structures or a post-purification lid opening.

Acknowledgement

We acknowledge the funding support from DARPA Young Faculty Award N66001-11-1-4136, ONR Young Investigator Program Award N000141110914, NSF CAREER Award CCF1054898, NIH Director's New Innovator Award 1DP2OD007292, and Wyss Institute for Biologically Inspired Engineering, Harvard University.

References

1. Kildishev AV, Boltasseva A, Shalaev VM (2013) Planar photonics with metasurfaces. *Science* 339:1232009
2. Atwater HA, Polman A (2010) Plasmonics for improved photovoltaic devices. *Nat Mater* 9:205–213
3. Mulvaney SP, Musick MD, Keating CD, Natan MJ (2003) Glass-coated, analyte-tagged nanoparticles: a new tagging system based on detection with surface-enhanced Raman scattering. *Langmuir* 19:4784–4790
4. Lim D-K, Jeon K-S, Hwang J-H, Kim H, Kwon S, Suh YD, Nam J-M (2011) Highly uniform and reproducible surface-enhanced Raman scattering from DNA-tailorable nanoparticles with 1-nm interior gap. *Nat Nanotech* 6:452–460
5. Eustis S, El-Sayed MA (2006) Why gold nanoparticles are more precious than pretty gold: noble metal surface plasmon resonance and its enhancement of the radiative and non-radiative properties of nanocrystals of different shapes. *Chem Soc Rev* 35:209–217
6. Pompa PP, Martiradonna L, Della Torre A, Della Sala F, Manna L, De Vittorio M, Calabi F, Cingolani R, Rinaldi R (2006) Metal-enhanced fluorescence of colloidal nanocrystals with nanoscale control. *Nat Nanotech* 1:126–130
7. Ming T, Feng W, Tang Q, Wang F, Sun L, Wang J, Yan C (2009) Growth of tetrahedral gold nanocrystals with high-index facets. *J Am Chem Soc* 131:16350–16351
8. Sun Y, Xia Y (2002) Shape-controlled synthesis of gold and silver nanoparticles. *Science* 298:2176–2179
9. Ruan L, Ramezani-Dakhel H, Chiu C-Y, Zhu E, Li Y, Heinz H, Huang Y (2013) Tailoring molecular specificity toward a crystal facet: a lesson from biorecognition toward Pt{111}. *Nano Lett* 13:840–846
10. Wang Z, Tang L, Tan LH, Li J, Lu Y (2012) Discovery of the DNA “genetic code” for abiological gold nanoparticle morphologies. *Angew Chem Int Ed* 51:9078–9082
11. Seeman NC (2003) DNA in a material world. *Nature* 421:427–431
12. Rothmund PWK (2006) Folding DNA to create nanoscale shapes and patterns. *Nature* 440:297–302
13. Douglas SM, Dietz H, Liedl T, Hogberg B, Graf F, Shih WM (2009) Self-assembly of DNA into nanoscale three-dimensional shapes. *Nature* 459:414–418
14. Han D, Pal S, Nangreave J, Deng Z, Liu Y, Yan H (2011) DNA origami with complex curvatures in three-dimensional space. *Science* 332:342–346
15. Wei B, Dai M, Yin P (2012) Complex shapes self-assembled from single-stranded DNA tiles. *Nature* 485:623–626
16. Ke Y, Ong LL, Shih WM, Yin P (2012) Three-dimensional structures self-assembled from DNA bricks. *Science* 338:1177–1183
17. Yan H, Park SH, Finkelstein G, Reif JH, LaBean TH (2003) DNA-templated self-assembly of protein arrays and highly conductive nanowires. *Science* 301:1882–1884
18. Kuzyk A, Schreiber R, Fan Z, Pardatscher G, Roller E-M, Hogele A, Simmel FC, Govorov AO, Liedl T (2012) DNA-based self-assembly of chiral plasmonic nanostructures with tailored optical response. *Nature* 483:311–314

19. Maune HT, Han S-P, Barish RD, Bockrath M, Goddard III WA, Rothmund PWK, Winfree E (2010) Self-assembly of carbon nanotubes into two-dimensional geometries using DNA origami templates. *Nat Nanotech* 5:61–66
20. Pilo-Pais M, Goldberg S, Samano E, LaBean TH, Finkelstein G (2011) Connecting the nanodots: programmable nanofabrication of fused metal shapes on DNA templates. *Nano Lett* 11:3489–3492
21. Schreiber R, Kempter S, Holler S, Schuller V, Schiffels D, Simmel SS, Nickels PC, Liedl T (2011) DNA origami-templated growth of arbitrarily shaped metal nanoparticles. *Small* 7:1795–1799
22. Sun W, Boulais E, Hakobyan Y, Wang WL, Guan A, Bathe M, Yin P (2014) Casting inorganic structures with DNA molds. *Science* 346:1258361
23. Douglas SM, Marblestone AH, Teerapittayanon S, Vazquez A, Church GM, Shih WM (2009) Rapid prototyping of 3D DNA-origami shapes with caDNAo. *Nucleic Acid Res* 37: 5001–5006

DNA-Directed Self-Assembly of Highly Ordered and Dense Single-Walled Carbon Nanotube Arrays

Hareem Maune and Si-ping Han

Abstract

Single-walled carbon nanotubes (SWNT or CNT) have unique and well-known high-performance material properties that can enable revolutionary increases in the performance of electronic devices and architectures. However, fabrication of large-scale SWNT-based ICs is an enormously challenging, unsolved problem, and self-assembly is likely needed for critical steps. Over the past several years, methods have been introduced to create ordered carbon nanotube structures using DNA guided self-assembly. In this chapter, we briefly review the challenges involved in using DNA to assemble SWNT nanostructures, and then give detailed methods to assemble dense, aligned SWNT arrays. In particular, we discuss the preparation of DNA wrapped single-walled nanotubes (DNA-CNTs) using commercial carbon nanotube products that are suitable for electronics applications. Then, we discuss methods to characterize DNA-CNTs using fluid mode atomic force microscopy (AFM). Finally, we give detailed procedures for assembly of DNA-CNTs into dense parallel arrays via linker induced surface assembly (LISA).

Key words Carbon nanotubes, Self-assembly, AFM imaging, Nanoelectronics, DNA linkers

1 Introduction

SWNTs hold enormous potential as components for nanoscale devices and architecture due to their unique structural and electronic properties [1]. For example, SWNTs are one of the most promising candidates for high-speed, low-power electronics. System-level simulations of suitable CNT based transistors show that high performance devices require placement of purified semi-conducting CNTs (sCNT) at very tight pitch (sub 10 nm inter CNT distance) to allow for sufficient density scaling and source/drain contact scaling [2, 3]. However, the traditional SWNT device fabrication methods rely on multiple expensive lithographic steps, or suffer from instability of CNT dispersions, or have low placement yield or placement precision, etc. Most importantly the conventional techniques lack the ability to control CNT placement and pitch, especially at sub-10 nm.

Fortuitously DNA bases can adsorb onto the SWNT sidewall via dispersive interactions, allowing large numbers of short single-stranded DNA (ssDNA) to attach to individual SWNTs [4]. Thus, stable colloidal suspensions of as-produced, single-walled CNTs (SWNTs) are easily obtained using DNA, suggesting that DNA based self-assembly could organize SWNTs into ordered structures.

Indeed, the ability of biomolecules to interact in ordered assemblies, adopt fixed nanoscale geometric shapes, and achieve a wide breadth of functions have spurred much interest in their use for bottom-up fabrication in solid-state device applications where the state-of-the-art top-down approaches are not practical or prohibitively expensive. Widespread, intensive efforts are directed towards the development of nucleic acids and proteins into nanowires, lithographic masks, and scaffolds for fabrication of next-generation bioelectronics [5–10]. Recent advances in DNA nanotechnology have exploited the exquisite nanometer scale spatial addressability of DNA to achieve precise control over organization of nanomaterials [11], such as nanoparticles, viruses, and proteins.

For most of these applications, however, the material component being organized is approximately spherical. On the other hand, single walled CNTs are very long wires with diameters ranging from 0.4 to 2 nm but lengths from ~50 nm to millimeter. Thus, self-assembly methods [8, 12] must not only control the position of multiple CNTs but also their orientations. This makes DNA-assisted self-assembly of CNTs a challenging problem.

We have utilized DNA for dynamic manipulation of carbon nanotubes (CNTs) [8, 12] via control of DNA base pairing through branch migration reactions and control of DNA-material interactions through manipulation of environmental factors such as temperature, and counterion composition of the DNA containing solution. These self-assembly techniques are applicable to carbon nanotubes and other nanomaterials including DNA structures [13].

In this chapter, we outline the linker-induced surface assembly (LISA) process for creating rafts of dense, aligned, DNA-wrapped CNTs (DNA-CNT) [12]. We discuss the challenges of wrapping CNTs efficiently with DNA and implementation of LISA process on various substrates.

LISA is used to create 2D parallel DNA-CNT arrays, with controlled inter-CNT pitch, without the use of large DNA assembly templates (Fig. 1). A simple DNA duplex nanostructure not only disperses the CNTs, but also induces their self-assembly. The internanotube pitch is controlled with nanometer precision by modulating the length of the DNA duplex (Fig. 2). This surface-based self-assembly method utilizes mica as the substrate and the substrate's interaction with metal cations and DNA to control the CNT diffusion on the surface.

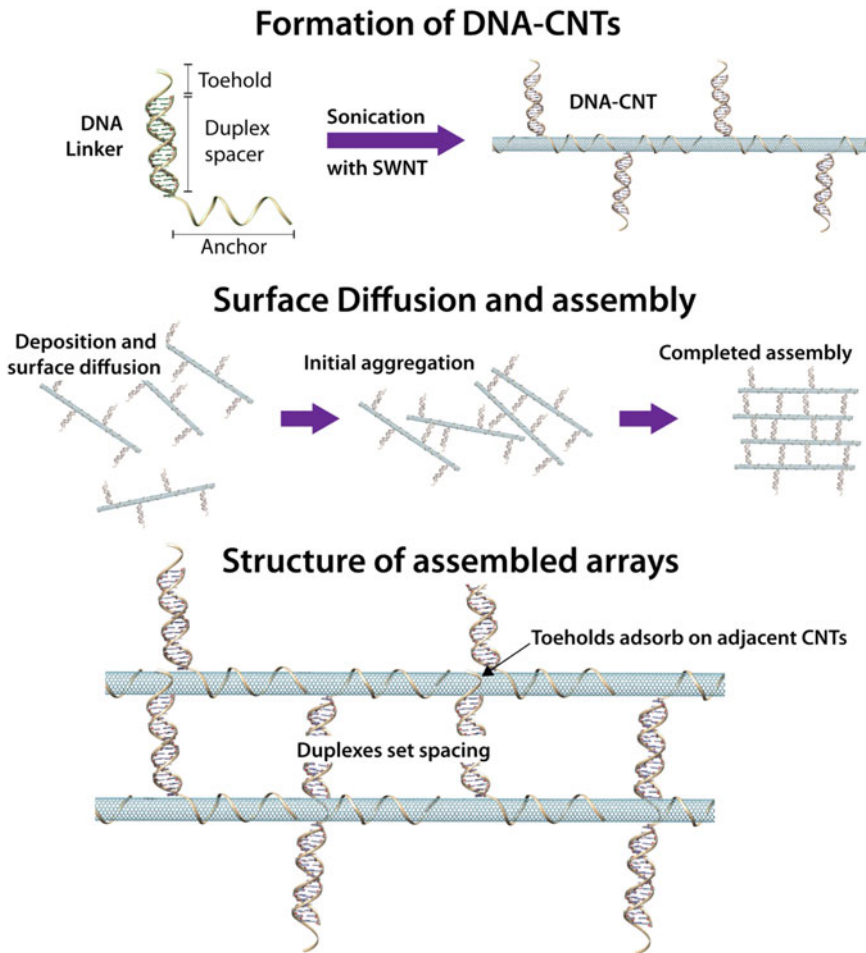


Fig. 1 Schematic of DNA-assisted CNT dispersion and the LISA process

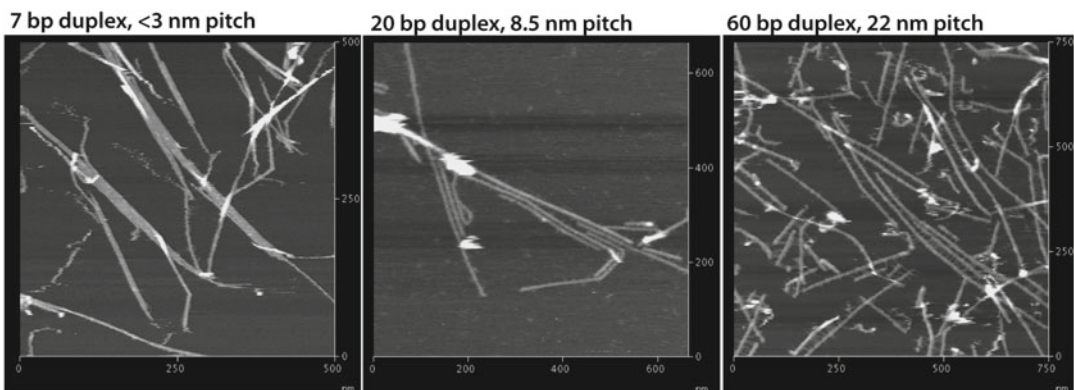


Fig. 2 AFM micrographs of DNA-CNT self-assembled arrays with three different duplex designs. The CNT pitch changes in accordance with the designed dsDNA spacer

We first disperse the CNTs with dsDNA linker construct (Fig. 1) and then implement the LISA process in three main steps as outlined in Fig. 3.

1. The DNA-CNTs are immobilized on a charged surface such as Muscovite mica or lipid bilayers via divalent cation mediated salt bridge interactions [14]. Both the CNTs and their attached linkers are aligned in-plane by the deposition substrate through electrostatic interactions.
2. Divalent Mg^{2+} cations are partially displaced by the addition of monovalent cations such as Na^+ to the solution, weakening the DNA interaction with mica. This disruption enables the DNA-CNTs to diffuse on the substrate in 2D while still associated with mica. As a result the toehold on DNA linkers can interact weakly with patches of exposed sidewall of nearby DNA-CNTs. Multiple weak sticky interactions between adjacent DNA-CNT stabilize and cooperatively bind them in parallel alignment. The inter-nanotube pitch is controlled with nanometer precision by modulating the length of the DNA duplex.
3. The mixture of divalent to monovalent ions is shifted to Mg^{++} by a gradual buffer exchange. This immobilizes the DNA-CNT array assemblies on mica that then can be dried or otherwise processed. Arrays assembled on either mica or DPPC can be then be transferred to other charged substrate via stamping.

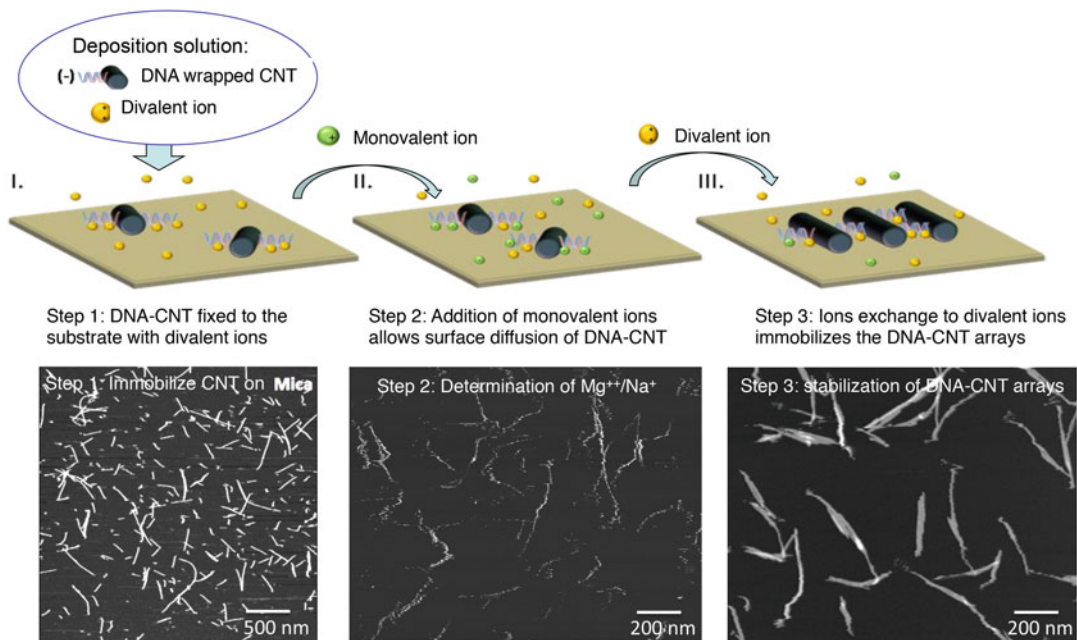


Fig. 3 Different steps to optimize LISA process for forming DNA-CNT arrays with precise CNT pitch and orientation

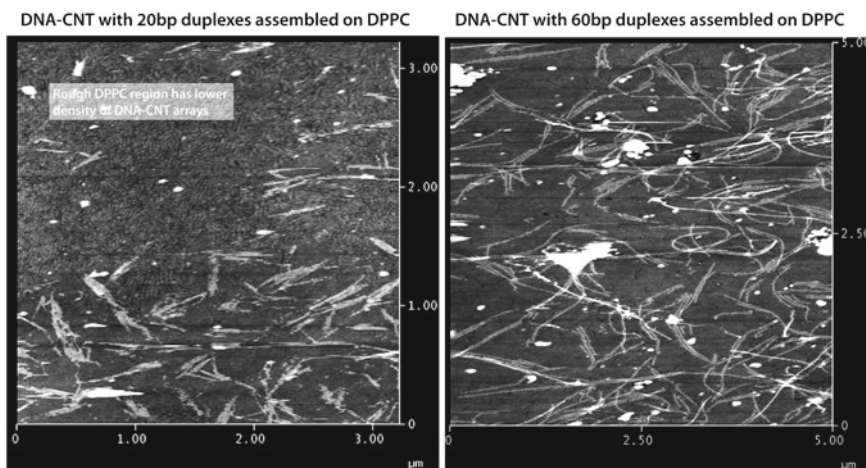


Fig. 4 AFM micrograph of the DNA-CNT arrays self-assembled on lipid-modified glass substrates. Rougher DPPC areas have lower DNA-CNT arrays

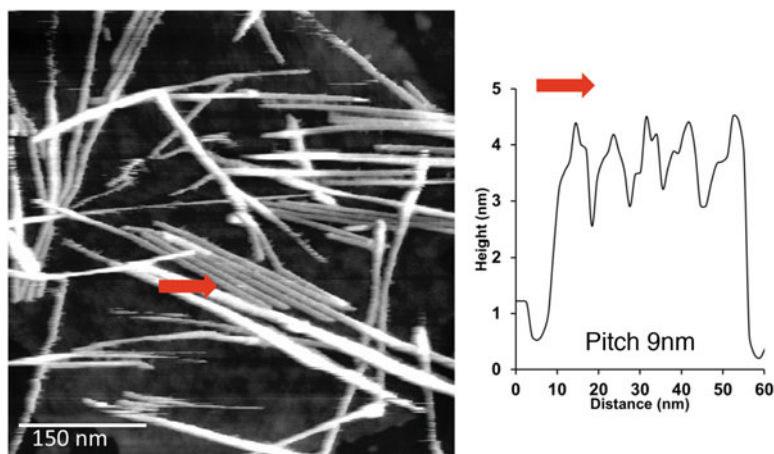


Fig. 5 AFM micrograph of the DNA-CNT arrays self-assembled on lipid-modified SiO_2 substrates

In our experience, LISA can be adapted to various charged substrates by simply varying salt, pH, temperature, etc. This chapter outlines a method for using lipid bilayers on glass and silicon dioxide for self-assembling DNA-CNT arrays (Figs. 4 and 5). It is most sensitive to the DNA-CNT dispersion quality. As DNA bases pi-stack onto the CNT walls to form the DNA-CNT conjugate, any residual surfactant or impurities that can displace DNA will adversely affect the DNA-CNT dispersion quality. For LISA process to be efficient and reproducible the CNT stock needs to be free from surfactants or other impurities.

2 Materials

1. DNA strands from Integrated DNA Technology.
2. Iso-nanotubes with 99, 95, and 90 % purity.
3. CoMoCat single-walled carbon nanotubes.
4. Ultrapure Millipore water from Millipore filtration system.
5. TAE buffer.
6. 1× TAE/Mg (10 mM tris-acetate, 1 mM EDTA, 12.5 mM magnesium acetate).
7. Master cycler.
8. DGU-sorted carbon nanotubes.
9. Bath sonicator.
10. Dipalmitoylphosphatidylcholine (DPPC) in powder form.
11. Sharp nitride lever probes for fluid AFM imaging from Bruker AFM probes.
12. Multimode and ICON AFM from Bruker.
13. Mica disk.
14. Steel mounting disks.
15. Electro dialyzer tank and dialyzer chambers.
16. 50K MWCO filters for electro dialyzer.

Images are collected by a Bruker Multimode VII system equipped with a fluid cell and a J scanner. The AFM was operated in tapping mode or peak force mode using the SNL silicon nitride soft contact mode AFM tips (2 nm nominal tip radius, smaller cantilevers used). Amplitude set point was typically ~150 mV, drive amplitude ~50–200 mV, integral gain of 1.5–2.5, frequency ~10 kHz, and scan rate is typically 1–3 Hz.

3 Methods

3.1 *Preparation of Surfactant-Free CNT Stock*

The dispersion of carbon nanotubes with DNA has been widely reported in literature [15]. However, most of studies involving the DNA wrapping of carbon nanotubes are done with small diameter, mixed chirality, CoMoCAT CNTs. For electronic devices, we use larger diameter, purified semiconducting, ARC discharge CNTs. Commercially available semiconducting CNTs are sorted using density gradient ultracentrifugation (DGU).

Briefly, during DGU, the CNTs are dispersed in aqueous solution in the presence of a combination of surfactants that selectively bind to different species of CNTs and thereby enhance the density differences between them. Surfactants typically include a combination of amphiphiles with anionic headgroups and alkyl tails like sodium dodecyl sulfate (SDS) and sodium dodecylbenzene sulfonate (SDBS) and/or bile

salts such as sodium cholate (SC). The surfactant-dispersed CNTs are usually placed in a density gradient column, centrifuged under very high relative centrifugal field, and induced to undergo spatial separation due to migration to different isopycnic point in the density gradient. Purified fractions of different CNT species after DGU have substantial surfactants present in the solution that can be washed away using solvents to create mats of dry CNTs.

We find that these mats have residual surfactant, which competes with the DNA interaction on CNT surface, and that this hinders the efficiency of DNA based self-assembly. In fact the residual concentration of the surfactant can shift the salt ratio required for LISA based assembly over a factor of 3. We have observed Mg^{2+}/Na^+ from as low as 0.2 to as high as 0.7. The magnesium to sodium ratio decreases with an increasing amount of residual surfactant on CNTs. This in turn adversely affects the stabilization of the DNA-CNT self-assembled structures after they form (step 3 in Fig. 3), leading to disruption of self-assembled structures even with the gentlest fluid displacement. In our experience, an Mg^{2+}/Na^+ ratio smaller than 0.35 starts affecting the stabilization step.

Thus, we have tested a few methods for cleaning the surfactant from the DGU-sorted CNTs and they have worked to varying degrees. Described here are the results for dry CNT stock preparation when starting from the surfactant dispersed aqueous CNTs that have not undergone any filtration. This provides a control for filtering CNT dispersions from high concentration surfactants. This method was tried with NanoIntegris's aqueous DGU chirality sorted CNTs (*see Note 1* for additional comments).

1. Fill the electro dialyzer tank with $1\times$ TAE/Mg buffer.
2. Place a 50 kDa MWCO membrane on one end of the dialyzer chamber and secure it tightly.
3. Add 1.5 ml CNT aqueous solution in the dialyzer chamber and close the chamber with another membrane.
4. Place the chamber in dialyzer tank and apply a voltage bias of 110 mV across the chamber for 1 h.
5. Turn off the voltage and reverse the chamber direction in the tank such that the membrane on the positive terminal side now faces the negative terminal side and vice versa.
6. Apply 11 mV voltage across the chamber for another 2 h. The CNTs will form a film and float off the membrane easily.
7. Remove the buffer from the tank and rinse the tank to remove white surfactant precipitated at the electrode.
8. Fill the tank with fresh the $1\times$ TAE/Mg buffer and replace the used membranes with new membranes while exchanging most of the solution in the chamber with $1\times$ TAE/Mg.
9. Set the bias voltage at 110 mV, run for 2 h, then switch the chamber to the opposite side, and run for another 2 h.

10. Repeat the above two steps four times.
11. Transfer the CNTs and liquid from the chamber to a vial.
12. Centrifuge the solution for 5 min at 20,000 rcf to get the CNTs crash to the bottom of the vial.
13. Decant the clear supernatant with pipette and replace it with equal volume of methanol.
14. Sonicate the vial quickly (10–15 s) to unbundle CNTs.
15. Repeat the methanol washing steps from centrifugation to collection of supernatant nine times.
16. Decant most of the clear supernatant and replace with water.
17. Centrifuge the vial for 20 min at 20,000 rcf to separate out the CNTs at the bottom.
18. Freeze the vial by plunging it into liquid N₂.
19. Open the cap and cover it with clean filter paper.
20. Place the vial in a 50 ml centrifuge tube and use lyophilization to obtain clean CNTs in dry form.

3.2 DNA-Linker Formation and CNT Dispersion

1. Make a 500 µl solution of 1× TAE/Mg with 33 M anchor strand and 36.3 M toehold strand. We first add the ultrapure water, then the appropriate volume of 10× TAE/Mg, followed by the anchor and toehold DNA strands.
2. Vortex and spin the DNA solution for few seconds. Anneal the strands together by heating up the solution to 90 °C and then cooling down to 20 °C at 1 °C per minute using the Eppendorf thermal cycler.
3. In a separate 2 ml microcentrifuge vial weigh out ~0.5 mg of solid CNTs and add the 500 µl of DNA-linker solution.
4. Wrap the cap of the vial with parafilm to avoid the cap from opening and causing any contamination during sonication.
5. Cool water in a bath sonicator to ~4 °C. Sonicate the CNT and DNA-linker mixture for 2 h at a constant temperature of 4 °C.
6. Centrifuge the DNA-CNT dispersion at 16,000 g for 90 min at 4 °C to remove the large CNT aggregates.
7. Carefully pipet out the stable DNA-CNT supernatant from any CNT pellet at the bottom of the vial and dispense it in a new microcentrifuge vial.
8. Store the final solution in appropriate aliquots at –80 °C to prevent slow aggregation of DNA-CNT over time.

This dispersion procedure is also compatible with other buffers. For example, dispersion using Na⁺-based buffers actually yields a higher concentration of DNA-CNTs than using Mg²⁺ ions (*see Note 2* for additional comments).

3.3 Determining DNA-CNT Concentration Needed for Self-Assembly

1. Cleave a circular, 1 cm diameter, mica piece that is attached to metal puck with glue. Make sure that the glue is retained under the mica and is not on the puck around mica.
2. In a high-humidity container, drop 2–5 μl of DNA-CNT solution on mica. Incubate for 5 min at room temperature.
3. Add 1 \times TAE/Mg buffer to bring the final volume to 100 μl .
4. Use tapping mode or peak force AFM technique in fluid to determine the DNA-CNT concentration on surface. We typically use Bruker Sharp Nitride Lever (SNL) probes.

The ideal DNA-CNT concentration for surface-based self-assembly is usually higher than ~ 20 CNTs/ μm . We typically find a starting DNA-CNT volume that provides the desired amount DNA-CNT in a few micron AFM scan and then optimize the $\text{Mg}^{2+}/\text{Na}^{+}$ ratio for DNA-CNT raft self-assembly conditions.

3.4 LISA Process for DNA-CNT Rafts on Mica

1. In high-humidity chamber, cast 2–3 μl of DNA-CNT on mica or as determined in Subheading 3.1.
2. Immediately add 17–18 μl of 1 \times TAE-Mg to bring the final volume to 20 μl and incubate for 5 min.
3. Add 50 μl of 1 \times TAE/Mg without mixing and incubate for 5 min.
4. Add 30 μl , of 1.5 M NaCl or NaOAc to bring the final volume to 100 μl .
5. Incubate using high-humidity container overnight at 33 $^{\circ}\text{C}$.
6. Add 25 μl of 1 \times TAE/Mg to the overnight incubation to increase the divalent cation concentration and incubate for 5 min at room temperature.
7. Add another 25 μl of 1 \times TAE/Mg to the overnight incubation to increase the divalent cation concentration and incubate for 5 min at room temperature.
8. Exchange the buffer to 1 \times TAE/Mg by removing 50 μl of the solution with a pipet, waiting 5 min for ions to reach equilibrium, and then by adding 50 μl of 1 \times TAE/Mg. Repeat the pipet assisted buffer exchange wash step five times. This step removes the unbound DNA-CNTs and immobilizes the bound CNTs on the surface of the mica.
9. For the final 50 μl buffer exchange, remove 50 μl of the buffer and add 50 μl of 10 mM nickel acetate-1 \times TAE/Mg mixture.
10. Using a pipet remove most of the buffer from the sample and serially dip the sample for 5 s in 30 ml of 20, 40 and 60% IPA consecutively and blow dry with compressed nitrogen.

We find that minimum volume of 100 μl of assembly buffer is required to do self-assembly studies using Bruker's fluid AFM setup.

Tapping mode AFM works best for visualizing the diffusion of DNA-CNT on mica substrate under fluid. For immobilized structures either the tapping mode or the peak force mode can be used.

The surface-based self-assembly optimization can be done by varying divalent to monovalent ionic ratio, temperature, concentration of DNA-CNTs, pH, etc. We typically start the experiments by immobilizing the DNA-CNT on mica using Mg^{2+} ions. Next we slowly add Na^+ ions to shift the equilibrium of Mg^{2+} and Na^+ ions at DNA/mica interface. This is visualized using real-time fluid AFM in tapping mode. Finally, at an appropriate Mg^{2+}/Na^+ ratio the DNA-CNT diffusion can be observed. We fix the Mg^{2+}/Na^+ ratio and vary the incubation temperature or time to obtain the optimal conditions for forming desired DNA-CNT rafts.

3.5 LISA Process for DNA-CNT Rafts on Lipid Modified Silica

1. Dissolve DPPC in 0.2 M NaCl and 0.01 M mono and disodium phosphate buffer (\sim pH 7.5) at 25 mg/ml concentration and form \sim 50 nm wide liposomes either using extrusion or sonication. The stock solution can be stored at 4 °C for 2 months.
2. Dilute lipid to 2.5 mg/ml concentration in either 1 \times TAE/Mg buffer or in 2 mM $CaCl_2$, 0.2 M NaCl, and 0.01 M mono and disodium phosphate immediately before forming lipid bilayer.
3. Deposit 30 μ l of spectroscopy-grade ethanol onto \sim 4 cm² pieces of glass cover slip, ignite it with a butane lighter, and allow it to burn. Repeat one or two times as needed. This step is performed just before lipid deposition and makes the glass substrate hydrophilic.
4. Add 50–100 μ l of 2.5 mg/ml DPPC to the glass substrate.
5. Seal in an airtight chamber and incubate in a Eppendorf PCR thermal cycler for 30 min at 50 °C. Cool down to room temperature at a rate of 1 °C every 10 s.
6. Wash the lipids on glass with a solution made of 1 \times TAE/Mg and 0.35 M NaCl buffer without exposing the surface to air. This is done by removing 50 μ l from the droplet with a pipette, adding 50 μ l of the washing solution, and repeating it 5–10 times.
7. Pipet off all buffer from substrate except for \sim 50 μ l of 1 \times TAE/Mg+0.35 M NaCl buffer.
8. Add 20 μ l of dispersed SWNTs in 1 \times TAEMg to the 50 μ l droplet.
9. Incubate at room temperature in a humidity-controlled chamber for at least 2 h.
10. Image under 1 \times TAE/Mg with 0.35 M NaCl buffer using tapping mode AFM.

3.6 LISA Process for DNA-CNT Rafts on Lipid Modified Thermal SiO₂

1. Extrude DPPC at 1–2 mg/ml in 0.2 M NaCl and 0.01 M Na₂HPO₄, at 50 °C for a minimum of 10–12 times and store at 4 °C until use.
2. Treat 3/4–1 cm² sized silicon substrates (100 nm thermally grown oxide) with reactive oxygen plasma for 10 s at 250 W just before use. Treated substrates can be kept under nitrogen for a few days before use.
3. Add 40 µl lipid solution on the wafer in a humidity-controlled container and incubate at 50 °C for 1 h.
4. Let the substrate equilibrate to room temperature for about 1–2 h.
5. Use pipet to vigorously wash the lipid film with 1× TAE/Mg at least ten times.
6. Observe the lipid bilayer quality using tapping mode AFM. If floating lipids are observed under the AFM, just wash a few more times.
7. Add 3–5 µl of neat DNA-CNT solution to the lipid films in 1× TAE/Mg and incubate for 5–10 min.
8. Place the sample in a humid chamber at room temperature (~18–22 °C), overnight.
9. Observe DNA-CNT raft assembly using tapping-mode fluid AFM. If needed samples can be gently washed with the buffer using a pipet to remove free DNA-CNT, etc.

At 4 °C the DPPC vesicles will eventually settle and may aggregate over time. Some settling of the vesicles has not been a problem for our experiments when used over the duration of a month. Using our lipid formulation it appears that longer O₂ treatments prevent good lipid film adhesion.

In principle, lipid films should be able to be cast with Mg⁺⁺ or Ca⁺⁺ and other divalent salts. However Ca⁺⁺ seems to produce the most stable films on silicon oxide preparation described here. In our experience, it is difficult to cast a stable lipid bilayer film using 1× TAE/Mg probably due to EDTA or phosphate chelation of the metal. Furthermore, we observe that with 0.1 M NaCl, the lipid films are uniform with little defects but with 0.01 M NaCl we get patchy films (*see Note 3* for discussion of AFM imaging of assembled rafts).

4 Notes

1. This cleaning method is not always required for NanoIntegris' DGU-sorted dry CNT films. The films are pre-washed by NanoIntegris. However, there is batch-to-batch "cleanliness" variation in the DGU sorted dry CNT films that can significantly affect the DNA-CNT self-assembly parameters. The LISA

process itself, once optimized, works under a wide range of salt conditions and is very consistent for a given stock of CNTs.

2. Final DNA-CNT dispersions in other buffers can be exchanged to Mg^{2+} buffer using spin filtration methods. For example, We have had good results dispersing the CNTs using 0.1 M NaCl as well as 0.1 M Na_2PO_4 and then exchanging them to magnesium-based buffer using YM-50 (50 KDa MWCO from Millipore) spin filter. This method was used for self-assembling DNA-CNTs onto large DNA nanostructures such as DNA origami, DNA ribbons, and DNA crystals. However, we have not optimized the DNA-CNT raft self-assembly conditions for such systems.
3. It is important that resolution of imaging would be set to the highest possible, and tapping force to the lowest as not to disrupt the film or the DNA-CNT self-assemblies. It helps to image lipid films at 1–3 μm scan sizes.

References

1. Avouris P (2009) Carbon nanotube electronics and photonics. *Phys Today* 62(1):34–40
2. Pfeiffer R, Pichler T, Kim YA, Kuzmany H (2008) Double-wall carbon nanotubes. In: Jorio A, Dresselhaus G, Dresselhaus MS (eds) *Carbon nanotubes: advanced topics in the synthesis, structure, properties and applications*. Springer, Heidelberg, Berlin, pp 495–530
3. Tulevski GS, Franklin AD, Frank D, Lobe JM, Cao Q, Park H, Afzali A, Han S-J, Hannon JB, Haensch W (2014) Toward high-performance digital logic technology with carbon nanotubes. *ACS Nano* 8(9):8730–8745
4. Zheng M, Jagota A, Strano MS, Santos AP, Barone P, Chou SG, Diner BA, Dresselhaus MS, Mclean RS, Onoa GB, Samsonidze GG, Semke ED, Usrey M, Walls DJ (2003) Structure-based carbon nanotube sorting by sequence-dependent DNA assembly. *Science* 302(5650):1545–1548. doi:10.1126/science
5. Maeda Y, Matsui H (2012) Genetically engineered protein nanowires: unique features in site-specific functionalization and multi-dimensional self-assembly. *Soft Matter* 8(29):7533–7544
6. Qun G, Chuanding C, Ravikanth G, Shivashankar S, Sathish A, Kun D, Donald TH (2006) DNA nanowire fabrication. *Nanotechnology* 17(1):R14
7. Willner I, Willner B (2001) Biomaterials integrated with electronic elements: en route to bioelectronics. *Trends Biotechnol* 19(6):222–230
8. Maune HT, S-p H, Barish RD, Bockrath M, Goddard IIA, RothmundPaul WK, Winfree E (2010) Self-assembly of carbon nanotubes into two-dimensional geometries using DNA origami templates. *Nat Nano* 5(1):61–66
9. Fink H-W, Schonberger C (1999) Electrical conduction through DNA molecules. *Nature* 398(6726):407–410
10. Surwade SP, Zhou F, Wei B, Sun W, Powell A, O'Donnell C, Yin P, Liu H (2013) Nanoscale growth and patterning of inorganic oxides using DNA nanostructure templates. *J Am Chem Soc* 135(18):6778–6781
11. Jones MR, Seeman NC, Mirkin CA (2015) Programmable materials and the nature of the DNA bond. *Science* 347(6224)
12. Han S-P, Maune HT, Barish RD, Bockrath M, Goddard WA (2012) DNA-linker-induced surface assembly of ultra dense parallel single walled carbon nanotube arrays. *Nano Lett* 12(3):1129–1135
13. Woo S, Rothmund PWK (2014) Self-assembly of two-dimensional DNA origami lattices using cation-controlled surface diffusion. *Nat Commun* 5:4889
14. Pastré D, Piétrement O, Fusil S, Landousy F, Jeusset J, David M-O, Hamon L, Le Cam E, Zozime A (2003) Adsorption of DNA to mica mediated by divalent counterions: a theoretical and experimental study. *Biophys J* 85(4):2507–2518
15. Zheng M, Jagota A, Semke ED, Diner BA, McLean RS, Lustig SR, Richardson RE, Tassi NG (2003) DNA-assisted dispersion and separation of carbon nanotubes. *Nat Mater* 2(5):338–342

Chapter 18

A Proximity-Based Programmable DNA Nanoscale Assembly Line

Xiaoyan Zhang, Xiaoqiang Ding, Jianzhou Zou, and Hongzhou Gu

Abstract

The assembly line is one of the key features of industrial production on the macroscopic scale, allowing programmability and sequential addition of parts to a final product. In this chapter, we use DNA to extend this notion to the nanoscale by the judicious combination of three DNA-based components: a DNA origami tile that provides a framework and track for the assembly process, three two-state DNA cassettes that can be programmed to donate cargo and are attached to the tile, and a DNA walker that can move on the track to collect cargo.

Key words Assembly line, DNA origami, DNA cassettes, DNA walker

1 Introduction

We often build products on the macroscopic scale by orienting two components together and then performing an operation to get them to cohere: riveting, welding or bolting metallic plates, screwing, nailing and gluing wood, sewing leather and textiles, or cementing bricks and stones. Assembly of a complex machine, such as an automobile, often takes place stepwise on an assembly line, where each construction task is broken down to its simplest components, and may be performed in part by independently programmable robots. The twentieth century, when assembly lines were developed, also witnessed impressive advances in chemical synthesis. Chemical synthesis differs from macroscopic assembly, because the precursors to conventional chemicals interact in all possible spatial orientations and positions, and products may result from the collisions of all molecules present, according to the laws of quantum mechanics and thermodynamics. In addition to continued progress in chemical synthesis, the early years of the twenty-first century have shown significant progress in nanoscience and nanotechnology. The aspects of nanoscience that are concerned with the construction of nanoscale species are clearly a subset of

chemistry, but there are potentially significant advantages to nanometer-scale assembly, owing to the relatively large sizes of the components. One of the potential strengths of nanoscale assembly is that it, too, holds the promise of programmed construction of target products by orienting and fastening individually selected components along an assembly line in a stepwise fashion.

One of the most convenient ways to prototype nanotechnological concepts is through structural DNA nanotechnology [1]. Using this approach, we have built a programmable assembly line on the nanoscale [2]. Any programmable assembly line requires three constituent parts: (1) devices whose states can be programmed to donate or not donate a component to the product; (2) a conveyor to move the growing product to the next station; and (3) a framework to position and orient the conveyor and the devices. For programmable devices, we have used a series of three cassettes (*see* Fig. 1 as an example, cassette-2 and cassette-3 are similar to cassette-1 in terms of structure and conformation except that they carry different gold nanoparticles) containing two-state programmable DNA-based nanomechanical devices [3, 4]; as a conveyor, we have used a novel DNA walker (*see* Fig. 2); to provide a framework, we have inserted the device-bearing cassettes [4, 5] into a DNA origami [6] tile, which also contains a track on which the walker can move (*see* Fig. 3). As the walker traverses its pathway along the origami tile, it encounters sequentially the three devices that contain components that can be added to the walker. If a device is programmed to add its component to the walker, a component will be transferred to the walker from the device; if the device is programmed not to donate the component, the transfer does not take place, and the walker will walk by it without receiving the component. Cargo donation (or not) is based on the proximity of the cargo component (or not) to the walker. The components consist of metallic nanoparticles tailed with a specific DNA strand. Including the null product, eight different products can be generated while walking, in response to the programming of the system.

Previously described walkers have been largely bipedal [7–10]. The walker used here has a different design (*see* Fig. 2); its walking structure is fundamentally triangular, based on a tensegrity triangle organization [11]. This walker has three “hands,” and four “feet,” all consisting of single-stranded DNA segments. The hands are used to accept and bind the cargo species that the walker can pick up. The feet make contact with the origami surface and are used for locomotion on the surface. The origami tile contains free single strands that provide a set of stations to which the walker’s feet can bind. To ensure the proper orientation of the walker towards the cargo sources, the fourth foot is bound at all stations where cargo is to be transferred from the two-state devices to the walker. Each step of the walker entails rotation of 120°; two steps are needed to move the walker

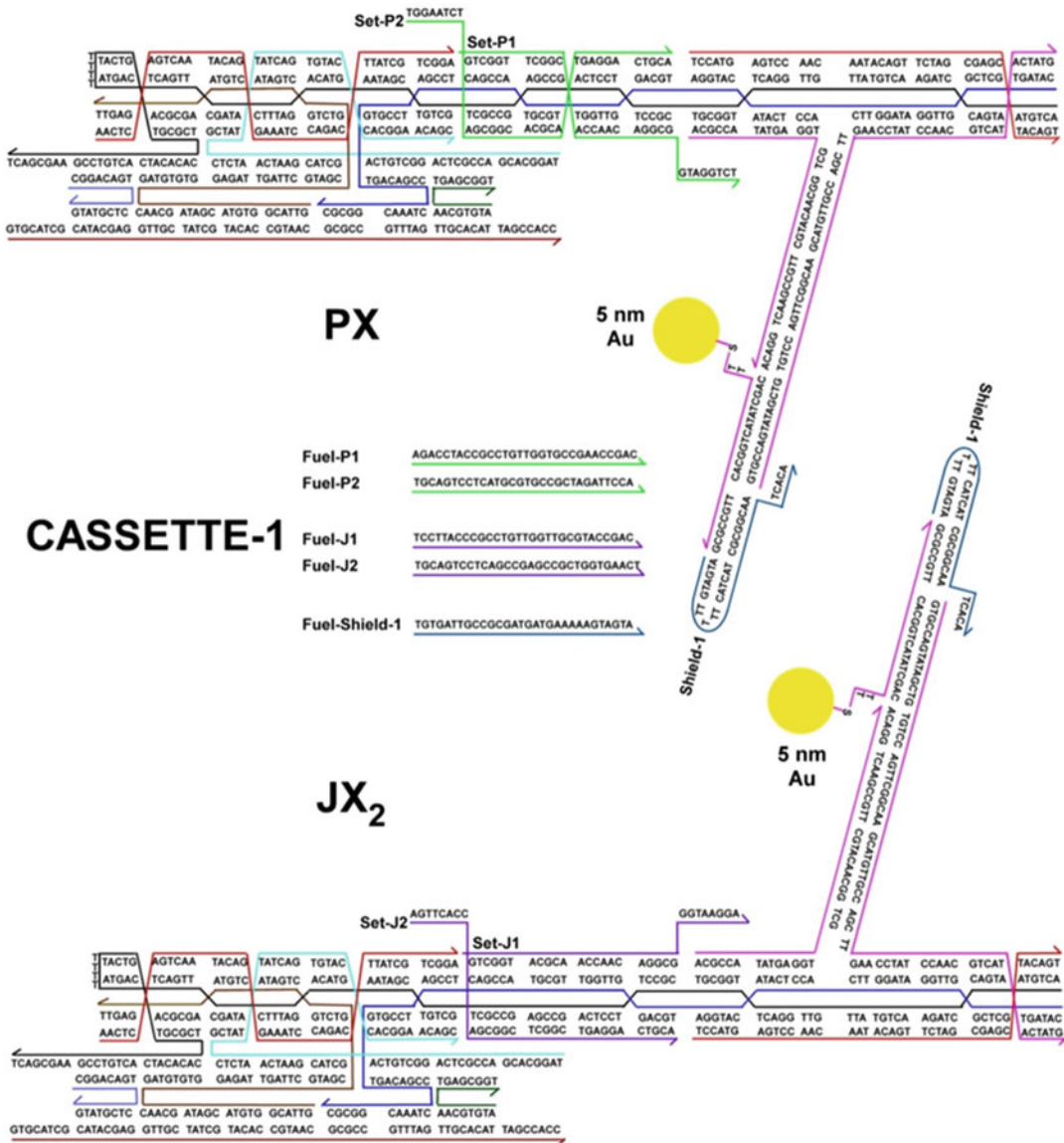


Fig. 1 Cassette-1 in the PX and JX₂ states. *Top*: PX state. *Bottom*: JX₂ state. Cassette-1 consists of five DNA duplexes. The bottom two duplexes form a DX motif, which can be inserted into the first slot of the origami by double cohesion. The top two duplexes form a PX/JX₂ motif and will stand out of the origami plane upon insertion. Strands Set-P1/2 and Set-J1/2 set the cassette to the PX and JX₂ state, respectively. Strands Fuel-P1/2 and Fuel-J1/2 are complementary to the set strands, which can be used to remove the set strands from the cassette. The fifth duplex acts like an arm and carries a 5 nm gold nanoparticle cargo through a thiol linkage. The overhang part of the cargo strand is protected by the Shield-1 strand, which can be removed by its complementary strand Fuel-Shield-1

from one cargo-transfer station to the next. All positional transitions of the walker and between the walker and the cargo-bearing arms are performed using the toehold-binding/branch migration methods of Yurke et al. [12].

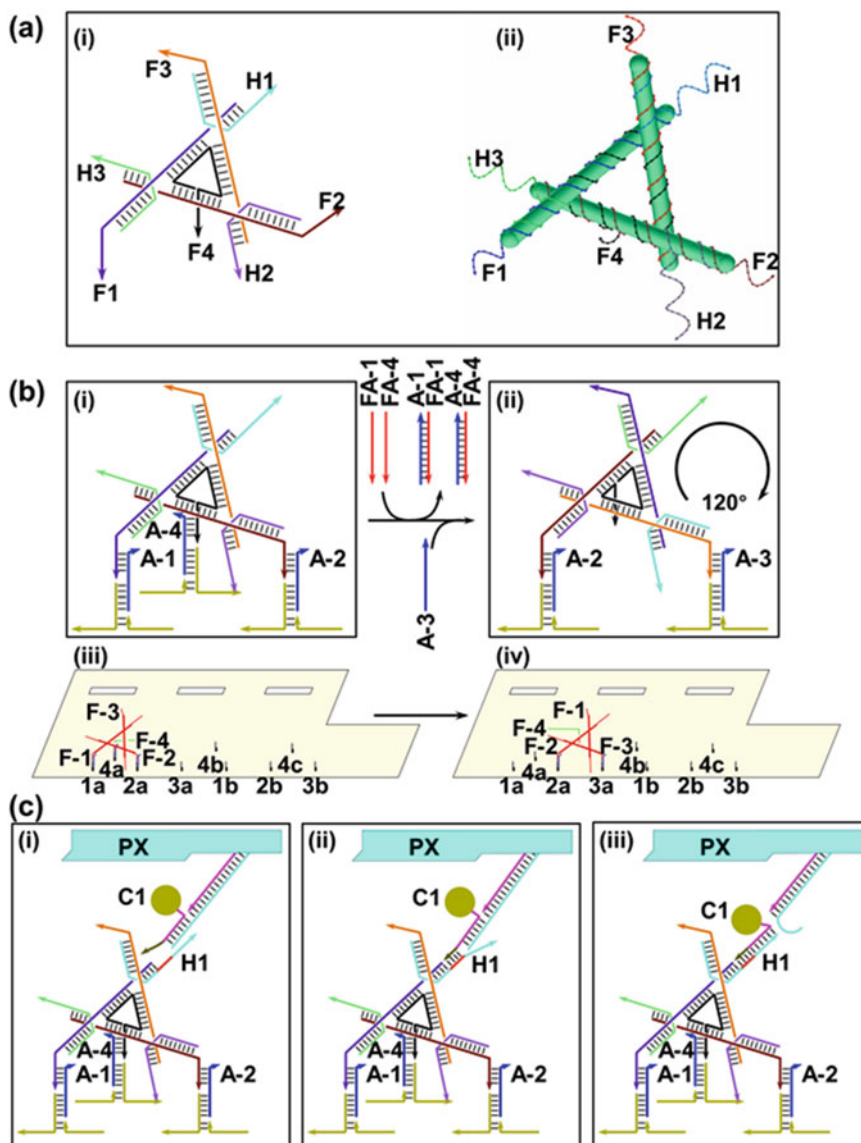


Fig. 2 Details of the walker, movement, and cargo transfer. **(a)** Walker structure. The drawing on the *left* is a stick figure indicating the three hands (H1-H3) and four feet (F1-F4). The image on the *right* shows the strand structure. **(b)** Movement. Walker reactions are shown in the upper two images, and movement on the origami is shown in the lower two images. A-*k* binds F*k* to the origami and FA-*k* is a fuel strand that removes A-*k*, undoing the corresponding binding. Foot-binding sites on the origami are labeled such that in its *n*th binding to the origami, F*k* binds to site *kn*. **(c)** Cargo transfer. The PX state bring the arm of cassette-1 close to H1 (*left*), the *brown* toehold binds its complement (*red; center*) and branch migration transfers the cargo strand to H1 (*right*)

2 Materials

Prepare all solutions using double-distilled water and analytical grade reagents. Prepare DNA samples at room temperature and store them at 4 °C. Diligently follow all waste disposal regulations when disposing waste materials.

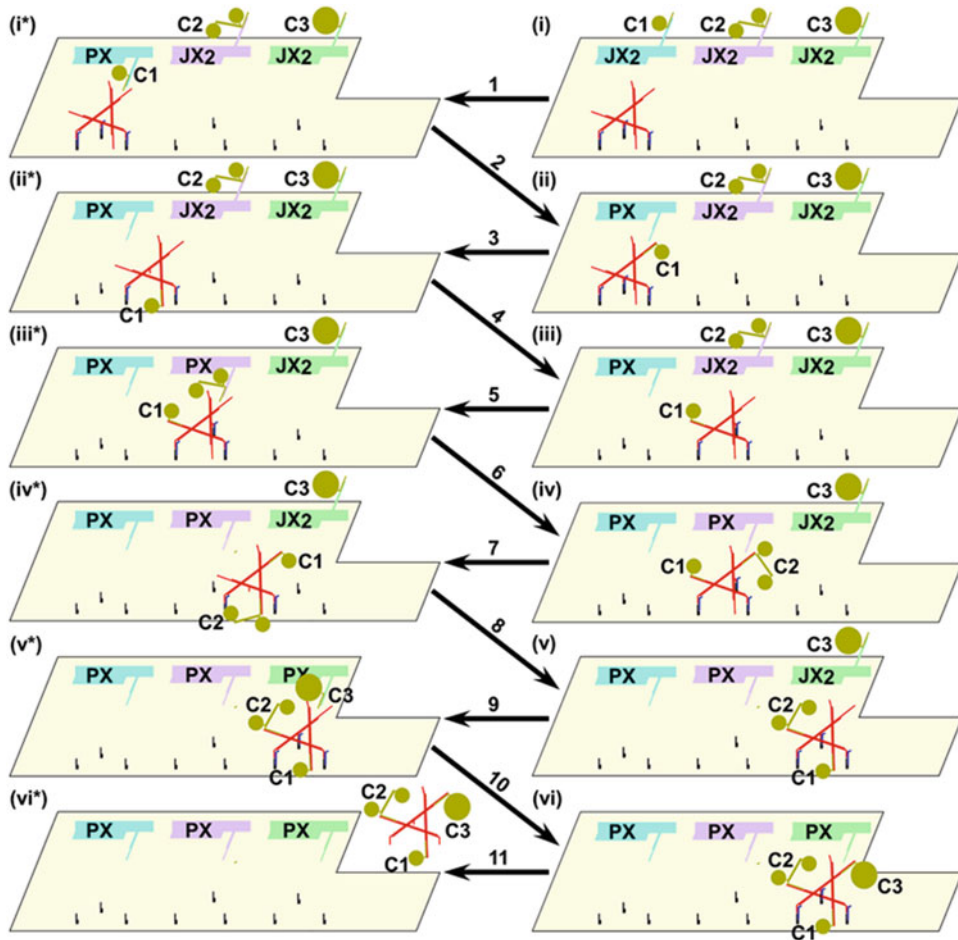


Fig. 3 The molecular assembly line and its operation. The basic components of the system are the origami tile (shown as a tan outline), programmable two-state DNA cassettes inserted in series into the tile (shown in blue, purple and green) and the walker (shown as a trigonal arrangement of DNA double helices in red). The cassettes have cargoes consisting respectively of a 5 nm gold particle (C1), a coupled pair of 5 nm particles (C2) and a 10 nm particle (C3) (indicated by green-brown dots), and their state can be PX (meaning on or “donate” cargo) or JX_2 (meaning off or “do not donate” cargo). In the example shown, the walker collects cargo from each cassette as it walk on the track (shown in black)

2.1 Buffers

1. $1\times$ TAE/Mg buffer (annealing buffer): 40 mM Tris-HCl, pH 8.0, 20 mM acetic acid, 2.5 mM EDTA, and 12.5 mM magnesium acetate.
2. Elution buffer: 500 mM Ammonium acetate, 10 mM magnesium acetate, and 1 mM EDTA.
3. $0.5\times$ TBE buffer: 89 mM Tris, 89 mM boric acid, 2 mM EDTA, pH 8.0.

2.2 DNA Oligonucleotides

1. Use *SEQUIN* [13] program to design DNA strands for the cassettes and walker molecules.

2. Synthesize DNA oligonucleotides on the DNA synthesizer using routine phosphoramidite chemistry, or purchase DNA oligonucleotides from companies.
3. Purify DNA strands by gel electrophoresis: Cut DNA bands out of 10–20% denaturing polyacrylamide gels. Elute DNA out of the gel slices in the elution buffer. Use ethanol (200 proof) in a volume ratio of 1:3 (buffer:ethanol) to precipitate DNA. Air-dry DNA pellet and resuspend DNA in deionized water. Quantify the concentration of each DNA strand by measuring the optical absorbance at 260 nm wavelength (OD_{260}).

2.3 Chemicals and Other Supplies

Bis (*p*-sulfonatophenyl) phenylphosphine dehydrate dipotassium salt (BSPP), sodium chloride, glycerol, gold nanoparticles, centrifugal cutoff filter, mica, AFM probes.

3 Methods

3.1 Preparation of Gold-DNA Conjugates

1. Mix 40 mg BSPP with 100 mL citrate-ion-stabilized gold nanoparticles (AuNPs) (*see Note 1*).
2. Stir the mixture overnight for ligand exchange.
3. Concentrate the mixture up to the micromolar range after phosphine coating (**steps 1 and 2**) by measuring the optical absorbance at 520 nm wavelength (OD_{520}).
4. Mix the gold nanoparticles from **step 3** with 5' end-thiolated (-SH) single-stranded (ss) DNA to a molar ratio of 1:1 (*see Note 2*).
5. Incubate the mixture in 0.5× TBE buffer containing 50 mM NaCl overnight at room temperature.
6. Separate gold-DNA conjugates carrying discrete numbers of copies of DNA strands by 3% agarose gel (*see Fig. 4*, running buffer 0.5× TBE, loading buffer 50% glycerol, 15 V/cm).
7. Collect the band (on the bottom) containing a 1:1 ratio of gold-DNA conjugates.
8. Electro-elute the conjugates into a pocket of dialysis membrane (molecular weight cutoff (MWCO), 10,000) at 10 V/cm for about 1 h.
9. Recover gold-DNA conjugates using a Microcon centrifugal filter device (MWCO, 50,000).
10. Quantify gold-DNA conjugates using OD_{520} .
11. Further stabilize the 1:1 gold-DNA conjugates by overnight incubation with short thiolated (-SH) oligonucleotides T₅-ssDNA ($[HS-T_5]/[Au] = 30$, in 0.5× TBE and 50 mM NaCl) at room temperature (*see Note 3*).
12. Use the same **steps 1–11** to prepare gold-DNA conjugates with differently sized gold (*see Note 4*).

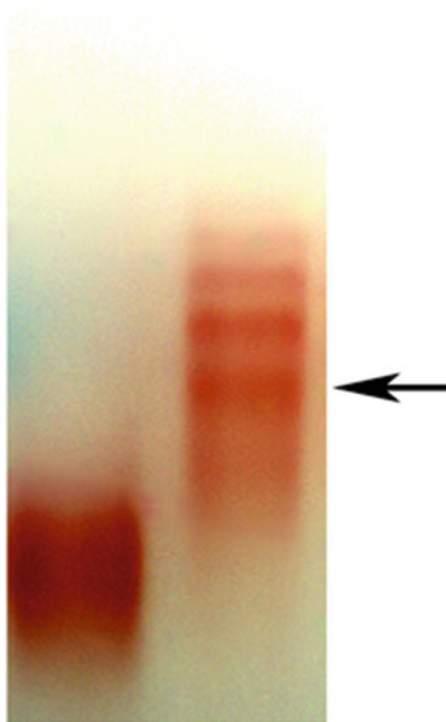


Fig. 4 Three percent agarose gels showing the gold-DNA conjugates. *Left lane:* Gold nanoparticles (AuNP) as a marker. *Right lane:* Gold-DNA conjugates. From *bottom to top*, each band corresponds to gold particles bearing an increased number of DNA strands. The first band (pointed out by an *arrow*) is collected for assembly of the cassettes

3.2 Formation of Hydrogen-Bonded DNA Devices

1. Stoichiometrically mix the component strands of a DNA device to a final concentration of 50 nM in 1× TAE/Mg buffer.
2. Heat the mixture to 70 °C in a 1 L water bath and let it cool to room temperature in about 16–20 h (*see Note 5*).
3. Confirm the formation and integrity of the DNA devices with non-denaturing polyacrylamide gel electrophoresis.

3.3 Formation of DNA Origami Tiles

1. Combine 5 μL of 30 nM (0.15 pmol) single-stranded M13 genomic DNA with the staple strands (1:5 molar ratio of M13 to staple strands) in 100 μL 1× TAE/Mg buffer. Please *see ref. [2]* for detailed sequence information of the staple strands.
2. Cool the sample from 90 to 60 °C on a thermo-cycling machine in 30 min.
3. Further cool the sample to 16 °C in 90 min.
4. Confirm the formation and integrity of the DNA origami with agarose gel electrophoresis and atomic force microscopy (AFM).

3.4 Purification of DNA Origami

1. Load 300 μL origami sample to a Microcon centrifugal filter device (MWCO, 50,000).
2. Spin the device at $300\times g$ for 10 min [14].
3. Discard the flow through and add 200 μL $1\times$ TAE/Mg buffer to wash the sample.
4. Spin the device at $300\times g$ for 10 min.
5. Repeat **steps 3** and **4** once.
6. Add 200 μL $1\times$ TAE/Mg buffer to the device.
7. Flip the device and spin the buffer down to a new tube.
8. Quantify the concentration of the purified origami sample by the measurement of OD_{260} .

3.5 Placing DNA Cassettes and Walker onto DNA Origami

1. Mix 200 μL of 1 nM (0.2 pmol) origami tiles with 4 μL each of 50 nM solutions containing cassettes-1, cassettes-2, and cassettes-3 (*see Note 6*) and the walker.
2. Add 0.2 pmol anchor strands A-1, A2, and A4 (*see Fig. 2b*).
3. Heat the mixture to 40 $^{\circ}\text{C}$ and slowly cool it to 4 $^{\circ}\text{C}$ over 1 day in a 2 L water bath placed in a sealed styrofoam box (*see Note 7*).
4. At room temperature, add equimolar quantities (0.2 pmol) fuel strands (*see Fig. 1*) to remove the shield strands on the DNA cassettes (*see Note 8*).

3.6 Walking on the DNA Origami

1. Add equimolar quantities (0.2 pmol) of fuel strands for anchor strands A-1 and A-4 to the system (*see Fig. 2b, see Note 9*).
2. Keep the system at room temperature for 2 h to remove the anchor strands and release the left foot of the walker.
3. Add equimolar quantities (0.2 pmol) of anchor strand A-3.
4. Keep the system at room temperature for another 2 h to bind the third foot of the walker with the corresponding extension of the origami helper strand.
5. Repeat 1–4 four times and walk the walker four steps to the end of the pathway (*see Note 10*).

3.7 Operation of Cassettes on the Origami

The default state of the three cassettes is JX_2 (OFF state), so the system begins with the state $(\text{JX}_2, \text{JX}_2, \text{JX}_2)$ (*see Note 11*). To switch to a different conformation, for example $(\text{JX}_2, \text{JX}_2, \text{PX})$ (*see Note 12*):

1. Add 4 μL each of 50 nM solutions containing strands Fuel-J1 and Fuel-J2 for cassette-3 to the 216- μL solution containing a 1:1:1:1:1 ratio of origami, cassette-1, cassette-2, cassette-3, and the walker.
2. Stir the solution 1 with a pipette for 5 min.

3. Keep the solution at room temperature for 2 h.
4. Add 4 μL each of 50 nM solutions containing strands Set-P1 and Set-P2 for cassette-3 to the solution.
5. Stir the solution with a pipette for 5 min.
6. Keep the solution at room temperature for 2 h.

3.8 Elution of the Walker Out of the Origami

1. Treat the system with the shield strands of the three cassettes for 2 h to protect the untransferred cargoes.
2. Add fuel strands of the walker to remove the anchor strands.
3. Keep the system at room temperature for 2 h and release the walker from the origami.
4. Treat the whole mixture with biotin-modified anchor strands (complementary with the extension part of strand 7 of the walker) at room temperature for 2 h.
5. Treat the whole mixture with magnetic streptavidin beads at room temperature for 45 min.
6. Place the mixture on a magnetic stand for another 45 min to allow the beads with the walkers to gather at the bottom.
7. Discard the supernatant liquid.
8. Add fuel strands (completely complementary with the biotin-modified anchor strands) to the system and release the walker from the beads.
9. Place the mixture on a magnetic stand for 45 min to allow only the beads to gather at the bottom.
10. Transfer the supernatant liquid (the walker) to another tube for TEM.

3.9 Atomic Force Microscopy Imaging by Tapping in Buffer

1. Spot 5 μL sample on freshly cleaved mica.
2. Leave the sample in the air to adsorb on mica for 2 min.
3. Add additional 25 μL of fresh $1\times$ TAE/Mg buffer to both the mica and the liquid cell.
4. Use commercial cantilevers with Si_3N_4 tips for buffer mode.
5. Perform AFM imaging on a NanoScope IV in “buffer in tapping mode.”

3.10 Atomic Force Microscopy Imaging by Tapping in Air

1. Spot 5 μL sample on freshly cleaved mica.
2. Leave the sample in the air to adsorb on mica for 1 min.
3. Wick out the excess sample from the mica with a piece of filter paper.
4. Wash the mica with 30 μL double-distilled water.
5. Wick out the water with a piece of filter paper.
6. Repeat 4–5 three times.

7. Cover the mica with a Petri dish.
8. Dry the mica in air for about 10 min.
9. Use commercial cantilevers with Si tips for air mode.
10. Perform AFM imaging on a NanoScope IV in “air in tapping mode” (*see* **Note 13**).

3.11 Transmission Electron Microscopy Analysis

1. Dip carbon-coated grid into DNA samples for 30 s.
2. Take the grid out and wick out the excess liquid with a piece of filter paper.
3. Place the grid on a piece of filter paper.
4. Cover the grid with a Petri dish and dry it in air for about 10 min.
5. Load the grid and collect TEM images on a JEOL 1200 EXII electron microscope operated at 60 kV.

4 Notes

1. Phosphine ligands lead to enhanced stability against higher electrolyte concentrations. It is necessary to replace citrate ions around gold nanoparticles with phosphine. Otherwise aggregation will form during the following concentration step.
2. If the thiolated ssDNA is shorter than 50 bases, we added equimolar complementary strand to make a duplex and increase the size of DNA. This gave us better separation of gold-DNA conjugates with different numbers of copies of DNA on the 3% agarose gel.
3. Short DNA components provide additional stability against the higher electrolyte concentrations necessary for DNA self-assembly.
4. Gold nanoparticles are chosen as cargoes because they can be easily visualized under AFM and TEM. Cargoes that can be carried by this assembly line should not be limited to nanoparticles. In principle, any small molecules that can be attached to DNA are good cargo candidates.
5. High temperature may cause the aggregation of gold-DNA conjugates. Annealing samples with gold nanoparticles above 70 °C is not recommended.
6. Previously we reported a DNA cassette that consisted of a sequence-programmable PX-JX2 device [3], combined with a domain for inserting it into a 2D DNA array; the state of the device can be switched when the cassette is inserted into an array [4]. In contrast to previously reported cassettes, those used here are held to the origami by double cohesion (two helices, each

with a sticky end, *see* Fig. 1), because this stronger interaction has proved more effective in several contexts [15, 16].

7. The three cassettes and the walker are assembled to their corresponding positions on the origami at the same time. Increasing temperature promotes the base-pairing interactions between cassettes and origami or walker and origami. However high temperature could denature the preformed cassettes, walker, or even origami. We found that starting the annealing at around 40 °C gave us over 90% yield of the successful placement of DNA cassettes and walker onto origami.
8. All cargo strands on the three cassettes are protected by the shield strands (Fig. 1). By doing so, cargo strands will not transfer from the cassettes to the walker during the process of placement of DNA cassettes and walker onto origami. Once the cassettes and the walker are settled on the origami, those shield strands are removed to expose the toehold of the cargo strands. Now the cassettes are ready for switching “on” to deliver cargo strands.
9. Each anchor strand (and each shield strand for cassettes) has unique sequences; thus to remove it a specific fuel strand is required.
10. Only foot 1–3 are involved in walking. The fourth foot positions the walker body close to the cassette whenever the walker pass by the transfer station near the cassette. For each step of walking, the walker rotates its body 120°.
11. To perform the assembly line with different kinds of cargo additions to the walker, we have preprogrammed the cassettes to the desired state before binding to the origami or dynamically switched the cassettes to the desired state during the walking process. The two methods generated almost the same results. And only the latter has been discussed in this protocol.
12. The PX-JX₂ device [3] is a two-state DNA nanomechanical machine; the two states (termed “PX” and “JX₂”) differ from each other by a half-rotation of one end relative to the other. In addition to these nanomechanical devices, the cassettes can also contain a robot arm [4], whose position is switched by the action of the device. These arms carry cargo components that can be added to the walker. Three of these independently programmable cassettes are used as the programmable elements in the assembly line [*see* ref. [2], figures S2–S4 for sequences]. In the PX state, a cargo particle can be added, because the particle and the walker are in proximity, but in the JX₂ state, it cannot be added, because the cargo particle is oriented away from the walker, and transfer of the cargo to the walker requires the proximity of these two components.

13. The tapping in air mode of AFM results in only the nanoparticles and the origami being visible. The individual nanoparticle components are not individually resolved. As more individual nanoparticles are added to the walker, under AFM we see the size of the nanoparticles increasing. To clearly visualize the pattern of nanoparticles on the walker, TEM experiment is performed.

Acknowledgements

H.G. thank members of the Seeman laboratory for helpful discussions. H.G. was supported by China “Thousand Youth Talents” (KHH1340004) and Fudan University startup (JJH1340110) grants.

References

1. Seeman NC, Lukeman PS (2005) Nucleic acid nanostructures. *Rpts Prog Phys* 68:237–270
2. Gu H, Chao J, Xiao SJ, Seeman NC (2010) A proximity-based programmable DNA nanoscale assembly line. *Nature* 465:202–205
3. Yan H, Zhang X, Shen Z, Seeman NC (2002) A robust DNA mechanical device controlled by hybridization topology. *Nature* 415:62–65
4. Ding B, Seeman NC (2006) Operation of a DNA robot arm inserted into a 2D DNA crystalline substrate. *Science* 314:1583–1585
5. Gu H, Chao J, Xiao SJ, Seeman NC (2009) Dynamic patterning programmed by DNA tiles captured on a DNA origami substrate. *Nat Nanotech* 4:245–249
6. Rothmund PWK (2006) Scaffolded DNA origami for nanoscale shapes and patterns. *Nature* 440:297–302
7. Sherman WB, Seeman NC (2004) A precisely controlled DNA bipedal walking device. *Nano Lett* 4:1203–1207
8. Shin JS, Pierce NA (2004) A synthetic DNA walker for molecular transport. *J Am Chem Soc* 126:10834–10835
9. Bath J, Green SJ, Allen KE, Turberfield AJ (2009) Mechanism for a directional, processive and reversible DNA walker. *Small* 5:1513–1516
10. Omabegho T, Sha R, Seeman NC (2009) A bipedal DNA Brownian motor with coordinated legs. *Science* 324:67–71
11. Liu D, Wang W, Deng Z, Walulu R, Mao C (2004) Tensegrity: construction of rigid DNA triangles with flexible four-arm junctions. *J Am Chem Soc* 126:2324–2325
12. Yurke B, Turberfield AJ, Mills AP Jr, Simmel FC, Newmann JL (2000) A DNA-fuelled molecular machine made of DNA. *Nature* 406:605–608
13. Seeman NC (1990) De novo design of sequences for nucleic acid structure engineering. *J Biomol Struct Dyn* 8:573–581
14. Ke Y, Lindsay S, Chang Y, Liu Y, Yan H (2008) Self-assembled water-soluble nucleic acid probe tiles for label-free RNA hybridization assays. *Science* 319:180–183
15. Ding B, Sha R, Seeman NC (2004) Pseudo-hexagonal 2D DNA crystals from double crossover cohesion. *J Am Chem Soc* 126:10230–10231
16. Constantinou PE, Wang T, Kopatsch J, Israel LB, Zhang X, Ding B, Sherman WB, Wang X, Zheng J, Sha R, Seeman NC (2006) Double cohesion in structural DNA nanotechnology. *Organic Biomol Chem* 4:3414–3419

DNA Walkers as Transport Vehicles of Nanoparticles Along a Carbon Nanotube Track

Jing Pan, Tae-Gon Cha, Haorong Chen, Feiran Li, and Jong Hyun Choi

Abstract

DNA-based molecular motors are synthetic analogs of naturally occurring protein motors. Typical DNA walkers are constructed from synthetic short DNA strands and are powered by various free energy changes during hybridization reactions. Due to the constraints set by their small physical dimension and slow kinetics, most DNA walkers are characterized by ensemble measurements that result in averaged kinetics data. Here we present a synthetic DNA walker system that exploits the extraordinary physicochemical properties of nanomaterials and the functionalities of DNA molecules, which enables real-time control and monitoring of single-DNA walkers over an extended period.

Key words DNA walker, Carbon nanotube, Quantum dot, DNA enzyme, Photo-regulation

1 Introduction

Synthetic oligonucleotides have been used to construct molecular motor systems composed of a short nucleotide walker strand hybridized with its complementary stator strands on a track. DNA's ability of specific base-pairing and multiple pathways to modulate their reaction kinetics enable various walker designs. The covalent modification of nucleotide strands also expand the library of possible walking mechanisms. Multiple chemical groups have been devised to construct DNA walkers that move autonomously and processively with controlled kinetics [1, 2].

Most DNA walkers have dimensions about several nanometers and several orders of magnitude slower kinetics compared to microtubule-based intracellular protein motors such as kinesins and dyneins. Due to these constraints, DNA walker systems are usually characterized by ensemble measurements such as gel electrophoresis [3, 4] and fluorescence resonance energy transfer (FRET) spectroscopy [5, 6]. These methods access kinetic information by analyzing accumulated signal output across the entire sample, while detailed insights on single walker behaviors are lost

during ensemble averaging. Single walker characteristics, when combined with statistical analysis, can reveal important aspects of the design and fabrication of DNA walker systems including the assembly quality, stepping yields, and walking processivity. Single molecule probing methods including atomic force microscopy (AFM) imaging [7, 8], optical particle tracking [9, 10], and single-molecule FRET [11, 12] have recently been demonstrated to be powerful experimental platforms for DNA walker studies. Design principles are extracted from single-molecule measurements, which lead to successful demonstration of a high-performance DNA walker system [13].

Here we present a deoxyribozyme (DNA enzyme or DNAzyme)-based walker system that moves on a carbon nanotube decorated with RNA fuel molecules, transporting a quantum dot (QD) (Fig. 1a) [9]. In particular, DNAzyme walker strands (green/red in Fig. 1a) are used as passivation ligands on a CdS QD (yellow sphere), which serves as both a cargo and an optical probe. RNA fuel strands (blue) adsorb onto a single-walled carbon nanotube (SWCNT), forming a linear, near-IR fluorescent track. The walker strand (*E*) consists of an enzymatic core (green) and two recognition arms (red). Initially, the DNAzyme conjugates with a fuel strand (*S1* in Fig. 1b) onto SWCNT surface. The enzymatic core cleaves the RNA strand in the presence of divalent metal cations (M^{2+}). After cleavage, the DNAzyme/RNA complex *ES1* becomes unstable and the walker strand migrates to the next RNA fuel strand (*S2*) forming a new complex *ES2*, as *ES2* is thermodynamically more favorable. The walker system completes this process repeatedly, resulting in autonomous and processive walking along the track. The visible fluorescence of the CdS QD is imaged over time against the near-IR fluorescence of the SWCNT to obtain the displacement and velocity of the walker system.

The system combines the stable optical signals from nanomaterials (i.e., QD and SWCNT) with the chemical functionality of DNA/RNA molecules to enable real-time tracking of a single walker over a long period. Design parameters including enzyme core type, recognition arm lengths, and environmental factors are

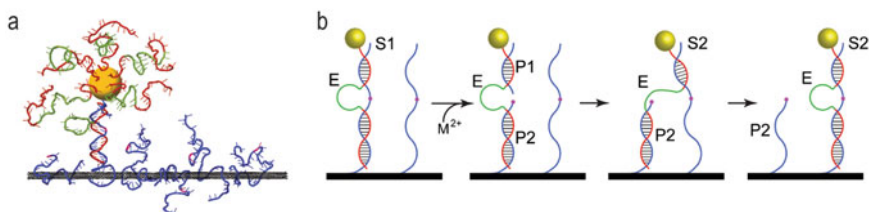


Fig. 1 (a) Schematic of the walker design (reprinted with permission from [9]. Copyright (2014) Nature Publishing Group) (b) Walking mechanism. M^{2+} denotes metal cations. E is the DNAzyme sequence. S1 and S2 are two adjacent RNA fuel strands. P1 and P2 are the upper and lower recognition arm after enzymatic cleavage (reprinted with permission from [13]. Copyright (2015) American Chemical Society)

identified and optimized to yield a walker that travels over 5 μm at a speed of 1 nm/s. Chemical and photochemical methods are demonstrated to regulate the walking kinetics [13].

2 Materials

All samples and buffers are prepared in deionized (DI) water (resistance = 18 M Ω). All chemical compounds are purchased from Sigma Aldrich unless specified otherwise.

2.1 DNA Walker Assembly

1. DNA sequence information: All DNA samples are purchased from Integrated DNA Technologies, Inc. and used without further purification. The DNAzyme and corresponding RNA substrate sequences are listed in Table 1. All strands are solubilized in DI water to make 1 mM final nucleotide concentration. The solution is then stored in $-20\text{ }^{\circ}\text{C}$.
2. Carbon nanotubes: Carbon nanotubes synthesized by two methods are used for walker track preparation. HiPco SWCNTs are purchased from NanoIntegris and CoMoCAT SWCNTs are obtained from SouthWest Nanotechnologies. Sodium cholate (SC) is used as surfactant to disperse SWCNTs in aqueous environment (*see Note 1*). Dialysis membrane tubes of 12–14 and 100 kDa molecular weight cutoff (MWCO) are used for surfactant exchange.

Table 1
Sequence of DNAzyme and corresponding RNA fuel strands

Nucleic acids	Sequence ^a
10–23 Enzyme	5'-AGT GCT GAT TCG GAC AGG CTA GCT ACA ACG AGA GTG ACT TT-3'
10–23 RNA fuel	5'-GTC ACT CrArU GTC CGA ATC AGC ACT TTT TTT TTT T-3'
8–17 Enzyme	5'-CCC GCA CCC CGC ACC CTC CGA GCC GGA CGA AGT TAC TTT T-3'
8–17 RNA fuel	5'-AGT AAC TrArG GGG TGC GGG GTG CTT TTT TTT TT-3'
Bipartite enzyme	5'-AGG CTA GGC TAG GCT AAG GAG GTA GGG GTT CCG CTC CAA TTC CTT T-3'
Bipartite RNA fuel	5'-GGA ATT GrArA CGA TAG CCT AGC CTA GCC TTT TTT TTT TT-3'
DZ7 enzyme	5'-AAT CGC AAG AAT CGG CAC GGC GGG GTC CTA TGT GGA GAC ACC TTT AGG TAA GGT GTG CAC GGA TTT-3'
DZ7 RNA fuel	5'-TCC GTG CTrG TGG TTC GAT TCT TGC GAT TTT TTT TTT TT-3'
Azo 10–23 enzyme	5'-AGT GCT GAT TCG GAC AGG CTA GCT ACA ACG AGA G/Azobenzene/TG ACT TT-3'

^a7/16-nt upper/lower recognition arm length is used for all cases with various enzymatic cores and in photo-regulation experiment. rArU is the RNA base and is the cleavage point

3. CdS QDs: Cadmium chloride (CdCl_2) is used as Cd^{2+} source. Sodium sulfide (Na_2S), purchased from Fisher Scientific, is used as S^{2-} source. DNAzyme strands are used as capping ligands to stabilize the synthesized CdS nanocrystals.
4. Dialysis buffer: 1× Trisaminomethane (Tris)-buffered saline with ethylenediaminetetraacetic acid or EDTA (TBS-EDTA): 20 mM Tris, 100 mM NaCl, 1 mM EDTA. 10× TBS-EDTA buffer is first prepared and subsequently diluted ten times upon usage (*see Note 2*).
5. Imaging buffer: 1× Tris-acetate (TA) buffer: 40 mM Tris. 50× TA buffer is first prepared by adding 242 g Tris base and 57.1 mL glacial acetic acid to 1 mL DI water. The pH of the prepared TA buffer is around 8.6. Acetic acid is used to adjust pH to 8. Metal (e.g., Mg^{2+} , Ca^{2+} , K^+) acetate solutions corresponding to designed experimental conditions are used to dilute the 50× TA buffer to final (1×) concentration.

2.2 Imaging Surface

1. Flow chamber components: Quartz slides and #1 (0.15 mm) cover slips, 1" polyimide double-sided tape, 10 μm Tygon tubing, 3 mL syringe, stainless steel needle.
2. Agarose film: Add 40 mg agarose powder into 2 mL DI water to make 2 wt.% agarose gel solution.

2.3 Equipment

Cole-Parmer ultrasonic processor, Beckman Coulter Optima Ultracentrifuge, Jobin Yvon Fluorolog-3 fluorometer, PerkinElmer Lambda 950 spectrophotometer, Branson benchtop sonicator, Carl Zeiss Axio Observer D1 microscope, Andor iXon 3 electron-multiplying charge-coupled device (EMCCD, 512 × 512 pixels), OMA-V 2-D liquid N_2 -cooled InGaAs camera (Princeton Instruments, 320 × 256 pixels), 405 and 658 nm diode lasers, and Newport Xenon arc lamp with filter set.

3 Methods

3.1 Sample Preparation

1. Surfactant-dispersed SWCNTs: Add 15 mg SWCNTs and 0.6 g SC to 30 mL DI water. This makes 2 wt.% SC concentration to ensure SC micelle formation. Probe-sonicate the mixture in ice bath for 1 h at 20 W. Remove the sonicated mixture from the ice bath and carefully weigh out an equal amount of solution in two Beckman centrifuge tube. Ultracentrifuge for 4 h at 134,000 × *g*. The top 70% supernatant is pipetted out from the centrifuge tube and stored in the dark at $-4\text{ }^\circ\text{C}$ (*see Note 3*).
2. DNA-dispersed SWCNTs: Prepare 1× TBS-EDTA buffer by adding 200 mL 10× buffer to 1800 mL DI water in a 2000 mL beaker. Add 100 μL of 1 mM RNA solution to 500 μL of SC-SWCNT solution in a 12–14 kDa MWCO membrane and

dialyze against $1\times$ TBS-EDTA buffer. Change buffer every 4 h four times, and then leave it overnight before taking the solution out of the dialysis membrane. An entire bottle of 1 L $10\times$ TBS-EDTA buffer and 24-h dialysis time should be used to obtain well-dispersed RNA-SWCNT sample (*see Note 4*). The RNA molecules self-assemble onto the nanotube sidewall through π - π stacking, while the SC molecules are gradually removed from the porous membrane. A second-stage dialysis is performed by replacing the 12–14 kDa membrane with 100 kDa membrane and dialyze for another 24 h. The excess free RNA strands that are not on the nanotube sidewall are removed from the second-stage dialysis.

3. Characterization of SWCNTs: SWCNT absorption (optical density or O.D.) at 632 nm is used to determine its concentration with the extinction coefficient of 0.036 O.D. $\text{mL } \mu\text{g}^{-1} \text{cm}^{-1}$. RNA concentration is determined by O.D. at 260 nm after subtracting SWCNT absorption background (*see Note 5*). RNA-SWCNTs display red-shifted optical signatures compared to SC-SWCNTs [14], which is then used to confirm the successful replacement of SC on the nanotube surface with RNA molecules after dialysis. SWCNTs with different chirality, indexed by chiral vector (n,m) , have distinct emission signatures [15]. The prevalent SWCNT species in the sample can be identified by measuring the photoluminescence excitation spectra (Fig. 2a).
4. DNA passivation of CdS QD: Mix $30 \mu\text{L}$ of 1 mM DNAzyme solution and $120 \mu\text{L}$ of 5 mM CdCl_2 solution in a glass vial. A magnetic stirrer is placed in the vial for stirring. $60 \mu\text{L}$ of 5 mM Na_2S is subsequently added to the vial with vigorous stirring, initiating the nucleation of nanocrystals (*see Note 6*). The solution turns light yellow upon Na_2S addition. $100 \mu\text{L}$ of TA buffer is added to the glass vial and incubated at 150 rpm for 6 h in the dark. The incubation allows the nucleated CdS nanocrystals to grow and ripen. As-synthesized nanocrystals are washed by a non-solvent method to remove unreacted excess precursors and DNAzymes. An equi-volume mixture ($300 \mu\text{L}$ each) of 3 M NaCl solution and isopropanol is mixed with the QD solution. The mixture is centrifuged at $18,000\times g$ for 10 min. The supernatant is discarded and the yellow pellet is re-dispersed by 30-s bath sonication in $100 \mu\text{L}$ $1\times$ TA buffer.
5. Characterization of CdS QDs: The concentration of the CdS QDs is characterized by the optical absorption based on the correlation proposed by Peng et al. [16]. The number of DNAzymes per CdS nanoparticle is determined by the concentration ratio of DNA vs. QD (*see Note 7*). TEM images are used to determine the size distribution of CdS nanocrystals. The average nanocrystal size is correlated to the emission peak wavelength. The nanocrystal obtained from the process

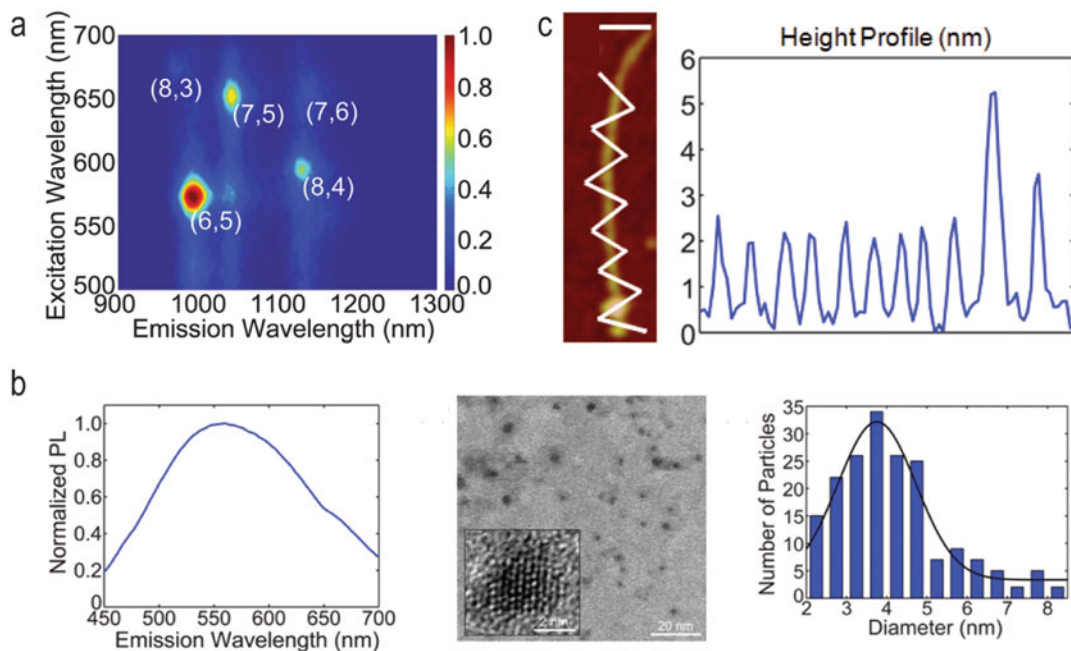


Fig. 2 Characterization of walker assembly. **(a)** Photoluminescence excitation spectra of RNA-SWCNT showing emission maxima from various nanotube species. **(b)** Optical emission spectrum and TEM images of the DNAzyme-CdS sample. The scale bar in the TEM image is 20 nm. Statistical analysis of the particle distribution from TEM images shows a particle size around 3.5 nm. **(c)** AFM image of a DNAzyme-decorated QD on an RNA-functionalized SWCNT. The scale bar is 100 nm. The height profile along the *white line* on the left column shows the RNA-wrapped SWCNT has a diameter of approximately 2 nm (reprinted with permission from [9]. Copyright (2014) Nature Publishing Group)

described here is around 4 nm with fluorescence emission centered at ~550 nm (Fig. 2b).

6. Conjugation of SWCNTs with QDs: RNA-SWCNT and DNA-CdS solutions are mixed at an equimolar ratio in $1\times$ TA buffer. Typically, a 10^4 -fold dilution of the as-synthesized DNA-CdS solution is required to achieve roughly a single nanocrystal per nanotube. The mixture is then incubated for 48 h at room temperature in dark for conjugation *via* DNA base-pairing.
7. Characterization of conjugation: The conjugation mixture is deposited onto freshly cleaved mica surface with equal volume of $1\times$ TA buffer containing 12.5 mM Mg^{2+} ($1\times$ TA- Mg^{2+} (12.5 mM)). The mica surface is incubated with the sample solution for 5 min. After incubation, the surface is washed by adding 90 μ L DI water and dried with compressed air. AFM measurement confirms the conjugation stoichiometry of SWCNTs and QDs (Fig. 2c).

3.2 Optical Measurements

1. Drill two 1 mm holes approximately 30 mm apart on the quartz slides for the inlet and outlet of a flow channel (*see Note 8*).

2. **Cleaning:** Place slides and cover slips in a staining jar. Add DI water and bath-sonicate for 10 min to remove dirt and contaminants. Rinse with DI water three times. Add acetone and bath sonicate for 10 min to remove water-insoluble dirt. Rinse with DI water three times. The cleaned slides and cover slips are dried using compressed air and stored in slide holder at 4 °C.
3. **Agarose film polymerization and sample immobilization:** Heat 2 wt.% agarose gel solution to 95 °C in a water bath. An aliquot of 100 μL of the heated agarose gel solution is spread on a clean cover slip for 12 h at room temperature. The solution of QD-SWCNT conjugates (30 μL) is deposited on the dried agarose film and evaporated for 4 h at room temperature.
4. **Flow chamber assembly:** Cut out 2 mm \times 30 mm area of a double-sided tape. This will serve as the flow channel. Align the flow channel with the drilled holes on the slides and sandwich the double-sided tape between cover slips and slides. Cut Tygon tubing to a 20 cm length and insert into the drilled holes of the slides. Connect the other end of the tubing to the sample or waste reservoirs. Seal the channel inlet and outlet with epoxy (Fig. 3a) (*see Note 9*).
5. **Optical stage setup and camera alignment:** Visible and near-IR cameras are connected to two exit ports of the microscope stand to image the walker and track its trajectory from two different spectral channels. The two cameras are aligned through a stage micrometer before each experiment. The (x,y) translation, rotation, and scaling are recorded as the transformation matrix for use in walking experiments. A third exit port is used to connect fluorometer through fiber optics for spectral measurement (Fig. 3b).
6. **Imaging scheme:** The visible image of a CdS QD and the near-IR image of a nanotube are first overlaid by using the transformation matrix from the previous step (Fig. 3c). The actual position of the CdS QD is resolved by fitting spot images to a Gaussian function and extracting the peak coordinates (Fig. 3d). The position of the walker is imaged against the nanotube track, which serves as a fiduciary marker for eliminating any effect from sample stage drift.
7. **Walking experiment:** Flow 100 μL 1 \times TA buffer slowly through the channel. Scanning through the sample to find a single-QD/single-nanotube conjugation spot (*see Note 10*). After confirming the single nanoparticle identity from the blinking behavior of a QD, the buffer in the channel is replaced by flowing 400 μL 1 \times TA- Mg^{2+} with desired Mg^{2+} concentration to start the walking experiment. Take measurements of both the QD and SWCNT images at certain time intervals (Fig. 4) (*see Note 11*).

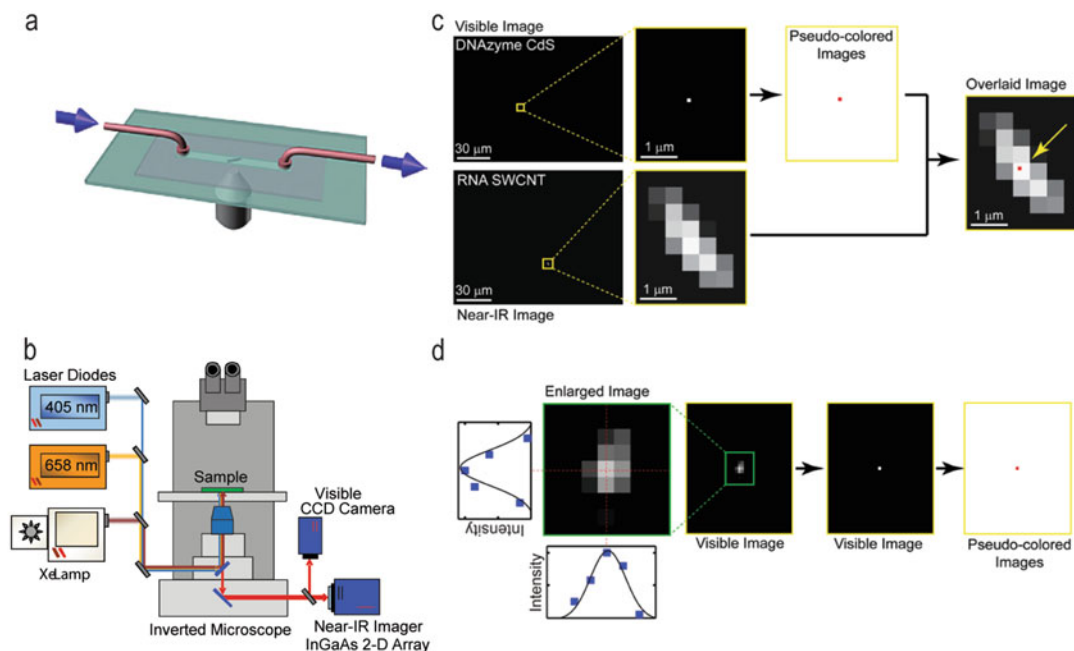


Fig. 3 Optical platform and imaging scheme. **(a)** Schematic of the flow chamber where the carbon nanotube tracks are immobilized on an agarose film. **(b)** Optical imaging platform which consists of two laser diodes (405 nm for CdS QDs and 658 nm for carbon nanotubes) and two cameras for imaging fluorescence in the visible (512×512 electron-multiplying charge-coupled device or EMCCD) and near-IR (320×256 InGaAs array) range (reprinted with permission from [13]. Copyright (2015) American Chemical Society) **(c)** Imaging scheme. *Left*: Raw image of the nanotube and QD. Scale bar is $30 \mu\text{m}$ in the original images and $1 \mu\text{m}$ in the zoom-in images. *Right*: Overlaid image of the nanotube and pseudo-colored, localized QD. **(d)** Gaussian fitting scheme to construct the pseudo-colored localized QD image and obtain its centroid position. ((a), (c), and (d) are reprinted with permission from [9]. Copyright (2014) Nature Publishing Group)

8. Data analysis for walking experiments: The displacement of a walker is directly measured from the walking experiment. The traveled distance of the walker is plotted against the measurement time and linearly fitted to obtain the walker speed (Fig. 5a).

3.3 Regulation of Walker Kinetics

The kinetics of a synthetic walker is modulated either by DNAzyme strands or by environmental factors such as cation species and concentration, pH, and temperature. Photo-regulation of walker kinetics can be also demonstrated by chemically modifying the nucleotide strands with photo-responsive azobenzene molecules. Here we describe the protocols for regulation through cations, DNAzyme sequence, and photo-control. More extensive results can be found elsewhere [13].

1. Cations: Flow $400 \mu\text{L}$ $1 \times \text{TA-Mg}^{2+}$ (10 mM) buffer into the channel to start the walking experiment. Make at least four measurements to obtain the walker speed under this condition. Flow $400 \mu\text{L}$ $1 \times \text{TA-Mg}^{2+}$ (50 mM) buffer to change the metal

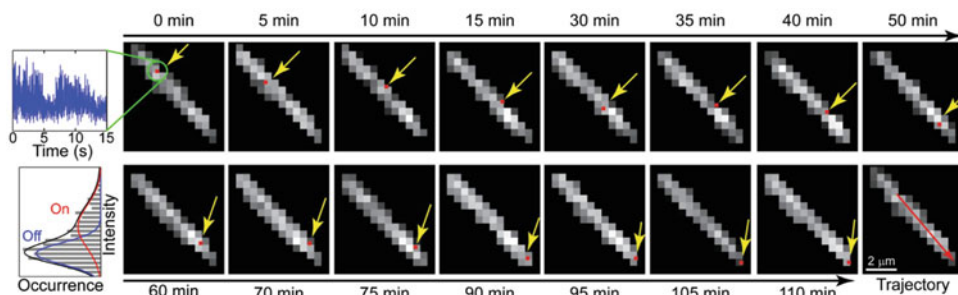


Fig. 4 Representative walking experiment results. *Left*: Blinking statistics of QD image to confirm the single QD identity. *Right*: QD imaged against a SWCNT track to monitor the DNA walker position over 110 min. The position of the QD is indicated by the *red dot* and the *yellow arrow*. The walking trajectory is shown as the *red arrow* in the last image (reprinted with permission from [13]. Copyright (2015) American Chemical Society)

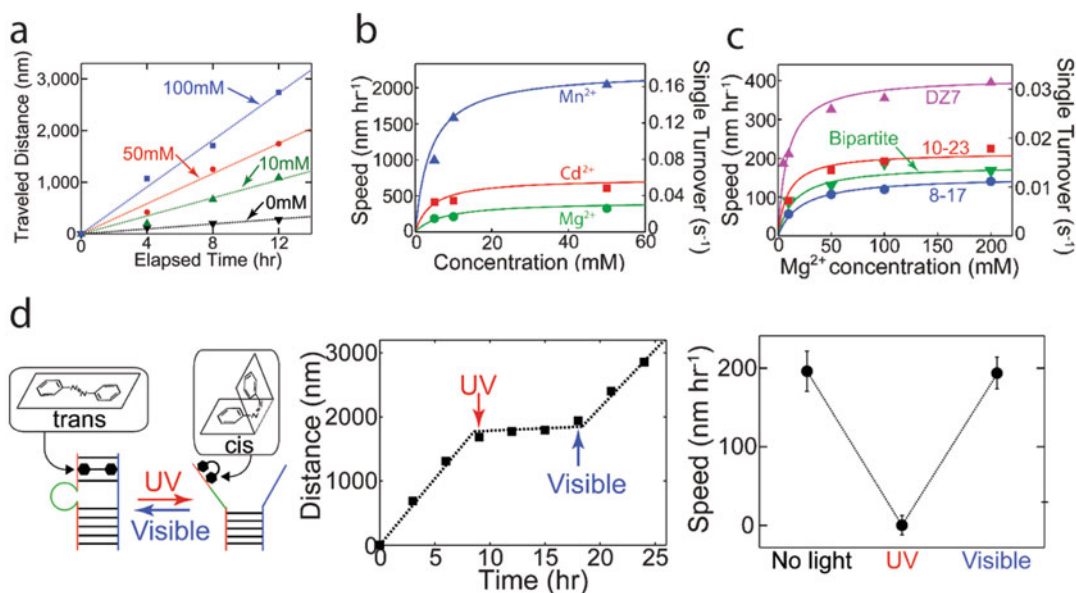


Fig. 5 (a) Distance vs. time plot is linearly fitted to obtain walker speed. Varying cation concentrations yield different walker speed (reprinted with permission from [9]. Copyright (2014) Nature Publishing Group) (b) and (c) Regulation of walker kinetics using cation species and DNAzyme sequences. (d) Photo-regulation of a DNA walker by incorporating photoisomerizable azobenzene moieties (*left*). Azobenzene molecules form the out-of-plane *cis* isomer under UV light, which does not allow duplex formation due to steric hindrance. Visible irradiation converts azobenzene into the planar *trans* isomer which allows base-pairing. Therefore, the walker stops upon UV illumination and resumes walking upon visible illumination (*center*). The walker speed can be fully recovered to the value before UV illumination after a UV-visible illumination cycle (*right*) (reprinted with permission from [13]. Copyright (2015) American Chemical Society)

cation concentration and take additional measurements under this condition. Repeat the experiment with $1\times$ TA-Mg²⁺ (100 mM) buffer. Walker speeds at 10, 50 and 100 mM Mg²⁺ concentrations are \sim 120, 160 and 220 nm/h, respectively. The speed *vs.* metal cation concentration plot is curve-fitted to

kinetics equations to obtain the reaction kinetics of enzymatic cleavage and strand displacement (Fig. 5b, bottom green curve) [9, 13]. Prepare 1× TA-Mn²⁺ and 1× TA-Cd²⁺ buffers and repeat this process to create faster walker kinetics sample (Fig. 5b, blue and red curve).

2. DNAzyme sequence: Prepare the walker assembly with corresponding DNAzyme and RNA sequence shown in Table 1 and perform walking experiment with 1× TA-Mg²⁺ at various Mg²⁺ concentrations for each DNAzyme sequence to produce the kinetics plots shown in Fig. 5c.
3. Photo-regulation: Prepare walker assembly with azobenzene modified DNAzyme sequence. The azobenzene moiety is incorporated in the upper recognition arm of the walker stand (Fig. 5d). Flow 400 μL 1× TA-Mg²⁺ (10 mM) buffer into the channel to start the walking experiment. Make at least four measurements to obtain walker speed at this condition. Shine UV light (300–400 nm) for 10 min at 10 mW. Image the sample for an additional four times. Shine visible light (485–700 nm) for 10 min at 10 mW. Take four more measurements. Plot the imaged QD positions as distance vs. time data to obtain the speed (Fig. 5d, center panel).

4 Notes

1. SC has a small aggregation number (2–3) and a small micelle size (~1 kDa), which makes them easily replaceable by RNA molecules during dialysis or buffer exchange. Carbon nanotubes dispersed by other surfactants (i.e., sodium dodecyl sulfate or SDS) can be also used, but the difference in average micellar molecular weight results in a different dialysis kinetics. A longer dialysis time is expected when other larger micelle size surfactants are used.
2. EDTA dissolves at a slow rate at neutral pH. Before adjusting pH with HCl, wait for all the EDTA powders to dissolve.
3. The concentration of the surfactant-dispersed SWCNTs is roughly 30 μg/mL. Sonication time affects the length of the prepared nanotubes. Longer sonication time will yield shorter nanotubes. If an ultracentrifuge is not available, use centrifugation at 15,000 rpm to separate large nanotube aggregations from well dispersed single tubes. However, a larger fraction of small nanotube bundles will be present in the solution.
4. Some aggregations might appear during dialysis, as the solubilizing ability of DNA/RNA is different from surfactants. If aggregations appear, centrifuge at 15,000 × *g* for 30 min to remove aggregations after dialysis. Typically, the decanted supernatant has a nanotube concentration of ~10 μg/mL.

5. To determine the number of nucleotide strands per nanotube, the molecular weight of a nanotube is estimated by assuming 300 nm average tube length and 1 nm tube diameter. The resulting molecular weight is approximately 3×10^6 amu. Based on the concentration of nucleotides and SWCNTs, there are approximately 80–100 RNA per nanotube.
6. It is important to keep the stirrer at 1000 rpm when adding Na_2S to the mixture. Otherwise, the added Na_2S will form aggregates immediately.
7. Approximately 10–30 DNA strands are present on a 3.5 nm QD. The number varies depending on the sequence of DNAszymes capping the QD.
8. Use water as lubricant and coolant as the drilling bit will become extremely hot. If water is not used, the drilling bit will be damaged after a few uses.
9. Too much epoxy will block the flow channel. To avoid epoxy blocking the channel, use a thin rubber plate with adhesive backing to cover the flow inlet and outlet first. Pierce a hole through the rubber plate and insert the tubing through the rubber plate. Apply epoxy on the rubber plate.
10. Finding the conjugation spot typically takes an hour depending on the sample quality.
11. Depending on the kinetic nature of the walker, different measurement intervals should be chosen. In case of slow walking speed, QD fluorescence will decrease in the image after several measurements due to photobleaching. Adding reducing agent (e.g., 20 mM dithiothreitol or DTT) will enhance the signal to noise ratio of the QD image as the reducing agent removes the surface charge traps from the QD.

Acknowledgement

This work is supported by the Office of Naval Research and the National Science Foundation.

References

1. Bath J, Turberfield AJ (2007) DNA nanomachines. *Nat Nanotechnol* 2(5):275–284
2. Pan J, Li F, Cha T-G, Chen H, Choi JH (2015) Recent progress on DNA based walkers. *Curr Opin Biotechnol* 34:56–64
3. Omabegho T, Sha R, Seeman NC (2009) A bipedal DNA Brownian motor with coordinated legs. *Science* 324(5923):67–71
4. Tian Y, He Y, Chen Y, Yin P, Mao C (2005) A DNAszyme that walks processively and autonomously along a one-dimensional track. *Angew Chem Int Ed* 44(28):4355–4358
5. Wickham SF, Bath J, Katsuda Y, Endo M, Hidaka K, Sugiyama H, Turberfield AJ (2012) A DNA-based molecular motor that can navigate a network of tracks. *Nat Nanotechnol* 7(3):169–173

6. Bath J, Green SJ, Turberfield AJ (2005) A free-running DNA motor powered by a nicking enzyme. *Angew Chem* 117(28):4432–4435
7. Wickham SF, Endo M, Katsuda Y, Hidaka K, Bath J, Sugiyama H, Turberfield AJ (2011) Direct observation of stepwise movement of a synthetic molecular transporter. *Nat Nanotechnol* 6(3):166–169
8. Yang Y, Goetzfried MA, Hidaka K, You M, Tan W, Sugiyama H, Endo M (2015) Direct visualization of walking motions of photocontrolled nanomachine on the DNA nanostructure. *Nano Lett* 15(10):6672–6676
9. Cha T-G, Pan J, Chen H, Salgado J, Li X, Mao C, Choi JH (2014) A synthetic DNA motor that transports nanoparticles along carbon nanotubes. *Nat Nanotechnol* 9(1):39–43
10. Michelotti N, de Silva C, Johnson-Buck AE, Manzo AJ, Walter NG (2010) Chapter six-a bird's eye view: tracking slow nanometer-scale movements of single molecular nanoassemblies. *Methods Enzymol* 475:121–148
11. Masoud R, Tsukanov R, Tomov TE, Plavner N, Liber M, Nir E (2012) Studying the structural dynamics of bipedal DNA motors with single-molecule fluorescence spectroscopy. *ACS Nano* 6(7):6272–6283
12. Tsukanov R, Tomov TE, Liber M, Berger Y, Nir E (2014) Developing DNA nanotechnology using single-molecule fluorescence. *Acc Chem Res* 47(6):1789–1798
13. Cha T-G, Pan J, Chen H, Robinson HN, Li X, Mao C, Choi JH (2015) Design principles of DNA enzyme-based walkers: translocation kinetics and photoregulation. *J Am Chem Soc* 137(29):9429–9437
14. Barone PW, Baik S, Heller DA, Strano MS (2005) Near-infrared optical sensors based on single-walled carbon nanotubes. *Nat Mater* 4(1):86–92
15. Bachilo SM, Strano MS, Kittrell C, Hauge RH, Smalley RE, Weisman RB (2002) Structure-assigned optical spectra of single-walled carbon nanotubes. *Science* 298(5602):2361–2366
16. Yu WW, Qu L, Guo W, Peng X (2003) Experimental determination of the extinction coefficient of CdTe, CdSe, and CdS nanocrystals. *Chem Mater* 15(14):2854–2860

INDEX

A

- Agarose gel electrophoresis.....22, 39, 46, 109–115,
117, 118, 159, 183, 205, 212, 242, 263
- Assembly line257–268
- Atomic force microscopy (AFM) 19, 22, 31, 34, 36,
37, 39, 86–89, 92, 93, 95, 111, 118, 127, 159–160, 186,
223, 230, 247, 249, 250, 253–255, 262, 263, 265–266,
268, 270, 274

C

- Carbonization.....222, 228–230
- Carbon nanotube (CNT) 218, 245–256, 269–279
- Colorimetric.....134, 137, 138, 140–143, 148
- Computer-aided design.....51–80
- Confined growth237–242
- Conjugation.....100, 103–105, 155–158,
191–193, 274, 275, 279
- Cryogenic electron microscopy (cryoEM).....22–23
- Crystallography3
- Cytosine-phosphate-guanosin (CpG) immunostimulatory
drugs.....122

D

- DNA 3–25, 27–39, 99–103, 105, 106, 109,
110, 153, 154, 156, 208–210, 237–242, 246–279
- brick.....41–48, 218–219, 238
- brick crystal45
- cassette.....261, 264–267
- crystal3–10, 219, 229, 256
- design261
- enzyme155–158, 270
- gridiron.....27–39
- linker.....21, 248, 252
- nanostucture.....11–25, 27–39, 94, 109–111,
113–118, 121–131, 133, 134, 138, 153, 159–161, 165,
166, 183, 191, 205, 212, 217–231, 238, 256
- nanotechnology 3, 11, 41, 51, 53, 80, 165,
217–231, 246, 258
- origami5, 6, 12, 28, 29, 34, 35, 41, 42, 55, 82,
113–115, 118, 121, 122, 153–162, 165, 188–190, 195,
204–206, 211, 218–222, 225, 227, 237–242, 256, 258,
263–265, 267
- walker258, 264, 265, 267, 269–279

- DNA-PAINT185–201
- Drug delivery.....121–131
- Dynamic light scattering (DLS).....24, 105, 106

E

- Enzyme activity.....133–150, 154, 160
- Enzyme cascade.....153–162

F

- Fluorescence microscopy122, 185, 186, 196
- Functionalization.....99–101, 103–105, 109

G

- Gold nanoparticles (AuNPs).....41, 99, 100, 111,
121, 238, 240, 242, 258, 259, 262, 263, 266
- G-quadruplex133–150

H

- Hydrofluoric acid (HF) etching224–226

I

- In vitro transcription83–91, 93

L

- Label-free135, 138, 237
- Liposome.....121, 174, 178–180, 183, 184, 254

M

- Membrane proteins203–211
- Metallization221, 231, 238
- Metal nanoparticles218, 237–242
- Methyltransferase (MTase)135–141, 150
- Modular.....42
- Motif5, 6, 11–25, 28, 29, 31, 34, 35, 51,
52, 55, 57, 59–61, 63–68, 75–78, 82, 83, 219, 259

N

- Nanoelectronics10
- Nanofabrication.....217–231
- NanoOctahedron.....166–183
- Nanoparticle117, 237–242, 246, 258,
259, 262, 263, 266, 268–279

Nanotechnology	3, 11, 27, 41, 51, 53, 72, 80, 84, 165, 217–231, 246, 257, 258	Self-assembly.....	11–18, 41, 82, 86, 126, 153, 187, 206, 217–219, 238, 245–256, 266
Nuclear magnetic resonance (NMR).....	82, 203–211	Silicon dioxide	249, 255
P		Single particle reconstruction	22–23
Photo-regulation	276–278	Star motif	11–25
Polyacrylamide gel electrophoresis (PAGE).....	19–21, 85, 87–95, 154–156, 158	Structural biology	203
Polyhedron	13–16, 219	Structural DNA nanotechnology	3, 41, 165, 217–231, 258
Polymeric bead pull-down.....	111, 117	Super-resolution imaging	185–201
Porous carbon material	228, 231	Surface.....	22, 25, 39, 48, 99–105, 122, 127, 155–160, 186, 190, 191, 194–196, 201, 221–223, 225, 230, 231, 238, 246, 248, 251, 253, 254, 258, 270, 272–274, 279
Protein-DNA conjugation.....	156–158	T	
Purification.....	6, 17–21, 38, 48, 85, 89–93, 104, 105, 155–158, 166, 174–177, 183, 193, 205–209, 212, 219, 240, 242, 243, 264, 271	Tensegrity.....	5–7, 9, 258
Q		Terminal deoxynucleotidyl transferase (TdT).....	135–139, 141–150
Quantum dot (QD).....	100, 104, 106, 121, 238, 239, 270, 272–274, 276–279	Thioflavin T (ThT)	134
R		Three-dimensional (3D)	3–25, 41, 56, 57, 71, 77, 122, 133, 237–242
Residual dipolar couplings.....	204, 205	Three-dimensional DNA nanostructures.....	11–25, 117
RNA.....	52, 58, 71, 75, 270–274, 278, 279	Transmission electron microscopy (TEM).....	23, 34, 36, 37, 39, 48, 87, 95, 105, 111, 118, 177, 178, 181–183, 239, 241–242, 266, 268, 274
nanoparticles.....	81–95	U	
nanotechnology	51, 72, 83, 84	Ultrafiltration	110–114
origami	51–80, 82–84	V	
sequence design	72–75	Vesicles	178, 180, 183–185, 255
structure prediction.....	56	W	
Rolling circle amplification (RCA)	122, 126–128, 130, 135	Wireframe	27–39, 219
S			
Secondary structure	52, 56, 57, 69–74, 76, 130, 147, 190		
Self-assembled monolayer (SAM).....	222–224		